

**MOTOR EQUIVALENCE IN ACTIONS
BY REDUNDANT MOTOR SYSTEMS**

by

Daniela Mattos

A dissertation submitted to the Faculty of the University of Delaware in partial fulfillment of the requirements for the degree of Doctor of Philosophy in
Biomechanics and Movement Science

Summer 2015

© 2015 Daniela Mattos
All Rights Reserved

ProQuest Number: 3718355

All rights reserved

INFORMATION TO ALL USERS

The quality of this reproduction is dependent upon the quality of the copy submitted.

In the unlikely event that the author did not send a complete manuscript and there are missing pages, these will be noted. Also, if material had to be removed, a note will indicate the deletion.



ProQuest 3718355

Published by ProQuest LLC (2015). Copyright of the Dissertation is held by the Author.

All rights reserved.

This work is protected against unauthorized copying under Title 17, United States Code
Microform Edition © ProQuest LLC.

ProQuest LLC.
789 East Eisenhower Parkway
P.O. Box 1346
Ann Arbor, MI 48106 - 1346

**MOTOR EQUIVALENCE IN ACTIONS
BY REDUNDANT MOTOR SYSTEMS**

by

Daniela Mattos

Approved:

Gregory E. Hickey, PT, Ph.D.
Chair of the Department of Physical Therapy

Approved:

Kathleen S. Matt, Ph.D.
Dean of the College of Health Sciences

Approved:

James G. Richards, Ph.D.
Vice Provost for Graduate and Professional Education

I certify that I have read this dissertation and that in my opinion it meets the academic and professional standard required by the University as a dissertation for the degree of Doctor of Philosophy.

Signed:

Mark Latash, Ph.D.
Professor in charge of dissertation

I certify that I have read this dissertation and that in my opinion it meets the academic and professional standard required by the University as a dissertation for the degree of Doctor of Philosophy.

Signed:

Darcy Reisman, PT, Ph.D.
Professor in charge of dissertation

I certify that I have read this dissertation and that in my opinion it meets the academic and professional standard required by the University as a dissertation for the degree of Doctor of Philosophy.

Signed:

Slobodan Jaric, Ph.D.
Member of dissertation committee

I certify that I have read this dissertation and that in my opinion it meets the academic and professional standard required by the University as a dissertation for the degree of Doctor of Philosophy.

Signed:

Jill Higginson, Ph.D.
Member of dissertation committee

I certify that I have read this dissertation and that in my opinion it meets the academic and professional standard required by the University as a dissertation for the degree of Doctor of Philosophy.

Signed:

Robert Sainburg, OTR, Ph.D.
Member of dissertation committee

ACKNOWLEDGMENTS

The path towards a Ph.D. is absolutely impossible without guidance and support. I would like to express my deepest gratitude to my professors with whom I worked. I came from Brazil to study motor control and the experience of being surrounded by experts in this field was very unique. I am extremely thankful to my advisor Dr. John Scholz (*in memorium*) for every effort he put towards my academic formation, for all the challenges, encouragements and his meticulous guidance. I would also like to thank Dr. Mark Latash. It was an honor to continue my studies under his mentorship and to be exposed to an extremely rich learning environment at PSU. I am also very thankful to Dr. Darcy Reisman for her guidance as my co-advisor. Several times her inputs were “just what I needed”. Moreover, Darcy’s trajectory is very inspiring for me. I am also grateful for the discussions with Dr. Gregor Schöner that were fundamental for the understanding of the topic. My sincere “obrigado” to my committee members: Dr. Robert Sainburg, Dr. Slobodan Jaric and Dr. Jill Higginson, for their time, attention, and valuable feedback. Thanks for all the opportunities, for the assistance during the moments of transition, and more importantly for helping me reach some of my personal goals as a scientist.

I would also like to thank all the members of Dr. Scholz’s lab at UDel: Geetanjali, Eunse, Shraddha, Pei Chun, Jennifer, and of the MCL at PSU: Satya, Stan, Mu, Florent, Hang Jin, Tao, Ali, Behnoosh, Yang, Yen and Sasha. Sharing space with you was not only a great source of technical support and academic experiences, but also comfort, culture and entertainment. I am also grateful for friends I met during

these years, especially Anna, As Danis (QPPE), Vivek and Melissa. You were like angels in the right place and time. Andrew was also fundamental throughout the process; I can't thank enough for his sincere friendship. Last, but not least, this journey could never be completed without the everlasting support and strength of my parents, brothers and closest friends – Thank you!

This research was supported by the National Institute of Health under grants NS-035032 and AR-048563.

TABLE OF CONTENTS

| | |
|---|------|
| LIST OF TABLES | viii |
| LIST OF FIGURES | ix |
| ABSTRACT | xvi |
| Chapter | |
| 1 INTRODUCTION | 1 |
| 1.1 Background | 1 |
| 1.1.1 The Redundancy Problem | 3 |
| 1.1.2 Principles, hypotheses and notions in motor control | 4 |
| 1.1.3 The UCM framework at different spaces | 12 |
| 1.1.3.1 Multi-Joint Synergies | 12 |
| 1.1.3.2 Multi-Muscle Synergies | 18 |
| 1.1.3.3 Multi-Finger Synergies | 22 |
| 1.1.4 Motor Equivalence | 27 |
| 1.1.5 Models supporting the UCM hypothesis | 29 |
| 1.2 Significance and Innovation | 31 |
| 1.3 Aims and Hypothesis | 32 |
| 2 UNPREDICTABLE ELBOW JOINT PERTURBATION DURING REACHING RESULTS IN MULTIJOINT MOTOR EQUIVALENCE | 36 |
| 2.1 Abstract | 36 |
| 2.2 Introduction | 37 |
| 2.3 Methods | 43 |
| 2.4 Results | 54 |
| 2.5 Discussion | 66 |
| 2.6 Conclusions | 73 |
| 3 MOTOR EQUIVALENCE (ME) DURING REACHING: IS ME OBSERVABLE AT THE MUSCLE LEVEL? | 75 |
| 3.1 Abstract | 75 |

| | | |
|-----|--|-----|
| 3.2 | Introduction | 75 |
| 3.3 | Methods | 80 |
| 3.4 | Results | 98 |
| 3.5 | Discussion | 108 |
| 4 | MOTOR EQUIVALENCE DURING MULTI-FINGER ACCURATE FORCE PRODUCTION | 119 |
| 4.1 | Abstract | 119 |
| 4.2 | Introduction | 120 |
| 4.3 | Methods | 124 |
| 4.4 | Results | 134 |
| 4.5 | Discussion | 143 |
| 5 | TASK SPECIFIC STABILITY OF ABUNDANT SYSTEMS: STRUCTURE OF VARIANCE AND MOTOR EQUIVALENCE..... | 154 |
| 5.1 | Abstract | 154 |
| 5.2 | Introduction | 155 |
| 5.3 | Methods | 158 |
| 5.4 | Results | 170 |
| 5.5 | Discussion | 184 |
| 6 | CONCLUSIONS | 194 |
| 6.1 | Aim 1 Findings | 194 |
| 6.2 | Aim 2 Findings | 196 |
| 6.3 | Aim 3 Findings | 198 |
| 6.4 | Aim 4 Findings | 202 |
| 6.5 | Concluding Comments and Future Directions | 204 |
| | REFERENCES | 208 |

Appendix

| | |
|---|-----|
| COMPUTATION OF VARIANCE AND MOTOR EQUIVALENCE ANALYSES REFERENT TO AIM 3 | 225 |
|---|-----|

LIST OF TABLES

| | |
|---|-----|
| Table 2.1 Movement time, peak velocity, and time of peak velocity. | 59 |
| Table 2.2 Targeting error..... | 60 |
| Table 2.3 Slope of change in ME and Non-ME components..... | 64 |
| Table 3.1 Average \pm SEM variable and constant error of pointer position at movement termination..... | 102 |
| Table 3.2 Example mode structure for two (S01 & S10) of the six subjects who had very similar muscle contributions (loading > 0.5) to the first two modes, but who could have very different muscle contributions to the other three modes. A third subject (S03) exhibited two modes (Mode 1 & Mode 4) similar to modes 2 and 1 respectively for the six similar subjects, although the percent of variance accounted for by the mode related to elbow extensor activation accounted for less of the total variance. | 103 |
| Table 3.3 The dot product between mode vectors (M1-5) for S01 paired with each of the remaining subjects..... | 104 |

LIST OF FIGURES

| | |
|---|----|
| <p>Figure 2.1 Cartoon depicting the experimental setup. Subjects wore safety goggles with a cardboard brim attached to the bottom to block vision of their arm and hand during approximately the first half of the reach. Either a spherical target or a cylinder (illustrated here) was hung from strings from a post to increase the need to control the terminal reach precisely. The Thera-Band was attached with hooks to padded cuffs placed around the upper arm and distal forearm so that they spanned the elbow joint.</p> | 44 |
| <p>Figure 2.2 Mean (\pmSD) of elbow joint excursion for a representative subject during the reach for the 3 conditions of stiffness (0-K, Low-K, and High-K) and for the spherical and cylindrical targets. θ_{elbow}, elbow joint angle. Flex, flexion; Ext, extension.</p> | 55 |
| <p>Figure 2.3 Time series (\pmSD) is shown of the resultant hand path (<i>top</i>) for the same subject as in Fig. 2 for the 3 stiffness conditions when reaching to the spherical (<i>left</i>) or cylindrical (<i>right</i>) targets. <i>Bottom</i>: mean (\pmSD) resultant velocity profiles associated with the reaches shown at <i>top</i>.</p> | 55 |
| <p>Figure 2.4 Time series (\pmSD) of the hand's orientation to coordinates of the cylindrical target (pitch, roll, and yaw) for reaching to both the spherical and cylindrical targets for a subject showing smaller changes in orientation (<i>A</i>) and a subject showing larger changes in orientation (<i>B</i>).</p> | 58 |
| <p>Figure 2.5 Time series (\pmSE) of the motor equivalent (ME, solid lines) and non-motor equivalent (Non-ME, dashed lines) components of the joint difference vector (JDV). Results are presented for each target (<i>left</i> and <i>right</i>) and in relation to the 2 performance variables (<i>top</i> and <i>bottom</i>). .</p> | 61 |
| <p>Figure 2.6 Average (\pmSE) of ME and Non-ME components for each performance variable at each 10% of the reach trajectory; <i>F</i> ratios and <i>P</i> values are based on the 4-way repeated- measures ANOVA performed over each 10% of the reach. The interaction performance variable [3-dimensional (3D) position vs. 3D orientation] by projection component (i.e., ME vs. Non-ME) was significant for the phases indicated.</p> | 62 |

| | |
|---|----|
| Figure 2.7 Average (\pm SE) for ME and Non-ME components for each stiffness condition for each 10% of the reach trajectory. <i>F</i> ratios and <i>P</i> values are based on the 4-way repeated-measures ANOVA performed over each 10% of the reach. The interaction stiffness (Low-K vs. High-K) by projection component (i.e., ME vs. Non-ME) was significant for the phases indicated. | 64 |
| Figure 2.8. Mean (\pm SE) of each component of joint configuration variance (V_{UCM} and V_{ORT}) computed at each phase of the reach and averaged across target type, performance variable, and stiffness. <i>F</i> ratios and <i>P</i> values are based on the 4-way repeated- measures ANOVA performed over each 10% of the reach. Only the main effect of variance component (V_{UCM} vs. V_{ORT}) was significant for the phases indicated. DOF, degree of freedom. | 65 |
| Figure 3.1 Illustration of experimental set-up for perturbed trials. Nonperturbed trials were identical, except for the attachment of the Thera-band. Subjects wore a pair of safety goggles that had the equivalent of the brim of a baseball hat attached to prevent subjects from viewing their reaching arm in the initial position. On nonperturbed trials, the experimenter acted as though they were applying the band by pulling gently on the wrist and shoulder attachments to prevent subjects from predicting when the perturbation would occur. | 82 |
| Figure 3.2 Illustration of methods to determine (top panel) EMG onsets for a given trial of both conditions and (middle and lower panels) the time of onset of a perturbation for a given trial of the PERT condition. EMG _{All Muscles} in the top panel is the sum of the rectified, filtered and normalized EMGs of all measured arm muscles for a given trial. EMG _{TRICEPS} is the sum of rectified, filtered and normalized the EMGs for a given PERT trial and the average of this sum across trials for the N-PERT condition. | 92 |
| Figure 3.3 Illustration of displacements of arm joint degrees of freedom for a representative subject with (black lines) and without (gray lines) the perturbation applied to the elbow. Thick lines are the mean across reaches. Thin lines are one standard deviation. Four joint motions exhibited much smaller adjustments to the perturbation and are therefore not illustrated. | 99 |

| | |
|---|-----|
| Figure 3.4 Example trajectories of elbow angle (top row), elbow flexors (2nd row), elbow extensors (3rd row) rectified, integrated and normalized to MVC EMG activities, and M-modes (last row) for N-PERT and PERT conditions. Data are averaged across trials of a representative subject after aligning trials based on EMG onsets..... | 100 |
| Figure 3.5 Motor equivalent (ME) and nonmotor equivalent (Non-ME) components of projections of (1) deviations of M-modes between PERT and N-PERT conditions (top row) and (2) deviations of the joint configurations between PERT and N-PERT conditions (lower row) related to stability of the pointer position (left column) and its orientation in 3D space (right column) for four phases of the reach..... | 107 |
| Figure 3.6 Average across subjects, \pm SEM of the index of cocontraction is illustrated for four phases of reaching for both the PERT and N-PERT conditions. | 108 |
| Figure 3.7 A: The ellipse shows a hypothetical data distribution across trials for the task of producing a constant total output by two effectors: $E_1 + E_2 = C$. Note the higher variance along the uncontrolled manifold (UCM) for the task as compared with variance orthogonal to the UCM. The task to change the magnitude of C (from C_1 to C_2) can be achieved with different amounts of motion along the UCM (motor equivalent motion), from minimal (from S_0 to S_1) to very large (from S_0 to S_3). B: If a preferred trajectory from S_0 to S_1 is perturbed (Pert), the corrective reaction may be directed toward the originally planned final state (Reaction-1) or to a state characterized by a larger amount of motion parallel to the UCM (Reaction-2 leading to S_2). We observed behavior corresponding to Reaction-2. | 113 |
| Figure 4.1 a A schematic of the experimental setup showing the subject's position and the sensor arrangement; b illustration of the feedback given to the subject on the monitor display. Signals for the maximum voluntary contraction (MVC), ramp force production, and cyclic force production with (TRACK) and without (N-TRACK) template are illustrated. A metronome paced the N-TRACK task; c schematic of force sensors mounted on linear motors. In the illustration, the ring force sensor is lifted. Moment arms with respect to mid-hand were 4.5, 1.5, -1.5, and -4.5 cm for the index (I), middle (M), ring (R), and little (L) fingers, respectively. Counterclockwise rotation (+) around the axis represents pronation moment..... | 126 |

Figure 4.2 Time profiles of a representative subject illustrating changes in total force (*upper plots*), individual finger forces (*middle plots*) and the motor equivalence analysis (*lower plots*) pre-, during-, and post-perturbation during the TRACK (*right plots*) and N-TRACK (*left plots*) task. The *black vertical lines* represent the perturbation onsets for PT_{UP} (middle finger lifted at 1 cm height) and PT_{DN} (middle finger lowered, at 0 cm height)..... 136

Figure 4.3 Finger force (*I* Index, *M* Middle, *R* Ring, *L* Little, *IMRL* total force) during different phases (means ± standard errors are shown): *Top* general adjustments: pre-, during-, and post-perturbation, *Middle and bottom* quick adjustments following PT_{UP} and PT_{DN}: Pre-Pert, Post-Pert50, Post-Pert100, Post-Pert150, and Post-Pert500. *Left and right plots* show the TRACK and N-TRACK conditions, respectively. Pre-perturbation phase for the PT_{UP} condition is the mean pre-perturbed cycles, and pre-perturbation phase for PT_{DN} condition is the mean of the last cycle before PT_{DN}. 137

Figure 4.4 Motor equivalence (*upper plots*) and UCM analysis (*lower plots*) with respect to the to the stabilization of the **a** total force (F_{TOT}) and **b** total moment of force (M_{TOT}) during phases pre-, during-, and post-perturbation for TRACK and N-TRACK tasks. *Left and right plots* show analyses in the mode and force spaces, respectively. Means ± standard errors are shown..... 140

Figure 4.5 Motor equivalence analysis during phases pre- and post-perturbation (Post-Pert50, Post-Pert100, Post-Pert150, and Post-Pert500) following PT_{UP} (*upper plots*) and PT_{DN} (*lower plots*) for TRACK (*left plots*) and N-TRACK (*right plots*) tasks in the mode space. Analysis in the force space (not shown) had similar profiles. Means ± standard errors are shown..... 142

Figure 4.6 An illustration of the idea of motor equivalence. Two effectors are involved in a common task $F_1 + F_2 = C$. In the initial steady state ($C = C_1$, cloud of data points 1), inter-trial variance is mostly along the UCM for this task (*dashed line*). A perturbation changes the output of the system to C_2 (cloud of points 2). It is expected to lead to larger deviation along the less stable direction (ME, along the UCM) as compared to more stable direction (nME, along ORT). A correction leads to the same output of the system, C_1 (cloud of points 3), again with a large ME deviation along the UCM. Note that the ME versus nME deviations may be associated with different structure of inter-trial variance as illustrated with the different shapes of the clouds of data points..... 151

Figure 5.1 *Left*: The experimental setup. The monitor shows the target position at the beginning of each trial and the cursor feedback for the F- and M-tasks. *Middle*: Visual feedback for the Jumping-Target Task with the four possible conditions of target jump. Only one target was shown at each time. *Right*: The *inverse piano* used to lift the index (I) finger during the Step I-Perturbation Task. The zero moment was computed with respect to the midline between middle (M) and ring (R) fingers. Clockwise direction was considered (+) and represented pronation moment of the forearm. 161

Figure 5.2 Phases of analysis for the Jumping-Target and Step I-Perturbation tasks. For the Jumping-Target task, the phase PRE- corresponded to the mean values between 2.0 and 2.5 s prior to the first target jump (1st jump), during (DUR-) was computed between 3.5 and 4 s after the 1st jump, and POST- to the mean values between 2.0 and 2.5 s after the second target jump (2nd jump). For Step I-Perturbation, the phases PRE- and POST- were computed between 2.0 and 2.5 s prior to and after the onset of the index finger lifting (I-lifting), respectively. 168

Figure 5.3 Force and moment time profiles of a subject during the Jumping-Target Task. The period highlighted in gray shows the target at a new position after the 1st jump. *Upper* plots show the total force (F_{TOT}) and the total moment of force (M_{TOT}) during each condition of target jump. *Middle* and *lower* plots show the finger forces and moment of force of the index (I), middle (M), ring (R), and little (L) fingers. Positive moment direction represents supination efforts. 172

Figure 5.4 Typical time profiles of the motor equivalence (ME, solid line) and non-motor equivalence (nME, dotted line) components during the Jumping-Target Task. Analysis was performed in the space of finger-modes. Each component was normalized by the square root of the number of DOF in each dimension. 174

Figure 5.5 Group means (\pm SE) of the motor equivalence (ME, gray bars) and non-motor equivalence (nME, black bars) components at phases: PRE-, during (DUR-), and POST- target-jump. *Upper* and *lower* plots show the continuous-feedback and frozen feedback variables, respectively. Visual feedback was removed for frozen-feedback variables at phases DUR- and POST- Target Jump. 175

Figure 5.6 Group means (\pm SE) of the V_{UCM} (gray bars) and V_{ORT} (black bars) components at phases: PRE-, during (DUR-), and POST- target-jump. The continuous-feedback and frozen feedback variables are shown in the *upper* and *lower* plots, respectively..... 177

Figure 5.7 Force and moment time profiles of a subject during the Step I- Perturbation Task. The period highlighted in gray shows the period of lifting of the index (I)-finger. *Upper* plots show the total force (F_{TOT}) and the total moment of force (M_{TOT}) for the F-task and M-task. *Middle* and *lower* plots show the finger forces and moment of force of the index (I), middle (M), ring (R), and little (L) fingers..... 179

Figure 5.8 Typical time profiles of the motor equivalence (ME, solid line) and non-motor equivalence (nME, dotted line) components during the Step I- Perturbation Task. Analysis was performed in the space of finger-modes. Each component was normalized by the square root of the number of DOF in each dimension. 5.8: Typical time profiles of the motor equivalence (ME, solid line) and non-motor equivalence (nME, dotted line) components during the Step I-Perturbation Task. Analysis was performed in the space of finger-modes. Each component was normalized by the square root of the number of DOF in each dimension. 182

Figure 5.9 Group means (\pm SE) of the motor equivalence (ME, gray bars) and non-motor equivalence (nME, back bars) components during the Step I- Perturbation Task at phases Pre-Perturbation and Post-Perturbation, *upper* and *lower* plots respectively. The scale of the *y*-axis is not consistent between plots. 183

| | |
|--|-----|
| Figure 5.10 Group means (\pm SE) of the V_{UCM} (gray bars) and V_{ORT} (back bars) components during the Step I-Perturbation Task at phases Pre-Perturbation and Post-Perturbation, <i>upper</i> and <i>lower</i> plots respectively..... | 184 |
| Figure 5.11 Scheme illustrating a hypothetical experiment where the goal of the task is to produce 10 N using the index (I) and ring (R)-fingers. When this task is repeated several times, and the force sharing between the I and R fingers (<i>I,R-sharing</i>) for each trial is plotted, the shape of the distribution will be an ellipse. The major axis corresponds to all the combinations of finger forces that satisfy the task, i.e. the UCM. Now, lets assume that one of the fingers is perturbed (eg. lifting of the I-finger) leading to increase in the force produced by both fingers. The total force will be larger than 10 N. Then, after some delay, the force of the I and R-fingers will decrease to maintain the total force close to 10 N, representing motor equivalence at the task-performance. It is likely that the force produced by the individual fingers will change relative to the unperturbed state. The <i>I,R-sharing</i> is illustrated in three states: 1- unperturbed, 2- during the perturbation; 3- after the correction. Note that most of the deviations in <i>I,R-sharing</i> lie along the UCM (ME component) as compared with deviations orthogonal to the UCM (nME component)..... | 187 |

ABSTRACT

The phenomenon of motor equivalence (ME) is one of the most remarkable features of purposeful behaviors in biological systems that allow reorganizing the degrees-of-freedom (DOFs) in the face of perturbations and still accomplishing the functional task. When a small perturbation is introduced to the system, salient variables of task performance are never perfectly unchanged, which poses additional challenges to the estimation of motor equivalence. The Uncontrolled Manifold (UCM) hypothesis proposes that the CNS uses a manifold (UCM) within the space of the elemental variables corresponding to desired values of a particular performance variable. Then, most of the variance in motor elements is expected to be confined to the UCM. Based on this hypothesis, the changes in elemental variables caused by an external perturbation are expected to lie mostly along the UCM, i.e. to represent ME with respect to the performance variable, while a smaller set of deviations in the elemental variables would cause errors in the performance variable (non-motor equivalent, nME). The overall goal of this dissertation was to quantify the ME phenomenon and, more specifically, to determine how different types of feedback contribute to the reorganization of motor elements to maintain stability of task-specific variables. Perturbations were provided during the course of either reaching arm movements or finger pressing tasks. Then, ME was quantified with respect to salient,

lower dimensional performance variables at several levels of description including joint angles, muscle groups, finger forces, and finger modes. The outcomes of this study suggest that ME is present throughout the course of actions, even when there is no perturbation. After the perturbation onset, there was an immediate increase in the amount of ME that became larger within time windows of 50 ms post-perturbation, accompanied by a smaller increase in the nME component. These effects remained high after a transient external perturbation. ME effects were also induced by a quick action without any physical perturbation. We observed a large increase in the nME component upon removal of visual feedback, while the changes in the ME component were inconsistent. These results suggest that ME modulation receives contributions from several sources: muscle mechanics, reflexes and voluntary responses. Visual feedback seems to play a critical role in organizing the task-specific stability in multi-finger pressing tasks. These results support the idea that the CNS makes use of the abundant DOFs, allowing for flexibility of motor patterns in the face of perturbations or quick changes in actions.

Chapter 1

INTRODUCTION

1.1 Background

The redundancy problem has traditionally been viewed as the central research topic in the motor control field (Bernstein 1967). Motor redundancy is defined as the multiplicity of solutions for the same task. Then, the problem becomes how to select a particular set of solutions from all the possible ones across various levels of analysis (muscle, groups of muscles, joints, forces) (Turvey, 1990). Since the redundancy problem was framed, there were several attempts to determine which variables are being “controlled” by the CNS when purposeful movements are performed. Bernstein himself proposed that the redundant degrees-of-freedom (DOFs) were eliminated (Latash, 2000). Currently, there are two qualitative different ways to approach Bernstein’s problem. The first one is based on notions of classic mechanics, control theory and engineering and assumes that the central controller finds an optimal solution to the task. “Redundancy reduction” (Guigon, Baraduc, & Desmurget, 2007) is used to implement the solution, for example, by proposing task constraints that will ultimately lead to a non-redundant system. These methods are often not task-specific and incompatible with the phenomenon of flexibility of motor patterns observed in redundant systems. Other researchers advocate that redundancy is explored during movement performance (Latash, Levin, Scholz, & Schoner, 2010; Latash, Scholz, & Schoner, 2007; Scholz & Schoner, 1999) and the controller facilitates groups of

equally acceptable solutions as opposed to finding a unique solution, this notion is known as the Principle of abundance (Gelfand & Latash, 1998; Latash, 2012a).

The phenomenon of motor equivalence refers to reorganization of motor elements in the face of perturbations to preserve stability of a particular task-specific performance variable, or the *task-specific stability*. This is a fundamental feature of everyday motor behaviors that allows dealing with unpredictable situations without compromising successful outcome of the task. Motor equivalence is only possible because of the extra DOFs and, therefore, a great research model to further explore the principle of abundance and its underlying mechanisms. However, the quantification of motor equivalence in a redundant system is not as trivial as it appears to be. When the system is perturbed, there will also be changes in salient performance variables. Then, how can one estimate the changes in motor elements that lead to error in the task performance versus the ones that lead to motor equivalence? This question can be answered by quantifying the stability properties of multi-DOFs system.

The UCM approach has been used to test stability properties of a redundant system in multiple ways. Within the traditional uncontrolled manifold (UCM) framework, variability arising in the system naturally from trial-to-trial is expected to be larger in the directions of low stability (those spanning the UCM) as compared to directions of high stability (ORT) (Scholz & Schoner, 1999; Schoner, 1995). A more direct method to test task-specific stability of a redundant system is to measure its response after a perturbation while subjects intend to perform a particular task. This method estimates the amount of motor equivalence (Martin, 2007) as the deviations of motor elements corresponding to no changes in salient performance variables (confined to the UCM), while the deviations that lead to changes in those variables are

addressed as the non-motor equivalent (nME) component (Schoner, Martin, Reimann, & Scholz, 2008).

The overarching goal of this proposal was to use both the traditional inter-trial variance and the less extensively explored motor equivalence methods to quantify the amount of task-specific reorganization of motor elements following perturbation across multiple levels of analyses (joint angles, muscles, finger forces and modes). This study also explores the role of several underlying mechanisms involved in the use of redundancy including mechanics and neural responses from peripheral afferents (cutaneous and proprioceptive), and voluntary responses, as well as visual feedback. Findings from this dissertation have direct contributions to the principle of motor abundance.

1.1.1 The Redundancy Problem

Purposeful natural movements typically involve the coordination of multiple DOFs. For example, when a person reaches to touch an external target, several joint rotations with at least 7 rotational DOFs are coordinated to position the hand in the 3-dimension (3D) space. Because the number of DOFs in the joint space exceeds the number of DOF strictly required for the target task, there are an infinite number of ways to combine the joint rotations and accomplish the task successfully. How the central nervous system (CNS) reduces the number of independent variables to be controlled has been a fundamental question in the motor control field (Turvey, 1990), defined as the Problem of Motor Redundancy. The redundancy at the joint kinematic level of description is known as the problem of inverse kinematics. To add further complexity to the problem, redundancy also exists in the muscular control: many

combinations of muscle forces can generate the torque around the joint (Latash, 2012b), which gives rise to the problem of inverse dynamics. Then, to produce a certain level of muscle activity, there are many motor units that can be recruited at different frequencies. The redundancy problem exists at any level of the description, from the macroscopic to microscopic variables. Despite the high amount of DOFs, behaviors produced by humans are highly coordinated, i.e. they have a spatial, temporal and functional order (Schoner & Kelso, 1988).

1.1.2 Principles, hypotheses and notions in motor control

A common approach to the redundancy problem is to effectively reduce the DOFs by applying a cost function that limits the choice of joint and muscle combination. Common examples of cost functions are: minimum time (Enderle & Wolfe, 1987), minimum jerk (Flash & Hogan, 1985), minimum torque change (Uno, Kawato, & Suzuki, 1989), minimum effort (Hasan, 1986), minimum discomfort (Cruse & Bruwer, 1987) and more complex cost functions (Rosenbaum, Meulenbroek, Vaughan, & Jansen, 2001). One of the most recent functions proposed is the weighted sum of the motor command squared and performance error used in the formulation of the optimum feedback control (Scott, 2004; Todorov & Jordan, 2002). Unlike the previous cost functions, the optimum feedback control solves the redundancy problem moment-by moment, using the available information to choose the best output (Todorov & Jordan, 2002), and therefore is compatible with features of motor flexibility. While having a cost function to describe a particular behavior could help to formalize well-established behaviors, the next step would be to link such functions to neurophysiological mechanisms. This step has been a challenge.

An alternative way to deal with the redundancy existent in motor systems was to start with developing a set of notions specific to biological systems. In order to introduce an adequate language to the motor control field, several principles and hypotheses have been proposed over the past decades including the principle of abundance, the principle of minimal interaction, the UCM hypothesis, and the equilibrium point hypothesis.

The Principle of Abundance & the Principle of Minimal Interaction

The abundance provided by the available DOFs allows for flexible solutions during actions. The potential benefits of the surplus of DOFs during movement coordination motivated Gelfand and Latash (1998) to reformulate the DOF-problem as the “Principle of Abundance”. This principle states that redundancy allows for the facilitation of a family of solutions organized into structural units (synergies) equally capable of solving the problem (Latash, Scholz, & Schoner, 2002). Then, based on the Principle of Abundance, the excess of DOF is not a “computational problem” that needs to be solved, but a positive characteristic of human’s behavior (Latash, 2012a).

The “Principle of Minimum Interaction” suggested that: “the interaction among elements of a multi-element system is organized so as to minimize the external input to each individual element (and, correspondingly, its output) while keeping the total output of the system compatible with the command signal from the hierarchically higher controller” (Latash, 2010a). Therefore, it assumes a hypothetical hierarchical organization of motor elements forming the structural units and the task being performed (Gelfand & Latash, 1998). At the higher level of the hierarchy, the CNS stabilizes the task performance. At the lower level, the contribution from each element

involved in the task is allowed to vary to preserve the stability of task-related performance (Schoner, 1995).

The concept of synergy

In contemporary literature the most emphasized feature of synergies is the preferred relations among the elements (Berniker, Jarc, Bizzi, & Tresch, 2009; Borzelli, Berger, Pai, & d'Avella, 2013; Cheung, d'Avella, & Bizzi, 2009; d'Avella & Lacquaniti, 2013; d'Avella, Portone, Fernandez, & Lacquaniti, 2006; Desmurget et al., 1995; Soechting & Lacquaniti, 1989), or sharing patterns among elements of a redundant system. A second essential feature of synergies is the error compensation/flexibility present when a purposeful action is performed by a redundant system (Latash et al., 2007). In one of the most classical examples of motor redundancy, Bernstein noticed that when professional blacksmiths hit the chisel with the hammer, the variability of the tip of the hammer across repeated strokes was lower than the variability of joint trajectories (Latash et al., 2007). This observation suggested that the joints compensated for each other errors during the movement performance, and the major goal of this compensation was to preserve the task-related performance variable, i.e., the preserve the trajectory of the tip of the hammer (Latash et al., 2007).

Other definitions of synergy incorporate the feature of task specific stability. For example, Turvey (1990) described synergies as a group of muscles crossing several different joints and capable of contracting independently of each other, behaving as a single task-specific unit. This organization was proposed to be flexibly adapted to task-performance and stable under transient perturbations (Turvey, 1990). Some years later, a broader definition of synergy that was proposed. Synergy was

explicitly defined as: “a neural organization of a multi-element system that (1) organizes sharing of a task among a set of elemental variables; and (2) ensures co-variation among elemental variables with the purpose to stabilize performance variables” (Latash et al., 2007). This definition regards synergy as a functional rather than an anatomic concept and not restricted to the muscular system. In fact, these structural units can be defined for subsystems within the organism, organism, or groups of organisms.

The notion of task-specific stability

Stability of a variable can be defined as the ability to return to the initial state when the variable is pushed away from its steady state, or the capacity to resist internal and external perturbations (Latash et al., 2007; Scholz & Schoner, 1999; Schoner, 1995). If the perturbation is phasic, all of the internal mechanical DOFs, not only the perturbed ones – readjust immediately in such way that the task performance is preserved. This is equivalent to the notion of attractor in dynamical systems, a preferred state or sequence of states that the system gravitates to when starting from arbitrary starting conditions and following arbitrary perturbations (Turvey, 1990). There are several sources of internal and external perturbation when a movement is performed; internal perturbations can be mechanical (e.g. joint interaction torques) or nervous (coupling among effector or sensory system).

The notion of task-specific stability comes from observations of invariances of trajectories in a particular reference frame (Atkeson & Hollerbach, 1985; Schoner, 1995). These invariances are indicative of the task performance of control, but the task performance is by no means fixed. For example, if invariances are observed at the level of the end-effector, they can be interpreted as evidence for end-effector control.

Similarly, regularities at the level of joint configurations are suggestive of joint-level control (Schoner, 1995). In this context, the concept of control variable is different than the one of “controller” used in the implementation of the internal model theory (Kawato, 1999; Kawato & Wolpert, 1998).

The Uncontrolled Manifold Hypothesis

The notion of synergies stabilizing salient performance variables is a central aspect of understanding how the CNS makes use of the motor abundance. The UCM approach developed by Schoner (1995) proposes that the task-specific stability of a particular variable can be quantified by comparing whether most of the inter-trials variability in the space of elemental variables lead to the preservation (lower variability) of the task performance (Scholz & Schoner, 1999).

The implementation of the UCM framework was necessary to overcome to the problem of incommensurability between elemental variables within the system and task variables. For example, the variability of joint rotations are measured in radians squared and the variability of the hand position measured in meters squared (Latash et al., 2010), and the direct comparison of the variability of these two different units has not meaning. Then, a formal mathematical model (Jacobian matrix in a linear approximation) is used to relate the changes in task space to changes in elemental variables (Latash et al., 2010; Scholz & Schoner, 1999). The UCM is approximated by the null space of the Jacobian matrix. In this method, the variability of elements is analyzed across trials and projected along (V_{UCM}) and orthogonal (V_{ORT}) to the UCM. Consider a simple example of a producing 10 N of accurate force with two fingers several times. Any combination of the finger force leading to preservation of the 10 N of total force lie along the UCM, while the combinations of finger force that lead to

values different than 10 N deviate from the UCM and represent task errors (Latash, Scholz, & Schoner, 2002). When this task is repeated, there will be a negative correlation between the finger forces mostly due to differences in the initial forces shared between fingers. Then, most of the across-trials variability in the finger force space will lead to accurate total force production ($V_{UCM} \gg V_{ORT}$), which is interpreted as evidence of force-stabilizing synergy.

A most recent formulation of the UCM hypothesis states that: “a neural controller acts in the space of the elemental variables and selects in that space a subspace (the UCM) corresponding to a desired value of a performance variable” (Alessandro, Carbajal, & d'Avella, 2013). The UCM control theory hypothesizes that combinations of elements within this solution set are less stabilized and relatively free to vary, while combinations that would change the goal outcome are resisted (Latash et al., 2007; Scholz & Schoner, 1999).

The equilibrium-point hypothesis

The concept of synergy and task-specific stability is an attractive approach to the redundancy problem. However, explicit links to neurophysiology remain to be discussed. An influential theory that provides a neurophysiological basis for movement control and coordination is the Equilibrium-Point (EP) hypothesis developed by Feldman (1966, 1986).

One of the precursors of the EP-hypothesis explored the characteristics of the *tonic stretch reflex* muscles in decerebrated cats (Matthews, 1959). The tonic stretch reflex is the force-length relation during slow muscle stretch at a constant rate (Feldman & Orlovsky, 1972). The experiments in humans started with measures of the torque-angle characteristic given by different amounts of forearm unloading starting

from the same arm posture and torque (Feldman, 2009). When the load was removed the subjects were instructed to “do not interfere” in an attempt to keep the descending command unchanged. Feldman found that the *torque-angle* characteristics for the elbow joint were compatible with the *force-length* characteristics found in Matthew’s experiments. In addition, when the initial joint angle was intentionally changed, a shift in the *torque-angle* characteristic along the angle axis was observed. This result led to the suggestion that some physiological variable was responsible for the shift in the characteristic during the voluntary change in the arm posture. A subsequent study performed in decerebrated cats showed that a fixed stimulation of several descending pathways led to an invariant relationship between muscle force and length (Feldman & Orlovsky, 1972). Moreover, an increase in the stimulation of the descending pathways led to preservation of the shape of the *force-length* curve, but the whole curve shifted along the length axis (Feldman & Orlovsky, 1972).

The similarities between the *torque-angle* and the *force-length* curves (called the invariant characteristic, IC) and the shifts in the curve along the x-axis with the changes in the initial angle of the elbow joint representing changes in the descending commands, led to the hypothesis that the CNS set values for the length, at which muscles will start to be recruited during the *tonic stretch reflex*. The threshold value is known as λ , corresponding to the threshold length, at which all muscles are in equilibrium (produce zero level of activity) (Latash, 2008). Another parameter estimated from the IC curve is the apparent stiffness represented by the IC slope. One consequence of the EP-hypothesis is that muscle force and joint torques are not pre-computed, but a consequence of specification of a value of the tonic stretch reflex threshold and external conditions (reflexes, muscle properties, external load).

The *tonic stretch reflex* is also a case of synergy that can be described considering a simple case of one muscle. If one motor unit stops firing, the force will decrease, and the muscle fibers will stretch, activating the muscle spindles that will increase the excitatory input to the alpha-motoneurons. Then, either the frequency of recruitment of motor units or the number of motor units recruited will increase in such a way that the balance of forces will be maintained. This mechanism will partly compensate for the initial force decrease (Latash, 2012b).

The EP-hypothesis states that the neural control specifies length threshold for muscle activation. This hypothesis was recently reformulated in terms of referent configuration (Latash, 2010a). In multi-DOF systems, the neural controller sets a time-varying referent configuration describing an equilibrium trajectory for a salient variable, at which muscles are at their threshold of activity (via the tonic stretch reflex). Then, the actual trajectory is attracted towards the referent one until the difference between them decreases and the muscle activity become minimal. This is in accordance with the principle of minimal final action that reflects the tendency to move to a state with minimal potential energy. Usually the referent values cannot be reached because of anatomical and environmental constraints, then muscles reach an equilibrium with non-zero levels of activity. The mapping of equilibrium trajectories onto muscle activations is still not well developed (Feldman & Levin, 1995). However, it is suggested that there is a hierarchical structure with control variables at each level representing subthreshold depolarization of neuronal pools that ultimately result in signals to alpha-motoneurons and lead to displacement of the salient variable (Latash, 2010a).

1.1.3 The UCM framework at different spaces

The UCM framework allows addressing whether hypothetical variables related to the task-performance are stabilized by the elements of the synergy in several natural tasks. Some of the behaviors tested include reaching (Yang, Scholz, & Latash, 2007), bilateral movement (Tseng & Scholz, 2005b; Tseng, Scholz, & Valere, 2006), pointing (Tseng, Scholz, & Schoner, 2002), sit-to-stand (Reisman, Scholz, & Schoner, 2002a; Scholz & Schoner, 1999), posture (Hsu & Scholz, 2012; Hsu, Scholz, Schoner, Jeka, & Kiemel, 2007), adaptation (Yang et al., 2007), learning (Yang & Scholz, 2005), finger pressing tasks (Latash, Scholz, Danion, & Schoner, 2001, 2002) and prehension (Gorniak, Zatsiorsky, & Latash, 2009).

The understanding of purposeful task coordination can be explored at different levels of description. In the UCM framework, elemental variables are defined as the DOFs that can be changed by the CNS independently of each other, at least theoretically. The elemental variables are defined differently depending on the level of analysis. At the joint level, it is assumed that joint rotations are individually manipulated. However, in studies of finger synergies and muscle synergies, modes play the role of the elemental variables. The notion of modes was introduced to isolate co-variations among elemental variables that are not task-specific (Latash et al., 2007). Studies of multi-DOF synergies at the joint, muscles, and fingers levels are reviewed.

1.1.3.1 Multi-Joint Synergies

The UCM approach has been useful to distinguish stabilization of different performance variables. Several potential performance variables have been investigated when individuals perform reaching movements including the arm's center of mass (CM) trajectory, hand path's orientation and position. The hand position can be further

decomposed into the vector pointing from the starting point to the center of the target (hand path extent), and the orthogonal vector (hand path direction) (Reisman & Scholz, 2003). The indices of stabilization of each of these performances may change as the reach progresses, due to, for example, influence of the velocity/acceleration on the joint mechanics, and more strict constraints of the task close to movement termination.

One of the first experiments that used the UCM framework investigated the multi-joint coordination during shooting with a laser pistol at a target (Scholz, Schoner, & Latash, 2000). To perform this task successfully, the gun barrel had to be aligned with the direction from the gun back-sight to the target. Several hypotheses were tested in this experiment related to the stabilization of different task-variables throughout the reach: the direction of the gun barrel to the target, the gun's position in space, as well as the arm's center of mass trajectory. There was a strong multi-joint synergy with respect to the stabilization of the gun's orientation from the movement onset and from different starting locations, while the alignment of the gun's barrel was crucial only at the time of pressing the trigger. An additional manipulation performed in the experiment, was using an elastic band crossing the elbow joint. Interestingly, when the joint was blocked the joint variance decreased, but this decrease was mostly due to lower V_{UCM} , reflecting less motor equivalent joint solutions for the task, as opposed to changes in the joint angles that led to errors in the task. Similar analysis showed that stabilization of the gun's spatial position, and center of mass position was only seen early in the movement and not at the time of shooting. This finding was related to the movement dynamics (such as arm's inertia) that could play a larger role at the movement onset. Overall, the results of this experiment suggested that different

task-related performance variables could be stabilized at different phases during the movement.

A subsequent experiment investigated the stabilization of several performance variables during a pointing task (Tseng et al. 2003) including movement extent, movement direction, and CM's path. As a general finding, most of the variability in the joint configuration led to stable performance variables in the different phases of reach. However, the control of the CM's path and movement extent were compromised near the peak velocity. At these timings, the joint interaction torques were probably higher and the control of these performance variables might be more difficult or not as critical. During the trajectory, the hand's path direction was less affected by the changes in the arm velocity than the hand's path extent (Tseng, Scholz, Schoner, & Hotchkiss, 2003), which led the authors to suggest that timing errors might compromise the control of hand's path extent (Tseng & Scholz, 2005b).

The UCM framework also allows investigating the benefits of the redundancy when simultaneous tasks are performed. Gera et al. (2010) investigated the stabilization of the hand's position and orientation simultaneously when subjects inserted objects into targets with matched shapes. The shapes tested (ball, trapezoid and five-point star) required different levels of orientation control of the hand at the time of insertion. For example, the ball shape had weak orientation constraint, while the trapezoid and five-point star shapes required control of orientation about all axes. An additional condition consisted of dropping a ball into a can, at conditions at which orientation was not constrained in any direction. This study showed that 3D hand orientation was weakly stabilized at the late phase of the object transport, and more strongly stabilized at the adjustment phase, when the shape of the target explicitly

constrained the hand orientation. The stabilization of the 3D hand position was observed during all phases of the movement, and was not affected by the orientation constraints. The principle of superposition was suggested to account for the ability to explore the motor abundance and preserve tasks simultaneously without interference. Hsu and Scholz (2012) also investigated the role of redundancy in the stabilization of multiple tasks. In this experiment, upper limb tracking movements with different degrees of difficulty were performed while standing. Good performance in this type of task involves both tracking accuracy and balance. Increasing indices of difficulty in upper limb target movements did not compromise the stability of the COM position. Moreover, there was a larger V_{UCM} component when the task difficulty increased, without a corresponding increase in the V_{ORT} component. These results suggested that multiple tasks could be successfully performed by exploring the available DOFs (Hsu & Scholz, 2012).

Tseng et al. (2002) investigated the role of arm dominance and vision on the use of redundancy. The effect of vision on the UCM-based variance analysis with respect to the pointer's tip path was mild and quantitative differences were apparent only closer to movement termination. At this particular phase, there was an increase in both the V_{UCM} and V_{ORT} components when individuals reached with their non-dominant arm, but such effect was not present during reaches with the dominant arm (Tseng et al., 2002). A different experiment investigated the bilateral coordination during a fast circle drawing task (Tseng et al., 2006). In this study, the V_{ORT} component increased during fast circle drawing with respect to the non-dominant hand and to the relative position and orientation between hands, while no major differences

between limbs were observed in the V_{UCM} component (Tseng & Scholz, 2005b). It was suggested that joint interaction torques might have an effect on interlimb stability.

The UCM approach was also applied to answer interesting questions related to bilateral arm movements: whether they are formed by preferential stabilization of each arm or a coupling among them. This question was investigated experimentally during pointing movement (Domkin, Laczko, Jaric, Johansson, & Latash, 2002) and also in tasks involving symmetric and asymmetric circular drawing (Tseng & Scholz, 2005b). In both studies there was a strong synergy of joints stabilizing the 2D hand path, regardless whether the UCM analysis was performed individually for each arm or for the bilateral arm movement with respect to the vectorial distance between hands. However, the bilateral motion did lead to changes in results of the UCM analysis. The index of synergy (V_{UCM}/V_{ORT}) was larger when the analysis was computed for the bilateral than the unilateral motion Domkin et al. (2002). In addition, Tseng and Scholz (2005b) found no differences between symmetric and asymmetric conditions in UCM analysis with respect to individual hand position. For the bilateral drawing there was larger V_{UCM} and V_{ORT} ; in addition, the V_{ORT} values for the asymmetric bilateral drawing were larger than for the symmetric movements. This study suggested separate control of bilateral hand's motion by intra-limb synergies, with additional superimposed synergies during the bilateral drawing.

The joint kinematics was also explored in a series of studies of motor adaptation/learning. A typical paradigm to study motor learning involves reaching in unusual force fields (Shadmehr & Moussavi, 2000; Shadmehr & Mussa-Ivaldi, 1994). Reaching from one target to another one usually leads to a straight path (Morasso, 1981). The individuals are typically requested to reach repeatedly under a force field

proportional to the movement velocity and perpendicular to the hand's path. The studies showed that the initial attempts of reaching under the force field led to a curved hand path. With practice, the quasi-static straight path was recovered. When the force field was turned off, the hand path becomes curved in the opposite direction of the applied force field. According to the authors, the evidence of motor adaptation to the force field suggests that an internal model that counterbalances the expected external force is created. Other types of internal models were suggested to account for different features of reaching (Franklin, Osu, Burdet, Kawato, & Milner, 2003; Osu, Burdet, Franklin, Milner, & Kawato, 2003). However, when the reaching in unusual force field paradigm was used to investigate the multi-joint coordination, the repeated reaches under a force field led to an increase in both V_{UCM} and V_{ORT} components computed with respect to hand's path. The adaptation effects showed a noticeable decrease in V_{ORT} at around time of peak velocity and at movement termination. The decrease in V_{UCM} was much smaller and was kept relatively high even at late practice (Yang et al., 2007). Yang and Scholz (2005) investigated the effect of practice of throwing a Frisbee. The amount of self-motion (a component of the joint velocity vector that does not affect the velocity of the hand) increased significantly after practice, possibly reflecting better compensation for perturbations due to the limb's dynamics (Yang & Scholz, 2005). Interestingly, the analysis with respect to hand orientation and movement direction showed improvement with practice (decrease in both components of joint variance, especially for V_{ORT}), while corresponding analyses with respect to movement extent and hand velocity revealed a decrease in V_{UCM} but didn't show a consistent decrease in V_{ORT} with practice.

1.1.3.2 Multi-Muscle Synergies

“The central nervous system knows nothing of muscles, it only knows movements”. This saying by the neurologist Hughlings Jackson (1889) suggests that the CNS sends a signal to groups of muscles as opposed to each muscle individually during the tasks. There are some examples in the literature of complex muscle organization that resemble those seen in motor behavior elicited both at the spinal cord (Fukson, Berkinblit, & Feldman, 1980; Lemay & Grill, 2004; Prochazka, Clarac, Loeb, Rothwell, & Wolpaw, 2000; Saltiel, Wyler-Duda, D'Avella, Tresch, & Bizzi, 2001) and in the brain (Graziano, Taylor, & Moore, 2002; Holdefer & Miller, 2002). Saltiel et al. (2001) found that the stimulation of interneuronal regions of the frog's spinal cord led to an organized motor output. Twelve muscles were grouped into seven factors using PCA analysis, and they could be combined to form natural behaviors such as jumping and swimming. The PC vectors were similar among frogs. In the brain, long-pulse stimulations directed to both the motor cortex and primary motor cortex evoked complex postures that resembled for example, defensive and hand-to-mouth movements (Graziano, Taylor, & Moore, 2002). Also, microstimulation of the motor cortex triggered combinations of synergies similar to those observed during natural grasping in rhesus macaques (Overduin, d'Avella, Carmena, & Bizzi, 2012).

Muscle synergies are typically described in the literature as patterns of muscle coactivation as a means of reducing the redundancy in the multi-muscle system (d'Avella, Fernandez, Portone, & Lacquaniti, 2008; d'Avella & Lacquaniti, 2013; d'Avella et al., 2006). As previously mentioned (at the “*the concept of synergy*” subsection), this notion does not incorporate the feature of the flexibility/error compensation. Therefore, other authors (Klous, Mikulic, & Latash, 2011; Krishnamoorthy, Scholz, & Latash, 2007; Robert & Latash, 2008) use the term

muscles modes (M-modes) in reference to proportional changes in muscle activation. M-modes are defined using matrix factorization methods such as PCA or non-negative matrix factorization (Tresch, Cheung, & d'Avella, 2006). The different methods of matrix factorization led to qualitatively similar M-modes (Tresch et al., 2006).

Previous studies explored whether different patterns of muscle activation during reaching could be reconstructed by a few M-modes. A large repertoire of movements involving pointing in different directions, external loads, forearm postures, speeds could be described by scaling M-modes in amplitude and shifting them in time (d'Avella et al., 2008; d'Avella et al., 2006). While the M-modes provide support for the hypothesis that the CNS sends signal to a set of muscles related to the reaching instead of sending signals to individual muscles, the matrix factorization analysis does not give information about the coordination among motor elements during reaching with respect to a particular task performance. The analysis of flexibility/error compensation of multi-muscle synergies can be run using the UCM framework. The use of the UCM analysis to multi-muscle synergies assumes a two-level hierarchical control. At the lower level, the muscles show patterns of parallel activation (M-modes) and at the upper level, the M-modes serve as the elemental variables, and their gains are flexibly combined to stabilize important performance variable.

The UCM approach to muscle synergies involves several computational steps (Krishnamoorthy, Latash, Scholz, & Zatsiorsky, 2003). First, groups of muscles (M-modes) are defined using PCA analysis with rotation and factor extraction. The M-modes are an estimative of the variables activated independently by the CNS. Then, the temporal profile of the modes is obtained by multiplying the PCs by the recorded muscle activation indices. The next step involves the computation of the Jacobian

matrix that defines the relationship between small changes in the M-modes and changes in a task-related performance variable, which is usually estimated by multiple linear regressions. Finally, the inter-trial variability in the M-modes lying along and orthogonal to the UCM (null space of the Jacobian matrix) is computed, defining the V_{ucm} and V_{ort} components.

The UCM analysis at the muscle-level has been more extensively applied for tasks involving postural control (Danna-Dos-Santos, Degani, & Latash, 2008; Danna-Dos-Santos, Shapkova, Shapkova, Degani, & Latash, 2009; Danna-Dos-Santos, Slomka, Zatsiorsky, & Latash, 2007; Krishnamoorthy, Goodman, Zatsiorsky, & Latash, 2003; Krishnamoorthy, Latash, et al., 2003; Krishnamoorthy, Latash, Scholz, & Zatsiorsky, 2004) such as preparation to self-initiated postural perturbation (Krishnamoorthy, Latash, et al., 2003), preparation to making a step (Wang, Zatsiorsky, & Latash, 2005, 2006), and voluntary sway of the COP (Danna-Dos-Santos et al., 2007). At the lower level of the hierarchical organization, the M-modes were reported to be similar in composition and number in tasks that did not challenge the postural stability. For example, when individuals performed a whole-body sway frequencies ranging from 0.125 Hz to 1.00 Hz (Danna-Dos-Santos et al., 2007), three M-modes were extracted accounting for at least 65% of the variance during body sway. The M-modes were similar across the wide range of frequencies and across subjects, but the third M-mode was more variable. M-modes were found to be similar even when the experiment involved more drastic modifications in the task, such as requiring changes in the COP in different directions (forward and backward), magnitude of perturbation (light and heavy), and tasks that involved explicit (voluntary sway) and implicit shifts in the COP associated with anticipatory postural

adjustments. However, the number and composition of M-modes increased from three to four/five when the level of difficulty became higher (Danna-Dos-Santos et al., 2008). Some of the tested manipulations that defied posture were: standing in a narrow base of support and applying high-frequency lower-amplitude muscle vibration to the Achilles tendons while standing on one foot. In these studies, the composition of the M-modes was classified into two classes related to the effect of the changes in muscle activity in a group: reciprocal (e.g. “*push back*” and “*push forward*”, when the significant loading coefficients are composed by dorsal and ventral muscles, respectively) and co-contraction modes, when muscles with opposing functions are significantly loaded in the same PC (Danna-Dos-Santos et al., 2007; Krishnamoorthy, Goodman, et al., 2003; Krishnamoorthy, Latash, et al., 2003). Interestingly, the number of co-contraction (joint-specific) M-modes increased in the most challenging conditions, which was related to an increase in the joint stiffness to preserve the task stability under perturbations (Krishnamoorthy et al., 2004).

A strong index of synergy, i.e. $V_{UCM} > V_{ORT}$, has been reported at steady state phases (Wang, Zatsiorsky, et al., 2006) or when individuals perform a voluntary body sway (Danna-Dos-Santos et al., 2007). This indicates that flexible combinations of M-modes preserved the center of mass COP trajectory (Danna-Dos-Santos et al., 2008; Danna-Dos-Santos et al., 2007; Krishnamoorthy, Goodman, et al., 2003). The task-specific stability feature can be expected to be present even when, at the lower level of the hierarchy, M-modes are inconsistent across tasks and subjects (Danna-Dos-Santos et al., 2009) or no muscle groupings are identified (Valero-Cuevas, Venkadesan, & Todorov, 2009), supporting the principle of motor abundance. There were also cases at which synergies decreased in preparation to a quick action, such in the leg that makes

a step (Wang et al., 2005). This task is discrete in its nature, and a decrease in the synergy index is proposed to facilitate a change in the corresponding performance variable.

1.1.3.3 Multi-Finger Synergies

The control of grasping is often described at two levels of hierarchy. At the higher level, the task is shared between the thumb and the virtual finger (represented by all fingers opposing the thumb (represented by all fingers opposing the thumb, Arbib, Iberall, & Lyons, 1985). At the lower level, the task is shared among the actual fingers. The finger interactions at the lower level have been investigated during multi-finger pressing tasks of accurate force or moment production using the UCM framework (Latash, 2012b). Mechanical and neural factors contribute to the covariation of finger forces during pressing tasks. Mechanical factors involve the anatomical connections among fingers such as shared muscle compartments and inter-digit tendinous connections (Kilbreath & Gandevia, 1994; Leijnse et al., 1993), and the action of inertial forces related to the movement. Neural factors involve overlap of the cortical representation of fingers and synergies (Rouiller, Moret, Tanne, & Boussaoud, 1996; Schieber, 1991). During force production tasks, fingers show patterns of coordination such as force deficit, enslaving, sharing and error compensation, described below:

Force Deficit: lower peak finger forces in multi-finger tasks as compared to single-finger tasks (Kinoshita, Kawai, & Ikuta, 1995; Li, Latash, Newell, & Zatsiorsky, 1998; Ohtsuki, 1981).

Enslaving: In a multi-finger force production task, if someone tries to produce force with one finger, other fingers will also apply some force unintentionally. The unintentional force production by non-instructed fingers is called “enslaving” (Danion et al., 2003). Because the UCM analysis assumes that elements can be changed by the CNS one at a time, the hypothetical modes (assumed to be independent of each other) are used as the elemental variables during finger-force production analysis (Latash et al., 2001; Scholz, Danion, Latash, & Schoner, 2002). Operationally, the modes have been defined by a linear transformation of force vectors into mode vectors. The transformation matrix is defined using data from a ramp force production task. In this task, individuals are required to produce force with individual fingers to measure the amount of force produced simultaneously by the other fingers. The coefficients of linear regression of individual finger forces when subjects attempt to press with one finger at a time form the enslaving matrix.

Sharing and the principle of minimization of secondary moments: The principle of minimization of secondary moments was introduced (Zatsiorsky et al. 1998) based on an observation of nearly invariant sharing pattern over a ramp force production (Li, 1998). According to this principle, the total force is shared among the finger such that the total moment with respect to the longitudinal axis of the forearm is minimal. Several studies supported this principle (Li et al. 1998; Zatsiorsky et al. 1998, 2000; Li et al. 2000), but violations were also found (Latash et al. 1998; Danion et al., 2001).

Error compensation: The phenomenon of error compensation has been described by several authors (Latash, Li, & Zatsiorsky, 1998; Li, Latash, & Zatsiorsky, 1998; Santello & Soechting, 2000). If the fingers do not act

synergistically, the sum of the variance of individual finger forces should be equal to the sum of total forces (Bienaimé Equality Principle). However, it was demonstrated that the sum of the variance of finger forces exceeds the sum of total force variance during a force ramp task, which suggests a negative co-variation among fingers, and supports the error compensation principle (Li, Latash, & Zatsiorsky, 1998). Further investigations found that total force is relatively preserved during tapping by individual fingers (Latash et al., 1998). There was an online compensation for expected changes in total force due to change in the force contribution of the tapping finger, and a feed-forward mechanism was suggested to account for this phenomenon (Latash et al., 1998). In this case, the negative co-variation reflects more the abundance (flexibility) of the system than the error compensation, due to feedback loops. The UCM framework is suitable to test whether the task variable is stabilized across trials, which also implies that there is a co-variation among finger forces to stabilize the task variable. One of the biggest advantages of the error compensation/flexibility feature of synergies is that the excess of DOFs is more of an advantage than a computational burden. Therefore, additional DOFs do not imply increased complexity in the task performance (Latash et al., 2001).

Force-moment multi-finger stabilization & Principle of superposition

One unexpected finding in oscillatory finger-pressing tasks requiring accurate force control was the implicit (non-instructed) multi-finger total moment stabilization. The across-trials analysis of force variance showed force-destabilizing covariation close to the force peak. Despite not explicitly instructed, the moment was stabilized during most of the cycle. The authors suggested that multifinger synergies are biased towards moment stabilization due to the need of precise moment control during

everyday tasks (Latash et al., 2001; Scholz et al., 2002). In Zhang, Zatsiorsky, and Latash (2007), individuals were explicitly instructed to produce cyclic pronation-supination moment of forces with respect to the midpoint between the middle and ring fingers. In this case, the fingers stabilized the moment but not the total force. The authors suggested that in pressing tasks, there are no force-stabilizing synergies unless such control is explicitly instructed. On the other hand, moment-stabilizing synergies are present when the control of the performance variable is and is not instructed (Zhang et al., 2007). The simultaneous stabilization of force and moment during accurate total force production supports the principle of superposition introduced in robotics. The principle of superposition states that actions can be divided into subtasks that are controlled individually without interference (Arimoto, Nguyen, Han, & Doulgeri, 2000; Arimoto, Tahara, Yamaguchi, Nguyen, & Han, 2001).

Discrete versus oscillatory force production, rate of force and timing variability

There are contradictory perspectives in the field about the control of discrete and oscillatory movement production. According to Schoner (1990), both tasks can be viewed as limit cyclic oscillators, with differences in their timing of initiation and termination. The other view suggests that discrete and oscillatory tasks involve different control mechanisms. In this view, oscillatory tasks require minimal correction and attention relying more on the feed-forward mechanisms and central pattern generators, while discrete tasks requires online monitoring and correction (de Rugy & Sternad, 2003; Sternad, de Rugy, Pataky, & Dean, 2002). During a pressing task study comparing both task conditions (discrete and cyclic), differences among discrete and cyclic finger force production were observed at slow force production, but not at fast speed (Latash, Scholz, Danion, et al., 2002). However, the rate of force

production affected the distribution of V_{UCM} and V_{ORT} . V_{ORT} was strongly influenced by the rate of force and the V_{UCM} by the force magnitude. The model of variability proposed by Simon Gutman/Goodman and his colleagues (Gutman & Gottlieb, 1992; Gutman, Latash, Almeida, & Gottlieb, 1993) led to the suggestion that most of amplitude related variance gets into V_{UCM} , while the time-related variance gets into V_{ORT} (Latash, Danion, Scholz, Zatsiorsky, & Schoner, 2003). A subsequent experiment investigated cyclic tasks at different frequencies. The increase in frequency led to a higher rate of force change, however it did not lead to an increase in V_{ORT} . These results suggested that timing variability decreases with the increase in frequency (Friedman, Skm, Zatsiorsky, & Latash, 2009). However, in a different study, subjects performed a discrete task (ramp production) and V_{ORT} increased with the force rate (Varadhan, Zatsiorsky, & Latash, 2010). The differences/similarities in the control mechanism of discrete and oscillatory tasks remains an area requiring further exploration.

Unintentional responses to external perturbation and control with referent configurations

Recent studies investigated the effect of a transient perturbation with implications for synergic control and the equilibrium-point hypothesis. Mechanical perturbations were directed to one of the fingers producing accurate force and imposed a controlled displacement. Lifting one finger leads to redistribution of the force shared among fingers. The force of the perturbed finger increases while there is a drop in forces of the other fingers, with a larger drop in the neighboring fingers (proximity effect). However, the compensation is not complete and leads to a net overall increase in the total force. The force-stabilizing synergies remained strong despite individuals

were instructed to not interfere with the external perturbation (Martin, Budgeon, Zatsiorsky, & Latash, 2011; Wilhelm, Zatsiorsky, & Latash, 2013). The results suggested equifinality at the task-performance variable, but not in the space of the elemental variables (finger forces and finger modes), supporting the idea of control with referent configuration (Wilhelm et al., 2013).

1.1.4 Motor Equivalence

In this dissertation we explored the phenomenon of motor equivalence. Here, motor equivalence reflects a change in the configuration of motor elements (i.e. changes in the sharing among elements) after a perturbation that leads to the preservation of the task-specific performance variable (Scholz & Schoner, 2014). Note that this phenomenon is only possible when the system exhibits sufficient motor redundancy. In the literature, the term “motor equivalence” has also been used to describe the ability to produce the same outcome using different end-effectors (Wing, 2000). A typical example is the ability to write with several parts of the body beyond the hand, such as toes or mouth (Bernstein 1967).

The definition of motor equivalence in the context of task-specific stability was demonstrated in a speech experiment. The lower lip was (unexpectedly) prevented from moving downward when subjects pronounced two types of sounds: /baeb/ and /baez/. A compensatory reaction in the upper lip was observed when the movement involved bilabial closure in /aba/, but not when the motion did not, /aka/ (Kelso, Tuller, Vatikiotis-Bateson, & Fowler, 1984). One of the difficulties in studying the motor equivalence phenomenon is to determine the extent to which motor equivalence reflects changes in motor elements that are associated with the task performance and those that are not.

One variant of the UCM analysis (Scholz et al., 2007; Schoner et al., 2008) allows measuring quantitatively the motor equivalence. In this case, one would use a set of unperturbed trials, and compute the null space of the Jacobian (\mathbf{J}) matrix relating small changes in the motor elements to changes in the tested performance variables. Similar to the UCM-based variance analysis, this null space reflects all possible combinations of motor elements that lead to the same value of the performance variable. Then, the deviation of elements during the perturbation is computed by subtracting it from the mean of the unperturbed trials. This deviation is projected into the null space (UCM) and orthogonal (ORT) spaces of \mathbf{J} , and the respective lengths of projection are computed. The deviations lying along the UCM reflects the motor equivalent adjustments (ME component) in the space of elemental variables that tend to preserve the value of performance variable. The ORT component represents the non-motor equivalent component (nME), i.e. the changes in the motor elements during the perturbation leading to different performance during the perturbation.

The motor equivalence approach was applied to a postural task (Scholz et al., 2007), testing whether the joint configuration would reorganize to keep the body COM steady after translations of a force plate at different amplitudes. The results showed that immediately after the transient perturbation, the ME increased significantly more than the nME component. The difference between components remained high at late phases after the perturbation and increased with larger amplitudes of perturbation. Thus, suggesting that the reorganization of the joints after the perturbation tend to preserve the pre-perturbed values of the center of mass (COM_{AP}). A second study measured motor equivalence relative to the hand position while subjects reached at different speeds (Scholz et al., 2011). The motion dependent joint interaction torques

increase at higher movement speeds, producing internal perturbations. The motor equivalence was computed between pairs of reaches at slow, moderate, and fast speeds. It was observed that most of the changes in the joint configuration due to the differences in the speed of reaching happened to preserve the end-point coordinate at the movement termination. If a specific sharing among motor elements were prescribed in detail at a higher level of control, one would expect the sharing patterns to be recovered in the experiments described. Therefore, these findings using the motor equivalent method draw into question strategies of movement control typically described in terms of configuration of motor elements. They are more compatible with the principle of abundance where all DOFs are used to stabilize important variables.

The motor equivalence analysis is a signature of the redundancy in motor system and a more direct method to test the task-specific stability as compared to the UCM-based variance analysis. In the former the motor elements of the system are purposefully perturbed, while in the UCM-based variance approach the changes in the motor element arise despite the attempt to perform exactly the same action across trials.

1.1.5 Models supporting the UCM hypothesis

Goodman and Latash (2006) developed a feed-forward model with two commands at the higher level of the hierarchy, related and unrelated to the task variable; the elemental variables are generated based on the knowledge of the decoupling among the subspaces forming the Jacobian. The function of the feedback is to update the mapping between changes in elemental variables and changes in task variables (the Jacobian), not for any explicit feedback corrections. This updating

process can be done through physiological feedback loops such as the central back-coupling mechanism (Latash, Shim, Smilga, & Zatsiorsky, 2005). Central back-coupling loops use self- and lateral inhibition among the elements that is suggested to stabilize a particular output at shorter delays when compared to proprioceptive feedback. These loops have been described for the Renshaw cell system (Rothwell, 1994).

Martin, Scholz, and Schoner (2009) developed a scheme of movement coordination based on neuronal dynamics that explains the motor equivalence observed after a movement is perturbed. There are two key concepts in the formulation of the model. The first one is a neuronal dynamics that generates time courses of equilibrium joint angles and velocities. The neuronal dynamics transforms the task space into effector space. It does so by decoupling the deviations in the joint velocities leading to changes in the task-performance from the ones that leave the task-performance unchanged. The neuronal dynamics possibly sets the threshold position for recruitment of motoneurons (Raptis, Burtet, Forget, & Feldman, 2010). The second key component is the back-coupling. This is a feedback mechanism that adjusts the equilibrium trajectory of the salient variable in the face of perturbations and acts primarily in the subspace within the UCM to produce motor-equivalent solutions with respect to the task-performance.

Martin's model uses an augmented Jacobian matrix (Jacobian augmentation technique: JAT model). The JAT introduces additional constraints to make the matrix invertible. Martin used a special matrix combined from vectors spanning the null-space of the Jacobian. Therefore, there is one solution to the problem (resolving the redundancy) and equations of motion can be implemented (Goodman & Latash, 2006).

The asymmetric distribution of the across-trials variance in the motor elements would be predicted by the “minimum intervention principle” used in the optimal feedback control. Such principle states that deviations from the average behavior are only corrected when they interfere with the task goals (Liu and Todorov 2007; Todorov 2004; Todorov and Jordan 2002). However, as previously mentioned, the OFC assumes task constraints based on optimization criteria solved moment by moment, the choice of the cost function is arbitrarily, and it is not clear whether the structure of variance should be dependent on feedback control (Goodman & Latash, 2006).

1.2 Significance and Innovation

The UCM-based method allows to test whether a hypothetical task-related performance variable is stabilized by a set of motor elements, whether several performance variables can be simultaneously stabilized, and to quantify the use of motor redundancy during motor learning and in cases of motor pathologies. These measures of coordination among elemental variables can be done during the course of movement. The findings suggest that variability does not necessarily reflect deviations from optimality or “incoordination”. In the clinical practice, when variability is viewed as “error”, therapists will guide movements toward more optimal patterns. However, when variability is understood as critical to natural movement production, one should consider the use of variability as part of the treatment as opposed to reinforcing stereotypical behaviors.

This study is innovative in terms of the method used that directly quantifies the changes in the motor elements leading to motor equivalence with respect to a performance variable and allows introducing a measure of within-a-trial synergy. This

is important because, by definition, the synergy is a neural organization that combines motor elements to preserve values of task-related performance variables. These neural structures arise due to the natural variability in redundant systems, but are also formed online during the course of the movement and in response to perturbation. In addition, the motor equivalence analysis was applied at different levels of description, e.g. multi-joints, multi-muscles and multi-finger synergies. The phenomenon of motor equivalence is investigated after a perturbation is introduced to the system of motor elements. However, the perturbation itself has some effects on the profile of the task-performance. Each of these methods has different strengths in terms of the research design, which shed light on the contributions arising from either mechanics or neural sources of motor equivalence. Moreover, the analysis of different time epochs after the perturbation helps to determine the underlying neurophysiology contributing to the typical increase in the motor equivalent component including responses due to short-latency loops, pre-programmed reactions and voluntary control. We believe that these findings about the role of diverse feedback mechanisms are important additions to the overall set of studies that support the principle of motor abundance.

1.3 Aims and Hypothesis

Aim 1: To determine how perturbations applied to the elbow joint lead to the use of motor equivalent joint configurations when individuals reach to targets with different constraints.

***Hypothesis 1.1:** Motor equivalence effects ($ME > nME$) with respect to the pointer tip's position and the hand's orientation will be present early in the reach*

until movement termination. Such effects will increase after the perturbation onset, and a further increase is expected when the perturbation is stronger.

Hypothesis 1.2: When the pointer is inserted into the cylindrical target, the motor equivalence effects will be larger with respect to hand orientation than position. In contrast, larger motor equivalence effects with respect to hand position than orientation are expected when individuals touch with the pointer the spherical target.

Hypothesis 1.3: The inter-trial variance in the joint configuration space will be structured in a specific way such that most of joint-configuration variance will lead to stable pointer tip position and hand orientation ($V_{UCM} > V_{ORT}$).

Aim 2: To determine whether muscle modes (M-modes) can be reorganized in a task-specific way when the elbow joint is partially blocked (perturbed) during reaching to a cylindrical target.

Hypothesis 2.1: Motor equivalence effects ($ME > nME$) will be present in the M-mode space with respect to the pointer tip position and hand orientation. These effects will increase across successive time windows of 50 ms immediately after the perturbation onset corresponding to the action of local reflexes, pre-programmed reactions and voluntary responses. The motor equivalence effects will be stronger for hand orientation than pointer-tip position.

Hypothesis 2.2: The motor equivalence effects after the perturbation are not primarily due to an increase in the index of co-contraction between elbow flexors and extensors at the post-perturbation phases as compared to unperturbed reaches.

Aim 3: To determine whether a signature of motor equivalence ($ME > nME$) would be present after a transient positional perturbation applied to an element (the middle finger) during a multi-element task (accurate four-finger cyclic force production). The motor equivalence will be computed with respect to the total force (F_{TOT}) produced by the four fingers and moment of force (M_{TOT}) about the longitudinal axis of the forearm/hand.

***Hypothesis 3.1:** Motor equivalence effect ($ME > nME$) with respect to F_{TOT} and moment M_{TOT} values will be present in-between the lifting and lowering phases of the transient perturbation of the middle finger in the spaces of both finger forces and modes. The motor equivalence effect will persist after the transient perturbation is over.*

***Hypothesis 3.2:** Motor equivalence in F_{TOT} ($ME > nME$) will increase along time windows of 50-ms immediately after the perturbation onset in the spaces of finger forces and modes corresponding to local reflexes, pre-programmed reactions and voluntary responses.*

***Hypothesis 3.3:** Most of the inter-trial variance in the spaces of finger forces and modes will be compatible with stable values of F_{TOT} and M_{TOT} ($V_{UCM} > V_{ORT}$) at steady states pre-, during-, and after- the middle finger perturbation.*

Aim 4: To determine whether changes in the action performed by an abundant system will lead to a motor equivalence signature ($ME > nME$). A secondary goal was to investigate the effects of removal of visual feedback on the ME and nME components.

Hypothesis 4.1: *An action that a priori lies primarily within the nME space will induce a change in the ME component.*

Hypothesis 4.2: *When the target values of the performance variables are changed back to their original values, the nME components will return to the original values, while the ME components will not.*

Hypothesis 4.3: *The amount of ME change will be insensitive to presence of visual feedback, while nME change will increase without visual feedback.*

Hypothesis 4.4: *The synergic structure of variance ($V_{UCM} > V_{ORT}$) will be observed for the variable receiving visual feedback but not for the “frozen-feedback” variable.*

Chapter 2

UNPREDICTABLE ELBOW JOINT PERTURBATION DURING REACHING RESULTS IN MULTIJOINT MOTOR EQUIVALENCE

2.1 Abstract

Unpredictable elbow joint perturbation during reaching results in multijoint motor equivalence. Motor equivalence expresses the idea that movement components reorganize in the face of perturbations to preserve the value of important performance variables, such as the hand's position in reaching. A formal method is introduced to evaluate this concept quantitatively: changes in joint configuration due to unpredictable elbow perturbation lead to a smaller change in performance variables than expected given the magnitude of joint configuration change. This study investigated whether motor equivalence was present during the entire movement trajectory and how magnitude of motor equivalence was affected by constraints imposed by two different target types. Subjects pointed to spherical and cylindrical targets both with and without an elbow joint perturbation produced by a low- or high-stiffness elastic band. Subjects' view of their arm was blocked in the initial position, and the perturbation condition was randomized to avoid prediction of the perturbation or its magnitude. A modification of the uncontrolled manifold method variance analysis was used to investigate how changes in joint configuration on perturbed vs. nonperturbed trials (joint deviation vector) affected the hand's position or orientation. Evidence for motor equivalence induced by the perturbation was present from the

reach onset and increased with the strength of the perturbation after 40% of the reach, becoming more prominent as the reach progressed. Hand orientation was stabilized more strongly by motor equivalent changes in joint configuration than was three-dimensional position regardless of the target condition. Results are consistent with a recent model of neural control that allows for flexible patterns of joint coordination while resisting joint configuration deviations in directions that affect salient performance variables. The observations also fit a general scheme of synergic control with referent configurations defined across different levels of the motor hierarchy.

2.2 Introduction

It has been suggested that the central nervous system's (CNS) plan for targeted reaching involves specifying a terminal joint configuration (Desmurget, Grea, & Prablanc, 1998; Grea, Desmurget, & Prablanc, 2000; Tillery, Ebner, & Soechting, 1995). If this is true, relatively invariant terminal joint configurations could be expected if reaching is performed repetitively from a fixed initial hand location and arm configuration to a fixed target location. Pointing to a given target location from different starting positions (Soechting, Buneo, Herrmann, & Flanders, 1995) or when reaching around obstacles compared with straight reaches (Torres & Andersen, 2006a) leads, however, to different terminal configurations. In addition, results of studies of unperturbed reaching from a fixed initial position by Cruse, Bruwer, and Dean (1993) have provided equivocal evidence for planning in terms of terminal joint postures.

Evidence exists for the preservation of the spatial orientation of the plane of the arm (which has a complex relationship to joint angle changes) and the 3D curvature of the hand path when performing 3D reaches over a wide range of movement speeds (Nishikawa, Murray, & Flanders, 1999). Similarly, monkeys

learning an obstacle avoidance task were shown to keep the spatial trajectories of individual joints relatively constant despite variations of movement speed (Torres & Andersen, 2006b). These results suggest that the entire temporal sequence of joint configurations for a given hand trajectory may be planned by the CNS (Rosenbaum, Meulenbroek, Vaughan, & Jansen, 1999). Such a strategy could presumably simplify trajectory control because differences in movement velocity could be achieved by simply scaling the transition time between a planned sequence of joint postures without significantly affecting the postures themselves (Hollerbach & Flash, 1982; Rosenbaum et al., 1999; Torres & Zipser, 2002). In contrast, a study of targeted reaching at different speeds by Thomas, Corcos, and Hasan (2003) showed that reaching at different speeds did not lead to a simple scaling of segmental kinematics.

Evidence exists for the preservation of the spatial orientation of the plane of the arm (which has a complex relationship to joint angle changes) and the three-dimensional (3D) curvature of the hand path when performing 3D reaches over a wide range of movement speeds (Nishikawa et al., 1999). Similarly, monkeys learning an obstacle avoidance task were shown to keep the spatial trajectories of individual joints relatively constant despite variations of movement speed (Torres & Andersen, 2006a). These results suggest that the entire temporal sequence of joint configurations for a given hand trajectory may be planned by the CNS (Rosenbaum et al., 1999). Such a strategy could presumably simplify trajectory control because differences in movement velocity could be achieved by simply scaling the transition time between a planned sequence of joint postures without significantly affecting the postures themselves (Hollerbach & Flash, 1982; Rosenbaum et al., 1999; Torres & Zipser, 2002). In contrast, a study of targeted reaching at different speeds by Thomas et al.

(2003) showed that reaching at different speeds did not lead to a simple scaling of segmental kinematics.

The challenge of answering the question of whether a movement's terminal joint configuration is planned in advance is that the motor system is inherently noisy. Thus even reaching from a relatively fixed initial hand position and arm posture will result in some trial-to-trial variation in the hand's path and its terminal position, as well as in the joint configuration. A method is needed, then, to distinguish between differences in joint configurations due to noisy control versus different movement plans. The uncontrolled manifold (UCM) approach provides tools that allow such differences to be tested quantitatively by comparing task-relevant to task-irrelevant variance in the space of the motor elements (i.e., joints or muscles). For example, recent investigations of a variety of upper extremity tasks used such tools to map joint variance across repetitive reaches onto end-effector variance. The results of those studies suggested that the CNS uses a family of joint postures that are equivalent with respect to producing a consistent hand path when performance occurs under identical task conditions (Scholz et al., 2000; Tseng et al., 2002; Tseng & Scholz, 2005a; Tseng et al., 2003; Yang et al., 2007). Such results make it difficult to argue that the CNS typically plans for specific joint configurations or muscle activation patterns (see, e.g., Krishnamoorthy, Goodman, et al., 2003; Krishnamoorthy et al., 2004; Krishnamoorthy et al., 2007), although the CNS can certainly plan for such detail when the task requires it (e.g., artistic endeavors). Further evidence that planning likely involves the specification of relatively global, performance-related variables comes from studies of motor equivalence. Motor equivalence often is defined as the preservation of a parameter most related to task performance despite changes in the

values of the underlying motor elements. It has been investigated by measuring the ability of individuals to complete a goal or produce accurate end-effector movements when the motor elements are perturbed (Schoner et al., 2008). For example, spinal frogs were shown to be able to remove noxious stimuli from their skin with their foot even immediately after restriction of a joint's motion (Berkinblit, Gel'fand, & Fel'dman, 1986). Kelso et al. (1984) found that despite the application of unexpected forces to perturb jaw movements during the production of different speech utterances, those utterances could still be perceived by independent listeners, indicating preservation of the acoustic goal. Moreover, they showed that the primary articulatory compensations occurred in effectors most appropriate for the production of a given utterance. Similar effects were reported by Cole and Abbs (1987) from studies of a perturbed precision grasp. Levin, Wenderoth, Steyvers, and Swinnen (2003) used a spring load to perturb the forearm during a two-joint, star drawing task and found that the kinematics of nonperturbed drawing was preserved with the perturbation by significant changes in muscle electromyographic patterns. Each of these studies evaluated the relative level of terminal goal achievement as the criterion for motor equivalence and provided evidence for changes in the activation of certain motor elements associated with this preservation. Despite these clear patterns of behavior, the idea of motor equivalence is less well defined conceptually than it appears. For example, the variable that describes the goal of a task, e.g., bilabial closure (Kelso et al., 1984), thumb-fingertip contact (Cole & Abbs, 1987), or foot contact (Berkinblit et al., 1986), will not be unchanged perfectly when a perturbation is applied. Small changes of these variables induced by the perturbation or by any other variations of task conditions that may occur naturally are generally observed. Thus a more relevant

definition of motor equivalence would be that changes in the configuration of motor elements that lead to changes in variables relevant to the task goals are small compared with other changes of the configuration not directly relevant to those goals. Those other changes of the articulatory configuration thus represent the “motor equivalent” solution to the task (Schoner et al., 2008). This definition presupposes, first, that there is a shared metric with which to compare the changes that occur at the level of the task goal to changes that occur at the level of the configuration of motor elements and, second, that there is a way to compare the many variables that describe the motor elements to the few variables that describe the task goal. Similar to the problem of assessing the role of natural variability of the motor elements during repetitive tasks mentioned above, the UCM approach provides a potential solution to these problems. A recent study applied a version of the UCM approach to resolve whether differences in the terminal joint configuration induced by reaching and pointing to targets at different velocities were due primarily to differences in the terminal pointer- tip position across speed conditions or reflected motor equivalence (Scholz et al., 2011). Different dynamics due to changes in joint interaction torques with movement speed were used to produce internal perturbations of the entire arm. The results of that study indicated that performance-relevant changes of the joint configuration across speed conditions, i.e., those that affected the terminal pointer-tip position, were significantly smaller than configuration changes that did not affect the terminal pointer position. The UCM method was also used to study postural perturbations induced by support surface movement and revealed that changes in joint configuration due to a perturbation were largely motor equivalent compared with preperturbation postural states (Scholz et al., 2007).

The present study had three goals. The first goal was to determine whether perturbation of a 10 degrees of freedom (DOFs) reaching task exhibited motor equivalence both at the target of reaching and during the reach path and, if so, where along that path it became manifest. For example, it is in principle unnecessary to preserve the pointer-tip path during the reach itself as long as the pointer ultimately reaches the target. A second goal was to determine how the use of motor equivalence was affected by different constraints imposed by two different target types, one with only position constraints, the other with both position and orientation constraints. A final goal was to confirm that the results from the motor equivalence analysis, comparing perturbed to nonperturbed trials, provided different information than the typical UCM variance analysis (Scholz & Schoner, 1999), which evaluates the structure of joint variance across repetitions of the same condition. We hypothesized that motor equivalence, related to the pointer tip's path and the hand's orientation, would be present from relatively early in the reach until movement termination because typical reaching movements occur in quasi-straight line paths (Abend, Bizzi, & Morasso, 1982; Morasso, 1981) and motor synergies are organized to stabilize important performance-related variables like the hand path (Latash et al., 2007). A second hypothesis was that the magnitude of the motor equivalence effect would depend on the strength of the perturbation, i.e., that the greater the tendency to perturb the arm, the stronger would be the restoring forces to preserve the hand path. Two different target types were used in this study: a cylindrical target, where subjects had to insert the pointer halfway into the cylinder, and a spherical target that had to be touched by the pointer. We hypothesized that the motor equivalence effect relative to the hand's orientation would be strongest when reaching to insert the pointer into a

cylindrical target because only that target had an explicit orientation constraint. Finally, it was predicted that motor equivalence analysis would provide different information about reaching coordination than the typical UCM variance analysis.

2.3 Methods

Subjects

Eight healthy males participated in the study, averaging 20.1 (\pm 1.5) years old, 184.2 (\pm 2.4) cm in height, and weighting 79.0 (\pm 7.8) kg. All participants were right handed as determined by the Edinburg handedness questionnaire (Oldfield, 1971). They gave informed consent as approved by the University of Delaware Human Subjects Committee.

Experimental procedures

Experimental setup

Participants sat on a chair in front of a table that had a rectangle cut out of one side into which the chair was placed. The participants sat with their trunk upright, feet flat on the floor, and arms supported laterally by the table (Fig. 2.1). The heights of both chair and table were adjusted to keep the shoulder of the arm that performed the task immediately next to the trunk in a slightly adducted position, the elbow in $\sim 90^\circ$ of flexion, and the forearm resting on the table in a neutral position. The subjects were instructed to hold a cylindrical shaped handle (5 cm in diameter and 11 cm high) with their most comfortable grasp. Solidly embedded in the center of one end of the handle was a 12-cm-long knitting needle that served as a pointer. To maintain the handle's

orientation in the hand during the trials, the handle and the subject's palm were covered with the loop-and-hook type of Velcro strips.

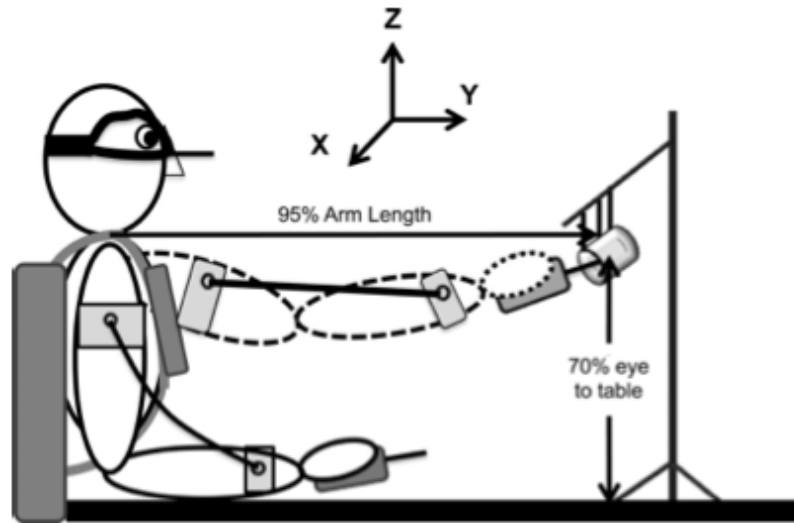


Figure 2.1 Cartoon depicting the experimental setup. Subjects wore safety goggles with a cardboard brim attached to the bottom to block vision of their arm and hand during approximately the first half of the reach. Either a spherical target or a cylinder (illustrated here) was hung from strings from a post to increase the need to control the terminal reach precisely. The Thera-Band was attached with hooks to padded cuffs placed around the upper arm and distal forearm so that they spanned the elbow joint.

Once the subjects held the handle, they were not allowed to change their grasp until the end of the data collection. After the subject was positioned, the chair was locked in place and the subject's trunk was secured to the chair with a harness to limit compensatory trunk movements, but still allowing normal scapular motion. To guarantee the reliability of the initial position throughout the experiment, a vacuum air bag was fitted underneath and around the lateral, medial, and back sides of the

participants' arm, leaving their elbow, forearm, wrist, and hand secured in a depression with rigid sides.

The experiment included reaching to two target types, providing different constraints on reaching: a spherical target (2.54-cm diameter; 3 positional constraints) and a cylindrical target (2.54-cm diameter, 5.08 cm wide; 3 positional and 2 orientation constraints). Each target's center was positioned at a distance corresponding to 95% of the subject's extended arm length (defined as the distance from the lateral aspect of the acromion process of the shoulder to the proximal interphalangeal joint of the index finger) and at 70% of the height of the subject's eye from the table while in the sitting position. The targets were suspended from a rigid pole by a string to require greater final position control than if subjects were able to forcefully hit the target. The cylindrical target was oriented at 45° relative to the global coordinate system, for which the y -axis pointed forward from the subject's body, rotated in the counterclockwise direction so that the opening in the cylinder into which the pointer was inserted faced toward the subject. The targets were suspended so that the centers of the spherical and cylindrical targets were in the same spatial location.

Instructions

The subjects were instructed as follows: "Following my 'go' command, begin reaching when you are ready and then move the pointer as quickly as possible to the target while still maintaining accuracy. You should stop at the target location without disturbing its position." It was emphasized that this was not a reaction time task. For the spherical target, subjects were instructed to lightly touch the target with the pointer-tip. For the cylindrical target they were told to insert the pointer-tip halfway

into the opening of the cylinder. Subjects were asked to try to perform all trials at the same speed and to touch/insert the pointer-tip as accurately as possible.

Experimental condition.

Each target condition involved 75 trials of reaching, 25 in each of three perturbation conditions that were completely randomized: 1) no perturbation (0-K); 2) a single elastic band (Thera-Band) placed across the elbow joint (stiffness = 4.8 N/m; Low-K); and 3) two elastic bands (stiffness = 12.5 N/m; High-K). Participants wore goggles with the brim of a hat attached, permitting them to see the targets clearly while eliminating the view of their arm. Cuffs with D-rings were placed around the upper arm and proximal to the wrist, to which hooks attached on each end of the Thera-Band could be attached. Prior to each trial, one experimenter attached the appropriate band (perturbed conditions) or pretended to attach the band (no perturbation condition) with a tug on the D-rings so that subjects could not tell whether or not there would be a perturbation. The bands were at their resting lengths in the initial position so that the subjects felt no pull in this position. This was confirmed verbally with subjects. Individuals performed practice trials or reaching with- out a band before the beginning of the experimental task. A break was permitted when requested by the subjects. Participants never reported fatigue.

Data collection

Three-dimensional kinematic data were collected with an eight-camera Vicon MX-13 motion-measurement system (Vicon, Oxford Metrics) at a sampling frequency of 120 Hz. The cameras were spread out in a circle around the subject and were spatially calibrated before each data collection. Rigid bodies with four reflective

markers each were placed on the right arm at 1) two-thirds of the distance between the neck and the acromion process, to acquire clavicle/scapula motion, and midway and along the lateral part of the 2) upper arm, 3) the dorsum of the forearm, and 4) the posterior surface of the hand. Individual markers used to estimate the joint locations were placed on the sternum notch, which served as the base frame of the local coordinate system, 2 cm below the acromion process, on the medial and lateral humeral epicondyles to estimate the elbow joint axis and on the radial and ulnar styloid processes of the forearm to estimate the wrist joint axes. An additional reflective marker was placed near the base of the pointer. The spherical and cylindrical targets were calibrated after each session by using the known fixed position of the pointer-tip relative to the hand rigid body and recording the hand while the subject held the pointer-tip statically at the target locations.

One static calibration trial was recorded with the arm extended forward prior to the experiment. In this trial, the arm was facing forward from the shoulder, with the upper arm, forearm, and hand aligned and held parallel to the floor with the thumb pointing upward. In this position, the arm was parallel to the global y -axis and all joint angles were defined as zero. The positive axes of each joint coordinate system in this position pointed laterally (x -axis), forward (y -axis), and vertically upward (z -axis). Joint angle computation involved computing the rotation matrices required to take the arm rigid bodies from the dynamic trial into the calibration position.

Data processing

Vicon Nexus 1.6.1 software was used to label the reflective markers and create the geometric model of their kinematic motion. The signals were then processed with a customized Matlab program (version 7.1, Mathworks). Marker coordinates were

low-pass filtered at 5 Hz with a bidirectional 4th-order Butterworth filter. The resultant velocity of the pointer-tip marker was obtained after differentiation of its x , y , and z coordinates. Kinematic variables of each trial were time-normalized to 100% for most analyses after differentiation.

Joint Angle Computation

The joint angles were calculated from the markers' coordinates as follows: The rigid bodies at each sample of an experimental trial were rotated into their static position in the calibration trial and used to compute the rotation matrices required to take one into the other (Soderkvist & Wedin, 1993). The product of these rotation matrices for adjacent segments was then used to extract Euler angles in Z - X - Y order. The result provided 10 rotational DOFs: 3 at the clavicle/scapula (abduction-adduction about the z -axis; elevation-depression about the x -axis, and upward-downward rotation about the y -axis) and shoulder (horizontal abduction-adduction about the z -axis; flexion-extension about the x -axis, and internal-external rotation about the y -axis) and 2 at the elbow (flexion-extension about an axis oblique to the local coordinate system; forearm pronation-supination about the y -axis) and wrist (flexion-extension about the z -axis; abduction-adduction about the x -axis). Rodrigues' rotation formula was used to rotate the elbow flexion-extension axes from the x -axis of the global coordinate frame to the axes formed by markers placed at the medial and lateral epicondyles (Murray, Li, & Sastry, 1994).

Movement time (MT)

Both movement onset and termination were determined for each trial as follows. The pointer-tip position was rotated into a local coordinate frame with the x -axis pointing from its average starting position before trial onsets to the calibrated

target position. The local coordinate along this axis, i.e., movement extent, was then differentiated. Onset and termination were determined as the times when the velocity profile along movement extent first exceeded or returned to, respectively, 5% of its peak velocity. The time between movement onset and movement termination was computed as movement time (MT).

Target error

Deviations of the pointer-tip at movement termination with respect to the calibrated target position (x -, y -, and z -coordinates) were obtained, and the constant errors (CE) and variable errors (VE) were computed (Schmidt & Lee, 2005).

Pointer-tip path and hand orientation

The path of the pointer-tip was obtained as the sequence of its global x -, y -, and z -coordinates. The resultant hand path was then calculated from these individual coordinates. Hand orientation for both target conditions was obtained by forming a target coordinate system for the cylindrical target, where the y^{target} -axis was the major axis of the cylinder, the x^{target} -axis was the minor axis, parallel to the floor, and the z^{target} -axis pointed upwards. Euler angles (roll, pitch, and yaw) were then extracted from the rotation matrix, computed at each sample in time, required to take a local coordinate system formed by the hand rigid body into the target coordinate system. The angles corresponded to rotation about the x^{target} -, y^{target} -, and z^{target} -axes of the target coordinate system, respectively.

Peak movement velocity

The x -, y -, and z -coordinates of the pointer-tip position were differentiated to obtain the end-effector velocity. The resultant pointer-tip velocity was calculated as

the norm of the differentiated coordinates at each point in the trial. The portion of the resultant velocity between the onset and termination of each reach was then extracted. A custom Matlab program was then used to automatically pick the peak of the resultant velocity and determine its time of occurrence within the reach (onset to termination). Averages across trials were obtained for each combination of target and perturbation strength.

Motor equivalence (ME) Estimate

The perturbation caused by extension of the elastic bands placed across the elbow joint will naturally lead to some deviation of the pointer-tip path compared with the nonperturbed condition. In fact, some variability of the pointer-tip path is expected across trials of reaching even without a perturbation. The goal of this analysis, then, was to provide a quantitative test to determine whether differences in the pointer-tip position between perturbed and nonperturbed reaches fully accounted for measured differences in the joint configuration, or whether more of this difference in the joint configuration was motor equivalent.

To investigate this question, all trials were time-normalized to 100% (movement onset to termination) and the average joint configuration across trials at each 1% of the three conditions (i.e., $\underline{\theta}_{0-K}$, $\underline{\theta}_{Low-K}$, $\underline{\theta}_{High-K}$) was calculated. Then, the geometric model describing how changes in the joint configuration from the mean of the nonperturbed condition ($\underline{\theta}_{0-K}$) affect either the 3D pointer-tip path or the 3D hand orientation was computed. From this, the Jacobian matrix (J) was computed, reflecting how small changes in a given joint angle while keeping other angles constant affects the 3D pointer-tip path or the 3D hand orientation. Details of the method can be obtained from recent publications (Scholz et al., 2011; Scholz & Schoner, 1999;

Scholz et al., 2007)Scholz et al. 2007, 2011; Scholz and Schoner 1999). The nullspace of this Jacobian provides a linear estimate of the subspace of joint space within which changes in the joint configuration have no effect on the performance variable of interest (i.e., the mean pointer-tip path or hand orientation of nonperturbed trials).

Then, a joint deviation vector ($JDV_{i0} = \bar{\theta}_{i-K} - \bar{\theta}_{0-K}$) between each stiffness (Low-K and High-K) condition and the nonperturbed (0-K) condition was obtained at each percentage of the reach. The JDV was then projected onto the nullspace of the Jacobian for the nonperturbed condition and into the complementary subspace, or range space. The length of the projection into the nullspace represents an estimate of the change in the joint configuration due to the perturbation that did not affect the performance variables, 3D pointer-tip path or 3D hand orientation, compared with the nonperturbed trials, while the length of projection into the range space estimates the effect of that change on the performance variable. Because the dimensions of the nullspace (dUCM = 7), a linear estimate of the UCM (i.e., the motor equivalent subspace), are larger than the dimensions of the complementary or range space (dORT = 3), we divide the respective projections by the square root of the dimension to make comparisons fairer. If the length of projection within the nullspace (ME or motor equivalent component) was significantly larger for a given stiffness/band condition than the projection into the range space (Non-ME, or non-motor equivalent component), then we concluded that most of the change in the joint configuration due to perturbation of the elbow joint primarily acted to preserve the 3D pointer-tip path and/or the 3D hand orientation, i.e., that the deviation was not primarily a reflection of induced differences in the performance variable.

Components of joint configuration variance

In addition, the typical UCM variance analysis was performed addressing how trial-to-trial variations of the joint configuration within a condition are structured, i.e., whether they led primarily to changes in the performance variable across repetitions (i.e., contributed to “bad” variance) or were more consistent with a stable pointer-tip path or 3D hand orientation across repetitions (“good” variance). The method used to estimate the two components of joint configuration variance is outlined in detail elsewhere (de Freitas, Scholz, & Stehman, 2007; Reisman & Scholz, 2003; Scholz et al., 2000) and is similar to that outlined above for estimating motor equivalence. In this case, however, the Jacobian and nullspace are computed based on the mean joint configuration of each condition. Then, for each percentage i of the reach trajectory of each trial j of a given condition k , the mean-free joint configuration is obtained (i.e., $\underline{\phi}_{ijk} = \underline{\theta}_{ijk} - \bar{\underline{\theta}}_{ik}$) and projected into the estimated UCM, or nullspace, and range space for that condition. The variance across trials of the projections into each subspace is then computed. Each variance component is then normalized by dividing by the number of dimensions of each subspace ($d_{\text{UCM}} = 7$ for “good” variance within the estimated UCM, or V_{UCM} , and $d_{\text{ORT}} = 3$ for “bad” variance in the range space, or V_{ORT}).

Statistical analysis

All statistical analyses were performed in SPSS version 18. A P value ≤ 0.05 was considered statistically significant for all analysis. A two-way, repeated-measures ANOVA with independent factors 1) target type (sphere vs. cylinder) and 2) stiffness (0-K, Low-K, High-K) was performed to identify their effects on each of the mean and

standard deviation of movement time, peak movement velocity, and time of occurrence of the peak. Post hoc comparisons of means were performed with the least significant mean (LSD) test.

A multivariate analysis of variance (MANOVA) was used to test for differences in constant and variable target errors (dependent variables = x -, y -, and z -coordinates) with factors 1) target type (sphere vs. cylinder) and 2) stiffness (0-K, Low-K, or High-K). Post hoc comparisons of means using the LSD test were performed for the dependent variables that exhibited significant univariate results.

For purposes of statistical analysis of both motor equivalence and joint configuration variance, the results for each subject were averaged across 10 equal phases of the reach trajectory (each accounting for 10% of the trajectory) in order to evaluate the evolution of these variables, since the perturbation strength increases along the reach trajectory because of the elastic nature of the elbow joint perturbation.

To evaluate motor equivalence effects, a four-way repeated-measures ANOVA with independent factors 1) target type (sphere vs. cylinder), 2) performance variable (3D path vs. 3D orientation), 3) stiffness (Low-K or High-K), and 4) component of projection (ME vs. Non-ME) was performed separately for each of the 10 phases of the reach. The M-matrix function in SPSS was used to further analyze significant interactions. If there was a significant interaction, e.g., projection component by stiffness, and M-matrix tests revealed that both ME and Non-ME components increased with the High-K perturbation, then the slope of change of each component from the Low-K to the High-K condition [e.g., $(ME_{\text{High-K}} - ME_{\text{Low-K}})/(12.5 - 4.8)$] was computed and a repeated-measures ANOVA was used to confirm which component was more affected by the stronger perturbation.

Finally, a four-way repeated-measures ANOVA was used to identify differences between the variance components V_{UCM} and V_{ORT} across conditions, with factors 1) target type (sphere vs. cylinder), 2) performance variable (3D path vs. 3D orientation), 3) stiffness (0-K, Low-K, or High-K), and 4) variance component (V_{UCM} vs. V_{ORT}). This was again performed for each 10% of the reach trajectory.

2.4 Results

Movement kinematics

Figure 2.2 shows the average (\pm SD) elbow joint angle (flexion-extension) for a representative subject during the reach for each stiffness condition (0-K, Low-K, and High-K) and both targets (spherical and cylindrical). Although the Thera-Band length was adjusted so that it became engaged nearly immediately after the subject began to reach, elbow movement was similar to the 0-K condition in the Low-K and High-K conditions up until \sim 25% of the reach path, after which time the torque produced by the band restricted elbow extension. The effect was slightly stronger for the High-K than for the Low-K condition regardless of target type.

Figure 2.3, *top*, presents for a representative subject the mean resultant path (\pm SD) of the pointer-tip when reaching to both the spherical (*left*) and cylindrical (*right*) targets. Figure 2.3, *bottom*, presents the mean resultant velocity \pm SD for the same reaches. All subjects showed similar pointer-tip/hand trajectories. Subjects showed more individual variation of the hand orientation path throughout the reaches, although the presence or absence of a perturbation did not appear to affect the hand orientation substantially.

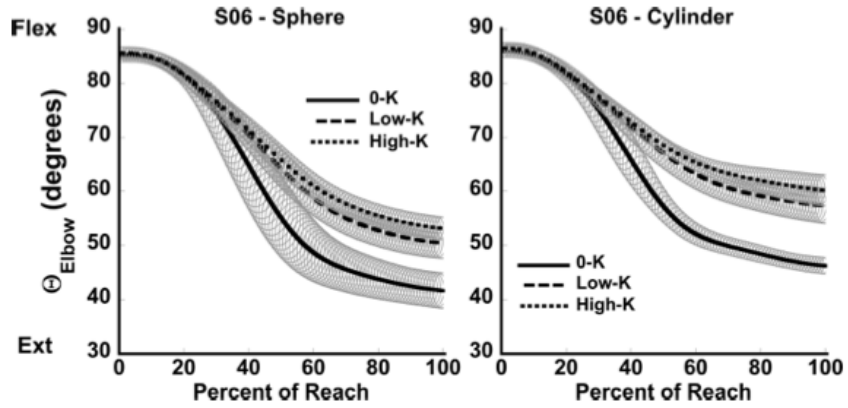


Figure 2.2 Mean (\pm SD) of elbow joint excursion for a representative subject during the reach for the 3 conditions of stiffness (0-K, Low-K, and High-K) and for the spherical and cylindrical targets. θ_{elbow} , elbow joint angle. Flex, flexion; Ext, extension.

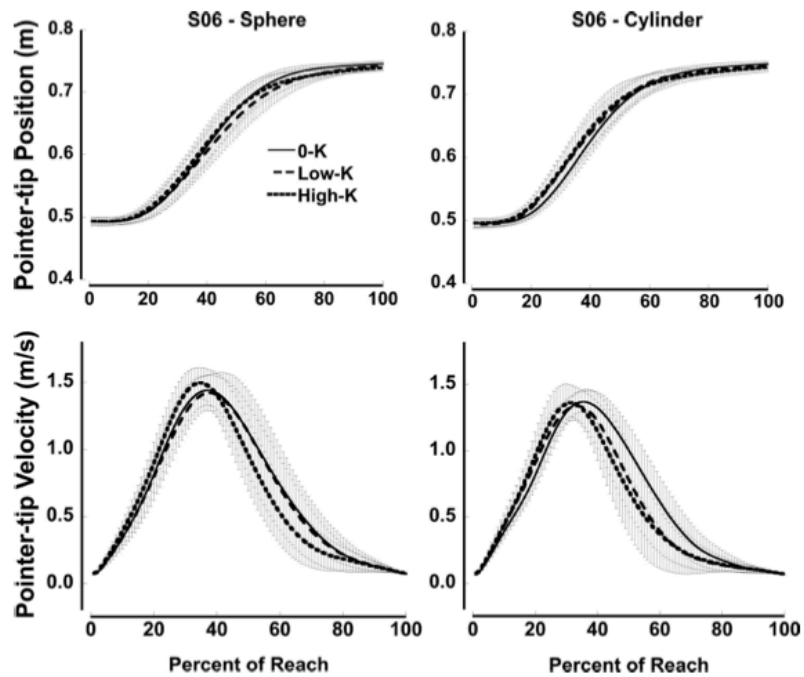


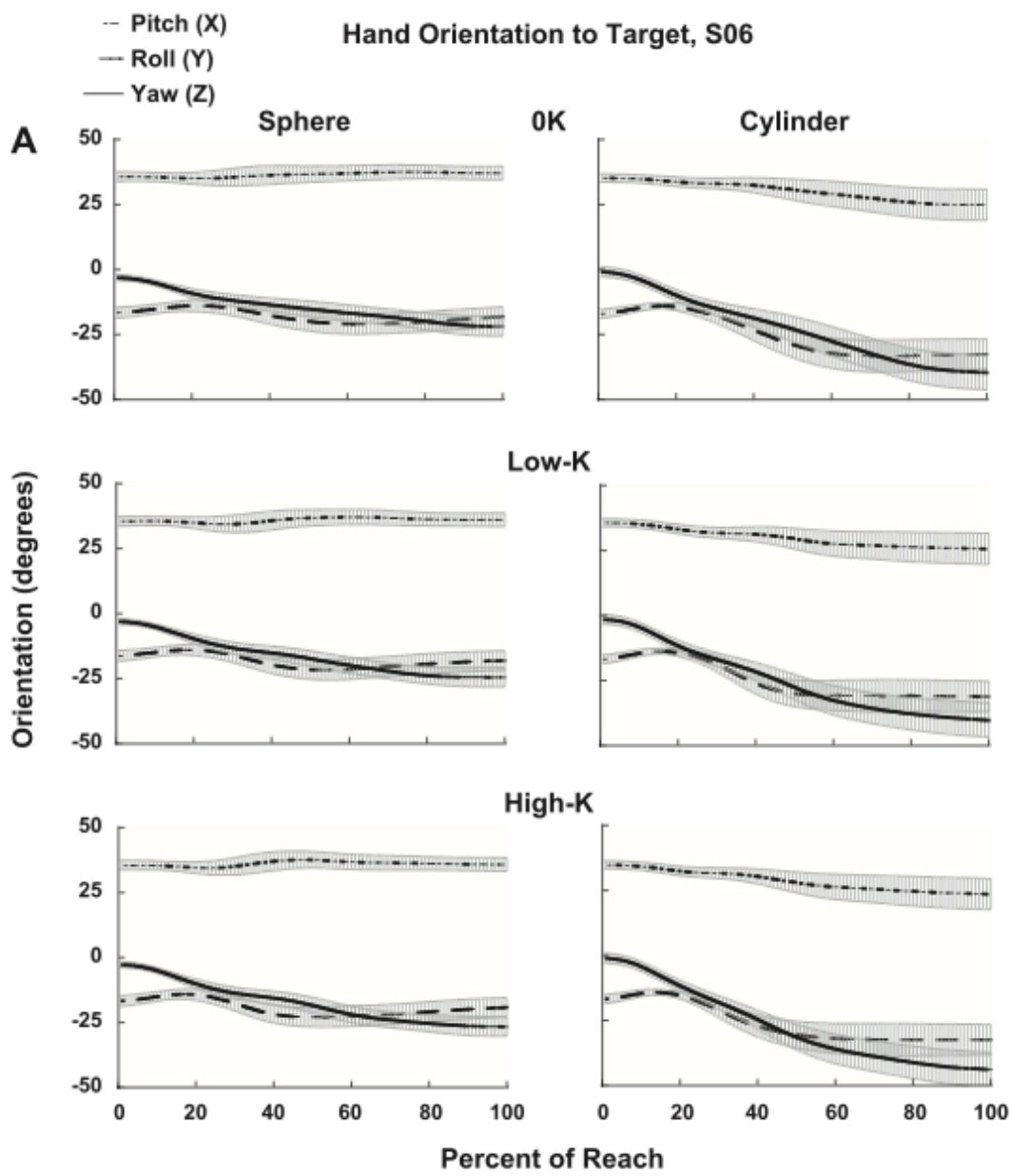
Figure 2.3 Time series (\pm SD) is shown of the resultant hand path (*top*) for the same subject as in Fig. 2 for the 3 stiffness conditions when reaching to the spherical (*left*) or cylindrical (*right*) targets. *Bottom*: mean (\pm SD) resultant velocity profiles associated with the reaches shown at *top*.

Figure 2.4 illustrates the mean hand orientation (\pm SD) relative to coordinates (pitch, roll, and yaw) for the spherical and cylindrical targets for two participants showing somewhat different changes in orientation across the reach. *Subjects 06* (Fig. 2.4A) and *08* (Fig. 2.4B) exhibited, respectively, the smallest and largest proportion of ME projection compared with Non-ME projection across the reach trajectory. Rotation about the z -axis (yaw) was most important, given the fact that the cylinder was rotated 45° about this axis in the x - y plane, and this coordinate changed the most. This was, of course, only critical for pointing to the cylindrical target, and it can be noted that the yaw rotation was greatest for this target condition for both subjects.

Movement time (MT)

Table 2.1 presents the mean and standard deviation of movement time, peak velocity of the pointer-tip, and time of occurrence of the peak as a percentage of the reach for the three stiffness conditions and both spherical and cylindrical targets across the subjects.

Both target type ($F_{1,7} = 16.342$, $P < 0.01$) and perturbation strength ($F_{1,7} = 14.881$, $P < 0.01$) affected the mean MT. No interaction between target type and perturbation strength was found ($P > 0.3$). MT was, on average, 59 ms longer for the cylindrical than the spherical target ($MT_{CY} = 0.811 \pm 0.037$ s vs. $MT_{SP} = 0.752 \pm 0.033$ s). In addition, MT was \sim 39 ms and 14 ms longer for the High-K condition compared with the 0-K ($P < 0.01$) and Low-K ($P < 0.05$) conditions, respectively. MT for the Low-K condition was also 25 ms longer than for the 0-K condition ($P < 0.01$). MT variability was not affected by target type ($P > 0.9$), perturbation strength ($P > 0.7$), or their interaction ($P > 0.6$).



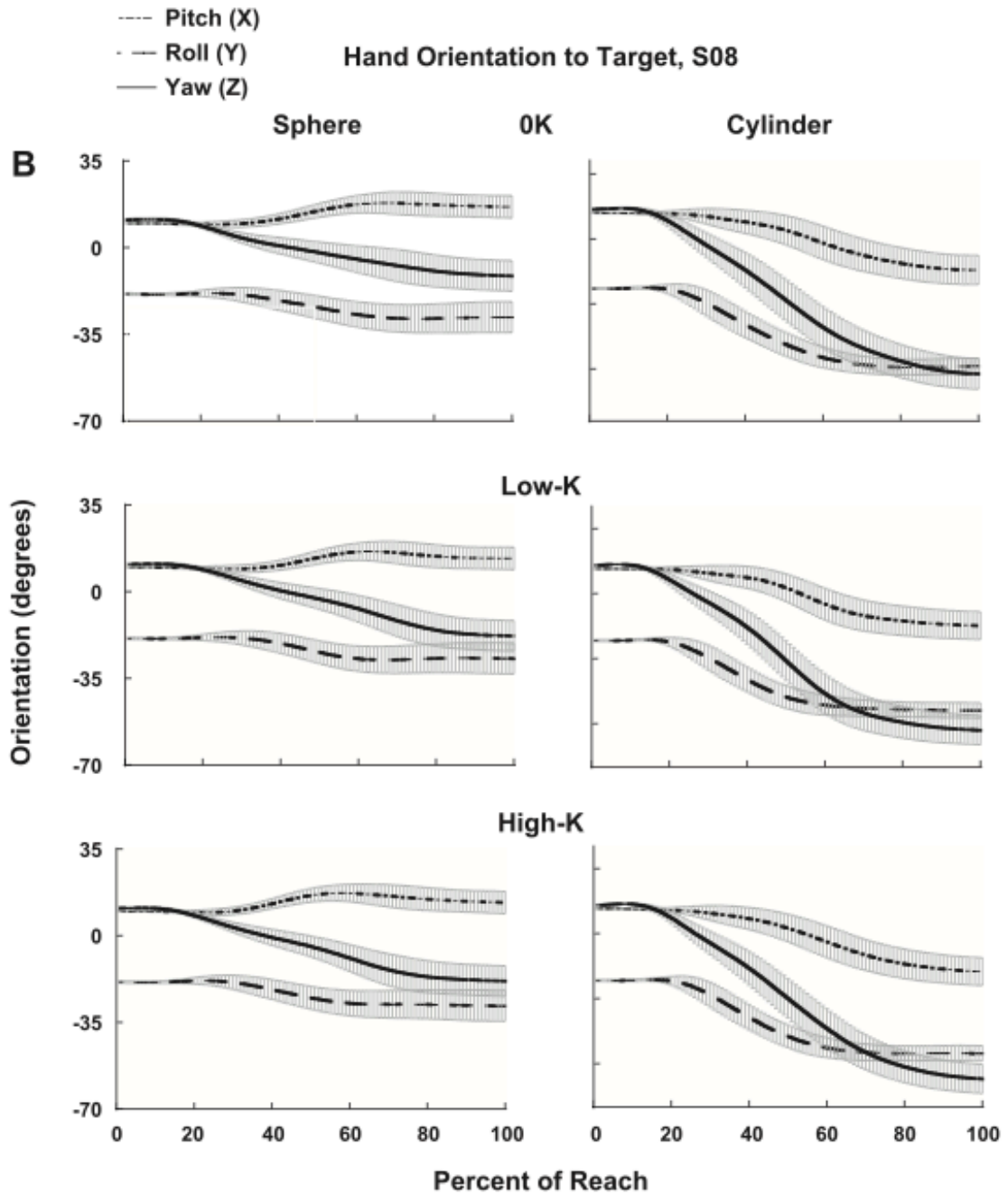


Figure 2.4 Time series (\pm SD) of the hand's orientation to coordinates of the cylindrical target (pitch, roll, and yaw) for reaching to both the spherical and cylindrical targets for a subject showing smaller changes in orientation (*A*) and a subject showing larger changes in orientation (*B*).

Table 2.1 Movement time, peak velocity, and time of peak velocity.

| Target | Stiffness | MT | | Peak Velocity | |
|----------|-----------|--------------|--------------|---------------|--------------|
| | | Mean, s | STDEV, s | Mean, m/s | % of Reach |
| Sphere | 0-K | 0.732 ± 0.08 | 0.088 ± 0.04 | 1.48 ± 0.11 | 40.43 ± 1.94 |
| | Low-K | 0.749 ± 0.10 | 0.080 ± 0.01 | 1.49 ± 0.11 | 40.08 ± 1.70 |
| | High-K | 0.774 ± 0.10 | 0.085 ± 0.03 | 1.43 ± 0.09 | 36.56 ± 1.68 |
| Cylinder | 0-K | 0.788 ± 0.10 | 0.082 ± 0.02 | 1.46 ± 0.10 | 36.61 ± 1.43 |
| | Low-K | 0.821 ± 0.11 | 0.084 ± 0.02 | 1.44 ± 0.09 | 35.10 ± 1.26 |
| | High-K | 0.824 ± 0.11 | 0.089 ± 0.02 | 1.47 ± 0.11 | 34.54 ± 1.32 |

Averages ± SE across subjects of movement time (MT) and its standard deviation (STDEV) and peak velocity and the percentage of the reach at which the peak of velocity occurred are presented. 0-K, Low-K, and High-K refer to no elastic band, low-stiffness band, and high-stiffness band crossing the elbow joint.

Target error

The MANOVA revealed that the CE of targeting (Table 2.2) depended on the stiffness condition (Wilks' $\lambda = 0.152$, $F_{6,24} = 6.26$, $P < 0.05$) for both the x -coordinate ($F_{1,7} = 13.740$, $P < 0.01$) and the y -coordinate ($F_{1,7} = 11.933$, $P < 0.005$). Post hoc tests revealed that CE in the x -dimension was significantly greater for the 0-K compared with either the Low-K ($P < 0.05$) or High-K ($P < 0.005$) condition, and for the 0-K compared with the High-K ($P < 0.005$) condition. Analysis of the y -dimension revealed that CE for the High-K condition was significantly larger and more negative compared with both the 0-K ($P < 0.005$) and Low-K ($P < 0.01$) conditions, indicating that there was more undershoot of the target when the arm was subjected to a stronger perturbation. However, CE was not different between target types ($P < 0.05$), and there was no interaction between target type and stiffness ($P > 0.2$).

Analysis of VE revealed no effect of target type (spherical vs. cylindrical, $P > 0.7$) or stiffness condition (0-K, Low-K, and High-K, $P > 0.5$). There was also not a significant interaction between these factors ($P > 0.7$).

Table 2.2 Targeting error.

| | Stiffness | x-Coordinate | y-Coordinate | z-Coordinate |
|----|------------------|---------------------|---------------------|---------------------|
| CE | 0-K | 0.0043 ± 0.0020 | -0.0104 ± 0.0032 | -0.0008 ± 0.0014 |
| | Low-K | 0.0022 ± 0.0021 | -0.0130 ± 0.0034 | -0.0020 ± 0.0016 |
| | High-K | 0.0002 ± 0.0020 | -0.0160 ± 0.0037 | -0.0022 ± 0.0016 |
| VE | 0-K | 0.0055 ± 0.0016 | 0.0064 ± 0.0018 | 0.0040 ± 0.0005 |
| | Low-K | 0.0062 ± 0.0019 | 0.0068 ± 0.0024 | 0.0062 ± 0.0026 |
| | High-K | 0.0044 ± 0.0002 | 0.0051 ± 0.0006 | 0.0043 ± 0.0005 |

Projection Components of the Joint Difference Vector (JDV)

To illustrate continuous changes in the ME and Non-ME components of the JDV projection, the averages ± SD across subjects are plotted in Fig. 2.5 for each target condition and performance variable (i.e., 3D pointer-tip position and 3D hand orientation). Of note, the component of the JDV lying in the nullspace (ME) was always somewhat larger than the component lying in the range space (Non-ME), particularly for the spherical target, and this difference became larger as the reach progressed beyond 30–40%. This was true independent of target type (sphere or cylinder) or performance variable (3D position vs. orientation). The continuous plots suggest that although the Non-ME component also increased with extension of the elastic band, the ME component increased by a greater amount.

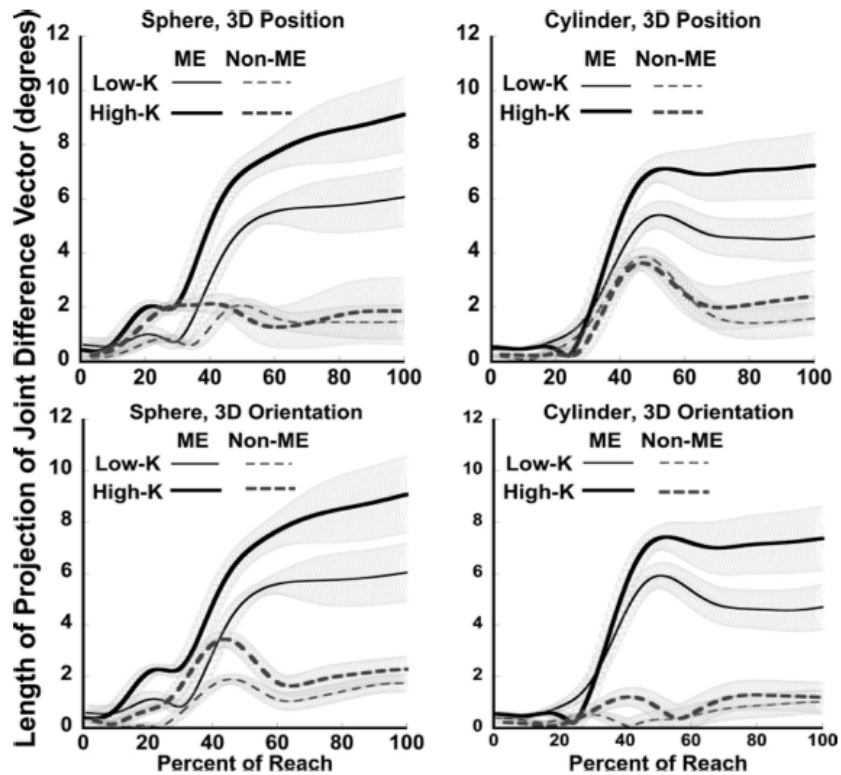


Figure 2.5 Time series (\pm SE) of the motor equivalent (ME, solid lines) and non-motor equivalent (Non-ME, dashed lines) components of the joint difference vector (JDV). Results are presented for each target (*left* and *right*) and in relation to the 2 performance variables (*top* and *bottom*).

The main effect of the projection component (ME > Non-ME) was significant no matter what phase of the reach was examined (all phases had $P < 0.05$). None of the three-way or the four-way interactions was found to be consistently significant across phases of the reach. The most consistent effects across phases were observed for the performance variable by projection component (Fig. 2.6) and stiffness by projection component (Fig. 2.7) interactions.

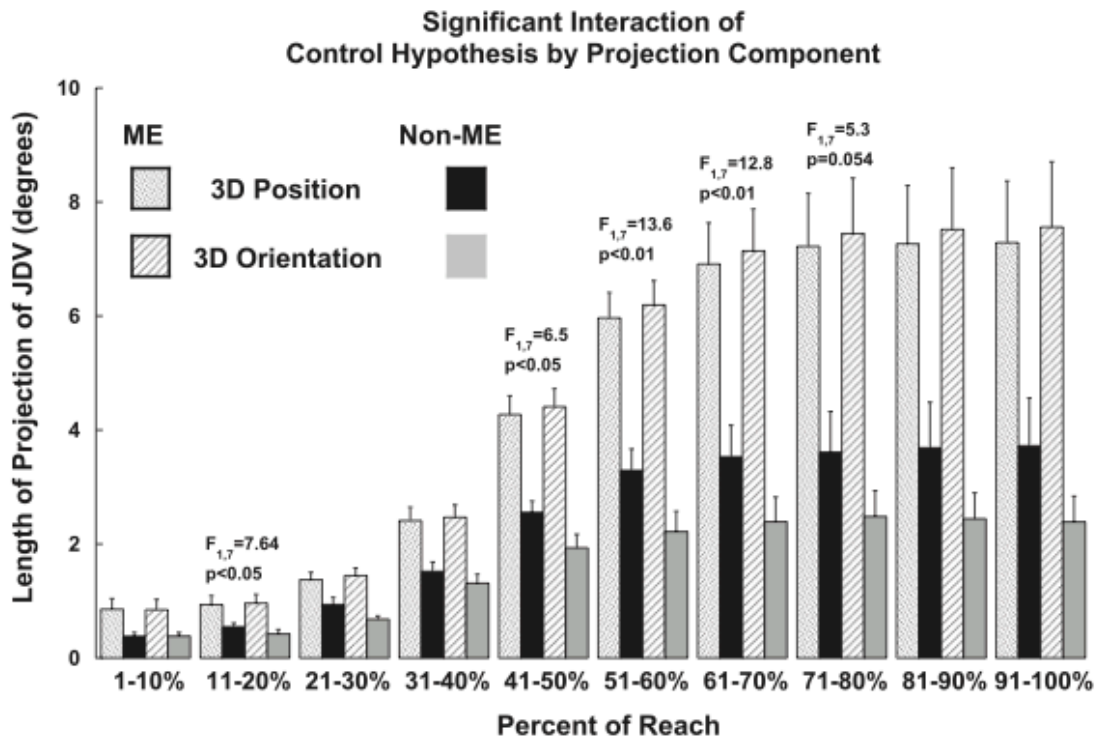


Figure 2.6 Average (\pm SE) of ME and Non-ME components for each performance variable at each 10% of the reach trajectory; F ratios and P values are based on the 4-way repeated-measures ANOVA performed over each 10% of the reach. The interaction performance variable [3-dimensional (3D) position vs. 3D orientation] by projection component (i.e., ME vs. Non-ME) was significant for the phases indicated.

The interaction of the performance variable and the projection component (Fig. 2.6) was nonsignificant during the early portion of the reach except for the second phase. After 40% of the reach (\sim 320 ms based on an average MT of \sim 800 ms), the differences in the projection component were dependent on the performance variable from 41% to 80% of the reach trajectory, and this interaction was close to significant thereafter. The ME component of the joint difference projection was approximately equal for 3D pointer-tip path and 3D hand orientation. However, as illustrated in Fig.

6, the Non-ME component was larger for 3D pointer-tip path, indicating that the difference in joint configurations between the nonperturbed and perturbed conditions led to a greater deviation of the 3D pointer-tip path from nonperturbed reaches than was the case for 3D hand orientation, regardless of the target type.

The interaction of stiffness and projection component (Fig. 2.7) was nonsignificant through the first 40% of the reach. Throughout the remainder of the reach, stiffness or perturbation strength significantly affected the projection component, as indicated in Fig. 2.7. The stronger perturbation caused by the stiffer band led to an increase in both the ME and Non-ME components compared with the low-stiffness condition, but the ME component increased more, as suggested by the significant stiffness by component interaction. This difference was further quantified by computing for each subject the slope of change between the two stiffness conditions (Low-K = 4.9 N/m; High-K = 12.5 N/m) for both ME and Non-ME components. The slopes were then compared by repeated-measures ANOVA (see METHODS). The slope (m) for the ME component was always larger than the slope for the Non-ME component for all phases of the reach trajectory (Table 2.3).

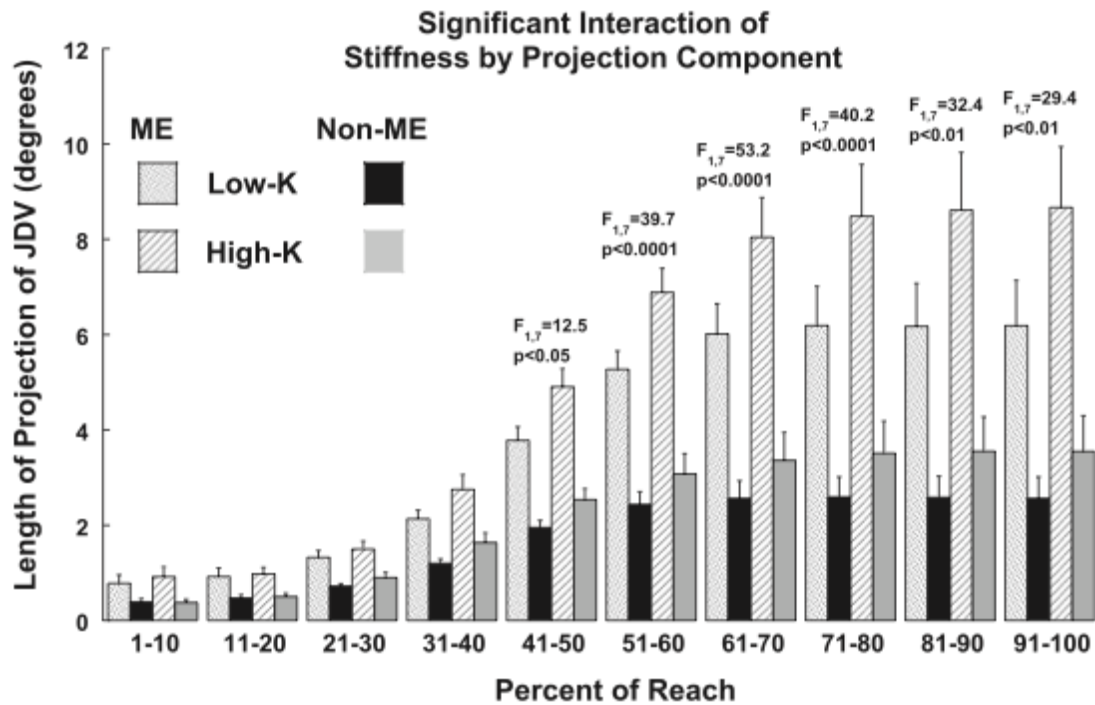


Figure 2.7 Average (\pm SE) for ME and Non-ME components for each stiffness condition for each 10% of the reach trajectory. F ratios and P values are based on the 4-way repeated-measures ANOVA performed over each 10% of the reach. The interaction stiffness (Low-K vs. High-K) by projection component (i.e., ME vs. Non-ME) was significant for the phases indicated.

Table 2.3 Slope of change in ME and Non-ME components.

| % of Reach | m_{ME} | m_{nME} | Statistical Test |
|------------|-----------------------|-----------------------|------------------------------|
| 41-50% | 0.00258 ± 0.00045 | 0.00134 ± 0.00027 | $F_{1,7} = 12.470, p=0.010$ |
| 51-60% | 0.00370 ± 0.00049 | 0.00147 ± 0.00044 | $F_{1,7} = 39.743, p<0.0001$ |
| 61-70% | 0.00467 ± 0.00063 | 0.00183 ± 0.00056 | $F_{1,7} = 53.227, p<0.0001$ |
| 71-80% | 0.00527 ± 0.00077 | 0.00211 ± 0.00064 | $F_{1,7} = 40.226, p<0.0001$ |
| 81-90% | 0.00560 ± 0.00086 | 0.00223 ± 0.00070 | $F_{1,7} = 32.417, p<0.001$ |
| 91-100% | 0.00570 ± 0.00089 | 0.00226 ± 0.00074 | $F_{1,7} = 29.352, p<0.001$ |

Mean \pm SE slopes (m) of the change Low-K and High-K conditions, based on each 10% of the reach, are presented. The slope for ME was always significantly larger.

UCM Variance Analysis

The analysis of variance components found no consistent main effects of target type, stiffness, performance variable, or interactions of these factors with the variance component across phases of the reach. The only consistent effect was that V_{UCM} was larger than V_{ORT} for all phases of reaching, (all $P < 0.05$). Figure 2.8 presents these results, collapsed across target type, performance variable, and stiffness condition (0-K, Low-K, and High-K).

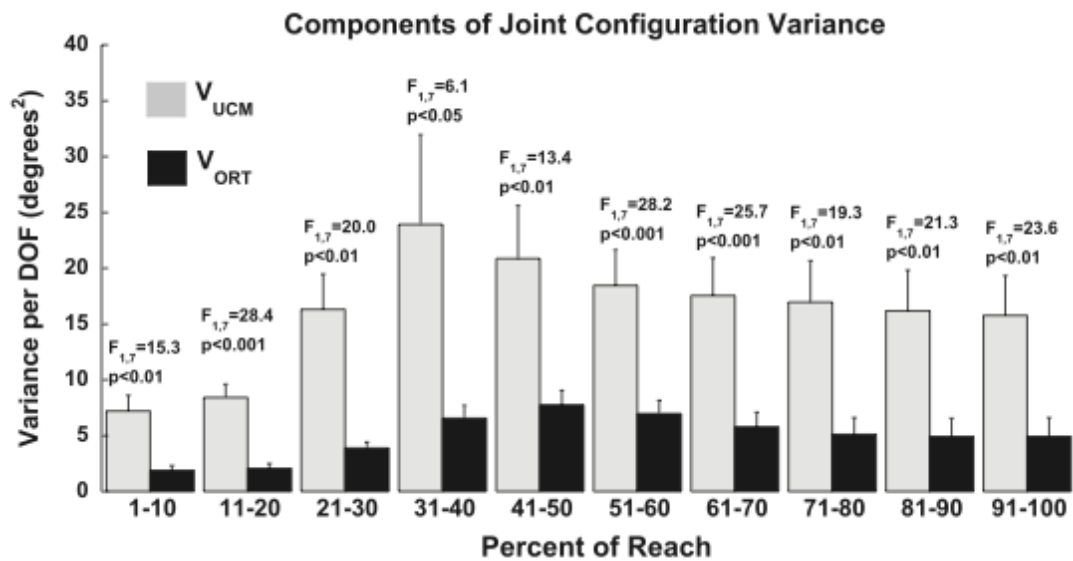


Figure 2.8. Mean (\pm SE) of each component of joint configuration variance (V_{UCM} and V_{ORT}) computed at each phase of the reach and averaged across target type, performance variable, and stiffness. F ratios and P values are based on the 4-way repeated-measures ANOVA performed over each 10% of the reach. Only the main effect of variance component (V_{UCM} vs. V_{ORT}) was significant for the phases indicated. DOF, degree of freedom.

2.5 Discussion

The present study investigated the extent to which motor equivalence is used to produce relatively stable values of variables most directly related to performance success in the face of a perturbation of reaching. If a larger component of the difference in the joint configuration between perturbed and nonperturbed trials had no effect on the pointer-tip path and/or hand orientation, variables most related to success of the pointing task, then this would provide stronger evidence for motor equivalence than has been provided in previous studies. This is a statistical question that required an appropriate method, for which we used a variation of the UCM method of analysis. The method was first introduced earlier in a study of postural stability in response to support surface perturbations (Scholz et al., 2007).

Results of the present study supported most of our hypotheses. Although the elbow perturbation led to significant differences in the anterior-posterior terminal pointer-tip location compared with nonperturbed reaches, the differences were relatively small, ~6 mm between the 0-K and High-K conditions. Perfect compensation for the perturbing force of the band is probably unrealistic given the nature of the task. Indeed, the ME component of the JDV, related to both the pointer-tip's path and the hand's orientation, was found to be significantly greater than the non-ME component throughout the reach.

Quantification of the joint configuration differences between perturbed and nonperturbed conditions revealed that most of that difference did not contribute to differences in the pointer-tip path or the hand orientation. Moreover, as predicted, the magnitude of motor equivalence depended on the strength of the perturbation, but only after ~40% of the reach trajectory, at approximately the time that elbow joint motion was affected by the perturbation (Fig. 2.2). The strongest perturbation (High-K

condition) resulted in a larger ME component than the weaker perturbation (Low-K), while the perturbation magnitude had a weaker effect on the Non-ME component of the JDV. This result is consistent with motor equivalence results computed at the termination of pointing in a recent report of the effect of reaching at different movement speeds (Scholz et al., 2011).

Contrary to one of our hypotheses, however, the target type had no effect on the amount of motor equivalence with respect to either the pointer-tip path or the hand orientation. For the spherical target, the projection components (i.e., ME vs. Non-ME) were not that different when computed relative to pointer-tip path versus hand orientation (Fig. 2.5, *left*). If anything, the Non-ME component related to the stabilization of hand orientation was greater early in the reach. For reaching to the cylindrical target, for which the pointer had to be oriented to insert it properly, the perturbation had a substantially larger effect on control of 3D position (higher Non-ME component) than for control of 3D orientation. Motor equivalence related to hand orientation was always larger than that for pointer-tip path regardless of the target type, a somewhat unexpected finding. Note that the ME and Non-ME variables were quantified per DOF in corresponding subspaces, so by itself, the number of constraints could not affect the proportion of ME value. The larger Non-ME values computed with respect to the pointer-tip path suggest that in perturbed trials the subjects were less concerned with keeping the end point trajectory consistent compared with keeping the end-effector orientation consistent.

The inequality $ME > \text{Non-ME}$ is far from being trivial. In the course of the unperturbed movement, the joint configuration changed to move the end point from the starting location to the target. If in the case of the perturbation the entire time

course of the movement slowed down, then we would expect the Non-ME component of JDV to be substantial. This is because at a given percentage of the movement cycle the joint configurations for the 0-K and, for example, the High-K conditions would differ in large part because of different pointer-tip positions. Although there was no difference in peak velocity among the conditions (Table 2.1), the timing of the peak was affected by the perturbation, occurring earlier in the perturbed conditions than in the 0-K condition. This effect can also be seen in the representative velocity plots in Fig. 3, although the differences were not huge, amounting at most to 4% of the cycle. Despite this delay, most of the change in the JDV due to the perturbation was motor equivalent and had no effect on the progression of the movement. Indeed, although both the ME and Non-ME components increased with greater perturbation strength, the ME component's increase was significantly greater than that of the Non-ME component.

The direct mechanical effects of the perturbation produced by the elastic band crossing the elbow joint were not limited to changing the trajectory of the elbow joint because of the mechanical joint coupling. Its effects on joint motion were complex, being both joint configuration and velocity dependent (see Zatsiorsky, 2002). Even during the first time interval, that is, from the time of movement initiation to 10% of MT (~80 ms), the deviation of the joint configuration (JDV) from its unperturbed trajectory was significantly larger within the ME subspace compared with the Non-ME subspace. Since it was impossible for the subject to predict when a perturbation would emerge, this time is too short for any conscious correction of the ongoing movement. There are two interpretations for this finding. First, the movement could be associated with a time profile of muscle activations that favored certain responses to

unexpected mechanical perturbations organized to keep the end point trajectory relatively immune to the perturbation. These are similar to “preflexes,” a term introduced by Dickinson and colleagues (2000) to designate peripheral responses of the muscles and tendons tuned in advance by the CNS. Second, there could be nonlocal, reflex like corrections at a latency of under 70 ms sometimes referred to as preprogrammed reactions, triggered reactions, or long-loop reflexes (cf. Chan, Jones, Kearney, & Watt, 1979; Gielen, Ramaekers, & van Zuylen, 1988). This latter explanation sounds less plausible because the first time interval was only 80 ms long, which seems too short to incorporate mechanically meaningful corrections in response to an unexpected smooth perturbation produced by the elastic band.

Results of the motor equivalence analysis suggest two different effects of “feedback” from mechanoreceptors. Traditionally, feedback would operate to stabilize the elbow joint against the band’s perturbation, given that the perturbation most directly affected elbow movement. However, the results of the pointer-tip path and hand orientation indicate stabilization of these more global performance variables, consistent with idea that cross-limb reflex pathways are crucially involved in producing interlimb synergies (Ross & Nichols, 2009). In addition, an additional type of “feedback,” referred to as “back-coupling,” that operates differently is likely. Back-coupling has been proposed in a model of reaching by Martin et al. (2009) as a mechanism that adjusts the referent trajectory of the end point to ensure equifinality of the actual trajectory in the face of perturbations. Martin et al.’s (2009) model contains components responsible for planning goal states and for movement initiation and timing, formulated at the level of the performance variables (e.g., hand position and/or orientation). The model also contains biomechanical dynamics of the effector system

as well as an associated muscle-joint model that takes into account the impedance properties of muscles based on a simplified version of Gribble, Ostry, Sanguineti, and Laboissiere (1998). According to the Martin et al. (2009) model, the descending motor command to the muscle-joint system is a set of equilibrium joint angles and velocity vectors. The neuronal dynamics of the model generates the time courses of these equilibrium joint angles based on an input signal that specifies the time course of the performance variable. In other words, this dynamics achieves the transformation from task space into joint space. It does so by coupling the equilibrium joint velocities such that joint velocity vectors that leave the performance variable unchanged are decoupled from joint velocity vectors that change the performance variable. This accounts for many of the signature features of movement tasks that have been reported previously based on UCM analyses (Martin et al., 2009). An alternative perspective, however, is that the descending commands do not specify joint angles or velocity vectors per se, but act to predetermine through threshold position control the spatial frame of reference in which the neuromuscular system is constrained to work (Raptis et al., 2010; see below). Nevertheless, the back-coupling in the Martin et al. (2009) model affects primarily the subspace of joint space where goal-equivalent joint configurations lie (i.e., the UCM) and explains motor equivalence: Deviations of the real from the equilibrium joint trajectory lead to an update of the equilibrium joint trajectory within the UCM. The result is the generation of a new, motor-equivalent plan.

This last point also suggests possible links of the data to the idea of control with referent configurations (reviewed in Feldman, 2009; Feldman, Goussev, Sangole, & Levin, 2007). Within this idea, the central controller is presumed to set a time

profile of a referent configuration of the body defined as a configuration at which all the muscles are at their threshold for activation. Thus the reaching tasks investigated here may have been guided primarily by changes in the referent position and referent orientation of the hand with respect to the environment, whereas individual DOFs were involved in the task or not depending on their capacity to minimize the difference between the actual hand position and orientation and their referent prototypes specified by the brain. Referent configurations may be unattainable because of external forces and anatomic constraints, which may explain why reaches were somewhat short of the target when working against the high band stiffness; in such cases, the body is predicted to come to equilibrium with nonzero levels of muscle activation.

Within a recent development of this general idea, neural control of natural movements is organized into a hierarchy (Latash, 2010a, 2010b); at each level of the hierarchy, neural signals can be adequately described as a set of referent values for salient variables. During a reaching movement, control at the highest level defines referent values for such variables as position and orientation of the end-effector. Movement is driven by a disparity between actual and referent values of those variables. At lower levels, the relatively low-dimensional input is transformed into a higher-dimensional set of referent values for appropriate variables formulated at a joint or muscle level. This mapping is organized in a synergic way: Families of referent configurations at a lower level may be facilitated as long as they correspond to the required referent configuration at the higher level.

In our experiment, salient variables were 3D pointer-tip path and hand orientation (for the cylindrical target). Referent values for those variables mapped onto

a redundant set of referent values (trajectories) in the joint space. This mapping was organized in a synergic way as demonstrated by the fact that most variance in the joint space was compatible with the same pointer-tip or hand position (orientation). This organization naturally channels effects of perturbations, internal or external, into the subspace of joint configurations compatible with the end point trajectory [similarly to results of a recent study by Gorniak, Feldman, and Latash (2009)].

Note that the elastic bands generated position-dependent forces. As a result, end point coordinates in the terminal position would be expected to differ between the two stiffness conditions if no correction of the referent configuration at the upper level of the hierarchy were implemented. Table 2 does show that reaches in the High-K condition had more CE in the y -dimension (AP) than did either the Low-K or 0-K condition. This would account for the higher Non-ME component of the JDV in the High-K versus Low-K conditions (Fig. 2.7) because the pointer was in a slightly different location at movement termination. Nevertheless, most of the JDV was motor equivalent and the ME component was significantly larger when the perturbation strength was greater, after ~40% of MT (Fig. 2.5). Hence, we suggest that higher-level corrections likely occurred to minimize deviations of salient variables, such as coordinates of the pointer-tip and hand orientation, from their average trajectories observed in unperturbed trials. These reasoning and conclusions have to be viewed as tentative since no explicit model of the arm reaction to different bands was studied.

A final point of interest is the results of the UCM variance analysis, performed here across repetitions of each condition, i.e., within each combination of target type and stiffness condition (0-K, Low-K, and High-K), performed for each performance variable (Fig. 2.8). Unlike the motor equivalence analysis, this analysis yielded no

effects of, or interactions among, stiffness conditions or performance variables. In all cases, V_{UCM} was substantially and significantly higher than V_{ORT} , the component of joint configuration variance that would induce variability of the 3D pointer-tip position or hand orientation. This result is consistent with the results of many previous studies (Freitas & Scholz, 2009; Freitas, Scholz, & Latash, 2010; Latash et al., 2003; Latash, Scholz, & Schoner, 2002; Reisman & Scholz, 2006; Reisman, Scholz, & Schoner, 2002b; Scholz & Schoner, 1999; Scholz et al., 2000; Tseng et al., 2002; Yang et al., 2007), further supporting the UCM control hypothesis (Latash et al., 2007; Martin et al., 2009; Schoner et al., 2008). Thus, despite differences among the conditions in the strength of perturbation, within a condition a similar variance structure emerged. The same mechanisms may be at play when investigating deviations of the joint configuration induced by different levels of perturbation, but the response is much stronger. This is probably due to the fact that feedback pathways are more strongly activated by external perturbations.

2.6 Conclusions

This study provides additional quantitative evidence for motor equivalence, here in response to mechanical perturbations during reaching. Evidence for motor equivalence was present throughout the entire reach, not only at or near movement termination. Moreover, the stronger the perturbation was, the stronger was the evidence for motor equivalence once the bands were clearly engaged. The results are consistent with a recent model of neural control in which the space of the motor elements is decoupled into motor equivalent and non-motor equivalent subspaces, allowing for flexible patterns of coordination while resisting deviations to the values of variables most related to task success. The results may also be compatible with the

hypothesis of hierarchical control with referent configurations at each level, and synergic mappings between control levels of the hierarchy

Chapter 3

MOTOR EQUIVALENCE (ME) DURING REACHING: IS ME OBSERVABLE AT THE MUSCLE LEVEL?

3.1 Abstract

The concept of motor equivalent combinations of arm muscles, or M-modes, was investigated during reaching to insert a pointer into a cylindrical target with and without an elbow perturbation. Five M-modes across 15 arm/scapula muscles were identified by principal component analysis with factor extraction. The relationship between small changes in the M-modes and changes in the position/orientation of the pointer were investigated by linear regression analyses. The results revealed a motor equivalent organization of the M-modes for perturbed compared with non-perturbed reaches, both with respect to hand position and orientation, especially in the first 100-ms postperturbation. Similar findings were obtained for motor equivalence computed based on changes in the joint configuration, although the kinematically defined motor equivalence was stronger for pointer orientation. The results support the hypothesis that the nervous system organizes muscles into M-modes and flexibly scales M-mode activation to preserve stable values of variables directly related to performance success.

3.2 Introduction

The fact that individuals can accomplish the same task using different effectors or in the presence of a perturbation (Hughes & Abbs, 1976; Kelso et al., 1984; Levin

et al., 2003; Scholz et al., 2011) attests to the remarkable flexibility of the central nervous system. This phenomenon is known as “motor equivalence”. The evidence for motor equivalence reinforces the notion of synergy - “working together toward a particular goal”, where elemental variables at different levels of analysis (e.g., muscles, motor units, joints or motor neurons) are organized to stabilize a performance variable of interest (Latash, Gorniak, & Zatsiorsky, 2008; Latash et al., 2007). It also suggests a hierarchical organization, where the individual control of elemental variables matters less than the interaction among them (Turvey, 2007).

Hughlings Jackson (1889) recognized some time ago that “*the central nervous system knows nothing of muscles, it only knows movements*”. This opinion brings attention to the fact that muscles are unlikely to be independently controlled by the CNS, a hypothesis supported by evidence from recent experiments using animal models to explore movements triggered by cortical (Graziano, Taylor, & Moore, 2002; Graziano, Taylor, Moore, & Cooke, 2002; Holdefer & Miller, 2002) and spinal cord stimulation (Saltiel et al., 2001). Such results indicate that combinations of muscle groupings express different motor behaviors, and that functionally relevant groups of muscles might be encoded at different levels of the CNS.

A variety of dimensional reduction approaches (e.g., principal component analysis, independent component analysis, nonnegative matrix factorization) have been used to identify groups of muscles that appear to work as single functional units of action (Turvey, 1990), referred to by some as muscle synergies (d'Avella et al., 2006; Ting, 2007; Tresch et al., 2006) and by others as muscles-modes (Asaka, Wang, Fukushima, & Latash, 2008; Danna-Dos-Santos et al., 2008; Krishnamoorthy et al., 2004; Latash et al., 2007), with important distinctions. The second term implies that

muscle groups play the role of elemental variables, on which synergies are built. The notion of synergies requires that different muscle groups work together in a flexible way to achieve the stability of or consistent changes in the values of important, functionally-relevant performance variables (Latash et al., 2007).

Functional muscle synergies have been investigated using the Uncontrolled Manifold (UCM) approach (Scholz & Schoner, 1999). This method provides a means for partitioning the variance of elemental variables into two components, only one of which produces motor error (“bad” variance), while the other (“good” variance) reflects flexible combination of the elemental variables that stabilize or provide consistent changes in a performance variable closely related to the task. Within this framework, muscle-modes represent combinations of muscle activations that reduce the number of DOFs manipulated by the CNS. It is important that the CNS has the ability to combine muscle-modes in different ways as the situation warrants to achieve performance stability, including the ability to compensate for perturbations (Latash et al., 2007). Many studies have investigated the role of functional muscle synergies from this perspective in the context of postural control (Danna-Dos-Santos et al., 2008; Danna-Dos-Santos et al., 2009; Krishnamoorthy, Goodman, et al., 2003; Krishnamoorthy, Latash, et al., 2003; Krishnamoorthy et al., 2004; Krishnamoorthy et al., 2007; Latash et al., 2007). These studies have focused on analysis of the two components of variance in the muscle-mode space with respect to different performance variables but did not investigate motor equivalence directly. Moreover, to our knowledge, no studies have investigated motor equivalence related to muscle activation in the context of more skilled activities such as reaching. Thus, the experiments presented in this article investigated the extent to which differences in

muscle-mode activations between perturbed and nonperturbed reaches displayed motor equivalence, i.e., were directed to minimize deviations of important performance variables from their unperturbed trajectories.

D'Avella and colleagues (2008; 2006) have provided evidence for the organization of arm muscles into a smaller number of functional groupings during the performance of reaching tasks by humans. However, their work did not investigate effects of perturbations and motor equivalence. Previous studies have reported that the number and composition of muscle-modes are not necessarily the same across subjects or similar tasks (d'Avella et al., 2008; Danna-Dos-Santos et al., 2008; Danna-Dos-Santos et al., 2009; Krishnamoorthy et al., 2004; Krishnamoorthy et al., 2007). One study of muscle control of a single finger also suggested that the muscle-mode structure might be absent: individual muscles can be units of control (Valero-Cuevas et al., 2009). Nevertheless, even in that study, an important finding was that the gains of the motor elements, whether muscle-modes or individual muscles, covaried to ensure low variability of the task variable (isometric force in an index finger task).

The current experiment is an extension of a previous study by our group (Mattos, Latash, Park, Kuhl, & Scholz, 2011) that established motor equivalence at the level of joint motions. There, deviations of the joint configuration that resulted from application of an unpredictable elastic resistance to elbow extension were primarily motor equivalent when compared with nonperturbed reaches. This was true both during the course of reaching and at movement termination, where accuracy of the pointer-tip position or pointer orientation was most crucial. The current experiment sought to determine whether a similar signature of motor equivalence could be identified at the level of muscle synergies and whether the amount of motor

equivalence differed during different phases of the reach. Synergies identified kinematically can result both from coupling of joint rotations due to biomechanical factors (e.g., joint interaction torques) and neural control. The muscle mode analysis used in the current study is based on quantifying coordinated electromyographic (EMG) activities of muscles recorded across the arm. EMG is an accepted method to identify changes in the neural drive to the motoneuron pools that innervate muscles. Thus, changes in muscle-mode magnitudes reflect coordinated changes in neural activation, due to local reflexes (40–60 ms postperturbation), preprogrammed reactions (~70–100 ms), or voluntary corrections (>100 ms).

In addition, it has been proposed that natural human movements are built on a hierarchy of synergies. For example, multijoint reaching to a target may be viewed as built on a multijoint kinematic synergy; each joint's trajectory may be viewed as built on a multimuscle synergy, while each muscle's activation pattern may be viewed as built on a synergy of motor units (Latash et al., 2008; Latash et al., 2007). Based on this hypothesis, one could predict that synergies defined at the muscle level would exhibit motor equivalent behavior with respect to stabilization of individual joint torques and related individual joint motion, but not necessarily with respect to stabilization of end-effector motion, which would depend on synergies defined across multiple joint motions. Thus, whether motor equivalence of muscle modes with respect to trajectories of the pointer tip's path and/or the hand's orientation were found in the current study, would provide an additional test of the hierarchical synergy hypothesis. Note that several recent studies have shown a trade-off between synergies at different levels of a hierarchy (Gorniak, Zatsiorsky, & Latash, 2007; Gorniak, Zatsiorsky, et al., 2009; Sun, Zatsiorsky, & Latash, 2011; Wu, Zatsiorsky, & Latash,

2012). These results suggest that having a strong synergy at the level of joint kinematics does not mean that a similar synergy will be seen at the level of muscle activations.

As in our previous study (Mattos et al., 2011), the task was reaching to insert a pointer into a cylindrical object, while an elastic resistance could be applied across the elbow. If motor equivalence in the space of muscle modes were to be found, we expected it to be strongest immediately after the onset of the elbow perturbation, and to be greater with respect to the pointer's spatial orientation rather than the position of the pointer-tip, based on our previous study (Mattos et al., 2011).

3.3 Methods

Subjects

Ten healthy subjects, averaging 23.1 ± 3.2 years of age, 175.4 ± 11.5 cm in height, and 76.6 ± 19.5 kg in weight, participated in the study. All participants were right-handed as determined by the Edinburgh handedness questionnaire (Oldfield, 1971) and had no reported neurological or motor disorders. They gave written informed consent as approved by the University of Delaware Human Subjects Committee in accordance with the Declaration of Helsinki.

Set-up Procedures

Subject's Initial Position

Participants sat on a chair in front of a table that had a rectangle cut out of one side into which the chair was placed. An illustration of the general experimental setup can be found in Figure 3.1. Participants sat with their trunk upright and their feet flat

on the floor. The heights of both the chair and the table were adjusted so as to support the reaching arm, with the shoulder in slight abduction and extension, the elbow in approximately 80° of flexion, and the forearm resting on the table in a neutral position. To guarantee the reliability of the initial position of the arm throughout the experiment, a vacuum air bag was fitted underneath and around the lateral, medial, and backside of the participants' arms, leaving their elbow, forearm, wrist, and hand secured in a depression with rigid sides.

Participants held a cylindrical handle, 5-cm in diameter and 11-cm long using a comfortable power grip. A 12-cm-long knitting needle served as a pointer and was solidly embedded in one end of the handle. The handle and the subject's palm were covered with the loop-and-hook type of Velcro strips, respectively, to maintain the handle's orientation in the hand constant during the trials. After positioning the subject, the chair was locked in place. The subject's trunk was secured to the chair with a harness to limit compensatory trunk movements but still allow normal scapular motion.

Target Position

The center of the target of reaching was positioned at a distance corresponding to 90% of the subject's extended arm length (defined as the distance from the lateral aspect of the acromion process of the shoulder to the pointer tip) and at 70% of the height of the subject's eye from the table while in the sitting position. The target was suspended from a rigid pole by a string to require greater final position control than if subjects were able to forcefully hit it; it offered little mechanical resistance when touched. It was oriented at 45° to each axis of the global coordinate system, for which the y-axis pointed forward from the subject's body, so that the opening of the cylinder

into which the pointer was inserted faced diagonally to the right of the subject's reaching (right) arm.

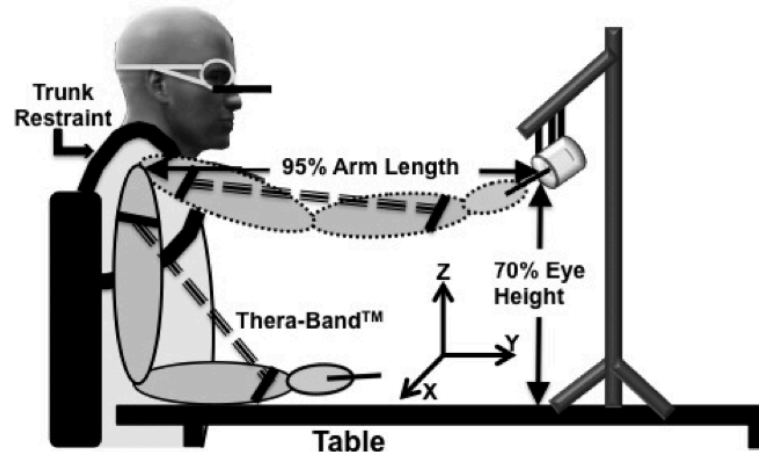


Figure 3.1 Illustration of experimental set-up for perturbed trials. Nonperturbed trials were identical, except for the attachment of the Thera-band. Subjects wore a pair of safety goggles that had the equivalent of the brim of a baseball hat attached to prevent subjects from viewing their reaching arm in the initial position. On nonperturbed trials, the experimenter acted as though they were applying the band by pulling gently on the wrist and shoulder attachments to prevent subjects from predicting when the perturbation would occur.

Elbow Perturbation.

Leather cuffs with D-rings attached were placed around the upper arm just distal to the armpit and immediately proximal to the wrist. Thera-Band (stiffness = 12.5 N/m) was used to produce an elastic perturbation of the elbow joint during perturbed reaches (Figure 3.1). The ends of the Thera-Band were wrapped around metal hooks that could easily be attached to the D-rings at the wrist and upper arm on perturbation trials. The length of the Thera-Band was selected to ensure that it

produced no force in the initial position. Subjects were asked after their experimental session whether they were able to determine when the elastic band was applied or not before movement initiation. All subjects indicated that they were unable to determine before a trial whether the band was applied.

Tasks

Estimation of Mode Vectors

To identify muscle modes in the space of 15 muscle activations, subjects were asked to perform a continuous set of movements in which they moved the hand-held pointer to the full extent of their reach anteriorly, to the right and left, across their body in alternation, and upwards, each direction performed twice. In addition, they traced a figure eight pattern parallel to the frontal plane twice before returning their arm to the initial position on the table. Participants were instructed to move all of their joints (wrist, elbow and shoulder) during the movement, and to perform the movements as fast as possible. Two trials were collected, each one lasting approximately 10 s. EMG signals of the 15 muscles were recorded and used to determine muscle-mode (M-mode) vectors, representing combinations of the muscles' activities. The M-mode vectors were used to transform EMGs from the reaching trials during the experiment proper into M-modes. Details of mode vector estimation are presented below.

Estimation of Motor Equivalence During Reaching

Ninety trials of reaching to insert the hand-held pointer into the cylindrical target that had 3 positional and 2 orientation constraints were performed across two conditions. Reaches of each condition were randomized across trials. In the Perturbed

(PERT) Condition, subjects performed 30 trials of reaching from the initial position to the target after the Thera- Band was attached with subjects' view of the arm occluded. The bands were at their resting lengths in the initial position so that the subjects felt no pull of the band in this position. In the Control (N-PERT) Condition, 60 trials were performed without the Thera-Band attached. More trials were performed in this condition to make it more difficult for subjects to guess when a perturbation might occur. Before these trials, the experimenter pretended to attach the band with a similar tug on the D-rings so that subjects could not tell whether the band was applied.

Individuals performed a few practice trials of reaching with and without an elastic band attached to the elbow before commencing the experimental trials. A break was permitted when requested by the subjects. Participants never reported fatigue.

Subject Instructions

Subjects were instructed in the main experimental task as follows: "Following my 'go' command, begin reaching when you are ready and then move the pointer as quickly as possible to the target while still being as accurate as possible. You should insert the pointer into the target without disturbing the target's position." It was emphasized that this was not a reaction time task. Participants were instructed to insert the pointer-tip to the depth marked by white tape (1.5-cm from its tip) placed on the cylinder. Subjects were instructed to attempt to perform all trials at the same speed and to hold their final position until receiving the command "Come back," after about three seconds.

Data Collection/Processing

Target and Pointer Position Calibration

Before the experimental trials, the positions of the four markers on the hand rigid body were recorded. In addition, two reflective markers embedded rigidly into a special calibration wand were recorded while the experimenter held the tip of the wand at the tip of the hand-held pointer used by subjects to point to the target in experimental trials. Knowing the distance along the calibration wand from its distal marker to its tip allowed determination of the instantaneous position of the pointer-tip during reaches by locating the two wand markers in the local coordinate system of the hand on the calibration trial and reconstructing them from the hand rigid body during the dynamic reaching trials. In addition, at the conclusion of each experimental session, the position of the cylindrical target (2.54-cm diameter, 5.08-cm wide) was determined by holding the tip of the same calibration wand at the center of the target and recording the position of its two reflective markers in global space. Knowing the distance from the distal marker to the tip and the positions of the two calibration wand markers allowed determination of the center of the target.

Movement Kinematics

An eight-camera Vicon MX-13 motion-measurement system (Vicon, Oxford Metrics), sampling at a frequency of 120-Hz, was used to collect movement of rigid bodies, composed of four reflective markers, attached to the upper trunk, between the neck and acromion, upper arm, forearm, and hand and individual markers placed at approximate joint locations (clavicular, shoulder, elbow, and wrist) and on the pointer. The cameras were spatially calibrated to the volume of the experiment before each

data collection. In addition two reflective markers were attached at both ends of the Thera-Band to estimate band excursion during the perturbed reaching trials.

One static calibration trial was recorded with the arm extended forward before the experiment (see Figure 1, Tseng et al., 2002). The arm was facing forward from the shoulder, with the upper arm, forearm, and hand aligned and held parallel to the floor with the thumb pointing upward. In this position, the arm was parallel to the global y -axis and perpendicular to the global x - and z -axes. All joint angles were defined as zero in this position (see below). The positive axes of each joint coordinate system in this position pointed laterally (x -axis), forward (y -axis), and vertically upward (z -axis).

Identifying Movement Onset and Termination

Vicon Nexus 1.6.1 software was used to postprocess the kinematic data. First, the reflective markers were labeled and tracked automatically by the Nexus software. The three-dimensional marker locations were then saved and further processed with a customized Matlab program (version 7.1, Mathworks Inc., USA). Marker coordinates were low-pass filtered at 5-Hz with a bidirectional fourth-order Butterworth filter. The derivatives of the pointer-tip marker's x , y and z coordinates were obtained and the resultant velocity computed. From the resultant, the reach onset and termination were determined, respectively, as the sample values were the resultant velocity exceeded or fell below 5% of the peak value. All trials were examined for double-peaked velocity profiles, which were eliminated from further analysis. Very few trials had double peaked velocities.

Joint Angle Computation

Joint angles were calculated from the marker coordinates as follows: The rotation matrices required to take the markers of each rigid body at each sample of an experimental reaching trial into their static positions in the calibration trial were estimated (Soderkvist & Wedin, 1993). The product of these rotation matrices from adjacent segments was then obtained and used to extract Euler angles in Z-X-Y order. The result provided 10 degrees of freedom of joint motions: three at the clavicle/scapula (abduction-adduction about the z-axis; elevation-depression about the x-axis, and upward-downward rotation about the y-axis) and shoulder (horizontal abduction- adduction about the z-axis; flexion-extension about the x-axis, and internal-external rotation about the y-axis) and two at the elbow (flexion-extension about an axis oblique to the local coordinate system; forearm pronation-supination about the y-axis) and wrist (flexion-extension about the z-axis; abduction-adduction about the x-axis). The Rodrigues' rotation formula was used to rotate the elbow flexion- extension axes from the x-axis of the global coordinate frame to the axis defined between the medial and lateral epicondyle markers of the humerus.

Motor Equivalence Analysis Based on Kinematics:

Step 1—Geometric Model and Kinematically Defined Jacobian Matrices

The Jacobian matrices were computed as the partial derivatives of the geometric model relating changes in joint angles to changes in either the pointer-tip position or the pointer orientation, i.e., $\Delta x = J(\theta^{\text{N-PERT}}) \Delta\theta$. Details of the method can be obtained from previous publications (Mattos et al., 2011; Scholz et al., 2011; Scholz & Schoner, 1999). The kinematic data were aligned based on the EMG events before computing the Jacobian matrices or performing the motor equivalence analyses.

Step 2—Motor Equivalence Analysis

For each kinematic sample of each trial of the PERT condition, aligned based on the EMG events, $\Delta\theta = \theta_0^{\text{N-PERT}} - \theta_i^{\text{PERT}}$ was computed, where $\theta_0^{\text{N-PERT}}$ is the joint configuration averaged across trials of the N-PERT condition and θ_i^{PERT} is the joint configuration for the i^{th} trial of the PERT condition. $\Delta\theta$ was then projected into the null-space of the Jacobian computed based on the N-PERT trials and the lengths of projection were computed within (ME component) and orthogonal to (Non-ME component) the null space. The average of the components across trials was computed for statistical analyses.

Electromyography (EMG)

Surface EMG signals were collected at 1080-Hz using a 16-channel wireless Aurion Zerowire EMG Telemetry system (Aurion Inc., Milan, Italy). The system transmits data from the EMG wireless modules (16-bit resolution, High pass filter: 10 Hz, Low-pass filter: 1 KHz) directly to a receiver unit. Self-adhesive Ag/AgCl electrodes (rounded rectangle shape, size 1 × 2 cm) were snapped to the EMG modules and attached parallel to the bellies of the following fifteen muscles on the right side of the body: superior trapezius (STRA), anterior deltoid (ADEL), medial deltoid (MDEL), posterior deltoid (PDEL), pectoralis major (PECT), biceps long head (BICP), brachialis (BRCH), triceps lateral head (LATR), triceps long head (LGTR), triceps medial head (MTRI), brachioradialis (BRRA), flexor carpi radialis (FCRA), flexor carpi ulnaris (FCUL), extensor carpi radialis (ECRA), and the extensor carpi ulnaris (ECUL). For each muscle, electrode placement was determined using standard placement locations and then confirmed by checking the EMG response when asking

subjects to perform related movements as well as isometric contractions. The interelectrode distance was 20-mm. The skin was cleansed with isopropyl alcohol and, if necessary, shaved with a medical razor. Each electrode's preamplifier was fastened using double-sided adhesive tape, and covered with cover-roll adhesive stretch tape. The upper arm and lower arm were bound with Coban self-adhesive wrap to secure the EMGs to the limb.

Initial EMG Processing

The raw EMG signals for MVC, mode estimation, and experimental reaching trials were band-pass filtered between 60-Hz to 350-Hz and then rectified and low-pass filtered at 30-Hz. The average baseline EMG values were computed before the beginning of each trial and subtracted from EMG activities for the entire trial. Then, the peak of two maximal voluntary contractions MVC trials for each muscle (see below) was used to normalize the EMG signals from the mode estimation and experimental reaching trials. All EMG signals for the experimental reaching trials were then integrated over 9 samples ($IEMG_{NORM}$) to equate the EMG sampling rate with the kinematic sampling rate.

Maximum Isometric Contractions (MVCs)

At the beginning of the data collection session, participants were asked to attempt performance of maximal voluntary movements against the resistance of the experimenter in appropriate directions to activate the recorded muscles. Participants were asked to attempt movement in each direction twice. The peak values of the filtered and rectified EMG signals were determined for each trial during the initial isometric portion of the trials (subjects often eventually overcame the isometric

resistance and moved slightly) with a customized Matlab program and the highest peak was subsequently used for normalization of the EMG data.

Motor Equivalence Analysis Based on EMG:

Step 1—Defining Muscle Modes (M-Modes)

The integrated, normalized EMG ($IEMG_{NORM}$) of two mode-estimation trials were used to provide a more general determination of the mode structure of the arm EMGs to be applied to the actual experimental trials. The EMGs from the two trials were concatenated, and then submitted to a principal component analysis (PCA) based on the muscle EMG correlation matrix, with Varimax rotation and factor extraction. The PCA was performed using the SPSS (IBM SPSS Statistics 19). PCA finds a set of mutually orthogonal components, each composed of linear combinations of each of the original factors (in this case, EMGs). The contribution of a given muscle to a principal component is referred to as the “loading” of that component. Those PCs, which contributed significantly to capturing the variance of the original dataset, were subsequently rotated using Varimax procedure. This procedure attempts to find a coordinate system rotation, which increases the large loadings and decreases the small loadings for any given component. PCA was used for this analysis instead of the frequently used NMF procedure because the results of NMF are nonorthogonal vectors, making computing variance per DOF impossible due to invalidation of the Pythagoras theorem for nonorthogonal subspaces.

Five principal components (PC's) were extracted for all subjects based on the criterion that all PCs had at least one muscle loading with absolute magnitude greater than 0.5. The average across subjects variance accounted for by the five M-modes was $76.28 \pm 3.25\%$. After the M-mode vector (matrix size = 5 PC's by 15 muscles) was

defined for each subject, the $IEMG_{NORM}$ data for each trial of the PERT and N-PERT conditions was converted into the M-mode space.

Step 2—Defining EMG Onsets

For each trial of each condition of a subject's data, EMG onset was determined as the sample value where the sum of the nonintegrated EMG_{NORM} , $\sum_{muscle=1}^{15} EMG_{NORM}$, across muscles deviated from the baseline value based on visual inspection (Figure 3.2, top panel). The sum over muscles was used because it resulted in a clearer determination of the onset compared with the EMG_{NORM} of individual muscles. Once the EMG onset was determined for each trial of both conditions, the trials were aligned at this sample value and cut so that the number of samples before EMG onset was consistent across trials, based on the trial with the fewest samples from data collection onset until the EMG onset. Likewise, the number of samples post-EMG onset was determined based on the trial with the fewest number of samples from EMG onset until the end of the trial, determined kinematically (i.e., 5% of peak resultant velocity of the pointer-tip).

Step 3—Defining Perturbation Onsets for Trials of PERT Condition

Perturbation onsets were based on the sum of the three triceps' heads, because this muscle showed the clearest change in response to the elastic perturbation of the elbow. Then, $\sum_{triceps=1}^3 EMG_{NORM}$ for a given trial of the PERT condition was superimposed on $\sum_{trial=1}^N \sum_{triceps=1}^3 EMG_{NORM} / N$ of the N-PERT condition, and the perturbation onset was chosen as the sample value where the value for the PERT trial

deviated upward from the average triceps activity of the N-PERT condition (Figure 3.2, bottom panel). This was confirmed by reference to the deviation of the elbow angle (Figure 3.2, middle panel).

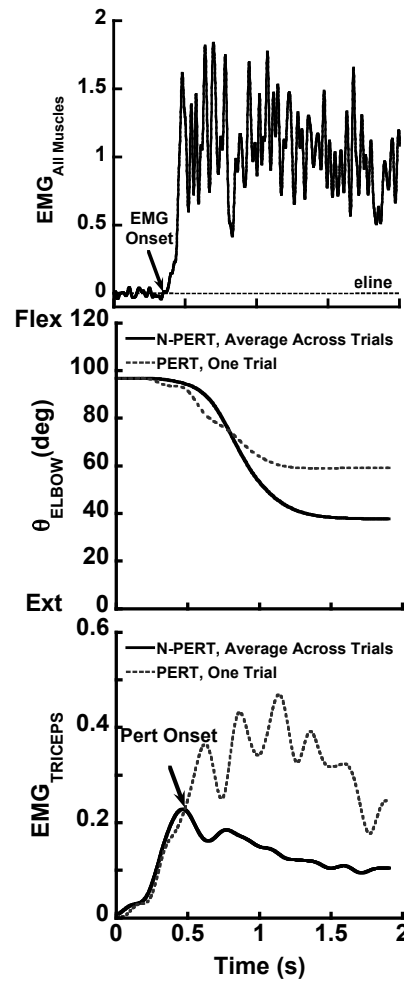


Figure 3.2 Illustration of methods to determine (top panel) EMG onsets for a given trial of both conditions and (middle and lower panels) the time of onset of a perturbation for a given trial of the PERT condition. $EMG_{All\ Muscles}$ in the top panel is the sum of the rectified, filtered and normalized EMGs of all measured arm muscles for a given trial. $EMG_{TRICEPS}$ is the sum of rectified, filtered and normalized the EMGs for a given PERT trial and the average of this sum across trials for the N-PERT condition.

Step 4 - Estimating Jacobian for Nonperturbed Trials Relating Changes in M-modes to Changes in Pointer Position or Pointer Orientation.

A Jacobian- like matrix for M-modes was estimated, similar to the Jacobian for kinematics (see below), by multiple linear regression analysis without the intercept, with the five M-modes as the independent variables and each of the three dimensions of pointer position and orientation as the dependent variables, e.g.,

$$\begin{aligned}
 P_x &= b_{x1} Mmode_1 + b_{x2} Mmode_2 + \dots + b_{x5} Mmode_5 \\
 P_y &= b_{y1} Mmode_1 + b_{y2} Mmode_2 + \dots + b_{y5} Mmode_5 \\
 P_z &= b_{z1} Mmode_1 + b_{z2} Mmode_2 + \dots + b_{z5} Mmode_5
 \end{aligned}
 \tag{3.1}$$

$$J_{position} = \begin{bmatrix} b_{x1} & b_{x2} & b_{x3} & b_{x4} & b_{x5} \\ b_{y1} & b_{y2} & b_{y3} & b_{y4} & b_{y5} \\ b_{z1} & b_{z2} & b_{z3} & b_{z4} & b_{z5} \end{bmatrix}
 \tag{3.2}$$

Where, P is the pointer-tip position with x, y, z-coordinates and b_{ij} are the unstandardized coefficients of the multiple regression analysis. The regression for orientation produces a similar Jacobian with M-mode changes related to the yaw, pitch and roll axes of pointer orientation. To increase the number of data points for the regressions, Jacobians were computed using consecutive 15 data samples across all trials of the N-PERT condition. Fifteen samples were chosen based on an evaluation of how changes in the number of samples used in the regression from as few as 6 to as many as 18 affected the b-values and their significance. Regressions with fewer than

15 samples resulted in noticeable changes in the b-values as additional samples were added. After 15 samples, a stable result was achieved.

The model evaluated, then, was $\Delta x = \underline{J}(\overline{muscle - mode}^{N-PERT}) * \Delta M\text{-mode}$, where Δx is the change in either the position or orientation variables, J is the Jacobian based on coefficients of the regression analysis, and $\Delta M\text{-modes}$ is the difference between perturbed and nonperturbed M-modes. Both the Jacobian $\Delta M\text{-modes}$ were computed at identical time points before and after the perturbation.

Step 5 - Computing Motor Equivalence.

The motor equivalence analysis asked how much of the change that occurred in the configuration of five M-modes when the perturbation was applied compared with the N-PERT condition was consistent with the same pointer-tip position or pointer orientation that occurred on the N-PERT trials. At each of the aligned data samples, the M-mode configuration for each trial of the PERT condition was subtracted from the mean across trials M-mode configuration of the N-PERT condition. This $\Delta M\text{-mode}$ configuration was then projected into the null-space of the EMG Jacobians for position and for orientation, based on the N-PERT trials as described above. Because the Jacobians were computed across 15 samples, the $\Delta M\text{-mode}$ configuration for every sample of 15 consecutive samples was projected into null space of the same Jacobian. The length of projection in the null space (ME component) provides an estimate of the extent to which the M-mode deviation was a reflection of flexible combinations of the 5 M-modes used to keep the pointer position or pointer orientation consistent in the PERT trials with its position or orientation for the N-PERT trials. The length of projection orthogonal to the null space (Non-ME component) reflected the extent to which the difference in the 5 M-modes between the

PERT and N-PERT conditions led to a change in the pointer position or pointer orientation. The mean across trials of the ME and Non-ME components for each subject was then computed for statistical analysis.

The goal of this analysis, then, was to identify whether the perturbation would change significantly the scaling of the M-modes so that they were no longer consistent with the nonperturbed Jacobian. If that were the case, a large nonmotor equivalent projection would be obtained. Alternatively, if the change in scaling induced by the perturbation reflected in the difference in perturbed and nonperturbed M-modes, then the projection of that difference would lie mainly in the UCM of the nonperturbed trials. Although the perturbation will affect the individual muscle activations, especially at the elbow, changing the scaling of the five M-modes, that change can be such that they tend to preserve the mean end-effector position or hand orientation or both, obtained on nonperturbed trials or could lead to very different end-effector positions or hand orientations. The only way to address this question is to reference the perturbed M-modes to the nonperturbed M-modes and how this difference relates to the nonperturbed Jacobian. The nonperturbed Jacobian used in the analysis is not affected by the position-dependent force field.

For both the EMG and kinematic analyses of motor equivalence, the projections were normalized by the square root of the subspace dimension. For example, for the analysis relating changes in five M-modes to changes in the 3D pointer-tip position, the orthogonal subspace in which changes of the pointer-tip position occur is three-dimensional whereas the null-space has two dimensions (5–3). Therefore, the ME component is the null-space projection divided by the square root of 2 while the Non-ME component is the orthogonal subspace projection divided by

the square root of 3. For the kinematic analysis, the orthogonal projection was normalized by the square root of 3 while the null-space projection was normalized by the square root of 7 (10–3).

Experimental Variables

Changes in the motor equivalence and nonmotor equivalence as a result of the perturbation were studied. In addition, two additional variables were investigated to help interpretation of the motor equivalence results.

Movement Time

Movement time was computed as the time between movement onset and termination, as defined above.

Variability of Pointer Position and Orientation.

Deviations of the pointer position at movement termination relative to the calibrated target position (x-, y-, z-coordinates) were obtained, and constant errors (CE) and variable errors (VE) were computed. Variable errors of pointer orientation, across repetitions, were also computed at movement termination.

Index of Cocontraction

A possible source of motor equivalent effects (i.e., ME > Non-ME) could be a selective increase in cocontraction on PERT trials compared with N-PERT trials. To test this, an index of cocontraction (iCC) between the elbow flexors and elbow extensors was computed for both conditions based on Rudolph et al. (2001):

$$iCC = \frac{EMG_{MIN}}{EMG_{MAX}} (EMG_{MIN} + EMG_{MAX}) \quad (3.3)$$

Where, EMG_{MIN} = level of activity in the less active muscle, EMG_{MAX} = level of activity in the more active muscle (to avoid division by zero errors). This index takes into account both the relative activation between elbow flexors and extensors as well as the magnitude of that activity.

Statistical Analysis

All statistical analyses were performed with SPSS (IBM SPSS Statistics 19). A $p < .5$ was considered statistically significant for all analysis.

One-way repeated-measures ANOVAs were used to test for differences between the N-PERT and PERT conditions for movement time and variability of the pointer position and orientation at movement termination.

Motor equivalence and iCC measures were averaged across four phases (1) before the perturbation onset (Pre-Pert), (2) from perturbation onset to 50-ms after the perturbation (Post-Pert 50), (3) from 51 to 100-ms postperturbation (Post-Pert 100) and (4) between 100-ms and 300-ms postperturbation (Post-Pert > 100). To evaluate motor equivalence both at the joint and muscle levels, three- way repeated-measures ANOVAs were performed with factors: 1) performance variable (3D position vs. 3D orientation), phase (Pre-Pert, Post-Pert50, Post- Pert100, and Post-Pert > 100), and component of projection (ME vs. Non-ME) of ΔM -mode or $\Delta\theta$.

Two way ANOVAs were performed to evaluate the effect of the condition (N-PERT vs. PERT) and phase (Pre-Pert, Post-Pert50, Post-Pert100, and Post- Pert > 100) on the index of cocontraction. Post hoc tests were performed using the M-matrix function in SPSS.

Before statistical analyses of motor equivalence, outliers (with values outside mean \pm 2 SDs) were replaced by the mean \pm 2 *SD*, depending on the direction of the deviation. This applied to only 6 of 160 values per data matrix (2 performance variables \times 4 phases \times 2 projection components \times 10 subjects). For all comparisons, if Mauchly's test of sphericity was significant, the Greenhouse-Geisser correction was used in the event that the significance with this correction differed from the standard statistics.

3.4 Results

Figure 3.3 illustrates the mean and standard deviation of changes of joint degrees-of-freedom affected by the elastic perturbation of the elbow during reaching trials. Only the six degrees-of-freedom showing a substantial effect are illustrated for simplicity. Note that the direction of effect of each joint differed with the perturbation.

Figure 3.4 illustrates time profiles of the averages across trials of the elbow angle (top row), linear envelopes of elbow flexor EMGs (second row), and elbow extensor EMGs (third row), and the five M-modes (bottom row) for the N-PERT (left column) and PERT (right column) condition of a representative participant. In trials of both conditions, there was a pronounced increase in the activity of the elbow flexor muscles at movement onset, likely related to lifting the forearm out of the trough used to stabilize the initial position. This was followed by a burst in the triceps to launch the hand to the target. For this subject, most of the contribution of the triceps activity came from activity of the medial head. Activity of other muscles (not shown) was somewhat more variable from trial to trial. The Thera-Band that was placed across the elbow joint provided a continuous perturbation during the reach during the PERT

condition (right columns), limiting elbow extension (Figure 3.4, top row) and leading to consistently higher triceps activity throughout the reach.

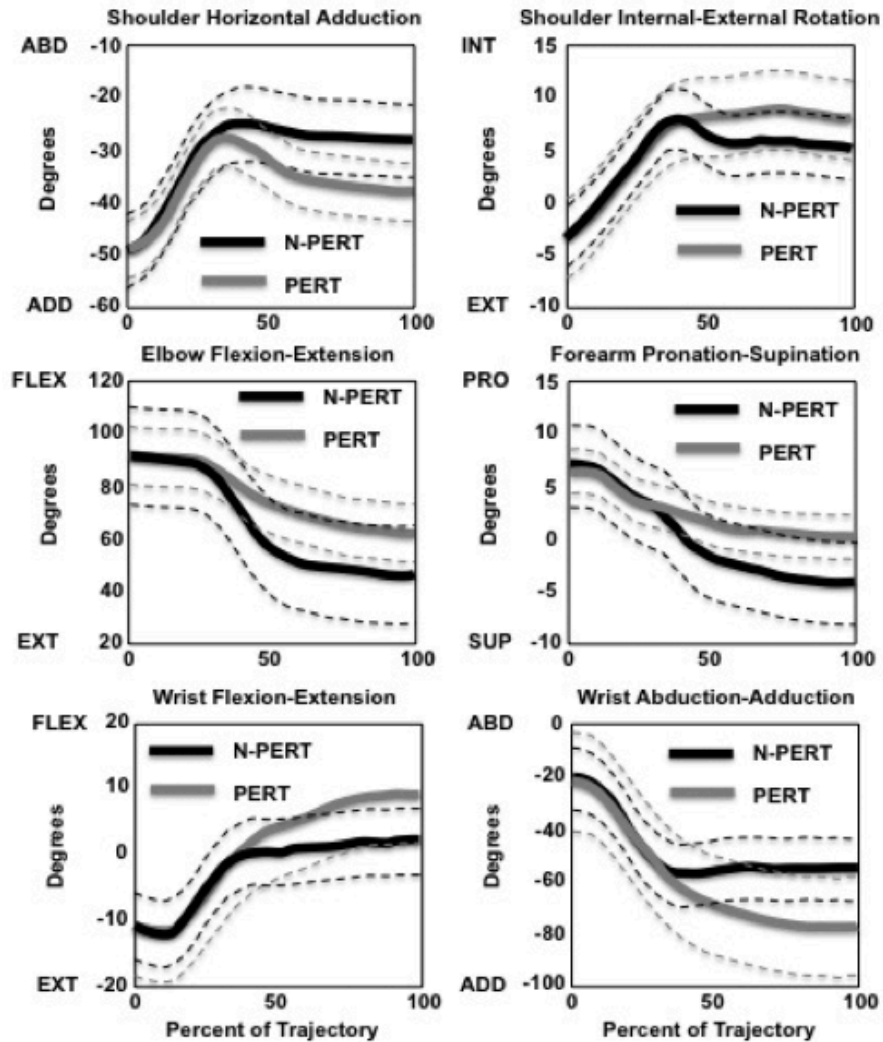


Figure 3.3 Illustration of displacements of arm joint degrees of freedom for a representative subject with (black lines) and without (gray lines) the perturbation applied to the elbow. Thick lines are the mean across reaches. Thin lines are one standard deviation. Four joint motions exhibited much smaller adjustments to the perturbation and are therefore not illustrated.

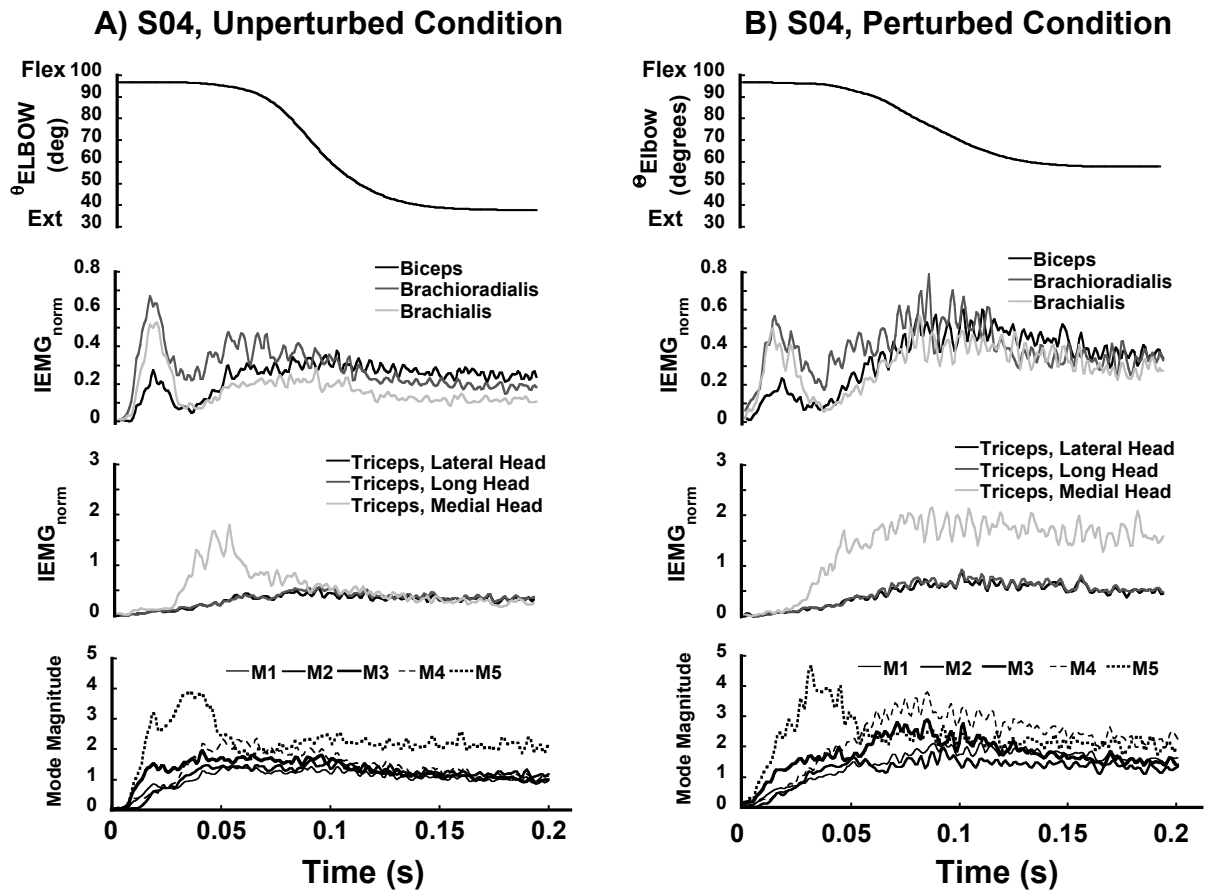


Figure 3.4 Example trajectories of elbow angle (top row), elbow flexors (2nd row), elbow extensors (3rd row) rectified, integrated and normalized to MVC EMG activities, and M-modes (last row) for N-PERT and PERT conditions. Data are averaged across trials of a representative subject after aligning trials based on EMG onsets.

Movement Time

The average ($\pm SEM$) of movement time was slightly lower for the N-PERT condition ($0.849\text{-s} \pm 0.029\text{-s}$) compared with the PERT condition ($0.898\text{-s} \pm 0.041\text{-s}$; $F_{1,9} = 5.13$; $p = .05$).

Variability of Pointer-Tip Position and Orientation at Movement Termination

Table 3.1 presents the average (\pm SEM) across-subjects variability of the pointer position and orientation at movement termination as well as the average (\pm SEM) constant error of targeting. Despite the perturbation being applied to the elbow, individuals were still able to complete the task with reasonable accuracy of the pointer position/orientation. The variable error of pointer position ($p > .64$) and pointer orientation ($p > .36$) did not differ between the PERT and N-PERT conditions, nor was there an interaction of condition by target coordinate (position, $p > .74$; orientation, $p > .95$). However, variable error differed among the three coordinate axes (position, $F_{2, 18} = 11.5$, $p < .01$; orientation, $F_{2, 18} = 18.3$, $p < .001$). For pointer position, variable error did not differ between the x and z-dimensions ($p > .78$), but both x ($F_{1,9} = 17.7$, $p < .01$) and z ($F_{1,9} = 14.1$, $p < .01$) dimensions had less variable error than did the y-dimension. Variable error of orientation was higher about the yaw (z: $F_{1,9} = 15.4$, $p < .01$) and pitch (y: $F_{1,9} = 24.6$, $p < .01$) axes than around the roll (x) axis, whereas variable error did not differ between the yaw and pitch axes ($p > .19$).

There was a significant effect of condition ($F_{1, 9} = 57.5$, $p < .001$) for constant error of the pointer position. Constant error was higher for the PERT compared with the N-PERT condition (Table 3.1). That is, the terminal distance between the pointer tip and target did differ between perturbed and nonperturbed conditions, although this difference is quite small, less than 1.7-cm. There also was a main effect of target coordinate ($F_{2, 18} = 18.0$, $p < .001$), but no significant interaction between condition and coordinate ($p > .06$). Constant error was substantially higher along the y-dimension than either the x ($F_{1, 9} = 22.7$, $p < .01$) or z ($F_{1, 9} = 26.0$, $p < .001$) dimensions but did not differ between the x and z dimensions ($p > .08$).

Table 3.1 Average \pm SEM variable and constant error of pointer position at movement termination.

| Performance Variable | | Variable Error | | Constant Error | |
|-----------------------|-----------|------------------|------------------|-------------------|-------------------|
| | | N-PERT | PERT | N-PERT | PERT |
| Position (mm) | x-axis | 3.81 \pm 0.316 | 3.78 \pm 0.301 | 1.36 \pm 1.53 | -2.16 \pm 1.53 |
| | y-axis | 4.88 \pm 0.548 | 5.09 \pm 0.379 | -11.79 \pm 3.05 | -17.53 \pm 2.84 |
| | z-axis | 3.59 \pm 0.321 | 3.85 \pm 0.394 | -2.57 \pm 2.94 | -6.90 \pm 2.86 |
| Orientation (degrees) | Yaw (z) | 7.03 \pm 0.905 | 6.46 \pm 0.910 | | |
| | Roll (x) | 3.85 \pm 0.698 | 3.43 \pm 0.647 | | |
| | Pitch (y) | 7.38 \pm 0.907 | 6.92 \pm 0.829 | | |

Yaw = rotation about the z-axis; roll = rotation about the x-axis; pitch: rotation about the y-axis.

M-mode Identification

Five M-modes were identified for all subjects. Typical time profiles for the M-modes are illustrated in the bottom row of plots in Figure 3.4. The linear regressions used to estimate how variation of the five M-modes affected pointer position or pointer orientation, the estimated Jacobian matrices, yielded, on average across subjects, adjusted R^2 values of 0.887 ± 0.019 and 0.825 ± 0.052 , respectively. Each of the individual M-modes was a significant predictor of both orientation and position for each subject in more than 50% of the movement trajectory with the exception of a total of ten cases out of 100 (six cases for position and four cases for orientation).

Three examples of the structure of M-mode vectors are illustrated in Table 3.2. Six of ten subjects had very similar muscle contributions to M-modes 1 and 2, as illustrated by S01 and S10. However, the muscle contributions to M-modes 3–5 could vary quite a bit across subjects, as also illustrated by these two examples. Subject S03 provides an example of one of the four subjects exhibiting a different M-mode organization. In this case, the variance explained was more evenly distributed across M-modes, with M-mode 1 being more similar to M-mode 2 of S01 and S10, while and the triceps heads loaded most strongly on M-mode 4 instead of M-mode 1.

Table 3.2 Example mode structure for two (S01 & S10) of the six subjects who had very similar muscle contributions (loading > 0.5) to the first two modes, but who could have very different muscle contributions to the other three modes. A third subject (S03) exhibited two modes (Mode 1 & Mode 4) similar to modes 2 and 1 respectively for the six similar subjects, although the percent of variance accounted for by the mode related to elbow extensor activation accounted for less of the total variance.

| Muscles | S01 | | | | | S10 | | | | |
|---------|---------------|---------------|---------------|---------------|---------------|---------------|---------------|---------------|---------------|---------------|
| | M1 | M2 | M3 | M4 | M5 | M1 | M2 | M3 | M4 | M5 |
| ADEL | 0.225 | 0.024 | 0.868 | 0.022 | 0.016 | -0.131 | 0.446 | 0.719 | -0.094 | 0.063 |
| MDEL | 0.654 | 0.023 | 0.631 | 0.099 | 0.016 | 0.030 | -0.096 | 0.850 | 0.275 | 0.032 |
| PDEL | 0.630 | 0.257 | 0.237 | -0.020 | 0.068 | 0.222 | -0.514 | 0.547 | 0.414 | 0.083 |
| PECT | 0.191 | 0.001 | 0.804 | 0.082 | 0.177 | -0.037 | 0.752 | 0.103 | -0.063 | 0.140 |
| STRA | -0.101 | 0.587 | 0.487 | -0.331 | -0.038 | 0.269 | 0.305 | 0.628 | -0.179 | -0.093 |
| BICP | 0.316 | 0.781 | 0.281 | 0.063 | 0.107 | 0.834 | 0.171 | 0.003 | 0.005 | -0.004 |
| BRRA | 0.028 | 0.802 | -0.022 | 0.340 | 0.199 | 0.798 | -0.112 | 0.186 | -0.088 | 0.212 |
| BRCH | 0.136 | 0.868 | -0.220 | 0.156 | -0.068 | 0.880 | -0.073 | -0.014 | -0.031 | -0.013 |
| LATR | 0.878 | 0.091 | 0.264 | 0.027 | -0.029 | 0.305 | -0.374 | 0.379 | 0.680 | 0.035 |
| LGTR | 0.832 | 0.115 | 0.351 | 0.036 | 0.071 | 0.051 | 0.120 | -0.005 | 0.881 | -0.159 |
| MTRI | 0.808 | -0.017 | -0.168 | -0.056 | -0.013 | -0.239 | 0.019 | -0.011 | 0.736 | 0.015 |
| FCRA | 0.008 | 0.120 | 0.060 | 0.936 | -0.118 | 0.160 | -0.056 | -0.035 | -0.113 | 0.907 |
| FCUL | -0.023 | 0.174 | 0.039 | 0.937 | 0.106 | -0.077 | 0.399 | 0.073 | 0.014 | 0.835 |
| ECRA | 0.183 | -0.021 | 0.039 | -0.002 | 0.908 | 0.599 | 0.557 | 0.109 | 0.164 | -0.107 |
| ECUL | -0.130 | 0.150 | 0.117 | -0.004 | 0.856 | 0.116 | 0.745 | 0.082 | 0.068 | 0.099 |
| %Var | 21.400 | 16.700 | 16.400 | 13.500 | 11.200 | 18.700 | 15.700 | 14.300 | 14.200 | 11.000 |

| Muscles | S03 | | | | |
|---------|---------------|---------------|---------------|---------------|---------------|
| | M1 | M2 | M3 | M4 | M5 |
| ADEL | 0.342 | -0.239 | 0.249 | -0.078 | 0.729 |
| MDEL | 0.845 | -0.285 | 0.068 | -0.036 | 0.123 |
| PDEL | 0.762 | 0.034 | -0.171 | 0.168 | 0.035 |
| PECT | -0.274 | 0.050 | 0.193 | 0.008 | 0.724 |
| STRA | 0.172 | 0.301 | -0.156 | 0.274 | 0.674 |
| BICP | 0.215 | 0.605 | 0.318 | 0.205 | 0.208 |
| BRRA | -0.056 | 0.781 | -0.182 | 0.037 | -0.037 |
| BRCH | 0.128 | 0.871 | 0.104 | 0.085 | 0.020 |
| LATR | 0.903 | 0.057 | 0.136 | 0.137 | -0.047 |
| LGTR | 0.769 | 0.336 | 0.228 | 0.077 | 0.139 |
| MTRI | 0.663 | 0.338 | 0.125 | -0.107 | -0.078 |
| FCRA | 0.100 | 0.141 | 0.896 | 0.017 | 0.092 |
| FCUL | 0.064 | -0.089 | 0.878 | 0.148 | 0.112 |
| ECRA | 0.111 | 0.040 | 0.080 | 0.925 | 0.060 |
| ECUL | 0.034 | 0.166 | 0.094 | 0.942 | 0.049 |
| %Var | 23.000 | 15.000 | 13.200 | 13.100 | 10.800 |

ADEL, MDEL & PDEL are the anterior, middle and posterior deltoids; PECT = pectoralis major; STRA = superior trapezius; BICP = biceps brachii; BRRA = brachioradialis; BRCH = brachialis; LATR, LGTR and MTRI are the lateral, long head and medial triceps; FCRA and FCUL are the wrist flexors, radialis and ulnaris, and ECRA and ECUL are the wrist extensors, radialis and ulnaris. Var = variance.

Table 3.3 presents the cosine of the angle (dot product) between corresponding M-mode vectors for S01 and all other subjects. M-mode 1 explained the most of the variance in EMG activity, whereas M-mode 2 explained the next highest amount of variance, etc., for all subjects. Note that S01, S04, S05, S08, S09 and S10 had the most similar EMG contribution to M-modes 1 and 2 (dot product close to 1.0), but could differ strongly for the other modes.

Table 3.3 The dot product between mode vectors (M1-5) for S01 paired with each of the remaining subjects.

| Subject | Reference S01 | | | | |
|---------|---------------|---------|-------|--------|--------|
| | M1 | M2 | M3 | M4 | M5 |
| S02 | 0.8542 | -0.0769 | 0.008 | 0.089 | 0.2737 |
| S03 | 0.2387 | 0.0735 | 0.780 | -0.023 | 0.0208 |
| S04 | 0.9181 | 0.8865 | 0.789 | -0.238 | 0.0340 |
| S05 | 0.9380 | 0.9227 | 0.266 | -0.059 | 0.0193 |
| S06 | 0.8590 | 0.0972 | 0.620 | 0.879 | 0.0287 |
| S07 | 0.7772 | 0.170 | 0.254 | 0.148 | 0.5146 |
| S08 | 0.8339 | 0.764 | 0.548 | 0.842 | 0.3416 |
| S09 | 0.9128 | 0.8114 | 0.866 | 0.069 | 0.0585 |
| S10 | 0.9332 | 0.8797 | 0.256 | 0.051 | 0.1462 |

Values closer to 1.0 indicate nearly identical mode vectors. Order of modes for all subjects is based on the order of percent of variance explained for that subject. Note that S01's mode structure was most similar to S04, S05, S08, S09 and S10 but only for the first two mode vectors.

Motor Equivalence: M-mode Space

In perturbed conditions, the deviation of M-mode variables was observed as early as 50-ms after the first visible changes in the EMG signals induced by the perturbation. These deviations were more pronounced in the ME component as compared with the Non-ME component, computed for both pointer- tip position and pointer orientation.

Figure 3.5 (top panels) depicts the projection components of Δ M-mode at different phases relative to the perturbation onset for 3D position (left panel) and 3D orientation (right panel) hypotheses. There was a significant effect of Projection Component ($F_{1,9} = 7.5, p < .05$), and an interaction between Projection Component and Phase ($F_{1,4,12.6} = 4.63, p < .05$; Greenhouse-Geisser adjustment). Post hoc tests using the M-matrix structure in SPSS revealed ME > Non-ME for all four time intervals, preperturbation, Post-Pert50, Post-Pert100, and for the remainder of the trial ($F_{1,9} > 5.68, p < .05$). There was a strong tendency for the ME component of the Δ M-mode projection to increase more than the Non-ME component between the preperturbation and Post-Pert50 phase ($F_{1,9} = 5.02, p = .052$). When comparing the preperturbation and the Post-Pert100 phases, ME increased significantly more than the Non-ME component ($F_{1,9} = 5.78, p < .05$). The ME and Non-ME components increased equally between the preperturbation and Post-Pert > 100 phases ($p > .12$). There were no other effects (all $p > .08$).

Motor Equivalence: Joint Configuration Space

Qualitatively similar results were seen in the joint configuration space: Deviations of the kinematic variables were particularly pronounced in the ME component, as compared with the Non-ME component, computed for both pointer-tip

position and pointer orientation. The projection components of $\Delta\theta$ at different phases relative to the perturbation onset for 3D position and 3D orientation hypothesis are illustrated in Figure 3.5, bottom panels. Analysis of the kinematic data revealed that all main effects and interactions were significant. The ME component of $\Delta\theta$ was greater than the Non-ME component for all phases ($F_{1,9} = 121.5, p < .001$). In contrast to the M-mode results, there was a significant three-way interaction of the performance variable (position vs. orientation), phase and projection component ($F_{1.44,12.98} = 4.87, p < .05$, Greenhouse- Geisser adjustment). This was due primarily to the fact that the difference between the ME and Non-ME components increased for later phases more when computed with respect to pointer orientation (Figure 3.5, lower right panel) than for pointer-tip position (Figure 3.5, lower left panel).

Index of Cocontraction

Cocontraction of muscles acting at the elbow joint increased throughout the course of the movement, but there were no major differences between the perturbed and unperturbed conditions. Figure 3.6 presents the index of cocontraction for both the PERT and N-PERT conditions. There was a main effect of the phase on the index of cocontraction ($F_{3,27} = 8.49; p < .05$), while the interaction between condition and phase approached significance ($F_{3,27} = 3.76, p = .054$) reflecting the tendency toward higher iCC index for the later phases under the PERT condition.

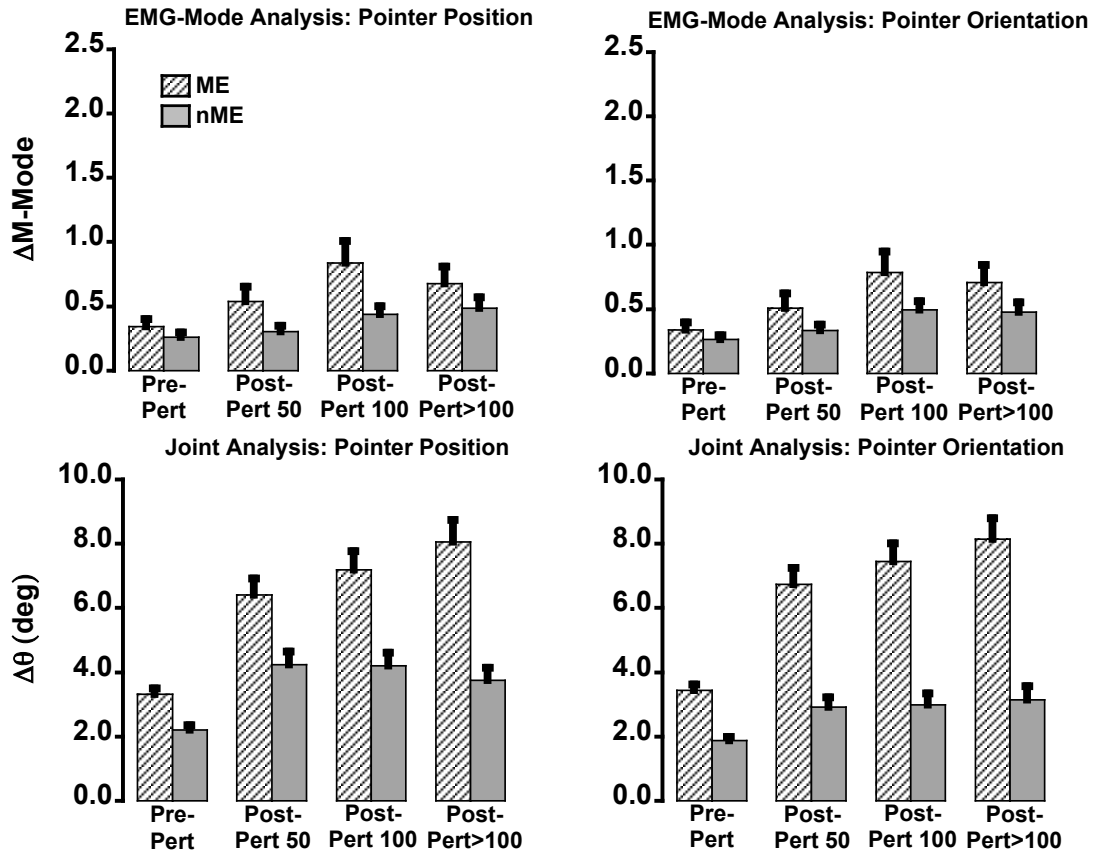


Figure 3.5 Motor equivalent (ME) and nonmotor equivalent (Non-ME) components of projections of (1) deviations of M-modes between PERT and N-PERT conditions (top row) and (2) deviations of the joint configurations between PERT and N-PERT conditions (lower row) related to stability of the pointer position (left column) and its orientation in 3D space (right column) for four phases of the reach.

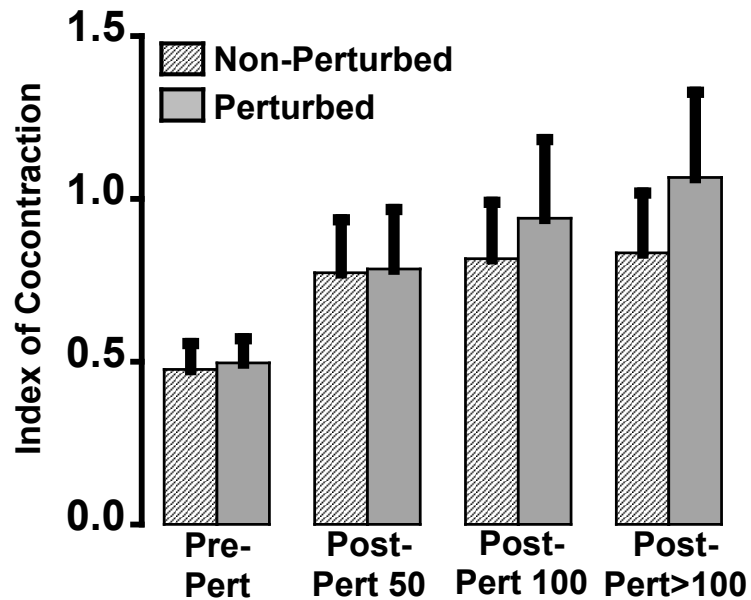


Figure 3.6 Average across subjects, \pm *SEM* of the index of cocontraction is illustrated for four phases of reaching for both the PERT and N-PERT conditions.

3.5 Discussion

The main result of the study is that unexpected perturbations during reaching movements produced muscle activation responses that had different magnitudes in two subspaces, motor equivalent and nonmotor equivalent. The differences between the magnitudes of the ME and Non-ME response components were seen as early as 50-ms after the first visible effects of the perturbation on muscle activations. The M-mode analysis is based on quantifying the coordinated electromyographic (EMG) activities of muscles across the arm. EMG is assumed to reflect changes in the neural drive to the motoneuron pools that innervate muscles. Thus, changes in M-mode magnitudes reflect coordinated changes in neural activation, due to local reflexes (40–60 ms postperturbation), preprogrammed reactions (~70–100 ms), or voluntary corrections (>100 ms). The observed differences between ME and non-ME components suggest

significant reflex and preprogrammed neural contributions to the previously reported results based on kinematic variables (Mattos et al., 2011).

Another hypothesis that stronger motor equivalence effects would be observed with respect to the pointer's spatial orientation was not confirmed at the level of muscle activation analysis, while it was confirmed by the analysis of the two components at the level of joint rotations. We also refuted the hypothesis that the early difference between the ME and Non-ME response was due to changes in muscle cocontraction. Implications of these results will be further discussed with respect to the general issue of motor equivalence, its importance for the scheme of control with muscle synergies, and the role of different factors for motor equivalence in space of different variables.

Motor Variance and Motor Equivalence

Two aspects of the motor behavior of redundant systems have been discussed recently (reviewed in Latash et al., 2007). The first aspect is related to the structure of motor variability estimated across repeated trials at the same motor task. The apparatus of the uncontrolled manifold (UCM) hypothesis (Scholz & Schoner, 1999) allows quantifying two components of variance within the redundant space of elemental variables. Figure 3.7A illustrates a typical data distribution across multiple trials at a task of producing a constant total output by two effectors ($E_1 + E_2 = C_{\text{TASK}}$). Contributions of each of the effectors were measured in individual trials and plotted in the state space of this simple system. Note that the cloud of data points is elongated along the line corresponding to perfect task performance (the UCM for this task). Variance along this line introduces no error into performance and may be addressed as “good” variance. Variance orthogonal to the line leads to errors in the sum ($E_1 + E_2$),

and may be called “bad” variance. Indices of synergies stabilizing the total output of systems similar to the one illustrated in Figure 3.7A have been quantified across populations, tasks and effector spaces as the relative amount of “good” variance in the total variance (reviewed in Latash et al., 2007).

The other aspect of motor behavior of such systems is related to the time evolution of the system during task performance. Imagine that the subject in the task $E_1 + E_2 = C_{TASK}$ tries to change the magnitude of C_{TASK} as a function of time. Figure 3.7B illustrates three possible trajectories that lead to transition of the system from a state corresponding to one value of $C_{TASK} = C_1$ to another state corresponding to $C_{TASK} = C_2$. One of the commonly used methods to compute trajectories of redundant systems is the so-called Moore-Penrose pseudo-inverse (Penrose, 1955; Whitney, 1969). This method computes a trajectory with the minimal sum of squared deviations of the elemental variables - shown in Figure 3.7B as the straight line from the initial state (S_0) to S_1 orthogonal to the UCM. This trajectory corresponds to zero motion of the system within the motor equivalent space and may be viewed as the most economical one. Two more trajectories are shown in Figure 3.7B leading from C_1 to C_2 . The second trajectory, S_0 to S_2 , has about equal displacements within the original UCM and orthogonal to the UCM. The third trajectory, S_0 to S_3 , shows a much larger component within the UCM (motor equivalent motion) as compared with the motion orthogonal to the UCM (range-motion).

Several earlier studies of joint kinematics during movement of redundant systems have shown significant motor equivalent components in trajectories of such systems, as well as self-motion related to changes in movement velocity (Scholz et al., 2011; Yang & Scholz, 2005; Yang et al., 2007). One of those studies showed also that

practice in an unusual force field leads to an increase in the relative amount of self-motion (Yang et al., 2007) - a counter-intuitive result suggesting that self-motion is not a by-product of the mechanical design of the human limbs, but a reflection of a purposeful neural strategy.

While many earlier studies explored the structure of variance in redundant systems (Danion et al., 2003; Domkin et al., 2002; Freitas et al., 2010; Kang, Shinohara, Zatsiorsky, & Latash, 2004; Krishnamoorthy et al., 2004; Latash et al., 2001; Latash, Scholz, Danion, et al., 2002; Park, Sun, Zatsiorsky, & Latash, 2011; Robert & Latash, 2008; Scholz & Schoner, 1999; Scholz et al., 2000; Wang, Asaka, Zatsiorsky, & Latash, 2006; Yang & Scholz, 2005; Zhang, Scholz, Zatsiorsky, & Latash, 2008), relatively few studies have explored the amount of motor equivalent motion and range-motion during natural movements and during responses to perturbations of such movements (Scholz et al., 2011; Yang & Scholz, 2005; Yang et al., 2007). Our current experiment quantified the amount of motor equivalent (ME, within the UCM) motion and Non-ME motion (range-motion) both before and immediately after an unexpected smooth mechanical perturbation. Using a spring-like resistance leads to smooth introduction of the perturbation over the movement time that allows to avoid phasic reflex and preprogrammed responses (Latash & Gottlieb, 1990). On the other hand, this method does not allow defining an exact time of the perturbation initiation. We used the earliest detectable deviations of the EMG signals from their pattern seen in averaged unperturbed trajectories as the time of effective perturbation initiation (see Experimental Procedure). Given that EMG responses are delayed as compared with the effective changes in peripheral receptor signals by a typical polysynaptic stretch reflex delay (about 40–50-ms), we feel safe to assume that

the changes observed within the Post-Pert50 time interval were of an involuntary nature. Indeed, this interval does not include times over 100-ms (shortest simple reaction time) after the estimated time when the perturbation produced perceivable changes in signals from peripheral receptors.

A major finding of the study is that the perturbation was associated with quick responses (deviations from unperturbed trajectories; Figure 3.5) in both muscle activation and kinematic spaces that were mostly confined to the ME subspace. Figure 3.7B illustrates a hypothetical trajectory between two values of the task variable and two possible reactions to a deviation from that trajectory induced by a perturbation. Reaction to the first deviation (solid line in Figure 3.7B) is directed to bring the trajectory back to its original path (in the space of elements), while the second reaction allows the trajectory to deviate substantially from the original path while still bringing it to the UCM corresponding to the next desired value of the performance variable (C_2). The latter solution would correspond to a larger relative amount of ME motion, and this is what we observed in the experiment. The relatively higher ME component, as compared with the Non-ME component, was seen immediately after the perturbation and the relative difference between the two showed a tendency to increase with time, particularly for the analysis in the joint angle space.

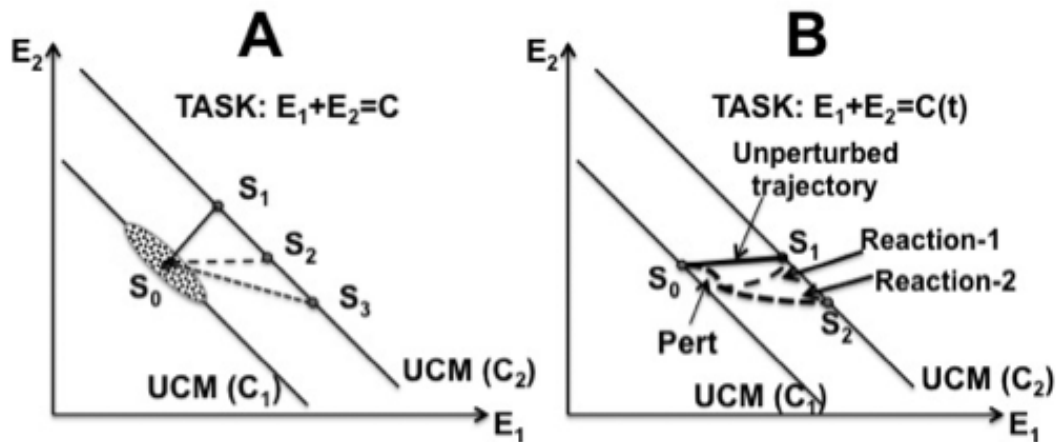


Figure 3.7 A: The ellipse shows a hypothetical data distribution across trials for the task of producing a constant total output by two effectors: $E_1 + E_2 = C$. Note the higher variance along the uncontrolled manifold (UCM) for the task as compared with variance orthogonal to the UCM. The task to change the magnitude of C (from C_1 to C_2) can be achieved with different amounts of motion along the UCM (motor equivalent motion), from minimal (from S_0 to S_1) to very large (from S_0 to S_3). B: If a preferred trajectory from S_0 to S_1 is perturbed (Pert), the corrective reaction may be directed toward the originally planned final state (Reaction-1) or to a state characterized by a larger amount of motion parallel to the UCM (Reaction-2 leading to S_2). We observed behavior corresponding to Reaction-2.

The difference between the ME and Non-ME components immediately following the onset of the perturbation, when defined in joint configuration space, can result both from coupling of joint rotations due to biomechanical factors (e.g., joint interaction torques), as well as neural control (Mattos et al., 2011). The very similar difference observed in the muscle activation space provides a strong argument for a significant neural contribution to this result. We considered two possible reactions to perturbations that could potentially contribute to the ME vs. Non-ME difference. The first is changing the amount of cocontraction within agonist-antagonist muscle groups

acting at individual joints. Cocontractions in the responses to unexpected perturbations have been reported in several studies (Latash, 2010a; Lewis, MacKinnon, Trumbower, & Perreault, 2010; Robert & Latash, 2008). Our analysis, however, failed to show significant changes in the cocontraction index during the first 100-ms following the identified time of the first muscle reaction to the perturbation. Note that the contrast between the ME and Non-ME components was seen during these time intervals in both joint configuration and muscle activation spaces. So, we view the cocontraction hypothesis as unlikely. An alternative is to assume that quick (reflex) muscle reactions to perturbations already show signs of a synergic organization directed at correcting errors in important performance variables (orthogonal to the corresponding UCMs) while allowing such errors to accumulate in the ME directions (within the UCM).

Several mechanisms have been offered to account for such reactions. Optimal feedback control (Todorov, 2004; Todorov & Jordan, 2002; Valero-Cuevas et al., 2009) predicts that corrective actions of the hypothetical neural controller would be directed at correcting deviations relevant for performance in the space of elemental variables, while ME deviations would be allowed to emerge. A similar prediction is made by schemes based on short-latency back-coupling loops (Latash et al., 2005), feed-forward synergic control (Goodman & Latash, 2006), and recent developments incorporating main ideas of the equilibrium-point hypothesis (Feldman, 1986, 2009) into the schemes for the neural control of multielement redundant systems (Latash, 2010c, 2012a; Martin et al., 2009). Currently, all these schemes make similar predictions with respect to predominance of ME trajectories in response to perturbations. Some of the schemes imply neural computations (Goodman & Latash, 2006; Todorov, 2004; Todorov & Jordan, 2002), while the rest are based on assuming

certain physical and physiological processes. Subjectively, we prefer the latter approach (Latash, 2010c, 2012a).

Multimuscle Synergies as Means of Building Motor Equivalent Solutions

The notion of muscle synergies has been interpreted in two ways. The first follows the traditional understanding of synergies as a number of elemental variables that change in parallel (Bernstein, 1967; Turvey, 1990). In the space of individual muscle activations as elemental variables, this definition leads to methods of synergy identification based on matrix factorization techniques such as principal component analysis and nonnegative matrix factorization (d'Avella & Bizzi, 2005; d'Avella et al., 2008; Ivanenko, Cappellini, Dominici, Poppele, & Lacquaniti, 2007; Saltiel et al., 2001). Application of such methods has allowed reducing the dimensionality of the original space of muscle activations to a lower-dimensional space of synergies. It has been shown that patterns of activation of large muscle groups during such tasks as standing, reacting to whole-body perturbations, walking and isometric force production can be represented using only a handful of variables (Ivanenko et al., 2007; Roh, Rymer, & Beer, 2012; Ting, 2007; Trumbower, Ravichandran, Krutky, & Perreault, 2010).

The alternative approach is based on a different definition of a synergy, namely a neural organization of elemental variables that stabilizes (reduces variance) a potentially important performance variable by covaried adjustments of the elemental variables (Latash et al., 2007). The existence of several elemental variables that show parallel changes is insufficient evidence to allow claiming that these variables are united into a synergy. Identification of muscle groups with parallel scaling of activation levels, even when their activities can be related to particular force (Roh et

al., 2012) or perturbation (Ting, 2007) directions as in the former understanding of synergies, represents only the first step in analysis of synergies according to the latter understanding. Such muscle groups are viewed as a lower-dimensional set of elemental variables (addressed as muscle-modes or M-modes), which are still redundant as compared with the sets of constraints associated with typical tasks. A number of studies, mostly using large muscle groups associated with whole-body actions, identified and quantified synergies stabilizing such variables as coordinates of the center of pressure and shear forces acting on the body of a standing person (Danna-Dos-Santos et al., 2008; Klous et al., 2011; Klous, Mikulic, & Latash, 2012; Krishnamoorthy, Latash, et al., 2003; Krishnamoorthy et al., 2004; Robert & Latash, 2008). Only a handful of studies applied the concept of multimuscle synergies in the latter meaning to arm actions (Krishnamoorthy et al., 2007).

In this study, we used the concept of multimuscle-mode synergies to explore possible causes of the predominantly motor equivalent deviations of joint trajectories in response to an unexpected perturbation reported earlier (Mattos et al., 2011). Indeed, it was possible that the perturbations produced joint deviations predominantly in the motor equivalent directions due to the mechanical joint coupling and effects of multijoint interaction in the specific joint configurations used in the study. It was important to explore whether motor equivalent deviations dominated in the muscle activation space. These effects could only be mediated by the central nervous system and would point at its important role in the organization of short-latency responses to perturbation in a redundant system. We did observe qualitatively similar results in the two spaces, those of M-modes and of individual joint rotations. This result

demonstrates that the specific trajectory deviations (predominantly motor equivalent or ME, see Reaction-2 in Figure 3.7B) are organized neurally.

Muscle synergies (in the meaning of multimuscule-mode synergies) may be viewed as the neural organizations that have three main purposes. First, the organization of muscles into groups (M-modes) reduces the dimensionality of neural variables. Second, covariation of M-mode activations in successive trials is organized to stabilize trajectory of important performance variables. Third, such muscle synergies are linked via short-latency loops to produce primarily motor equivalent deviations in cases of unexpected perturbations. The combination of the second and third purposes may be viewed as the means of ensuring stability of a multielement action. In this case, the word “stability” means both “low variance across trials” and “preserving trajectory of important variables under perturbations”.

Motor Equivalence in Different Spaces

The notion of motor equivalence was originally used by Bernstein (1967) in his classical studies of writing with an implement held by different effectors or attached to different body parts (reproduced later, Raibert, 1977). The term implied using variable sets of effectors (and, obviously, different muscle activation patterns) to achieve the same global goal. In general, the term does not necessarily imply motor redundancy. For example, different combinations of joint trajectories can accomplish the task of reaching to a target in two-dimensional space performed by a two-joint limb. If, however, not only the final state but also trajectory of important performance variables matters, motor redundancy becomes a necessary condition for having multiple motor equivalent solutions. Several studies have documented stabilization of the whole time profile of an important task-related variable by multijoint (multidigit)

synergies, even when only the final value of that variable was required by the task (Domkin, Laczko, Djupsjobacka, Jaric, & Latash, 2005; Domkin et al., 2002; Shim, Latash, & Zatsiorsky, 2003; Tseng et al., 2002; Tseng & Scholz, 2005a; Tseng et al., 2003).

Natural human movements may be viewed as being built on a control hierarchy involving several synergies. For example, multijoint reaching to a target may be viewed as built on a multijoint kinematic synergy; each joint's trajectory may be viewed as built on a multimuscle synergy, while each muscle's activation pattern may be viewed as built on a synergy of motor units (Latash et al., 2008; Latash et al., 2007). In our study, we considered two spaces of variables, those of joint rotations and those of muscle activations (reduced to M-modes). Motor equivalence was defined in both cases similarly, with respect to the end-effector position and orientation, both changing in time. The similarity of the effects of the perturbation on the relative amount of ME and Non-ME motions is not a trivial result. It suggests that muscle activations are organized into a synergy stabilizing not individual joint rotations but the endpoint trajectory. This result questions the aforementioned idea of a hierarchy of levels of synergies (Latash et al., 2008; Latash et al., 2007). It is more compatible with the view that motor elements at all levels of analysis are united into synergies stabilizing the ultimate task-related variables, not intermediate variables within the assumed hierarchy.

Chapter 4

MOTOR EQUIVALENCE DURING MULTI-FINGER ACCURATE FORCE PRODUCTION

4.1 Abstract

We explored stability of multi-finger cyclical accurate force production action by analysis of responses to small perturbations applied to one of the fingers and inter-cycle analysis of variance. Healthy subjects performed two versions of the cyclical task, with and without an explicit target. The “inverse piano” apparatus was used to lift/lower a finger by 1 cm over 0.5 s; the subjects were always instructed to perform the task as accurate as they could at all times. Deviations in the spaces of finger forces and modes (hypothetical commands to individual fingers) were quantified in directions that did not change total force (motor equivalent) and in directions that changed the total force (non-motor equivalent). Motor equivalent deviations started immediately with the perturbation and increased progressively with time. After a sequence of lifting–lowering perturbations leading to the initial conditions, motor equivalent deviations were dominating. These phenomena were less pronounced for analysis performed with respect to the total moment of force with respect to an axis parallel to the forearm/hand. Analysis of inter-cycle variance showed consistently higher variance in a subspace that did not change the total force as compared to the variance that affected total force. We interpret the results as reflections of task-specific stability of the redundant multi-finger system. Large motor equivalent deviations

suggest that reactions of the neuromotor system to a perturbation involve large changes in neural commands that do not affect salient performance variables, even during actions with the purpose to correct those salient variables. Consistency of the analyses of motor equivalence and variance analysis provides additional support for the idea of task-specific stability ensured at a neural level.

4.2 Introduction

Stability of human movements is one of their most crucial characteristics for success in changing and unpredictable external conditions. The problem of ensuring action stability is complicated by the fact that movements involve redundant sets of elements at any level of analysis (cf. motor redundancy, Bernstein, 1967). Recently, the problem of motor redundancy has been reformulated as motor abundance (Latash, 2012a). According to this view, the seemingly redundant sets of elemental variables (those produced by elements at a selected level of analysis) are allowed to vary as long as these variations are compatible with low variance (high stability) of a task-specific performance variable (Schoner, 1995). The introduction of the uncontrolled manifold (UCM) hypothesis (Scholz & Schoner, 1999) was an important step toward analyzing variance to learn about different levels of a motor control hierarchy. According to this hypothesis, a neural controller acts to limit variance at the level of elemental variables to a sub-space (UCM) within which performance variables specific to a task do not vary.

The UCM approach allows overcoming the problem of comparing elemental and performance variables expressed in different units by using a formal model that relates small changes in elemental variables with changes in performance variables,

the Jacobian matrix, \mathbf{J} (Latash et al., 2001; Scholz & Schoner, 1999). The UCM is commonly approximated by the null-space of \mathbf{J} . In contrast, the combinations of elemental variables along the orthogonal to the UCM space lead to errors in performance.

In this method, the inter-trial variability of elemental variables is analyzed within the UCM, V_{UCM} (“good variability”), and orthogonal to it, V_{ORT} (“bad variability”). If $V_{\text{UCM}} > V_{\text{ORT}}$, a conclusion is drawn that the performance variable is preferentially stabilized in the action. An extensive number of studies have demonstrated that purposeful movements lead to a structure of the trial-to-trial variability in the space of elemental variables ($V_{\text{UCM}} > V_{\text{ORT}}$) reflecting a family of goal-equivalent solutions used to solve a particular task (Latash et al., 2001; Li, Latash, & Zatsiorsky, 1998; Scholz et al., 2002; Scholz et al., 2000; Schoner, 1995).

One consequence of the motor abundance is the phenomenon of motor equivalence. This notion has been used in the field of movement studies for many years as the ability to accomplish the same task using different effectors (Wing, 2000) or with different contributions from a set of effectors (Hughes & Abbs, 1976; Kelso et al., 1984; Levin et al., 2003). A conceptual problem with this classical formulation is that in reality, the task level performance is never exactly identical under the different circumstances. Assessing motor equivalence thus requires comparing the amount of change at the task level with the amount of change at the level of elemental variables. Because these two levels have different metrics (e.g., distances in space for the task level, and joint angles at the elemental level), this comparison cannot be made directly. Similarly to the mentioned analysis of variance, the analysis of differences between the trajectories of task-specific performance variables when a motor task is

solved under different conditions must be based on a metric at the level of elemental variables. Jacobian \mathbf{J} linking the two levels can then be used to quantify components of trajectories that lead to a change in the performance variables and components that do not.

Recently, such an analysis of motor equivalence has been developed within the UCM hypothesis framework (Scholz et al., 2007; Schoner et al., 2008). In that analysis, unexpected movement perturbations were applied, and the deviations of elemental variables in the perturbed trials from the unperturbed movements were projected onto the corresponding UCM space and its orthogonal complement, ORT. Deviations within the UCM space are motor equivalent (ME) components, while deviations within the ORT are non-motor equivalent (nME). For instance, a perturbation that affects the position of the hand in space is expected to induce changes within the ORT subspace in the joint configuration space followed by corrective actions within ORT. Large ME deviations suggest that different joint configurations are used to achieve the same task performance.

Only a few previous experiments have tested the effects of perturbations using the described UCM-based approach (Scholz et al., 2007; Schoner et al., 2008). Motor equivalence was observed at the end of a reaching movement when comparing reaching at different speeds (Scholz et al., 2011). Because differences in movement speed disappear when the movement ends, the remaining difference between joint configurations within the UCM space reflected different solutions to the movement task at different speeds. In a subsequent reaching study, individuals were instructed to insert a pointer into spherical and cylindrical targets. At random trials their elbow joint extension was limited by an elastic band (Mattos, Kuhl, Scholz, & Latash, 2013;

Mattos et al., 2011). Most of the deviations in both joint configuration and muscle activation spaces during the perturbation were ME, starting immediately with the perturbation and lasting until the end of the movement. The cited studies analyzed ME and nME components when the perturbation was continuously applied to the moving effector. This made it difficult to decide if the observed reorganization of joint configurations was a consequence of the mechanical effect of the perturbation itself or reflected changes at the level of neural control of those movements.

A problem in assessing motor equivalence is distinguishing between ME components that are reflections of the direct, mechanical, effects of the perturbation and ME components that reflect a reorganization of the multi-degree-of-freedom movement at the neural control level. The main goal of this study was to address this problem by observing (1) how ME components evolve in time while a perturbation is held constant and (2) whether ME components persist after the perturbation is removed. ME components that persist after a perturbation has been removed reflect a change in the neural solution to the degree-of-freedom problem.

We used a cyclic multi-finger accurate force production task and the “inverse piano” device (Martin et al., 2011) that allows applying controlled perturbations in the course of task performance. The perturbation consisted of lifting by 1 cm and keeping elevated the middle fingerpad and then lowering it back to the pre-perturbation position. Each of the two phases led to immediate adjustments of all finger forces (Martin et al., 2011; Wilhelm et al., 2013) as well as to corrective actions that kept task performance accurate. Note that after the lifting-lowering sequence, the external conditions of the task returned to the pre-perturbation ones. The motor equivalence analysis was done at two time scales. The Micro-analysis involved time windows of

50 ms starting from the perturbation onset to 500 ms post-perturbation. This analysis was aimed at distinguishing corrections due to the action of various physiological mechanisms, from peripheral reactions of tissues to action of reflexes and reflex-like responses, and to voluntary corrections. The Macro-analysis explored steady states before, during and after the perturbation. After the perturbation, the observed ME vs. nME structure was hypothesized to reflect primarily changes in neural control. Overall, our main hypothesis was that strong ME components would be observed in all phases of the action reflecting the task-specific stability of the four-finger system with respect to total force. In addition, we used the more traditional UCM-based analysis of the two components of variance computed across cycles, V_{UCM} and V_{ORT} . The inequality $V_{UCM} > V_{ORT}$ was expected across conditions (Friedman et al., 2009; Latash et al., 2001).

4.3 Methods

Subjects

Eleven healthy adult subjects (8 males, 3 females), averaging 26.27 ± 5.29 years old, mass 69.39 ± 12.85 kg, height 1.72 ± 0.12 m took part of this study. All subjects were self-reported right hand dominant and had no history of any neurological or musculoskeletal disorder that could affect the upper arm. Subjects gave written informed consent as approved by the Office for Research Protection of the Pennsylvania State University.

Equipment

This experiment used the “inverse piano” device details in Martin et al. (2011) that consists of four unidirectional piezoelectric force transducers (208C01; PBC

Piezotronics Inc) individually connected to linear actuators (PS01-23x80; LinMot). Each sensor top was covered with sandpaper (300 grit) to increase the friction between the sensor and the fingertips. The sand paper also thermo-insulated the sensors from the body heat. The sensors were mounted within slots in a steel frame (140 x 90 mm), with 3-cm of distance between the centers of the sensors in the mediolateral direction, allowing for adjustments in the anterior-posterior direction as needed. The frame was attached to a wooden board (460 x 175 x 27 mm) to support the subject's arm. The signals from each sensor were sent through a DC-coupled signal conditioner (PCB) to a 16-bit analog-to-digital converter (CA-1000; National Instruments). A Labview-software (National Instruments) was developed to run the experiment, acquire, and record the force signals from individual fingers at 200 Hz, as well as to control the linear actuators through a controller (E-400-AT; LinMot). In addition, the customized Labview program recorded the timings of perturbation onset. See Figure 4.1 for a schematic representation of the experimental setup.

Experimental procedure

Subject position

Subjects sat on an adjustable chair in front of the table with their right forearm supported, facing a 19" monitor, placed 0.8 m away from the subject at the eye level. The monitor was used to provide visual feedback for the subjects. The right arm was at 60° of shoulder abduction, 120° of elbow flexion, hand pronated, and the wrist in neutral position. Foam paddings were placed under the subject's forearm and palm for comfort. Once the initial position was adjusted, the subject's forearm was fixed with

two Velcro straps to prevent changes in the elbow and shoulder joint angles throughout the trials.

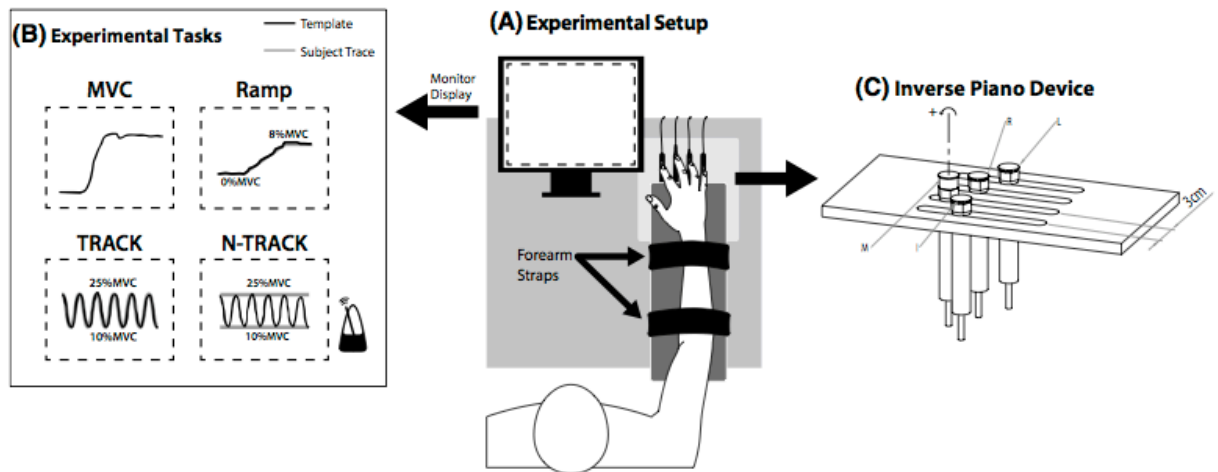


Figure 4.1 **a** A schematic of the experimental setup showing the subject's position and the sensor arrangement; **b** illustration of the feedback given to the subject on the monitor display. Signals for the maximum voluntary contraction (MVC), ramp force production, and cyclic force production with (TRACK) and without (N-TRACK) template are illustrated. A metronome paced the N-TRACK task; **c** schematic of force sensors mounted on linear motors. In the illustration, the ring force sensor is lifted. Moment arms with respect to mid-hand were 4.5, 1.5, -1.5 , and -4.5 cm for the index (I), middle (M), ring (R), and little (L) fingers, respectively. Counterclockwise rotation (+) around the axis represents pronation moment.

Experimental tasks

For all tasks, the subjects started each trial by placing all fingers on the top of the sensors and relaxing; the initial forces were set to zero, such that the sensors measured only the active downward forces. Finger pressing tasks using the index (I), middle (M), ring (R), and little (L) fingers were performed as follows.

Maximal voluntary contraction (MVC) task

Subjects were instructed to press on the sensors with all four fingers as hard as possible and reach maximal force within 6 s. Verbal encouragement as well as visual feedback on the total force was provided. Two trials, at least 30 s apart, were recorded per subject, and the trial with maximal peak force was selected. The MVC task was used to normalize the Ramp, Tracking and Non-Tracking Tasks (described below).

Ramp task

Subjects placed all the fingers on the sensors and tracked a ramp template with one finger at a time. The visual feedback on the force produced by the instructed finger (master-finger) was provided; however, the other three fingers (slave-fingers) also produced forces due to the phenomenon of enslaving (Danion et al., 2003; Zatsiorsky, Li, & Latash, 1998). The total duration of the ramp task was 8 s, which was divided in 3 parts: a horizontal line corresponding to 0% MVC for 2 s, an oblique line from 0 to 8% of MVC over 6 s, and another horizontal line corresponding to 8% of MVC for 2 s. After a few familiarization trials, two ramp trials were collected for each finger; the order of the fingers was randomized. This task was performed in two conditions: 1) all fingers at the same level; and 2) the middle finger lifted by 1 cm. The Ramp Task was used to estimate the enslaving index among fingers, and to compute finger modes (see later).

Tracking (TRACK) and non-tracking (N-TRACK) cyclic force production tasks

We explored two tasks involving and not involving an explicit force trajectory presented on the screen. The no-tracking task was expected to lead to higher nME

components across all comparisons as compared to the tracking task. In the TRACK task, subjects were instructed to track a sine-like signal changing between 10 and 25 % of each subject's MVC at 0.5 Hz with the cursor representing the current total force. The target was displayed on the monitor as a solid blue line. In the N-TRACK task, two horizontal lines were displayed on the monitor corresponding to 10 and 25 % of each individual's MVC. Subjects were instructed to produce smooth force oscillations in between the targets at 0.8 Hz controlled by audio beeps of a metronome, each beep representing half cycle. All subjects reported 0.8 Hz to be a comfortable frequency to perform this task. For both tasks, the total trial duration was 22 s. Each trial had two perturbations involving lifting (PT_{UP}) and lowering (PT_{DN}) of the M finger by 1 cm over 0.5 s. This manipulation increased and decreased the M finger force, respectively. The onset of PT_{UP} varied randomly between 6 and 10 s from the trial initiation, the M finger remained at the lifted position for 6 s, followed by PT_{DN} . Twenty-four trials were performed, with not less than 30-s interval between trials, and 2-min break after every six trials to avoid fatigue. Additional rest intervals were offered as needed. Subjects had 2–10 familiarization trials before data collection. Accurate total force production was emphasized at all times.

Data processing

The main outcome variables of this study were those of the motor equivalence and variance analyses described below. The UCM-based methods of analysis of inter-trial variance were used with finger forces and modes as elemental variables. As indicated by previous studies (Latash et al., 2001; Li, Latash, & Zatsiorsky, 1998) in multi-finger tasks, the total moment of force can be stabilized by the co-variation of

fingers forces (or modes) without being explicitly instructed by the task. Therefore, the analyses were performed with respect to both total force and moment of force.

Initial data processing

The digital signals were converted to force units, and force signals were filtered with a fourth-order, zero-lag Butterworth low-pass filter with a cutoff frequency of 5 Hz. The low cutoff frequency was used to eliminate the high-frequency noise caused by the motors during the perturbation. The frequency spectrum analysis showed that most of the power of the data was under 5 Hz. The total force was computed by summing the individual finger forces.

Enslaving matrix and finger modes

Finger forces during the oblique part of the Ramp Task were extracted. Linear regressions of the total force (F_{TOT}) produced by the four fingers against individual finger forces were used to estimate the 4 x 4 enslaving matrix, $[E]$, formed by the regression coefficients (k) for trials performed by each master finger, $i = (I, M, R, L)$:

$$F_{TOT} = k_{iI}\Delta f_I + k_{iM}\Delta f_M + k_{iR}\Delta f_R + k_{iL}\Delta f_L \quad (4.1)$$

$$[E] = \begin{bmatrix} k_{II} & k_{IM} & k_{IR} & k_{IL} \\ k_{MI} & k_{MM} & k_{MR} & k_{ML} \\ k_{RI} & k_{RM} & k_{RR} & k_{RL} \\ k_{LI} & k_{LM} & k_{LR} & k_{LL} \end{bmatrix} \quad (4.2)$$

The diagonal entries of the enslaving matrix represent the fraction of F_{TOT} produced by the master-finger, while the off-diagonal entries represent the fractions of F_{TOT} produced by the slave-fingers. The total amount of enslaving (EN) for each

subject was computed as the sum of the off-diagonal entries. The enslaving matrix was used to convert finger force data into finger modes:

$$\mathbf{m} = \mathbf{E}^{-1}\mathbf{f}, \quad (4.3)$$

where, \mathbf{f} is the 4×1 finger forces vector, and \mathbf{m} is the 4×1 finger mode vector. We performed further analysis in two spaces, \mathbf{f} and \mathbf{m} . Note that \mathbf{m} are hypothetical variables that, unlike forces, can be manipulated by the central nervous system one at a time (Danion et al., 2003).

Total moment of force

The total moment of force, M_{TOT} , produced by the fingers about the longitudinal axis of the forearm/hand was computed as follows:

$$M_{TOT} = d_I f_I + d_M f_M + d_R f_R + d_L f_L, \quad (4.4)$$

where d_i and f_i stand for the force and the lever arm for each finger i , respectively ($i = I, M, R, \text{ and } L$). As indicated in Figure 4.1, the force sensors were 3-cm apart; hence, $d_I = 4.5$ cm, $d_M = 1.5$ cm, $d_R = 1.5$ cm and $d_L = -4.5$ cm. Pronation and supination directions are represented by positive and negative signs, respectively. The moment estimation assumed no change in the point of application of the force in the medium-lateral direction.

Analysis of motor equivalence

Lifting the M finger led to force changes in all fingers, as compared to unperturbed conditions, which were expected to include an increase in the M finger force, a drop in the other finger forces, and an overall increase in F_{TOT} (Martin et al., 2011) Hence, a change in the sharing of F_{TOT} among the four fingers was expected. The motor equivalence analysis tested whether most of the changes in individual

finger forces and modes due to the perturbation preserved F_{TOT} produced pre-perturbation (ME) or leads to different values of F_{TOT} (nME). Similar analyses were performed with respect to M_{TOT} produced by the fingers forces/modes.

Individual cycles were identified as intervals between successive points when force derivative reached 5% of its maximal value in that cycle; for the TRACK task the definition of cycles was based on the template used as feedback to the subjects. Only full cycles were included in the analysis. Then, the average forces and modes ($x_{0,AV}$) produced by the fingers before the onset of PT_{UP} (Pre-Pert) were computed. Therefore, the N-TRACK Pre-Pert cycles were time normalized to the mean number of samples across all cycles and trials for each subject separately. This normalization was not necessary for the TRACK condition given that the number of samples for each cycle was consistent when subjects tracked the sine template. To align $x_{0,AV}$ with the cycles produced at each j trial, $x_{0,AV}$ was time normalized for each cycle of the j trial and reproduced approximately 10 and 16 times to match the number of cycles in the TRACK and N-TRACK conditions, respectively. Then, the deviation vector ($\Delta x_j = x_j - x_{0,AV}$) between the force/mode during the perturbed trials (x_j) and the mean Pre-Pert ($x_{0,AV}$) was obtained for each sample of j trial. To analyze the adjustments during PT_{DN} , the last cycle before the PT_{DN} was used as the Pre-Pert cycle.

The Jacobian (\mathbf{J}) matrices reflecting how changes in individual finger forces/modes affect F_{TOT} were defined. For \mathbf{f} -based analyses, $\mathbf{J}_F = [1,1,1,1]$. For \mathbf{m} -based analyses, $\mathbf{J}_M = [1,1,1,1] \cdot [\mathbf{E}]$. Analysis with respect to M_{TOT} used $\mathbf{J}_{MOM} = [d_I, d_M, d_R, d_L]$, where $d_I = 4.5$ cm, $d_M = 1.5$ cm, $d_R = 1.5$ cm and $d_L = -4.5$ cm. To estimate ME and nME components Δx was projected onto the null- and orthogonal spaces of the corresponding \mathbf{J} . The length of Δx projection onto the null- and range spaces

reflects the ME and nME deviations in the $\mathbf{f}(\mathbf{m})$ space, respectively. For quantitative comparison, the projections onto the ME space were normalized by the square root of three (dimensionality of the null-space, Mattos et al., 2011). More detail can be found in Appendix.

UCM-based variance analysis

This analysis investigated whether the trial-to-trial variance in the $\mathbf{f}(\mathbf{m})$ pattern led to changes in F_{TOT} (V_{ORT}) or kept F_{TOT} unchanged (V_{UCM}). This computation was similar to the ME analysis described above. In this case, however, the trial-to-trial variance of the de-measured $\mathbf{f}(\mathbf{m})$ data for each time sample was projected onto the null (V_{UCM}) and range spaces (V_{ORT}) of the corresponding \mathbf{J} during each phase of the analysis. Each variance component was normalized to the number of DOF in each dimension ($DOF_{UCM}=3$; $DOF_{ORT}=1$). The analysis was also performed for M_{TOT} . Details of this analysis can be found in (Latash et al., 2001).

Definition of phases of analysis

We analyzed effects of finger perturbation on the ME and nME components of \mathbf{f} and \mathbf{m} changes within different time windows immediately following initiation of the perturbation as well as at steady states (Micro and Macro analyses, respectively). To evaluate the Macro adjustments, three phases were defined as follows: Pre-perturbation (Pre-Pert): mean of all the full cycles before the PT_{UP} , During perturbation (During-Pert): mean of all the full cycles performed with the M finger lifted by 1 cm, and Post-Perturbation (Post-Pert): mean of all the full cycles after PT_{DN} when the M finger was lowered to the initial position. To evaluate the micro adjustments, four phases were defined for each perturbation as follows: 1-50 ms post-

perturbation (Post-Pert50), 51-100 ms post-perturbation (Post-Pert100), 101-150 ms post-perturbation (Post-Pert150), and 151-500 ms post-perturbation (Post-Pert500). The phases were selected to reflect purely mechanical effects of the perturbation (Post-Pert50), effects that could get contribution from spinal reflexes (Post-Pert100), effects that could include action of long-loop reflexes or pre-programmed reactions (Post-Pert150), and effects of all of the above plus those of voluntary corrections (Post-Pert500) (Prochazka et al., 2000).

Statistical analysis

All statistical analyses were performed with SPSS (IBM Statistics). The significance level was set as $p < 0.05$ for all analyses. Paired t tests were performed to test the differences between the enslaving indices, EN, measured in two finger configurations. The effects of phase in the analysis of both macro- and micro-adjustments on the forces/ modes of individual fingers and total force were tested using one-way ANOVA. Three-way repeated-measures ANOVAs were used to test the effects of *Projection-Component* (Motor Equivalence Analysis: two levels, ME and nME; UCM Analysis: two levels, V_{UCM} and V_{ORT}), *Phase* (Macro-Analysis: three levels, Pre-Pert, During-Pert, and Post-Pert; Micro-Analysis during PT_{UP} and PT_{DN} : five levels, Pre-Pert, Post-Pert50, Post-Pert100, Post-Pert150, and Post-Pert500), and *Condition* (two levels, TRACK and N-TRACK) computed with respect to F_{TOT} and M_{TOT} . M-Matrix was used for post hoc pairwise comparisons.

4.4 Results

Enslaving matrix

Indices of unintentional finger force production (enslaving, EN) were computed over trials when the subjects were instructed to press with one finger only. To confirm that these indices could be used for analysis using finger modes (see Methods), we compared EN indices across finger configurations (with the M finger lifted and not lifted) and also across force increase and force decrease segments of the ramp trials. Overall, there were no significant differences in the EN indices across the finger configurations and force directions. On average, EN was 0.81 ± 0.31 when all four fingers were at the same level and 0.76 ± 0.29 when the middle finger was lifted by 1 cm.

Force change patterns: macro-analysis

The subjects showed consistent performance of the main task in conditions both with (TRACK) and without (N-TRACK) a target line on the screen. Lifting and lowering the M finger (perturbations) introduced large changes in the individual finger forces, while the changes in the total force (F_{TOT}) time profile were relatively modest. This is illustrated in the top two panels of Fig. 4.2. Relatively minor differences between the perturbed (black, dashed line) and non-perturbed (gray, solid line) conditions can be seen in F_{TOT} . For the TRACK task, when the M finger was lifted, F_{TOT} remained unchanged ($F_{1,10} = 1.96, p = 0.19$), and there was a tendency for an increase in F_{TOT} for the N-TRACK task ($F_{1,10} = 4.94, p = 0.051$). For the TRACK task, F_{TOT} showed a tendency to decrease when the M finger was lowered as compared to during perturbation ($F_{1,10} = 4.21, p = 0.067$) and pre-perturbation ($F_{1,10} =$

6.966, $p < 0.05$). For the N-TRACK task, F_{TOT} also decreased after perturbation compared with the F_{TOT} applied when the M finger was lifted ($F_{1,10} = 6.97$, $p < 0.05$), but the pre- and post-perturbation conditions only approached significance. Despite being significant in some comparisons, the decrease in F_{TOT} was below 0.26 N, which represents only 1.9 % of the pre-perturbation F_{TOT} .

In contrast, individual finger forces showed rather dramatic changes induced by the perturbation in both tasks (the middle panels of Fig. 4.2; for across-subjects comparisons, see the top panels of Fig. 4.3). Lifting the M finger led to an increase in its force in both tasks ($F_{1,10} > 5.3$, $p < 0.05$) and to a significant decrease in the force of the R and L fingers for the TRACK task, and of the I and R fingers for the N-TRACK task ($F_{1,10} > 5.9$, $p < 0.05$); the decrease in the L finger force for the N-TRACK task approached significance ($F_{1,10} = 4.21$, $p = 0.067$). Lowering the M finger back to the initial position led to a drop in its force ($F_{1,10} > 10.0$, $p < 0.01$) and an increase in the forces by the I and R fingers ($F_{1,10} > 7.4$, $p < 0.05$) while the change in the L finger force was under the significance level. This was true for both TRACK and N-TRACK tasks. After the M finger was lowered to the initial position, force sharing among the four fingers differed from the pattern seen prior to the perturbation (compare the time intervals before the first vertical dashed line and after the second one).

The overall effect of the lifting–lowering perturbation was a significant increase in the M finger force in the TRACK task ($F_{1,10} = 9.18$, $p < 0.05$) but not in the N-TRACK task. There was a significant drop in the R finger force for both tasks ($F_{1,10} > 6.9$, $p < 0.05$) while other finger force changes were under the significance level.

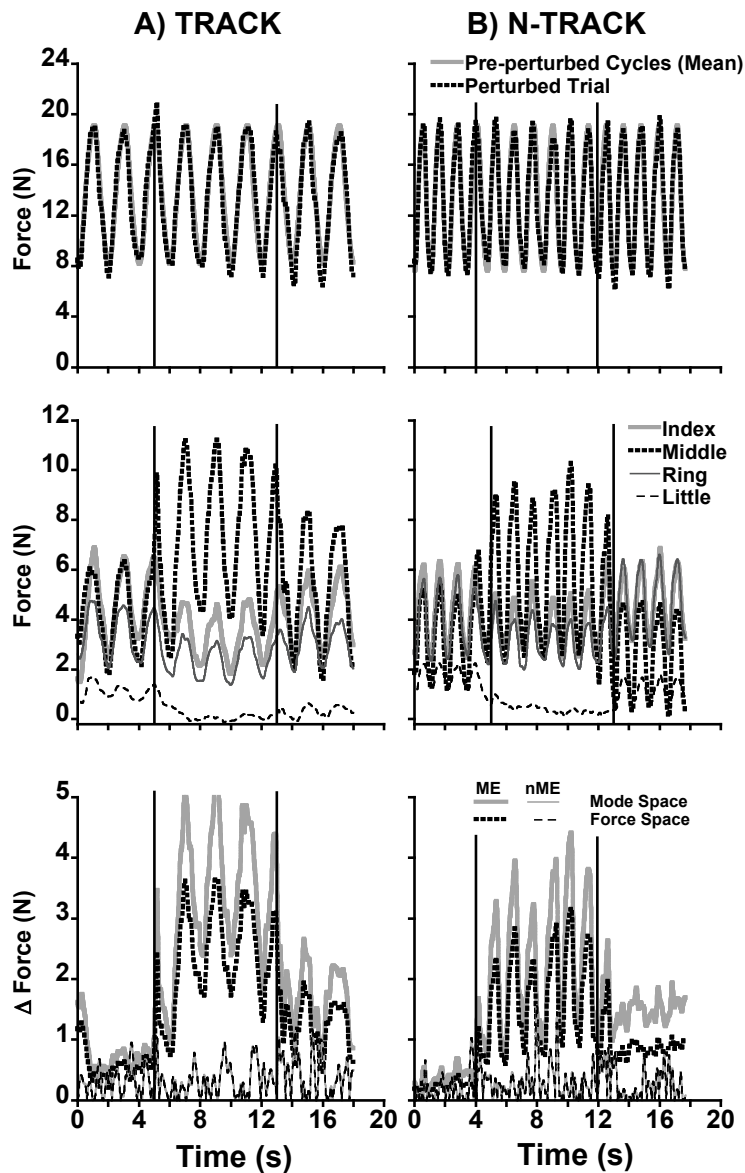


Figure 4.2 Time profiles of a representative subject illustrating changes in total force (*upper plots*), individual finger forces (*middle plots*) and the motor equivalence analysis (*lower plots*) pre-, during-, and post-perturbation during the TRACK (*right plots*) and N-TRACK (*left plots*) task. The *black vertical lines* represent the perturbation onsets for PT_{UP} (middle finger lifted at 1 cm height) and PT_{DN} (middle finger lowered, at 0 cm height)

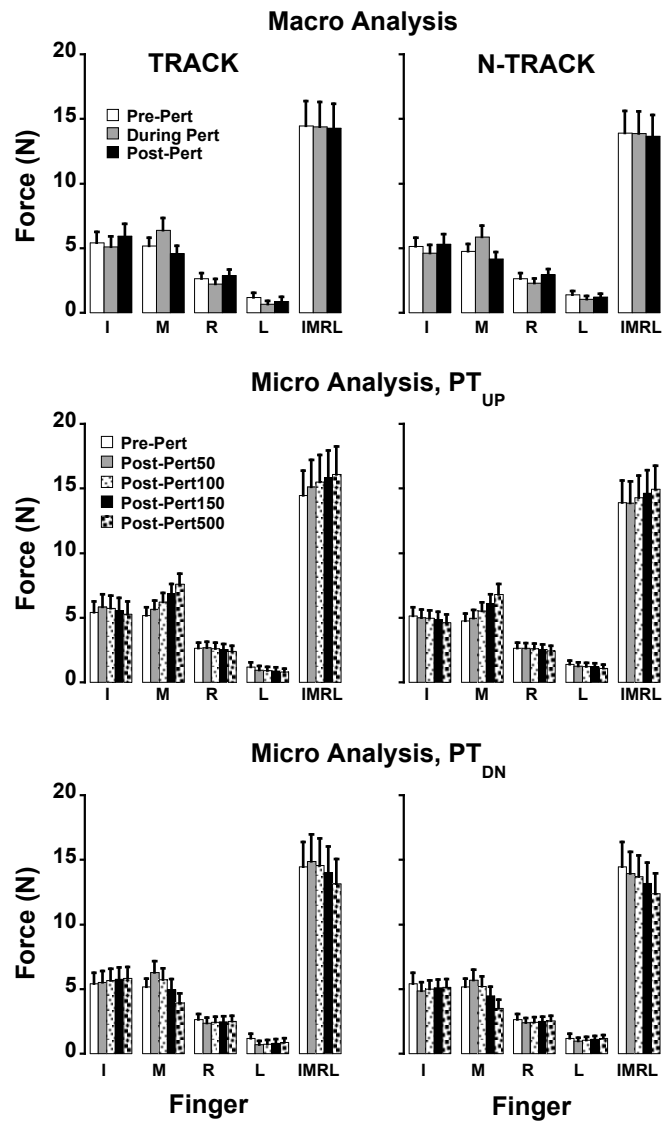


Figure 4.3 Finger force (*I* Index, *M* Middle, *R* Ring, *L* Little, *IMRL* total force) during different phases (means \pm standard errors are shown): *Top* general adjustments: pre-, during-, and post-perturbation, *Middle and bottom* quick adjustments following PT_{UP} and PT_{DN} : Pre-Pert, Post-Pert50, Post-Pert100, Post-Pert150, and Post-Pert500. *Left and right plots* show the TRACK and N-TRACK conditions, respectively. Pre-perturbation phase for the PT_{UP} condition is the mean pre-perturbed cycles, and pre-perturbation phase for PT_{DN} condition is the mean of the last cycle before PT_{DN} .

Force change patterns: micro-analysis

During the processes of the M finger lifting and lowering, finger forces showed consistent patterns of changes with time. The group average forces after the initiation of the perturbation are illustrated in the middle (for the M finger lifting phase, PT_{UP}) and in the bottom (for the M finger lowering phase, PT_{DN}) panels of Fig. 4.3. There was a gradual increase in the M finger force during PT_{UP} and its decrease during PT_{DN} while the I and R fingers showed opposite trends of force change (effect of *Phase*, $F_{1,381,18,811} > 6.6$; $p < 0.05$). No significant effects of *Phase* on the L finger force were observed. Pairwise contrasts showed significant differences between all pairs of phases for the M finger force ($p < 0.05$) with the exception of Pre- Pert versus Post- Pert50. For the I and R fingers, almost all force comparisons between phases starting from Post- Pert50 were significant with a few exceptions.

The forces of the I, R, and L finger showed changes in the opposite direction to the changes in the force of the M finger, while F_{TOT} changed with the M finger force. In particular, both F_{TOT} and M finger force increased when the M finger was lifted. Pairwise comparisons confirmed significant differences across phases ($p < 0.05$) with a few exceptions such as Pre-Pert versus Post-Pert50 for both tasks and PRE-pert versus Post-Pert100 for N-TRACK. F_{TOT} decreased when the M finger was lowered and its force decreased. The following significant pairwise contrasts were found: Pre-Pert versus Post-Post500 for both tasks $F_{1,10} > 17.0$, $p < 0.01$, Pre-Pert versus Post-Pert100 for N-TRACK $F_{1,10} = 7.1$, $p < 0.05$ as well as all comparisons between Post-Pert phases for both tasks: $F_{1,10} > 11.0$, $p < 0.01$).

Motor equivalence: macro-analysis

When two components of the finger force/mode (\mathbf{f}/\mathbf{m}) changes, motor equivalent (ME) and non-motor equivalent (nME), were quantified (see Methods), the ME component showed a dramatic increase during the perturbation (between the two vertical lines in the bottom panels of Fig. 4.3). In fact, the ME component was dominating even during the Pre-Pert cycles reflecting the fact that deviations of finger forces from the average performance were primarily within the subspace leading to no changes in F_{TOT} (the UCM). These results are illustrated in the top panels of Fig. 4.4a using the averaged across subjects data for the TRACK and N-TRACK tasks, in both \mathbf{m} (Fig. 4.4a, left plots) and \mathbf{f} spaces (Fig. 4.4a, right plots). It is obvious that in both spaces, both tasks, and all three phases, the ME component (dotted bars) was much larger than the nME one (gray and black bars) ($F_{1,10} > 49.0, p < 0.0001$).

There were differences in the magnitude of both ME and nME components across the three main phases, Pre-Pert, During Pert, and Post-Pert ($F > 17.0, p < 0.001$). Both components increased after the M finger was lifted and decreased after the M finger was lowered in both \mathbf{f} and \mathbf{m} spaces; Post- Pert components were larger than Pre-Pert (pairwise contrasts, $p < 0.05$). The differences among the three phases were larger for the ME than non-ME component in both \mathbf{f} and \mathbf{m} spaces (interactions *Projection-Component* \times *Phase*, $F > 17.0, p < 0.001$; with all pairwise contrasts at $p < 0.01$).

The motor equivalence analysis with respect to M_{TOT} is presented in the upper plots of Fig. 4.4b. The relative magnitude of ME and nME components differed across phases in both \mathbf{f} and \mathbf{m} spaces (*Projection-Component* \times *Phase*: $F > 11.70, p < 0.005$). In the pre-perturbed cycles, nME was higher than ME ($F_{1,10} > 22.83, p < 0.001$). During perturbation, both ME and nME components increased ($F_{1,10} > 19.0, p <$

0.0001) and ME became significantly higher than the nME component, which indicates that most of deviations in the sharing pattern of finger f and m led to no changes in M_{TOT} ($F_{1,10} > 25.0, p < 0.001$). Post- perturbation the ME and nME components did not differ in the m space ($F_{1,10} = 0.529, p = 0.484$) while $nME > ME$ in the f space ($F_{1,10} = 6.41, p < 0.05$). After the perturbation, the ME component decreased ($F_{1,10} > 6.90, p < 0.05$), while the nME component did not change ($F_{1,10} < 4.1, p > 0.07$) for both f and m spaces analyses.

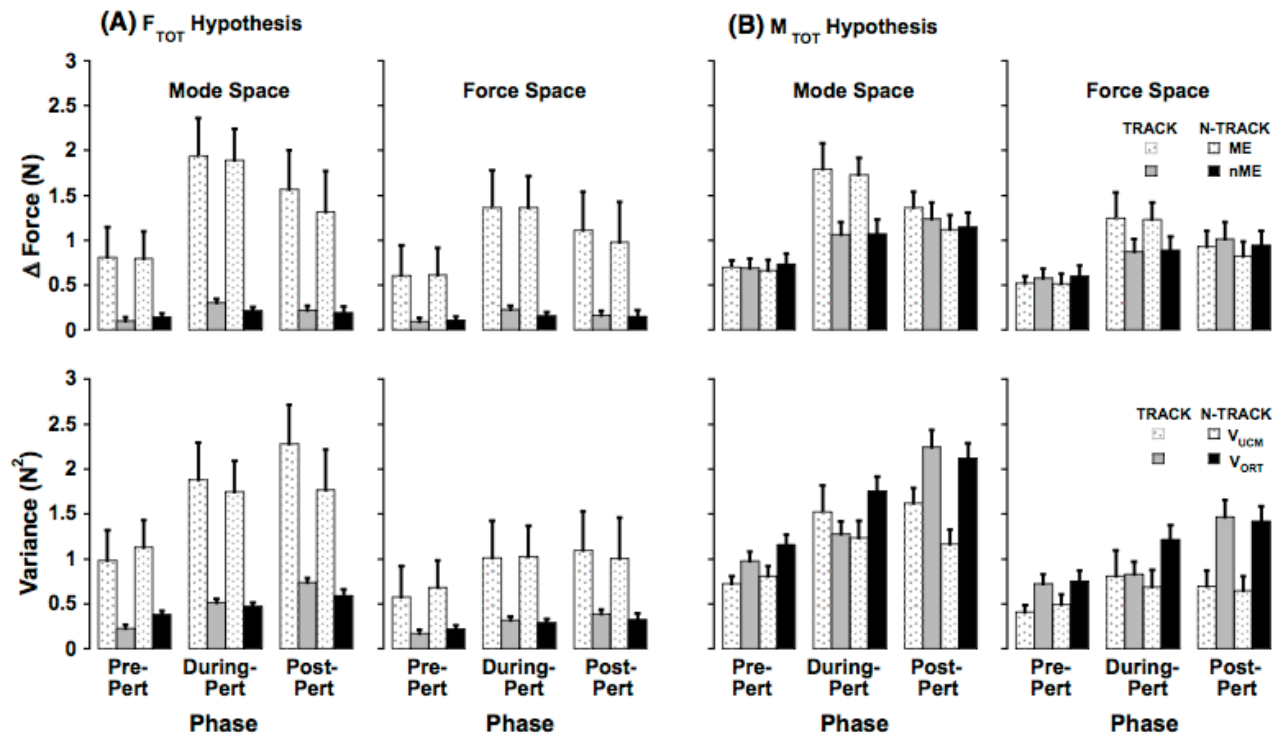


Figure 4.4 Motor equivalence (*upper plots*) and UCM analysis (*lower plots*) with respect to the to the stabilization of the **a** total force (F_{TOT}) and **b** total moment of force (M_{TOT}) during phases pre-, during-, and post-perturbation for TRACK and N-TRACK tasks. *Left and right plots* show analyses in the mode and force spaces, respectively. Means \pm standard errors are shown.

Motor equivalence: micro-analysis

The analysis of the ME and nME components over the time of the M finger lifting and lowering showed a consistent pattern: There was a gradual increase in the ME component over the phases accompanied by a smaller and less consistent increase in the nME component. These findings are illustrated in Fig. 4.5 for both TRACK and N-TRACK tasks (left and right panels of Fig. 4.5) and for the finger lifting (PT_{UP}) and finger lowering (PT_{DN}) phases of the perturbation. The predominance of the ME component (gray bars) is obvious in all the graphs.

These results were confirmed by the main effects of *Projection-Component* ($F > 35, p < 0.0001$) and *Phase* ($F > 78, p < 0.0001$) with a significant *Projection-Component* \times *Phase* interaction ($F > 45, p < 0.001$). For the PT_{UP} during the TRACK task, all pairwise comparisons between phases were significant with the exception of nME component between the Pre-Pert versus Post-Pert 50 and versus Post-Pert 100. During the N-TRACK task, analysis in both *f* and *m* spaces showed significance in all pairwise comparisons for the ME component, while only the difference between Pre-Pert and Post-Pert50 was significant for the nME component. The differences between the TRACK and N-TRACK tasks were confirmed by significant *Task* \times *Phase* ($F > 9.0, p < 0.01$) and *Projection-Component* \times *Task* \times *Phase* ($F > 4.1, p < 0.05$) interactions. Pairwise comparisons, however, failed to show significant differences in the nME component between Post-Pert50 and Post-Pert100 for the TRACK task. Note that quick adjustments were not tested with respect to the total moment of force because the primary task performance was the total force, and not total moment.

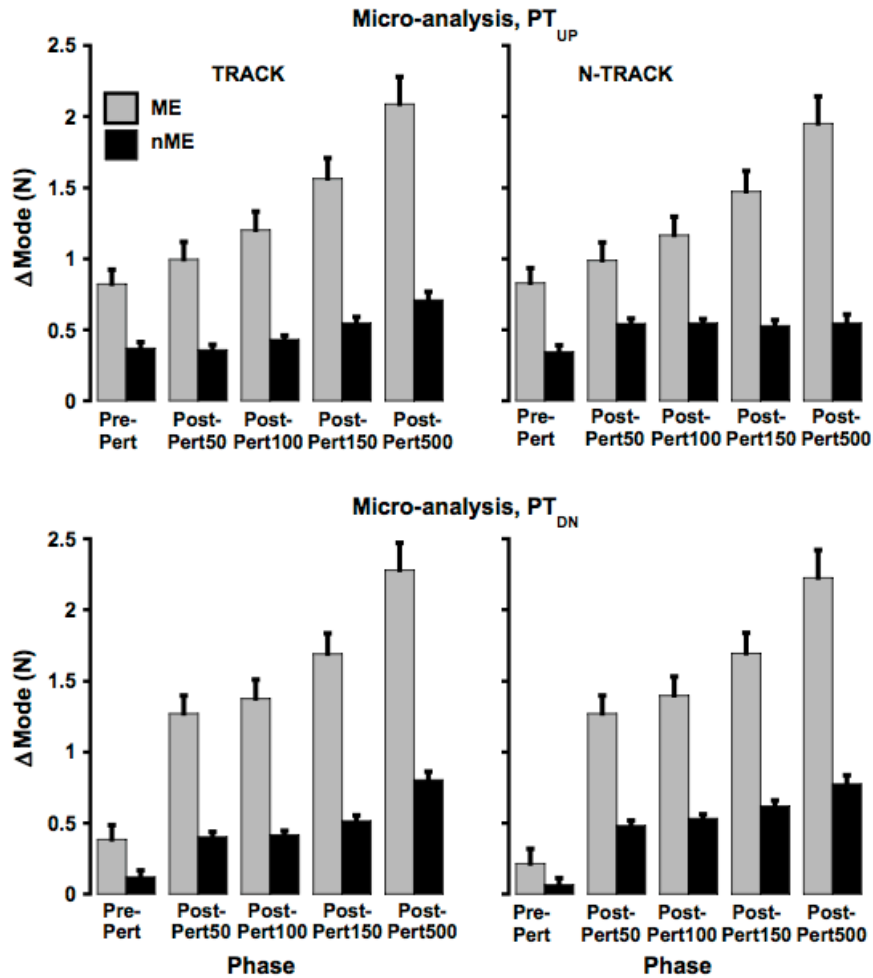


Figure 4.5 Motor equivalence analysis during phases pre- and post-perturbation (Post-Pert50, Post-Pert100, Post-Pert150, and Post-Pert500) following PT_{UP} (upper plots) and PT_{DN} (lower plots) for TRACK (left plots) and N-TRACK (right plots) tasks in the mode space. Analysis in the force space (not shown) had similar profiles. Means \pm standard errors are shown.

Analysis of the structure of variance

Analysis of across-cycle variance performed for each phase of the cycle confirmed that most variance in both \mathbf{f} and \mathbf{m} spaces was compatible with no changes in F_{TOT} (within the corresponding UCM; effects of *Variance-Component*, $F_{1,10} > 12.1$;

$p < 0.01$). These results are illustrated in the bottom panels of Fig. 4.4 for the TRACK and N-TRACK tasks. The UCM-based analysis revealed that compared to the Pre-Pert force cycles, the increase in the variance During-Pert and Post-Pert (effect of *Phase*, $F > 4.3$, $p < 0.05$) was primarily within the UCM (*Variance-Component* \times *Phase* interaction, $F > 3.54$, $p < 0.05$).

For the **f**- and **m**-based analysis, pairwise contrasts confirmed an increase in V_{UCM} from Pre-Pert to During-Pert and Post-Pert ($p < 0.05$) while there were no differences in V_{UCM} During-Pert and Post-Pert. V_{ORT} Post-Pert was higher than During-Pert, and both were significantly larger than V_{ORT} in the Pre-Pert steady state ($p < 0.05$). There was no main effect of *Task* and no other significant effects.

For the analysis with respect to M_{TOT} , ANOVA revealed a significant *Variance-Component* \times *Phase* ($F > 6.08$, $p < 0.05$) in both **f** and **m** spaces. Overall, the across-trials variance did not stabilize M_{TOT} as illustrated in Fig. 4.4b (lower plots, $V_{\text{ORT}} > V_{\text{UCM}}$). The main effect of task approached significance for the **m** analysis (*Projection-Component* \times *Task*: $F_{1,10} = 3.614$; $p = 0.086$). The lower left plot of Fig. 4.4b shows a progressive increase of V_{ORT} during- and post-perturbation in the **m** space ($F_{1,10} > 6.88$, $p < 0.025$). In the **f** space (right plots Fig. 4.4b), V_{ORT} magnitude was not affected by the perturbation ($F_{1,10} = 4.278$, $p = 0.065$), but it increased significantly after the perturbation ($F_{1,10} = 5.28$, $p < 0.05$). In contrast, V_{UCM} in both **f** and **m** spaces increased with the perturbation ($F_{1,10} > 6.04$, $p < 0.05$), but did not change after the perturbation ($F_{1,10} < 0.34$, $p > 0.574$).

4.5 Discussion

Our main hypothesis formulated in the Introduction has been confirmed in the study. In particular, ME components dominated finger force deviations from the

average pre-perturbation performance for the analyses in both spaces of elemental variables (f and m) during all phases of the task. A perturbation led to an increase in the ME component with respect to the pre-perturbation cycles. The Micro-analysis showed that deviations from the mean unperturbed sharing pattern due to the changes in the middle finger position were mostly in the ME space and these responses were partially due to mechanical factors, such as coupling among the fingers and responses of the extrinsic multi-tendon muscles to the perturbation, since ME was observed in the period Post-Pert50, before any mechanical effects mediated by reflex loops could be expected. ME increased substantially along the post-perturbation phases suggesting contributions of local reflexes, pre-programmed and voluntary actions to the motor equivalence. In addition, the UCM-based analysis of variance (Scholz & Schoner, 1999) showed that most of the variance of individual finger forces/modes across trials was compatible with unchanged total finger force (was within the UCM computed for the total force; Latash et al. 2001; Scholz et al. 2002). All these results were consistent between the TRACK and N-TRACK conditions.

Mechanisms for motor equivalence

Motor equivalence (ME, deviations of finger forces/modes that did not affect total force) was observed in our experiment immediately following a perturbation and then ME increased in time while the perturbation was kept constant. The non-motor equivalent (nME) component also increased, but to a lesser extent. These results are consistent with those in earlier studies of ME during multi-joint reaching (Mattos et al., 2013; Mattos et al., 2011). In contrast to those earlier studies, the perturbation was removed in our experiment. When the perturbation was removed, individuals did not recover their pre-perturbation force/moment sharing patterns. The persistent change

from pre- to post-perturbation was large within the UCM, showing ME induced by the transient perturbation and observed under conditions equivalent to the pre-perturbation baseline.

The modulation of finger forces observed as ME within the first 50 ms of the onset of the perturbation may be due to reflexes (Brown & Loeb, 2000). Reflexes rely on the force-length and force-velocity muscle characteristics that change with muscle activation and hence can be tuned by the central nervous system. Interestingly, the amount of ME increased progressively on a time scale of 100 to 500 ms as shown in Figure 4.2. This increase likely involved the action of spinal reflexes and long-loop responses as well as voluntary reactions. ME observed shortly after the perturbation also might reflect the structure of the mechanical perturbation itself, e.g., how much of the mechanical effect of the perturbation lied within the UCM and how much lied in the ORT subspace.

The persistent change in the sharing pattern observed after the transient perturbation can be interpreted within the neuronal dynamics model of multi-joint movement by Martin and colleagues (Martin et al., 2009), if the ideas of that model are transferred to the multi-finger task setting of this experiment. According to that model, neural activation variables that generate control signals to muscles converging on each joint are coordinated in such a way that the UCM and ORT subspaces are decoupled. This means that both descending and feedback signals produce two effects, those that do and do not lead to changes in a salient performance variable (F_{TOT} in our study), and these effects do not interfere with each other. The second element of the model is a form of back-coupling similar to the one introduced earlier (Latash et al. 2005), which uses sensory information about the actual joint configuration to produce

changes in muscle activation that may affect both UCM and ORT subspaces. Through this back-coupling, the neural control signals respond to sensed changes in each elemental variable leading to larger changes within the UCM, which translate into ME deviations of the system. The fact that ME increases with time is consistent with the gradual updating of the neural commands by the neural dynamics driven by input from the back-coupling.

Task-specific stability and its behavioral consequences

We would like to analyze the main results of our study within a scheme based on a few assumptions (Latash, 2010a; Martin et al., 2009). First, we accept the main axiom of the equilibrium-point hypothesis (Feldman, 1986; Feldman, Rachmilewitz, & Izak, 1966) and its later development as the referent configuration (RC) hypothesis (Feldman, 2009) that neural signals associated with the control of a movement can be adequately represented as subthreshold depolarization of neuronal pools leading to the emergence of referent values for salient, task-specific variables (given the external force field) - RC_{TASK} . The differences between referent and actual values of these variables lead to muscle activation via a chain of few-to-many mappings organized into a hierarchy, which leads to RCs at hierarchically lower levels, for example those associated with the control of individual limbs, digits, joints, muscles, etc. All muscle activations contribute to moving actual body configuration towards the RC_{TASK} . If this configuration is not attainable, e.g., due to external or anatomical constraints, a new equilibrium state is reached with non-zero muscle activations.

Second, we assume that the few-to-many (redundant) mappings are organized in a synergic way, that is, variance at the lower (higher-dimensional) level is larger in directions that do not affect the RC at the higher (lower-dimensional) level. This can

be achieved via the aforementioned central back-coupling loops and/or feedback loops from peripheral receptors (Latash et al., 2005; Martin et al., 2009). This assumption is readily compatible with the main ideas of the UCM hypothesis.

Stability of performance within this scheme is ensured with respect to task-related, salient variables. In contrast, elemental variables at lower levels of the assumed hierarchy are expected to show relatively large deviations in directions that keep those salient variables unchanged, i.e., within the UCM for those variables. Indeed, several recent experiments have provided evidence for equifinality of task-specific variables under transient perturbations, i.e., their return to pre-perturbation values, while elemental variables showed large deviations from their pre-perturbation values (Wilhelm et al., 2013; Zhou, Solnik, Wu, & Latash, 2014a). Those studies used changes in external mechanical variables as the means to introduce perturbations. Similar effects, however, may be expected from changes in neural, task-related variables.

A series of recent studies (Mattos et al., 2013; Mattos et al., 2011) have shown that an unexpected perturbation during an ongoing movement leads to immediate large deviations within a redundant set of elemental variables (joint rotations and muscle modes, cf. Krishnamoorthy, Latash, et al., 2003), with a large ME component. This component becomes even larger during movement correction although, obviously, it leads to deviations in the joint configuration and muscle activation spaces that, by definition, have no effect on task-related variables. In other words, most of the corrective action was not correcting anything. This result is hardly compatible with theoretical approaches based on ideas of action optimization (Diedrichsen, Shadmehr, & Ivry, 2010; Todorov & Jordan, 2002). It is, however, a natural consequence of the

general theoretical scheme described above. In particular, these results support the aforementioned model of movement control proposed by Martin and colleagues (Martin et al., 2009).

Our main observations in this study generalize the earlier finding to multi-finger action with several important distinctions. First, we studied cyclic tasks that, according to some authors (Hogan & Sternad, 2007), have qualitatively different control as compared to discrete tasks studied in the mentioned works by Mattos and her colleagues. Within our scheme, there is no distinction in the control of discrete and cyclic tasks, and our results in the current study of cyclic tasks are qualitatively similar to those in earlier studies of discrete tasks.

Previous experiments suggest that sharing patterns of force in multi-finger pressing tasks are chosen to minimize pronation and supination moments acting on the hand (minimization of secondary moments, Li, Latash, Newell, et al., 1998; Zatsiorsky et al., 1998; Zatsiorsky, Li, & Latash, 2000). During multi-finger accurate cyclic force production, similar to the task used in this experiment, subjects showed stabilization of the total moment of force (M_{TOT}) in a sense $V_{UCM} > V_{ORT}$ in the space of finger modes (Latash et al., 2001; Scholz et al., 2002). The authors have suggested that moment stabilization is a default developed during everyday tasks. Our results provide indirect support for the hypothesis on unintended moment stabilization. Indeed, there were large ME components in the deviations of finger forces (and modes) computed with respect to M_{TOT} as the performance variable. However, the relative magnitude of ME deviations in the analysis with respect to M_{TOT} was smaller than for the analysis with respect to F_{TOT} . We also failed to see the signature of M_{TOT} stabilization in the analysis of inter-cycle variance (see Fig. 4.4): In contrast to the results of this analysis with

respect to F_{TOT} ($V_{UCM} > V_{ORT}$), analysis with respect to M_{TOT} showed an opposite inequality ($V_{UCM} < V_{ORT}$). The difference in the current results from those in the cited earlier studies has to be explored in future,

Earlier studies of the ME and nME components in response to perturbations explored unidirectional perturbations that led to a new force field (Mattos et al., 2013; Mattos et al., 2011). Our study used transient perturbations, such that at the end of the trial the subjects were performing the task in the same external conditions as prior to the perturbation. Nevertheless, there was a significant increase in the ME component suggesting that effects of perturbations on the two components of motion (ME and nME) are seen even when the system apparently returns to a pre-perturbation state. These results follow naturally the introduced theoretical scheme: Each of the two components of the perturbation (PT_{UP} and PT_{DN}) contributed to ME motion, which was not corrected by the subject, while the nME motion was corrected.

Robustness of the results in the two spaces of elemental variables, finger forces and finger modes (cf. Danion et al., 2003) provides extra validity for the conclusion that stability at any of the lower levels of the hierarchy is structured with respect to task-specific variables with higher stability (lower variance) in directions that lead to changes in those variables (ORT, leading to nME deviations) as compared to directions that do not (UCM, leading to ME deviations).

Motor equivalence and UCM

The analysis of the structure of inter-trial variance within the UCM hypothesis and analysis of the two components, ME and nME, do not have to lead to similar outcomes. The UCM-based analysis of inter-trial variance quantifies deviations of the system from its average across trials behavior (Scholz & Schoner, 1999). Assuming

that each trial starts from somewhat different initial conditions and is associated with somewhat different changes in external conditions, variance is expected to be larger in directions of low stability (those spanning the UCM) as compared to directions of high stability (ORT). Hence, the signature inequality $V_{UCM} > V_{ORT}$ has been used as a proxy of different stability properties in sub-spaces computed with respect to a potentially important performance variable (reviewed in Latash et al. 2007).

Figure 4.6 illustrates a task of producing a constant force with two effectors: $F_1 + F_2 = C_1$. If the CNS organizes stability of $(F_1 + F_2)$, a cloud of data points elongated along the UCM (the dashed, slanted line) is expected in a series of trials (the cloud 1). Imagine now that an external perturbation changes the total force to C_2 . Since the two-effector system is less stable along the UCM (shown with the slanted dashed line), in addition to the deviation orthogonal to the UCM leading to a change in the total force (ORT, solid, thick line in Figure 4.6), a large deviation is expected along the UCM. If the subject in this mental experiment tries to bring the force back to C_1 , the corrective action may also be expected to lead to a large deviation of the two forces along the UCM. The deviations along the UCM are ME, while orthogonal to the UCM deviations – are nME. In multi-finger pressing tasks, the ME component represents a change in the force sharing pattern leading to the same total force, while changes in the magnitude of total force correspond to the nME component. Relative magnitudes of the ME and nME components are independent of the shape of data point distribution (compare the data clouds 1, 2, and 3), and hence this analysis is complementary to analysis of variance components within the UCM-framework. However, within our theoretical scheme, both of these potentially independent analyses are expected to lead to qualitatively similar results because they both reflect

different task-specific stability in different directions within a redundant space of elemental variables. This was indeed the case for the analyses with respect to F_{TOT} .

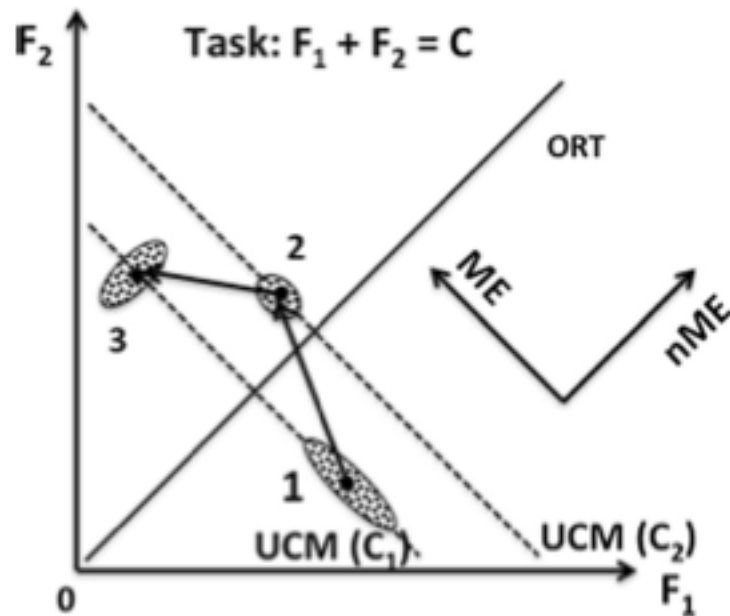


Figure 4.6 An illustration of the idea of motor equivalence. Two effectors are involved in a common task $F_1 + F_2 = C$. In the initial steady state ($C = C_1$, cloud of data points 1), inter-trial variance is mostly along the UCM for this task (*dashed line*). A perturbation changes the output of the system to C_2 (cloud of points 2). It is expected to lead to larger deviation along the less stable direction (ME, along the UCM) as compared to more stable direction (nME, along ORT). A correction leads to the same output of the system, C_1 (cloud of points 3), again with a large ME deviation along the UCM. Note that the ME versus nME deviations may be associated with different structure of inter-trial variance as illustrated with the different shapes of the clouds of data points.

The analyses with respect to M_{TOT} , which was not an explicit task-related variable, led to conflicting results. We observed relatively large ME components but

no signs of stabilization of M_{TOT} in the across-cycles variance indices. The relatively similar amounts of ME and nME components observed in the analysis with respect to M_{TOT} suggest that the neural controller did not consider M_{TOT} as an important performance variable. Note that stabilization of F_{TOT} and M_{TOT} are in competition. Indeed, stabilization of F_{TOT} requires negative co-variation of forces across cycles, while stabilization of M_{TOT} requires positive co-variation of forces produced by finger pairs acting in opposite direction (IM and RL). Both variables can be stabilized simultaneously as shown in earlier studies (Scholz et al., 2002; Zhang et al., 2008). So, the strong stabilization of F_{TOT} observed on our experiment ($V_{UCM} \gg V_{ORT}$) might contribute to the inequality $V_{UCM} < V_{ORT}$ observed for M_{TOT} . It is possible that the practice given to the subjects, the instruction emphasizing accurate F_{TOT} production, and the presence of perturbations played a role in the current results being different from those in earlier reports (Latash et al., 2001; Scholz et al., 2002).

We would like to emphasize the consistency of results obtained so far in studies of motor equivalence in different spaces of elemental variables, joint configuration space (Mattos et al., 2011), muscle mode space (Mattos et al., 2013), and finger force/mode spaces (the present study). The results were also consistent across discrete and cyclic tasks and tracking and no-tracking tasks. Overall, they provide so far the most consistent support for the scheme for the neural control of natural movements performed by redundant sets of elements.

Concluding comments

To summarize the main lesson from this study, consider the following example. Imagine that you press with a finger on the top of a long spring (similar to the one in the pen) placed vertically (cf. Valero-Cuevas, Smaby, Venkadesan,

Peterson, & Wright, 2003). The spring shows relatively high resistance to deformation (high stability) along its axis and relatively low resistance (low stability) orthogonal to its long axis. Even if you try your best to compress the spring slowly and accurately, at some point it will buckle (the so-called Euler's buckling). This buckling action is a consequence of different stability of the spring in different directions. Similarly, in our experiments, as well as in the previous studies (Mattos et al., 2013; Mattos et al., 2011), a purposeful action along a desired direction (trying to correct total force) led to large deviations orthogonal to that direction (ME). Those deviations were not part of the movement plan but natural consequences of the physics of the system resulting in its lower stability in directions spanning the UCM and contributing to the ME component.

Chapter 5

TASK SPECIFIC STABILITY OF ABUNDANT SYSTEMS: STRUCTURE OF VARIANCE AND MOTOR EQUIVALENCE

5.1 Abstract

Task specific stability is one of the most remarkable features of biological abundant systems. It allows reorganizing elements after perturbations, while being motor-equivalent with respect to values of salient performance variables. The main goal of this study was to test a hypothesis that self-triggered transient changes in performance of a steady-state task would result in motor equivalence. A secondary goal was to estimate effects of removing visual feedback on the amount of reorganization of motor elements. Healthy subjects performed two variations of a four-finger pressing task requiring accurate production of total force (F_{TOT}) and moment (M_{TOT}). In the Jumping-Target task, a sequence of target jumps induced transient changes in either F_{TOT} or M_{TOT} . In the Step-Perturbation task, the index finger was lifted by 1 cm for 0.5 s using the “inverse piano” device. Visual feedback could be frozen for one of these two variables in both tasks. Deviations in the space of finger modes (hypothetical commands to individual fingers) were quantified in directions that did not change F_{TOT} and M_{TOT} (ME component) and in directions that changed F_{TOT} and M_{TOT} (nME component). The changes in performance led to an increase in both the ME and nME components. After the sequence of target jumps leading to the same $\{F_{TOT}; M_{TOT}\}$ combination, the changes in finger modes had a

large ME component. Without visual feedback, a large increase in the nME component was observed without consistent changes in the ME component. Results from the Step-Perturbation task were qualitatively similar. These findings suggest that both external perturbations and purposeful changes in performance trigger a reorganization of elements of an abundant system, leading to large ME motion. These results are consistent with the principle of motor abundance corroborating the idea that a family of solutions is facilitated to stabilize values of important performance variables.

5.2 Introduction

All natural human movements involve more elements than necessary to perform typical tasks and, hence, allow numerous ways of performing such tasks. In each particular case, however, a single solution is observed from a potentially infinite set. How do such single solutions emerge? This question constitutes the essence of the so-called problem of motor redundancy or the Bernstein problem (Bernstein, 1967; Turvey, 1990). Earlier approaches assumed that the central nervous system (CNS) added constraints (eliminated redundant degrees-of-freedom, DOFs) and/or used optimization principles to find unique solutions each time a movement is produced (Prilutsky & Zatsiorsky, 2002; Vereijken, Vanemmerik, Whiting, & Newell, 1992).

More recently, two theoretical advances have led to a different approach to the problem of motor redundancy. The first is the idea of task-specific stability (Schoner, 1995) formalized as the uncontrolled manifold (UCM) hypothesis (Scholz & Schoner, 1999), and the second one is the principle of abundance (Gelfand & Latash, 1998; Latash, 2012a). According to these ideas, the CNS does not select unique solutions to motor problems but unites all the elemental variables of apparently redundant sets in a

way that facilitates families of solutions equally able to solve the task within a permissible error margin. This is reflected in different stability in the space of elemental variables in directions leading to no changes in salient performance variables (UCM, low stability) as compared to stability in directions leading to changes in those variables (orthogonal to the UCM, high stability).

In a series of recent studies, quick reactions to external perturbations were used to explore actions by apparently redundant (we are going to address them as “abundant”) sets of elemental variables during multi-joint and multi-finger tasks (Mattos et al., 2013; Mattos, Schoner, Zatsiorsky, & Latash, 2015; Mattos et al., 2011; Scholz et al., 2007). These studies have shown, in particular, that correction of a perturbation leads to a large amount of motion in the space of elemental variables that produces no changes in the task-specific performance variables (the so-called motor equivalent, ME, motion). Commonly, ME motion was much larger than motion leading to changes in the perturbed performance variable (non-motor equivalent, nME). Such large amounts of the apparently wasteful ME motion have been interpreted as reflecting low stability within the corresponding UCMs. This interpretation has been complicated by a few factors. First, in some of the mentioned studies (Mattos et al., 2013; Mattos et al., 2011), the perturbation acted during the entire movement time and, hence, in perturbed trials, the task was performed in a different force field. Second, even in studies with transient perturbations (Mattos et al., 2015), effects of the perturbations could last for some time and superimpose on the effects of the corrective actions. One of the main goals of the current study has been to address these problems and explore the amounts of ME and nME change when task demands are modified rapidly and transiently. In particular, a perturbation that a priori

lies primarily only within the nME space, will also induce change within ME (Hypothesis-1). Moreover, when the target values of the task variables are changed back to their original values, we predict that nME components return to their original values, while the ME components do not (Hypothesis-2).

A secondary question is related to the role of sensory signals of different modalities in bringing about the large amounts of ME motion during corrective actions. In the mentioned earlier studies, the subjects received both visual and natural somatosensory feedback. In this study, we manipulated visual feedback for one of the two task-specific performance variables. Our third hypothesis was that the amount of ME change would be insensitive to presence of visual feedback, while nME change would increase without visual feedback. This hypothesis is based on the idea of back-coupling feedback loops from motion-sensitive somatosensory receptors to neural mechanisms ensuring task-specific stability (Latash et al., 2005; Martin et al., 2009).

To address these hypotheses, we used two tasks. Both tasks required the subjects to produce accurate combinations of total pressing force (F_{TOT}) and total moment of force (M_{TOT}) by a set of four fingers. In one task, no perturbation was applied while the target could jump requiring a quick change in F_{TOT} or M_{TOT} ; after a short delay, the target jumped to the initial state. Visual feedback was provided for the “jumped” variable only, while it was frozen for the other variable. In the other task, a finger was perturbed (lifted) using the “inverse piano” device (Martin et al., 2011). This led to changes in both F_{TOT} and M_{TOT} . In different trials, visual feedback was available at all times for one of the variables and frozen for the other variable. In both conditions, we predicted comparably large amounts of ME motion for both variables

while much larger nME motion was expected for the frozen-feedback variable (Hypothesis-3).

To link the current experiment to earlier studies of four-finger force/moment production (Latash et al., 2001; Scholz et al., 2002), we also explored the structure of inter-trial variance in the space of commands to fingers (finger modes, Danion et al., 2003; Latash et al., 2001). We expected to see larger amounts of variance within the UCM than within orthogonal to the UCM space ($V_{UCM} > V_{ORT}$) for the variable receiving visual feedback but not for the “frozen-feedback” variable (Hypothesis-4).

5.3 Methods

Subjects

Eight healthy young adult subjects (mean age 30.37 ± 5.10 yr.; six males, two females) took part of this study. All subjects were self-reported right-hand dominant and had no history of injury or pain in the upper limb for the last six months. Subjects signed the informed consent form as approved by the Office for Research Protection of the Pennsylvania State University.

Equipment

The “inverse piano” device (Figure 5.1, right panel) was used to provide finger perturbations (Martin et al., 2011). This equipment consists of four unidirectional piezoelectric force sensors (208C01; PBC Piezotronics Inc.) mounted within slots of a steel frame (140 x 90 mm), 3-cm apart in the medio-lateral direction. The anterior-posterior position of the sensors was adjusted to fit the individual subject’s anatomy. Each sensor was covered with sandpaper (300 grit) and connected to linear actuators

(PS01-23x80; LinMot). The signals coming from the sensors were sent through a DC-coupled signal conditioner (PCB) to a 16-bit analog-to-digital converter (CA-1000; National Instruments). A customized Labview program (National Instruments) was written to acquire and record the individual force signals at 200 Hz, and also to control the linear actuators through a controller (E-400-AT; LinMot). The timing of perturbation onset was recorded.

Procedure

Subject position

Subjects sat on a chair with their right arm resting on a table. In the initial position, the upper arm was slightly abducted, 60° of shoulder abduction, 120° of elbow flexion, forearm pronated, and the wrist in neutral position. Cushioned paddings were placed under the forearm and hand for comfort. The forearm was secured to the platform with two straps to stabilize the initial posture. A monitor was placed 0.8 m away from the subject, at the eye level. The monitor was used to set tasks and provide visual feedback. The subject position is illustrated in Figure 5.1.

Experimental tasks

This study consisted of two main experiments preceded by maximal voluntary contraction (MVC) finger pressing tasks and one-finger tasks with accurate ramp force production (Ramp-tasks). In every trial, the subjects started with all four fingers (I: index, M: middle, R: ring and L: little) relaxed on the top of the force sensors facing the computer display. Then, the sensor signals were set to zero, which allows recording voluntary downward forces without an effect of fingers/hand's weight. Once the subject was ready, data collection started.

MVC task

Subjects were instructed to press as hard as possible on the sensors with all four fingers during 6 s. Visual feedback on the total force profile was provided as well as verbal encouragement. The maximal peak total force between two attempts was chosen as MVC. The MVC task was used to normalize the force and moments of force used in the main experimental tasks.

Ramp-task

Subjects placed the four fingers on the sensors and tracked a ramp template displayed on the monitor with one finger at a time. The ramp had three segments, two horizontal lines at 0% and 8% of MVC for 4 s, with an oblique line in-between from 0-8% MVC over 6 s. After a couple of practice trials, two trials were collected for each finger, and the trial with the trace most closely following the template was used to compute finger modes (see below). This task was used to estimate unintended finger force production by non-instructed fingers (Danion et al., 2003; Zatsiorsky et al., 1998).

Main Tasks (Jumping-Target and I-Perturbation Tasks)

Subjects performed several target-matching tasks. The visual target consisted of a white circle, 1.5-cm in diameter, placed at the center of the screen. A moving cursor (a dot with the diameter of 1 mm) was shown online, with the x -coordinate corresponding to total moment of force (M_{TOT}) value, and y -coordinate corresponding to total force (F_{TOT}) value as illustrated in Figure 5.1 (left panel). Zero value of M_{TOT} computed with respect to the midline between the M and R fingers corresponded to the center of the screen while zero F_{TOT} corresponded to the bottom of the screen.

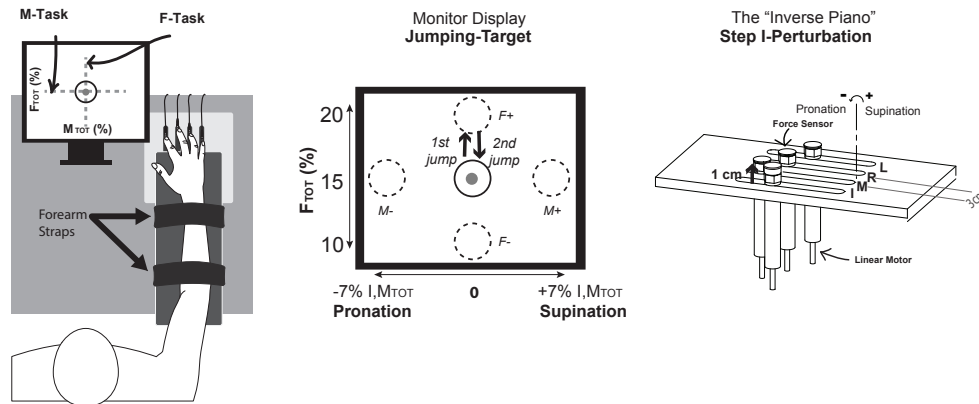


Figure 5.1 *Left*: The experimental setup. The monitor shows the target position at the beginning of each trial and the cursor feedback for the F- and M-tasks. *Middle*: Visual feedback for the Jumping-Target Task with the four possible conditions of target jump. Only one target was shown at each time. *Right*: *The inverse piano* used to lift the index (I) finger during the Step I-Perturbation Task. The zero moment was computed with respect to the midline between middle (M) and ring (R) fingers. Clockwise direction was considered (+) and represented pronation moment of the forearm.

At the trial onset, the target was always located at the center of the screen corresponding to $F_{TOT} = 15\%$ MVC and zero M_{TOT} . Individuals were instructed to try to bring the cursor into the center of the target as quickly and accurately as possible, and keep the cursor inside of the target until the end of the trial. Pilot trials showed that individuals usually take ≈ 2 s to bring the cursor into the target, and to stabilize the required combination of F_{TOT} and M_{TOT} . For all trials, further manipulations, such as target “jumps” on the screen or perturbation of the I-finger (see later) started randomly between 5 – 7 s from the start of the trial. The perturbation onset was

randomized to avoid changes of $\{M_{TOT}; F_{TOT}\}$ in preparation to the perturbation. Each trial lasted 15 s.

Jumping-Target Task: This part of the experiment (Figure 5.1, middle plots) involved quick changes in the target position. In those trials, at a random time between 5 and 7 s from the beginning of the trial, the target suddenly assumed a new position on the screen, remained in that position for 4 s, and then returned to its initial position ($F_{TOT} = 15\%$ MVC and $M_{TOT} = 0$) until the end of the trial. The subjects were instructed to always try to keep the cursor in the middle of the target, which required quick changes in either F_{TOT} or M_{TOT} . In the F-Jumping-Variable the target changed to either 20% (F+) or 10% (F-) of MVC. After the target jump was initiated, the x -coordinate of the cursor was “frozen” and supplied no information on M_{TOT} ; as a result the subjects received feedback only on F_{TOT} . Similarly, in the M-Jumping-Variable, the target jumped to the right (M+, requiring supination M_{TOT}), or to the left (M-, requiring pronation M_{TOT}). The target jump amplitude corresponded to $\pm 7\%$ of the maximal moment produced by the I-finger. In this condition, the position of the cursor along the y -axis was frozen. The F- and M-Jumping-Variable trials were performed in two blocks, and the order was balanced across subjects. Each block included a total of 30 trials, with 15 trials for each direction of target jump (either F+/F- or M+/M-). Three familiarization trials for each condition were provided at the beginning of each block. There was at least a 30-s interval between the trials and breaks of 3 min before each block.

I-Perturbation Task: This part of the experiment (Figure 5.1, right panel) was designed to analyze differences in the inter-trial structure of variance and motor equivalence as a function of perturbations applied to the I-finger and visual feedback.

The individuals were instructed to keep the cursor in the middle of the target. At random times between 5–7 s from the beginning of the trial, the *I*-finger was smoothly lifted by 1 cm over 0.5 s. The *I*-finger remained lifted until the end of the trial (Step, I-Perturbation). The perturbation led to an increase in both F_{TOT} and the pronation moment. The subjects were instructed to correct the effects of the *I*-finger perturbation as quickly as possible and keep the cursor in the center of the target at all times. After the perturbation onset, the cursor visual feedback was manipulated in two subtasks: F- and M-Task. In the F-Task, only force feedback was displayed, while the cursor *x*-coordinate was frozen. In the M-Task, the moment feedback was displayed, and the *y*-coordinate was frozen. The order of F- and M-tasks was block randomized among subjects. There were three practice trials for familiarization with the protocol at the beginning of each condition. More trials were provided as needed to guarantee that the subjects understood the task. There were at least 30-s intervals between trials.

Data processing

The experimental tasks required simultaneous accurate production of F_{TOT} and M_{TOT} ; therefore the motor equivalence and the inter-trial variance analysis in mode-forces (see computation below) were performed with respect to both F_{TOT} and M_{TOT} .

Initial data processing

The acquired signals were converted into force units, and low-pass filtered at 5 Hz with the 4th order zero-lag Butterworth filter. We used a relatively low cutoff frequency due to the vibrations seen in the signal during the finger perturbation when the actuators were active. Note, however, that most analyses were performed using steady-state phases. The total force was computed by summing the individual finger forces.

Enslaving matrix and finger modes

The amount of enslaving was computed using the finger forces in the oblique part of the Ramp Task. Linear regressions were performed between the individual finger forces and the total force for each instructed finger, $i = (I, M, R, L)$, the regression coefficients (k) were used to estimate the 4×4 enslaving matrix, $[E]$:

$$[E] = \begin{bmatrix} k_{II} & k_{IM} & k_{IR} & k_{IL} \\ k_{MI} & k_{MM} & k_{MR} & k_{ML} \\ k_{RI} & k_{RM} & k_{RR} & k_{RL} \\ k_{LI} & k_{LM} & k_{LR} & k_{LL} \end{bmatrix} \quad (5.1)$$

The finger-force was converted into modes using enslaving matrix as follows:

$$m = E^{-1}f, \quad (5.2)$$

where, f is the 4×1 finger forces vector, and m is the 4×1 finger mode vector. Further analysis was performed in the mode space, hypothetical neural commands that can be manipulated one at a time (Danion et al., 2003). The relative contribution to the F_{TOT} produced by the master-fingers is represented by the diagonal entries of the E matrix, while the off-diagonal entries represent the slave-finger force contributions.

Total moment of force

The total moment of force, M_{TOT} , was computed with respect to a horizontal axis parallel to the forearm/hand and passing through the mid-point between the centers of the force sensors for the M and R fingers:

$$M_{TOT} = d_I f_I + d_M f_M + d_R f_R + d_L f_L, \quad (5.3)$$

Where d_i and f_i represent the force and the lever arm for each finger i , respectively $i = [I, M, R, L]$. The center of the force sensors were 3-cm apart; hence, d_I

= -4.5 cm, $d_M = -1.5$ cm, $d_R = 1.5$ cm and $d_L = 4.5$ cm. Supination and pronation moments are represented by positive and negative values, respectively. The moment estimation assumed no change in the point of application of the force in the medio-lateral direction. Note that this value was not equal to the actual total pronation-supination moment.

Analysis of motor equivalence

This analysis quantified the amount of deviations in the space of finger-modes that led to either preservation of a selected performance variable, F_{TOT} or M_{TOT} , (ME component) or deviations in that variable (nME component). We quantified such deviations caused by corrective actions in both the Jumping-Target task and the I-Perturbation task. The signals were aligned by the onset of the target motion (Jumping-Target) or I-finger perturbation (I-Perturbation). For each trial, j , the average finger-mode ($m_{j,AV}$) produced between 2.0 and 2.5 s before the onset time was computed. In this time window the finger-modes were relatively steady. Then, the deviation vector ($\Delta m_j = m_j - m_{j,AV}$) between the mode (m_j) and the time-averaged finger-mode ($m_{j,AV}$) were obtained for each time sample. The mean across trials, Δm , was computed next. The Jacobian (\mathbf{J}) matrices reflect how changes in individual finger modes produce changes in F_{TOT} and M_{TOT} : $\mathbf{J}_F = [1, 1, 1, 1] \cdot [\mathbf{E}]$ and $\mathbf{J}_M = [d_L, d_M, d_R, d_L] \cdot [\mathbf{E}]$, respectively and $d_L = -4.5$ cm, $d_M = -1.5$ cm, $d_R = 1.5$ cm, and $d_L = 1.5$ cm, where the operator “ \cdot ” indicates matrix multiplication. The UCM was defined as the three-dimensional null-space of the Jacobian matrix \mathbf{J} (standing for either \mathbf{J}_F either \mathbf{J}_M), spanned by the basis vectors $\boldsymbol{\varepsilon}_i$, ($i=1,2,3$) solving:

$$\mathbf{J} \cdot \boldsymbol{\varepsilon}_i = 0 \quad (5.4)$$

Then, mean deviation mode vector, Δm , was projected onto the null- and orthogonal spaces of the corresponding \mathbf{J} as follows:

$$\Delta m_{\parallel} = \sum_{i=1}^3 (\varepsilon_i^T \cdot \Delta m) \cdot \varepsilon_i \quad (5.5)$$

$$\Delta m_{\perp} = \Delta m - \Delta m_{\parallel} \quad (5.6)$$

where Δm_{\parallel} , is the null-space component and Δm_{\perp} , is the orthogonal component of the mean deviation mode vector. Both components are still four-dimensional mode vectors. The extent of ME and nME changes of the modes was assessed by computing the length of these vectors, normalized by the square root of the number of DOF in the corresponding dimension ($\text{DOF}_{\text{UCM}}=3$, $\text{DOF}_{\text{ORT}}=1$; see Mattos et al. 2011): $ME = \sqrt{\sum_{n=1}^4 \Delta m_{\parallel,n}^2 / 3}$ and $nME = \sqrt{\sum_{n=1}^4 \Delta m_{\perp,n}^2 / 1}$.

UCM-based variance analysis

This analysis investigated whether the trial-to-trial variance in the finger-mode combinations was compatible with changed (V_{ORT}) or consistent (V_{UCM}) value of a performance variable, F_{TOT} and M_{TOT} . For the variance analysis, at each time sample, the mean, \bar{m} , across trials, j , of the mode vector, m_j , was computed and used to make the mode vector at each time sample and each trial, j , mean-free: $\delta m_j = m_j - \bar{m}$. The mean-free mode vector was projected onto the null (V_{UCM}) and orthogonal (V_{ORT}) spaces of the corresponding \mathbf{J} using the basis vectors, ε_i , of Eq. 4:

$$\delta m_{\parallel,j} = \sum_{i=1}^3 (\varepsilon_i^T \cdot \delta m_j) \cdot \varepsilon_i \quad (5.7)$$

$$\delta m_{\perp,j} = \delta m_j - \delta m_{\parallel,j} \quad (5.8)$$

The variance across trials per DOF along (V_{ucm}) and orthogonal (V_{ort}) to the UCM was then computed as follows:

$$V_{ucm} = \sum_{j=1}^{N_{trials}} |\delta m_{\parallel,j}|^2 / 3 \quad (5.9)$$

$$V_{ort} = \sum_{j=1}^{N_{trials}} |\delta m_{\perp,j}|^2 / 1 \quad (5.10)$$

where the vertical bars indicate the computation of the length of each mode vector. The normalization again takes into account the dimensionality of each subspace ($\text{DOF}_{UCM} = 3$; $\text{DOF}_{ORT} = 1$).

Definition of phases of analysis

We computed the mean components of variance and ME indices within steady-state phases as illustrated in Figure 5.2. For the *Jumping-Target* task, the steady state phase “PRE-” was computed as the average value between 2.0 and 2.5 s prior to the first target jump (1st jump), the phase during target jump (DUR-) corresponded to the time window 3.0-3.5 after the 1st jump, and the phase was post- target jump was computed between 2-2.5 s after the second target jump, when the target return to its initial position. For the *I-Perturbation* trials, the pre- and post-perturbation phases were computed over 2-2.5 s before and after the onset of the I-finger lifting, respectively. Note that in the PRE-phase the deviations in finger modes were computed with respect to the same time interval (see above – Analysis of motor

equivalence). Thus the difference vector of the time profile of finger-mode (Δm_j) from its average ($m_{j,AV}$) was zero on average, of course. The fluctuations around that mean, had ME and nME components, illustrated in the time profiles in Figure 5.4 between -2.5 and -2.0 s. Because lengths are positive numbers, the mean length of either component is larger than zero.

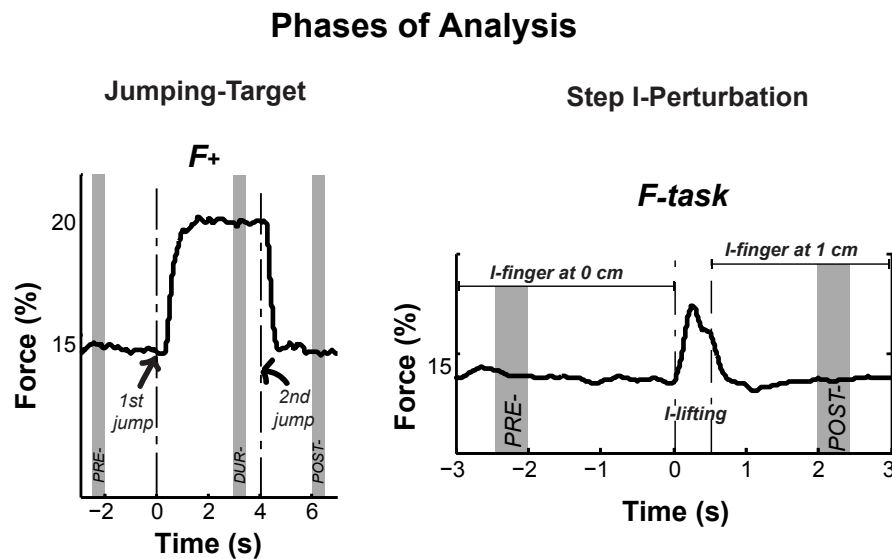


Figure 5.2 Phases of analysis for the Jumping-Target and Step I-Perturbation tasks. For the Jumping-Target task, the phase PRE- corresponded to the mean values between 2.0 and 2.5 s prior to the first target jump (1st jump), during (DUR-) was computed between 3.5 and 4 s after the 1st jump, and POST- to the mean values between 2.0 and 2.5 s after the second target jump (2nd jump). For Step I-Perturbation, the phases PRE- and POST- were computed between 2.0 and 2.5 s prior to and after the onset of the index finger lifting (I-lifting), respectively.

Statistical analysis

In the Jumping-Target experiment, the Jumping-Variable could involve transient changes of either F_{TOT} or M_{TOT} . We quantified the $\{ME; nME\}$ and $\{V_{UCM}; V_{ORT}\}$ components with respect to both F_{TOT} and M_{TOT} . This was done to verify the effects of the quick changes in each of the variables at phases DUR- and POST- target jumps on the components. We also estimated how visual feedback removal after the target jumps affected the outcome variables. Thus, separate 3-way ANOVAs were used with respect to each of the two performance variables for each Jumping-Variable. We divided the analyses of the continuous- and frozen-feedback variables. In the first one, when the target jumped to different values of force or moment, the performance variables analyzed were F_{TOT} and M_{TOT} , respectively. In the second case, the performance variable was M_{TOT} when force changed, and F_{TOT} when moment changed. The factors of the 3-way ANOVAs were: *Projection Component* (ME vs. nME or V_{UCM} vs. V_{ORT}), *Phase* (PRE-, DUR-, and POST-) and *Direction*. *Direction* had two levels, F+ and F- for the F-Jumping-Variable, and M+ and M- for the M-Jumping Variable.

In the I-Perturbation experiment, we also provided visual feedback only on force (F-task) or only on moment (M-task). Note that in this experimental design the external perturbation was always the same for both conditions of visual feedback. To test the effects of perturbation and visual feedback we performed 3-way ANOVAs for the F_{TOT} and M_{TOT} separately. The factors were: *Projection Component* (ME vs. nME or V_{UCM} vs. V_{ORT}), *Phase* (PRE- and POST-), and *Task* (F- and M-Task).

The Greenhouse-Geisser adjustment to the DOFs was applied whenever violations of sphericity were observed. Two-way ANOVAs and paired *t*-tests were performed for target post-hoc comparisons. *Paired t*-tests were also performed to

compare differences in the finger forces and moment of force between PRE- and POST-phases. Bonferroni corrections were applied. The level of significance was set to 0.05. All statistics were performed with SPSS statistical software (v. 20, IBM).

5.4 Results

1. Jumping-Target Tasks

In this part of the experiment, the target jumps could lead to a change in the target location along the vertical axis (requiring changes in F_{TOT}) or along the horizontal axis (requiring M_{TOT} changes). Visual feedback was provided only on the Jumping-Variable, i.e. if the target jumped along the vertical axis, individuals could observe changes in F_{TOT} , while M_{TOT} visual feedback was frozen. As expected, the subjects kept the values of the Jumping-Variable practically unchanged after the target returned back to its initial location. This was not true, however, for the frozen-feedback variable, which could show a large drift.

Figure 5.3 (*upper plots*) illustrates the time profiles of F_{TOT} and M_{TOT} for each of the four conditions. For F_{TOT} , the group mean \pm SD was 11.05 ± 3.30 N PRE- and 11.12 ± 3.19 N ($t_7 = -1.23$, $p > 0.25$) after- the target jumped up and then back to the original position (F+ Jumping-Variable); and it was 11.00 ± 3.34 N and 10.98 ± 3.19 N ($t_7 = 0.41$, $p > 0.69$), before and after the target jumped down and then back to the original position (F- Jumping-Variable), respectively. For M_{TOT} , the group mean \pm SD prior and after- the target jumped to the right and then back to the original position was -0.02 ± 0.24 Nm and 0.05 ± 0.41 Nm ($t_7 = -0.39$, $p > 0.70$), respectively; and

before and after the target moved to the left and then back to the original position M_{TOT} was -0.06 ± 0.26 Nm and -0.25 ± 0.46 Nm ($t_7 = 0.86$, $p > 0.41$), respectively.

In contrast, the values of the frozen-feedback variables (*i.e.* F_{TOT} for M+ and M- Jumping-Variable, and M_{TOT} for F+ and F- Jumping-Variable) showed major drifts. M_{TOT} drifted towards negative values (pronation). The group mean \pm SD of M_{TOT} PRE- and POST- changes in the F+ Jumping-Variable was -0.48 ± 0.42 Nm and -6.20 ± 1.65 Nm ($t_7 = 10.59$, $p < 0.001$), respectively; and PRE- and POST- changes in the F- Jumping-Variable, M_{TOT} was -0.27 ± 0.20 Nm and -5.83 ± 2.10 Nm ($t_7 = 7.82$, $p < 0.001$), respectively. The drifts in F_{TOT} were not consistent across subjects; the standard deviations were large (~ 5 N). Therefore, although F_{TOT} showed large deviations from the initial value in the M-tasks, there were no significant differences between F_{TOT} PRE- and POST- target jumps (all $t_7 < 1.845$, $p > 0.1$).

The respective changes in the individual finger forces and moments for the Jumping-Variable with continuous and frozen-feedback during the course of the trial can be seen in the middle and lower panels of Figure 5.3. For the continuous-feedback variable, there were large changes in the relative amount of force produced by the M and L- fingers when the target returned to the initial position across conditions (all $|t_7| > 2.63$, $p < 0.05$), the I- and R-fingers showed less consistent changes across subjects. There were also changes in the moment of force magnitudes, but with large variability among subjects.

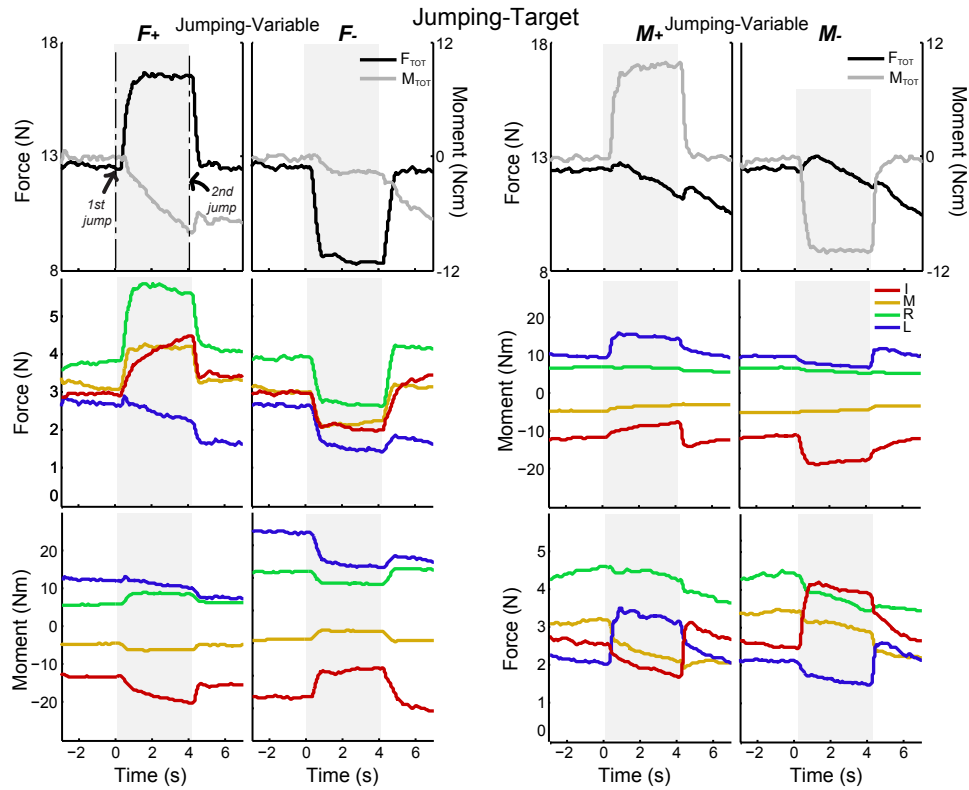


Figure 5.3 Force and moment time profiles of a subject during the Jumping-Target Task. The period highlighted in gray shows the target at a new position after the 1st jump. *Upper* plots show the total force (F_{TOT}) and the total moment of force (M_{TOT}) during each condition of target jump. *Middle* and *lower* plots show the finger forces and moment of force of the index (I), middle (M), ring (R), and little (L) fingers. Positive moment direction represents supination efforts.

Motor equivalence analysis

Figure 5.4 presents the ME and nME components for a representative subject, i.e., the amount of deviations in the mode space that left the performance variable unchanged, or changed, respectively. The area highlighted in gray shows the 4-s time window between the two target jumps, to a new location and back to the old location on the screen.

The analysis with respect to the continuous-feedback variable is shown in the upper plots of Figure 5.5. The ME and nME components were compared PRE- and POST- the sequence of two jumps, i.e., when the target was in the same place on the screen. For the continuous-feedback variable with respect to F_{TOT} , the ANOVA showed a significant 3-way interaction *Projection Component* \times *Phase* \times *Direction* on F_{TOT} ($F_{1.370,9.592} = 12.20$; $p < 0.005$), and a significant 2-way interaction *Projection Component* \times *Phase* ($F_{1.483,10.384} = 12.20$; $p < 0.001$) with respect to M_{TOT} . Prior to the first target jump, the ME (solid lines) component was significantly larger than nME (dotted lines) in F_{TOT} ($p < 0.05$). This effect was likely related to the variance structure and is discussed in detail in the Discussion. No differences between components were observed in M_{TOT} at PRE-phase ($p > 0.1$). At DUR-phase when the task-performance variable changed, both components were larger: ME ($p < 0.05$) and nME ($p < 0.001$). These results were observed for both F_{TOT} and M_{TOT} performance variables. The direction of target jump had an effect in the F_{TOT} analysis: the amount of ME ($p < 0.001$) was larger in F+ compared to F- target jumps (see DUR- in the upper-left plots, Figure 5.5). Finally, when the target returned to the initial position in the POST-phase, both ME and nME components were larger as compared to the PRE-phase, the time interval before the target jumps, but the relative increase in the ME component was larger. These findings across subjects are illustrated with the group means presented in Figure 5.5.

In contrast, for the frozen-feedback variable (lower plots of Figure 5.5) the ANOVA revealed a significant interaction *Projection Component* \times *Phase* ($F_{1.870,13.083} = 12.310$; $p < 0.05$) for F_{TOT} and a significant interaction *Projection Component* \times *Phase* \times *Direction* ($F_{1.258,8.807} = 7.081$; $p < 0.05$) for M_{TOT} . Both ME and nME

components increased at phases DUR- and POST- leading to no difference between the two in the final state ($p > 0.9$). For the M_{TOT} analysis, the increase in the ME ($p < 0.05$) and nME ($p < 0.0001$) components was larger in the Jumping-Variable F+ than F- (see these differences in the DUR-phase, lower left plot of Figure 5.5).

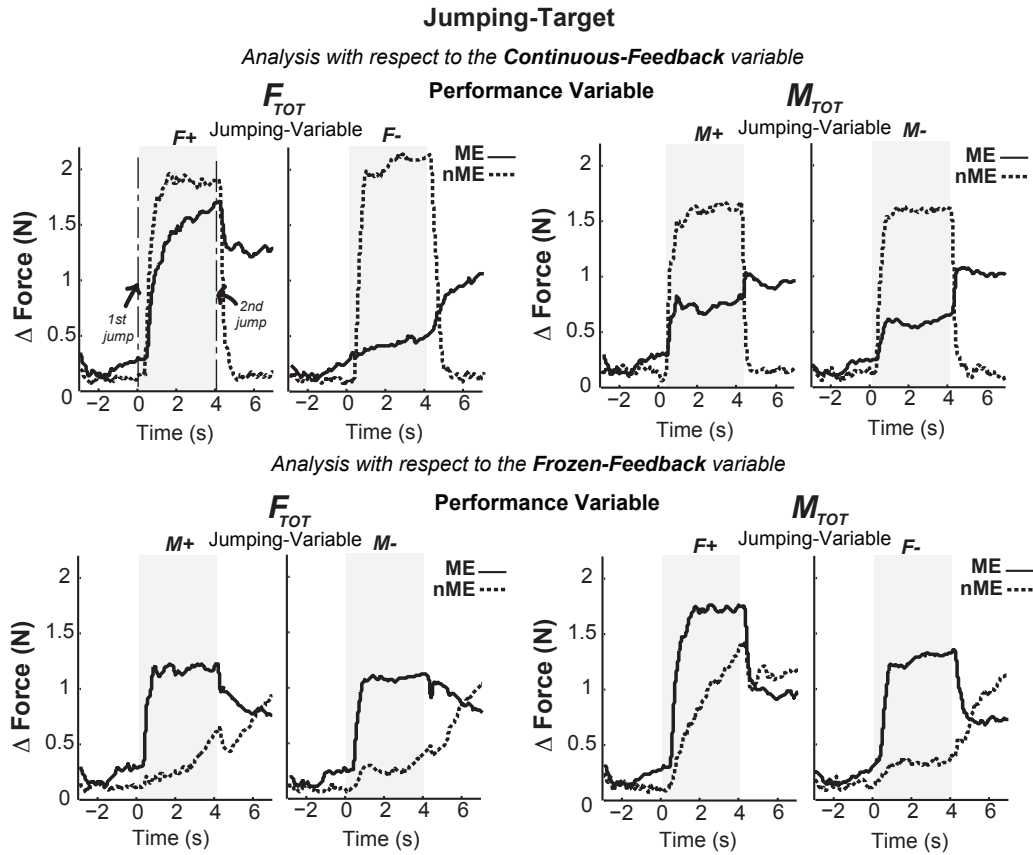


Figure 5.4 Typical time profiles of the motor equivalence (ME, solid line) and non-motor equivalence (nME, dotted line) components during the Jumping-Target Task. Analysis was performed in the space of finger-modes. Each component was normalized by the square root of the number of DOF in each dimension.

Jumping-Target

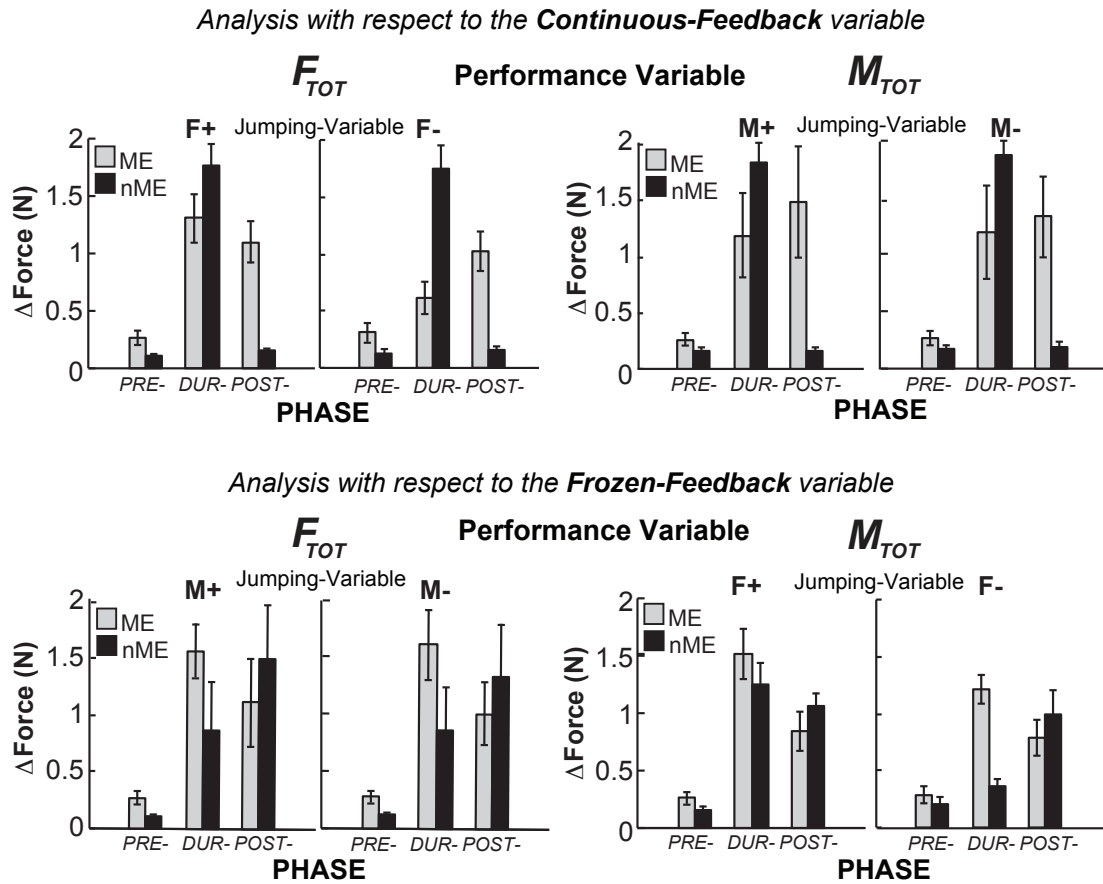


Figure 5.5 Group means (\pm SE) of the motor equivalence (ME, gray bars) and non-motor equivalence (nME, black bars) components at phases: PRE-, during (DUR-), and POST- target-jump. *Upper* and *lower* plots show the continuous-feedback and frozen feedback variables, respectively. Visual feedback was removed for frozen-feedback variables at phases DUR- and POST- Target Jump.

Analysis of the structure of variance

Analysis of the inter-trial variance in the space of finger modes is illustrated in Figure 5.6 with the group means for the two variance components (V_{UCM} – gray; V_{ORT} – black). The upper plots show the data for the continuous-feedback variable. For

F_{TOT} , the inequality $V_{UCM} > V_{ORT}$ was evident across the three phases while the M_{TOT} differences in V_{UCM} and V_{ORT} approached significance ($F_{1,7} = 4.855$; $p = 0.063$). F_{TOT} showed larger V_{UCM} for F+ Jumping-Variable than when the target jumped to lower levels of force production in F-. The lower plots (Figure 5.6) illustrate the data for the frozen-feedback variable. When visual feedback was removed following the first jump, the V_{UCM} and V_{ORT} components became similar (all $p > 0.2$). The 3-way ANOVA revealed a significant effect of *Projection Component* ($F_{1,7} = 5.650$; $p < 0.05$) for F_{TOT} . In contrast, for M_{TOT} analysis, there was only a significant interaction *Projection Component* \times *Phase* \times *Direction* ($F_{1,372,9.602} = 5.553$; $p < 0.05$). In the analysis with respect to M_{TOT} , V_{ORT} was larger in the F+ jumps than F- at DUR- ($p < 0.05$) and POST- ($p < 0.05$) phases. The difference in the amount of V_{UCM} in F+ versus F- during the target jump (DUR-) was close to significance ($p = 0.060$). These results were supported by a significant *Phase* \times *Direction* ($F_{1,604,11.229} = 25.573$; $p < 0.0001$) and *Projection Component* \times *Direction* ($F_{1,903,13.322} = 4.855$; $p < 0.001$) interactions in the M_{TOT} -analysis.

2. I-Perturbation Tasks

Step perturbation of the I-finger led to different adjustments in the finger forces and modes depending on the visual feedback provided. Figure 5.7 illustrates typical time profiles of F_{TOT} and M_{TOT} (top panels) and of the individual finger forces and moments for the continuous and frozen-feedback variables (middle and bottom panels) for a representative subject. The left plots show the time series for the F-task, when F_{TOT} was the continuous-feedback variable and M_{TOT} was the frozen-feedback variable. The right plots show the data for the M-task: M_{TOT} was the continuous-

feedback variable and F_{TOT} was the frozen-feedback variable. The time window highlighted in gray corresponds to the lifting of the I-finger by 1 cm.

Jumping-Target

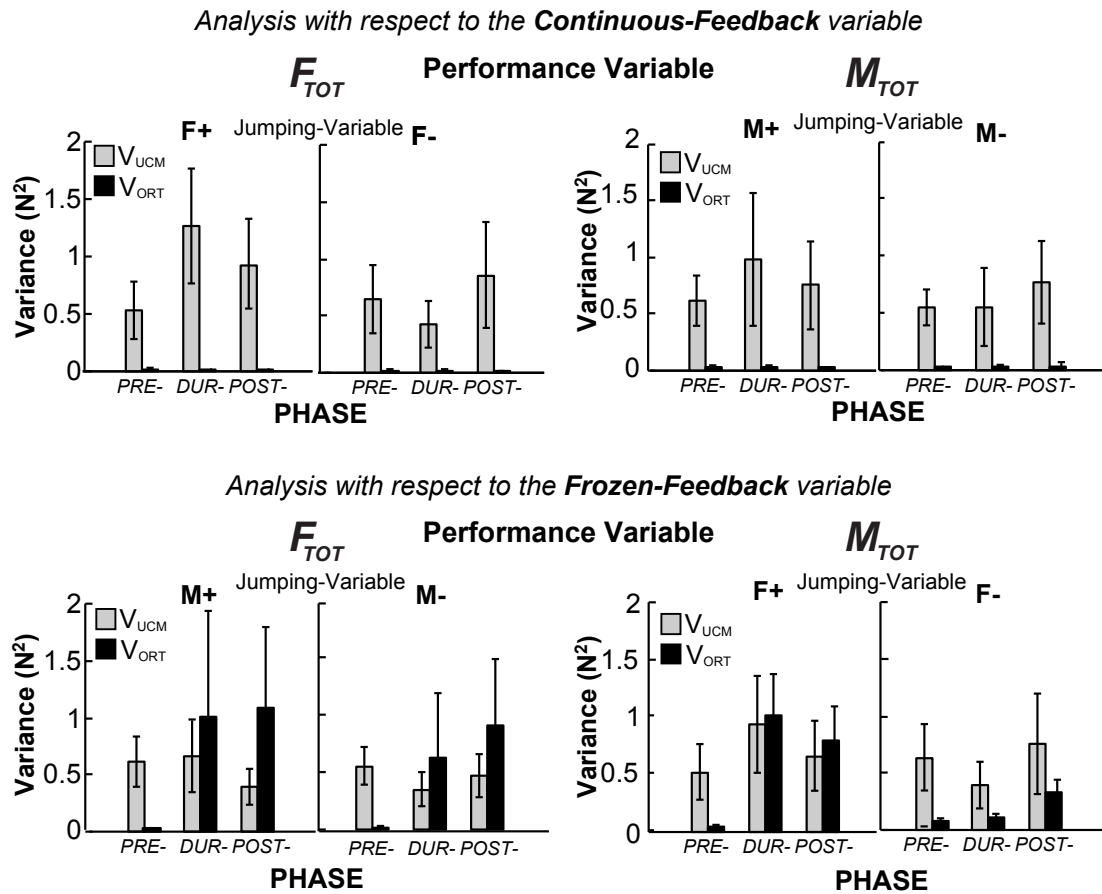


Figure 5.6 Group means (\pm SE) of the V_{UCM} (gray bars) and V_{ORT} (black bars) components at phases: PRE-, during (DUR-), and POST- target-jump. The continuous-feedback and frozen feedback variables are shown in the *upper* and *lower* plots, respectively.

Note that the values of the continuous-feedback variable (F_{TOT} for F-task, and M_{TOT} for the M-task) were similar PRE- and POST-perturbation. The group average \pm SE of F_{TOT} was 11.08 ± 3.27 N and 11.08 ± 3.15 N ($t_7 = 0.08$, $p > 0.90$) PRE- and POST-perturbation, respectively; the average values of M_{TOT} were 0.19 ± 0.42 Nm and 0.01 ± 0.48 Nm, respectively ($t_7 = 0.0843$, $p > 0.42$). In contrast, the frozen-feedback variable showed major deviation from its initial values. In particular, M_{TOT} in the F-task drifted towards negative values (pronation), from -0.08 ± 0.65 Nm to -13.05 ± 7.35 Nm ($t_7 = 5.260$, $p < 0.001$). In the M-task, the changes in F_{TOT} after the visual feedback removal were inconsistent across subjects, the mean values PRE- and POST-perturbation were 11.02 ± 3.20 N and 9.41 ± 4.63 N ($t_7 = 1.044$, $p > 0.33$).

In the F-task, after the I-finger was lifted, the force of the I-finger increased ($t_7 = -4.623$, $p < 0.01$) while the M, R and L fingers showed a force drop ($t_7 > 2.581$, $p < 0.05$). The individual finger moments also changed. There was an increase in the pronation moment by the I, R and L-fingers ($t_7 > -2.672$, $p < 0.05$). The M-finger was the only one showing a significant increase in the supination moment ($t_7 = -2.581$, $p < 0.05$) post-perturbation.

In the M-task, when the I-finger was lifted, the changes observed for the individual finger forces and moments varied across subjects. The differences between the individual finger forces produced PRE- and POST-perturbation were not significant (all $t_7 < 1.84$, $p > 0.10$). Also, no statistical significance was found in the moment of force of individual fingers between the conditions PRE- and POST-perturbation (all $t_7 < -1.84$, $p > 0.10$).

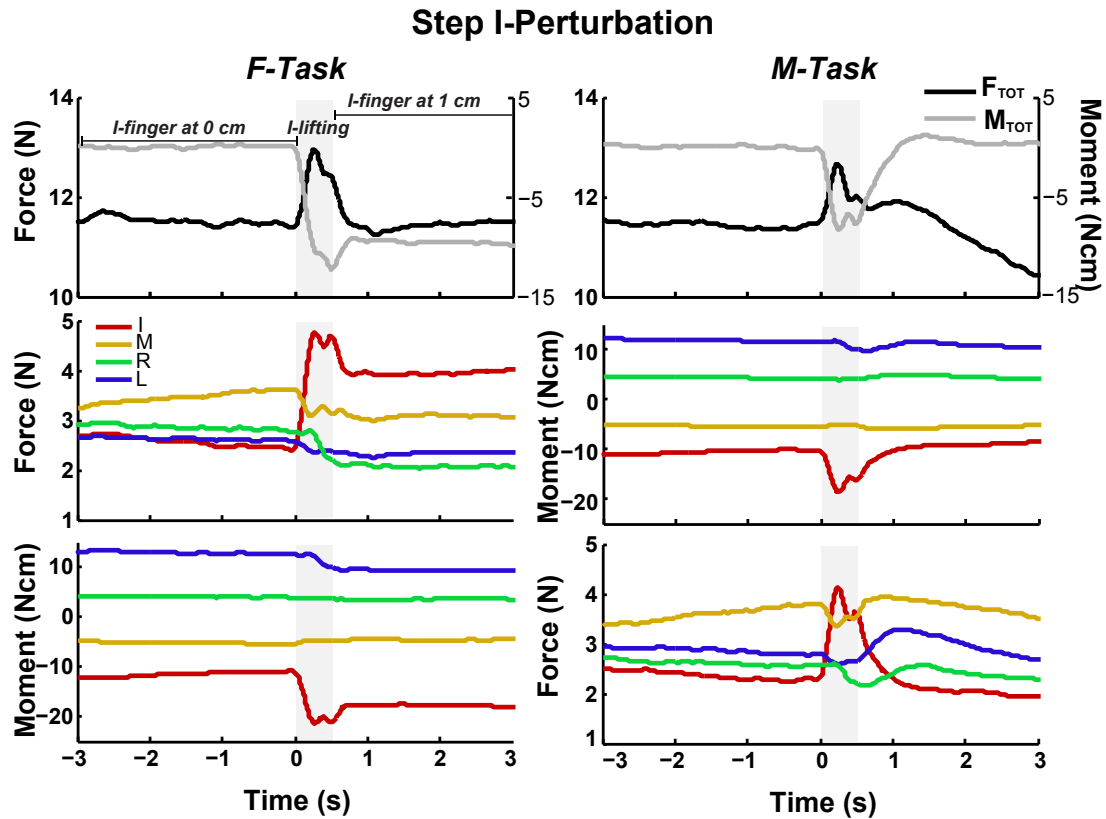


Figure 5.7 Force and moment time profiles of a subject during the Step I-Perturbation Task. The period highlighted in gray shows the period of lifting of the index (I)-finger. *Upper* plots show the total force (F_{TOT}) and the total moment of force (M_{TOT}) for the F-task and M-task. *Middle* and *lower* plots show the finger forces and moment of force of the index (I), middle (M), ring (R), and little (L) fingers.

Motor equivalence analysis

The time profiles of the ME and nME components for a representative subject are illustrated in Figure 5.8. For the continuous-feedback variable (top panels), there was an increase in the ME component (solid line) accompanied by minor changes in the nME component (dotted line) from the initial steady state to the final steady state (after the gray area). In contrast, for the frozen-feedback variable (bottom panels), the

ME component increased after the I-finger perturbation, but the increase of the nME component was also large. The respective group averages from the motor equivalence analysis are illustrated in Figure 5.9. Note the different scales of the y -axes in the top (PRE-perturbation) and bottom (POST-perturbation) panels.

Prior to the perturbation, the ME component was larger than the nME component across tasks for the F_{TOT} performance variable ($F_{1,7} = 16.415$; $p < 0.01$), and this difference was close to significance for M_{TOT} ($F_{1,7} = 4.622$; $p = 0.068$). Because the motor equivalence analysis within the phase prior to the perturbation computes a difference vector that is mean free, the ME and nME components in this phase are non-zero because the lengths of difference vectors are positive numbers. The larger ME relative to the nME component may come from the larger variance within the UCM than within ORT, a contamination of the mean by variance for positive measures (see Discussion). In the post-perturbation phase, the difference between ME and nME components was significant both for F_{TOT} ($p < 0.01$) and M_{TOT} ($p < 0.05$) continuous-feedback variables. There was no difference between these components for the frozen-feedback variable. This was true with respect to both performance variables (all $p > 0.1$).

Regarding the effects of the perturbation, there was an increase in the ME component at the post-perturbed phase for both tasks. In the F_{TOT} -analysis, the increase in ME was smaller for the frozen- as compared to the continuous-feedback variable (Sig. *Phase x Task*: $F_{1,7} = 8.603$; $p < 0.05$), while the ME increase was similar in both tasks with respect to M_{TOT} despite the differences in feedback (Sig. *Phase*: $F_{1,7} = 12.284$; $p < 0.01$). When continuous feedback was provided to the subjects there was no difference in the nME component between the PRE- and POST-conditions (the top

and bottom panels have different y-scales) indicating that values of the task-performance were preserved. However, this was not true when visual feedback was removed. In this case, there was a larger nME in F_{TOT} (right panel, Sig. *Phase* \times *Task*: $F_{1,7} = 6.255$; $p < 0.05$) and M_{TOT} (left panel, Sig. *Phase* \times *Task*: $F_{1,7} = 26.102$; $p = 0.001$) analyses. These findings were supported by a significant interaction *Projection Component* \times *Phase* \times *Task* computed separately each task performance variable F_{TOT} ($F_{1,7} = 10.050$; $p < 0.05$) and M_{TOT} ($F_{1,7} = 21.268$; $p < 0.005$).

Analysis of the structure of variance

We performed the variance analysis to verify whether the structure of variance would be preserved with respect to salient performance variables prior to and after the perturbation of the index finger, and to explore the effects of the visual feedback removal. The group average results of this analysis prior to and after the I-perturbation are illustrated in Figure 5.10 in the upper and lower plots, respectively. At the PRE-perturbation phase, feedback was provided for both F_{TOT} and M_{TOT} . Therefore, no differences were expected in the structure of variance prior to the perturbation.

The across-trials variance in finger-mode was structured ($V_{UCM} > V_{ORT}$) to preserve F_{TOT} at both phases when continuous feedback was provided (*Projection Component*: $F_{1,7} = 7.023$; $p < 0.05$). Similar finger-mode structure ($V_{UCM} > V_{ORT}$) was observed for the M-task at pre-perturbation ($t_7 = 3.189$; $p < 0.05$). The visual feedback removal led to a significant increase in V_{ORT} ($t_7 = -3.127$; $p < 0.05$) and no difference in V_{UCM} ($t_7 = -0.946$; $p = 0.376$); as a result, post-perturbation $V_{UCM} \sim V_{ORT}$ ($t_7 = -0.132$; $p = 0.899$). This finding was supported by a significant *Projection Component* \times *Phase* interaction ($F_{1,7} = 6.293$; $p < 0.05$). In the analysis with respect to M_{TOT} , $V_{UCM} > V_{ORT}$ for the continuous-feedback variable ($F_{1,7} = 8.790$; $p < 0.05$), and for the

frozen-feedback variable this difference approached significance ($F_{1,7} = 4.430$; $p = 0.073$) without other effects.

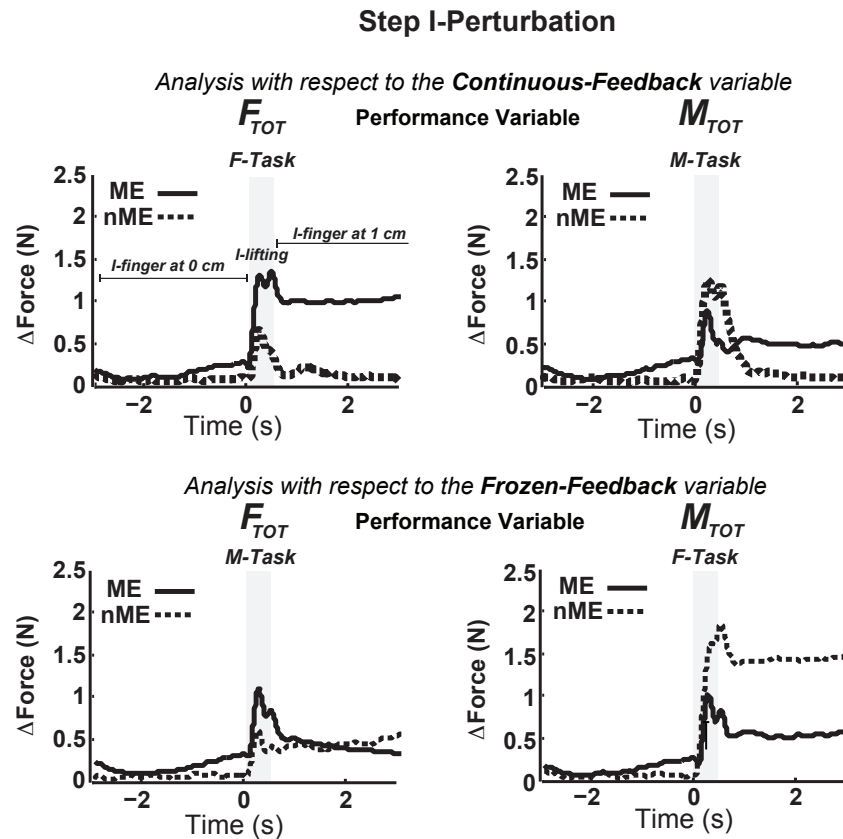


Figure 5.8 Typical time profiles of the motor equivalence (ME, solid line) and non-motor equivalence (nME, dotted line) components during the Step I-Perturbation Task. Analysis was performed in the space of finger-modes. Each component was normalized by the square root of the number of DOF in each dimension. 5.8: Typical time profiles of the motor equivalence (ME, solid line) and non-motor equivalence (nME, dotted line) components during the Step I-Perturbation Task. Analysis was performed in the space of finger-modes. Each component was normalized by the square root of the number of DOF in each dimension.

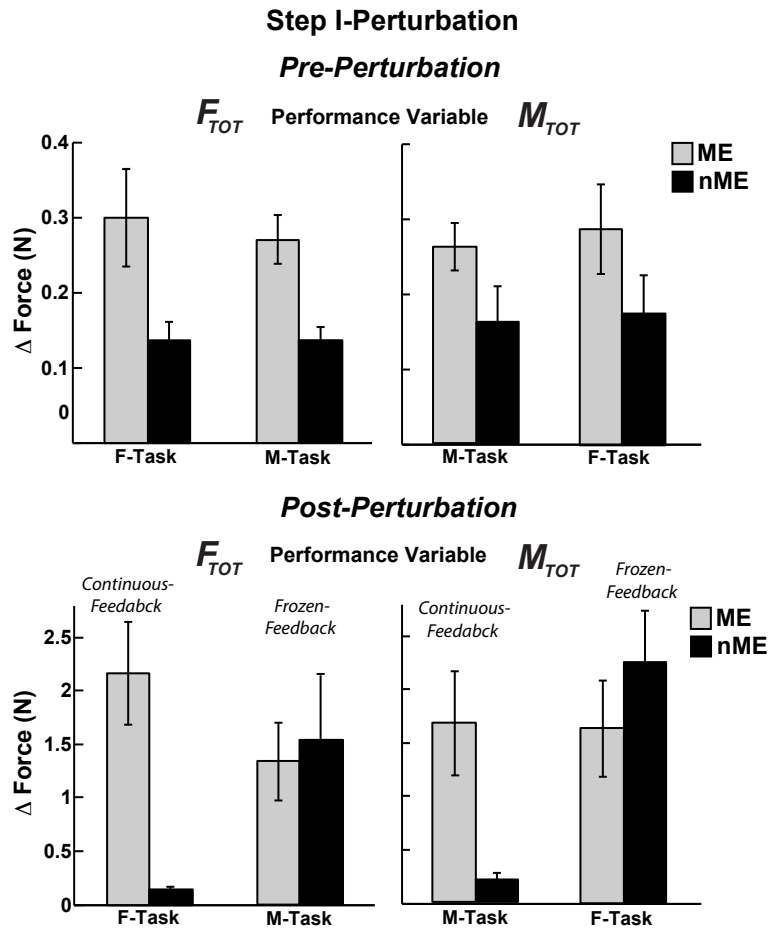


Figure 5.9 Group means (\pm SE) of the motor equivalence (ME, gray bars) and non-motor equivalence (nME, back bars) components during the Step I-Perturbation Task at phases Pre-Perturbation and Post-Perturbation, *upper* and *lower* plots respectively. The scale of the y-axis is not consistent between plots.

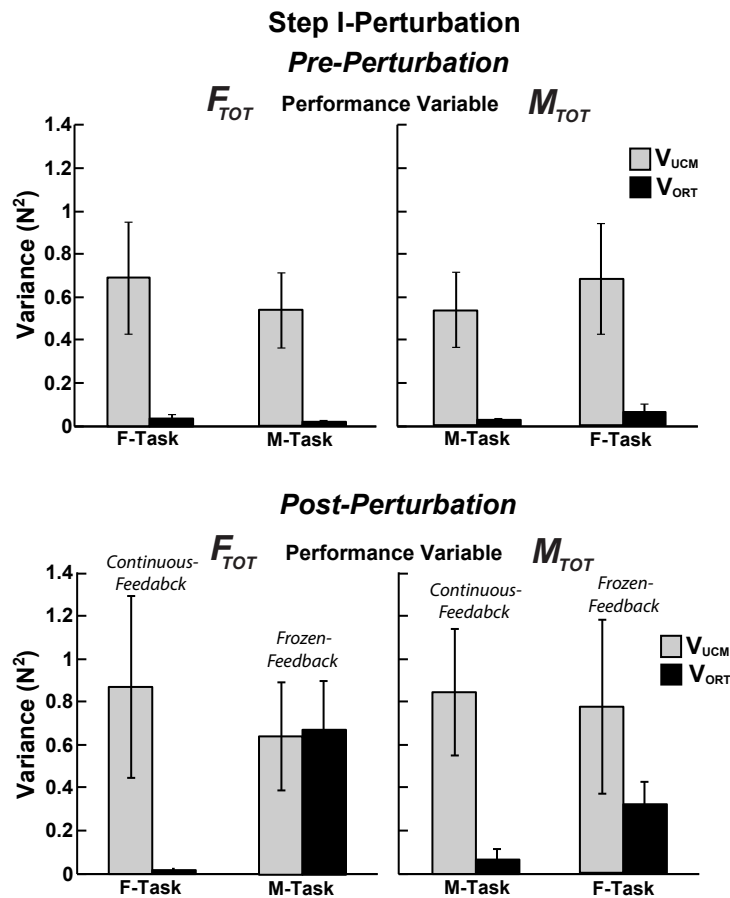


Figure 5.10 Group means (\pm SE) of the V_{UCM} (gray bars) and V_{ORT} (black bars) components during the Step I-Perturbation Task at phases Pre-Perturbation and Post-Perturbation, *upper* and *lower* plots respectively.

5.5 Discussion

The results largely confirmed the hypotheses formulated in the Introduction. We found a larger increase in the ME component when the task a priori required an increase only in the nME component (Hypothesis-1). More importantly, after the sequence of target jumps, the nME component returned to values close to pre-perturbed ones, while the ME component remained large (Hypothesis-2). A larger ME

effect ($ME > nME$) was also found after the step perturbations of the index finger. The effects of visual feedback removal were mostly along the ORT component resulting in a dramatic increase in the nME component (Hypothesis-3). Lastly, corroborating with previous experiments, there was a strong UCM effect ($V_{UCM} > V_{ORT}$) throughout the phases of analysis, except when visual feedback was removed on the task variable, relative to which was variance analyzed (Hypothesis-4). In those cases, variance in ORT increased after the visual feedback was frozen (DUR- and POST-). Further, we discuss implications of these findings on issues of the neural control of redundant (abundant) systems and task-specific stability of performance.

Task-specific stability in abundant systems

Traditional methods to study stability involve the application of small perturbations to the system of interest. Within the UCM hypothesis, analysis of inter-trial variance has been used to produce indices reflecting stability of multi-element systems in different directions. Indeed, assuming somewhat different initial conditions and force fields across trials, one expects relatively high inter-trial variance in less stable directions and low inter-trial variance in more stable directions. Relatively recently, a complementary method has been introduced based on observation of system's trajectories during quick actions (Mattos et al., 2011; Scholz et al., 2011). This method assumes that a neural input into the system associated with a quick action may be viewed as a perturbation expected to cause relatively large deviations of the system in directions of low-stability. If a system produces a desired value or time profile of a salient performance variable, large deviations in directions that keep this variable unchanged (motor equivalent, ME) are expected. Large ME deviations have

been observed in several earlier studies (Mattos et al., 2013; Mattos et al., 2015; Mattos et al., 2011; Scholz et al., 2011; Scholz et al., 2007).

In all the mentioned studies, mechanical perturbations were applied and the system's response was quantified. Our current study is the first to document large ME deviations during quick actions of a multi-element system in the absence of any perturbations. Indeed, in the jumping-target trials, ME was quantified after a sequence of target jumps on the computer screen leading to the same final combination of task variables, $\{F_{TOT}; M_{TOT}\}$. The second condition resembled previous experiments in using perturbations to the elements (cf. Mattos et al., 2013; Mattos et al., 2015; Mattos et al., 2011). While only one finger was explicitly perturbed (the index finger), all finger forces were affected partly due to the well-known phenomenon of enslaving (lack of individualization, Kilbreath & Gandevia, 1994; Schieber, 1991; Zatsiorsky et al., 1998) and partly due to the mechanical coupling among the fingers. Both conditions showed large ME deviations while nME deviations could differ depending on the available feedback.

We illustrate the idea of task-specific stability and the two methods of its analysis (inter-trial variance and ME) in Figure 5.11. Imagine that a person presses with two fingers to produce a certain level of force ($F_1 + F_2 = 10$ N) several times. The cloud of data points across repetitive trials may form an ellipsoid with the major axis parallel to the solution subspace (the UCM, the slanted solid line). Such data distributions are characterized by the inequality $V_{UCM} > V_{ORT}$ and have been interpreted as signatures of a two-finger force-stabilizing synergy (Latash et al., 2001; Scholz et al., 2002). They reflect lower stability of the two-finger system along the UCM as compared to the orthogonal (ORT) direction.

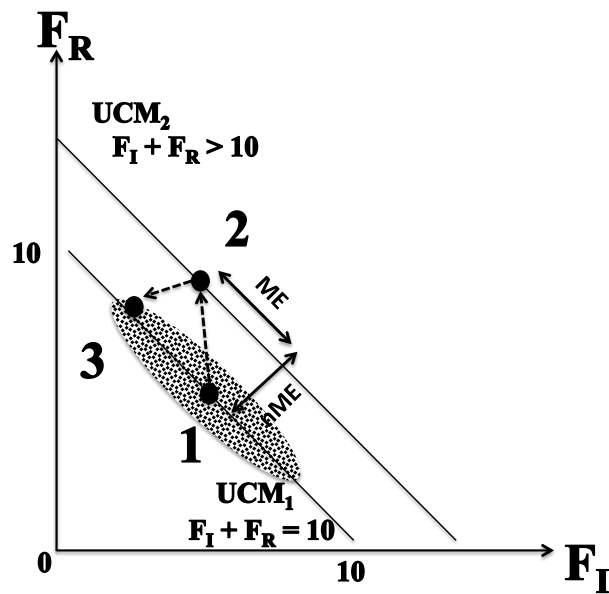


Figure 5.11 Scheme illustrating a hypothetical experiment where the goal of the task is to produce 10 N using the index (I) and ring (R)-fingers. When this task is repeated several times, and the force sharing between the I and R fingers (*I,R-sharing*) for each trial is plotted, the shape of the distribution will be an ellipse. The major axis corresponds to all the combinations of finger forces that satisfy the task, i.e. the UCM. Now, let's assume that one of the fingers is perturbed (eg. lifting of the I-finger) leading to an increase in the force produced by both fingers. The total force will be larger than 10 N. Then, after some delay, the force of the I and R-fingers will decrease to maintain the total force close to 10 N, representing motor equivalence at the task-performance. It is likely that the force produced by the individual fingers will change relative to the unperturbed state. The *I,R-sharing* is illustrated in three states: 1- unperturbed, 2- during the perturbation; 3- after the correction. Note that most of the deviations in *I,R-sharing* lie along the UCM (ME component) as compared with deviations orthogonal to the UCM (nME component).

Now, consider that a perturbation is introduced into the system, for example one of the fingers is lifted. This would lead to a change in the force produced by both fingers. There will be an error in the task performance ($F_1 + F_2 > 10$ N). Note, however, that the system is likely to deviate along both ORT and UCM directions, and

the deviation along the UCM direction is ME. If the subject of this mental experiment introduces a correction, total force is expected to drop close to the initial level but the individual finger forces may be expected to deviate along the UCM. These ME deviations have no effect on performance and, therefore, are not corrected. Similar effects may be expected from a voluntary quick total force change to a new level and its return to the initial level (same illustration as in Fig. 11 applies). Such a transient action is expected to lead to $ME > nME$ as it was observed in our experiment.

Structure of variance and motor equivalence

The use of quantitative analysis of ME within the UCM hypothesis is relatively recent. These studies have typically measured ME after either external perturbations applied to the whole system (Scholz et al., 2007), or to some of its elements (Mattos et al., 2013; Mattos et al., 2015; Mattos et al., 2011), or as a consequence of modified movement dynamics due to changes in the speed of reaching by a multi-joint effector (Scholz et al., 2011). The common finding among these studies is that ME deviations become larger with time after the perturbation and get contributions from mechanical reactions, reflex responses, and also voluntary corrections.

According to the general scheme (as in Fig. 5.11), both ME and structure of variance reflect task-specific stability. They, however, show different sensitivity to aspects of the action. For example, the system may show large deviations in a performance variable from an initial state resulting in large nME component such that $ME < nME$ (Figs. 5.4, 5.5). It may still be characterized by the $V_{UCM} > V_{ORT}$ inequality in both the initial and the final states (Fig. 5.6). On the other hand, V_{UCM} shows high sensitivity to the magnitude of the performance variable (V_{UCM}) while

V_{ORT} shows high sensitivity to its rate (Friedman, Latash, & Zatsiorsky, 2011; Goodman, Shim, Zatsiorsky, & Latash, 2005), thus it is possible to observe $V_{ORT} > V_{UCM}$ (or $V_{ORT} \sim V_{UCM}$) accompanied by $ME > nME$ (Mattos et al., 2015).

The ME effect ($ME > nME$) and the variance structure can also influence one another. Such interaction is expected when the difference of a finger-mode vector (Δm_j) from the pre-perturbed average is small, for example in the PRE-phase of the Jumping-Target and Step I-Perturbation tasks. The ME/nME components are computed as the length of the projections of the Δm_j , i.e. positive numbers. The mean Δm_j is zero in the PRE-phase. However, both ME and nME components are positive and their means are non-zero. For a broader data distribution, such an operation results in the mean shifted to larger values (Hansen, Grimme, Reimann, & Schoner, in press). Because the variance of the data is larger in the UCM than in ORT, $ME > nME$ is expected for small deviations from the mean. However, this type of interaction does not dominate in the POST-phase when Δm_j values are certainly different from zero.

An additional observation was that the difference in the structure of the inter-trial variance was different for different force levels required during the target jumps. When the target jumped to forces corresponding to 20% of the MVC there was a strong force-stabilizing synergy in a sense $V_{UCM} > V_{ORT}$. However, the target jumps to lower levels of force (10% of the MVC) resulted in $V_{ORT} \sim V_{UCM}$. These observations may be related to the mentioned dependence of V_{UCM} on the total force level. While higher force levels lead to more variance (Newell, Carton, & Hancock, 1984), when an abundant set of fingers is involved in the task, most of the variance is V_{UCM} (Goodman et al., 2005). Also, lower force levels required relaxation of the force producing muscles, which has been shown to lead to more variable performance than that during

force increase (Li, 2013; Shim et al., 2003; Shim, Olafsdottir, Zatsiorsky, & Latash, 2005).

Links to control with referent configurations

The ideas of the UCM hypothesis and of the neural control using referent spatial coordinates for salient variables have recently been united into a single scheme (Latash, 2010a). The referent configuration (RC) hypothesis 2009 (Feldman, 2009) is a generalization of the equilibrium point-hypothesis (Feldman, 1966, 1986) to multi-effector systems. According to this hypothesis, the CNS specifies a RC of the body, at which all the muscles are at their thresholds for activation via the tonic stretch reflex loop. The RC is typically not achievable due to anatomical and external constraints. As a result, the body reaches a state characterized with a non-zero level of muscle activations and non-zero forces on the environment. At the highest, task-specific level, the RC_{TASK} corresponds to referent coordinates of task-specific variables. In particular, in our experiment, setting values of $\{F_{TOT}; M_{TOT}\}$ may be associated with setting a vertical referent coordinate for the virtual finger (an imagined digit with the action equivalent to that of all four fingers, Arbib et al., 1985) and an angular referent coordinate (Latash, 2010a). Since the conditions were isometric, the differences between the actual and referent coordinates resulted in the production of non-zero $\{F_{TOT}; M_{TOT}\}$.

Mapping of the two task-specific referent coordinates to those for the four individual fingers is an example of a redundant problem (Bernstein, 1967). This mapping is organized in a synergic way, which means that any deviations in individual finger referent coordinates are channeled into a sub-space that does not affect the

performance variables (the UCM). This leads to the characteristic inequality $V_{UCM} > V_{ORT}$. Within this study, we do not address the next levels within the motor control hierarchy, which are also organized in a similar way, for example the mapping of finger referent coordinates onto referent coordinates for the many muscles affecting each finger's action.

Any intentional action is expected to be organized at the highest level of the hierarchy and represent shifts of referent coordinates for $\{F_{TOT}; M_{TOT}\}$. By itself, the action does not specify actions of individual fingers and referent coordinates for fingers change according to the task-specific organization of the mapping from the task-specific level to the finger level. This mapping ensures stability of the $\{F_{TOT}; M_{TOT}\}$ pair of variables and is expected to lead to large ME components of finger force (mode) changes and $V_{UCM} > V_{ORT}$. Note that both synergic signatures were observed across tasks and conditions in our study.

Unintentional drift in variables without visual feedback

When visual feedback was provided on one of the two performance variables only, the other variable (the frozen-feedback variable) showed a large-amplitude drift despite the instruction to the subjects to keep both variables at the initial levels. Removing visual feedback during steady-state accurate force production tasks is known to lead to a slow drift in the force level (Ambike, Zatsiorsky, & Latash, 2015; Slifkin, Vaillancourt, & Newell, 2000; Vaillancourt & Russell, 2002; Vaillancourt, Slifkin, & Newell, 2001). In those earlier studies, the subjects were not explicitly instructed to correct target forces, while our subjects were always instructed to keep the $\{F_{TOT}; M_{TOT}\}$ values at the target level. A study comparing the two instructions

reported more consistent behavior under the “do not interfere” instruction compared to the “correct quickly” instruction (Latash, 1994). Therefore, the instruction used in our experiment to correct the continuous-feedback variable could also play a role in the observed inconsistent force drifts among subjects.

The drift in M_{TOT} during the changes in force was consistently towards pronation during both Jumping-Target and I-Perturbation trials. In earlier studies, an interpretation has been offered of the force drift (and also of the hand position drift in multi-joint tasks, Zhou et al. 2014, 2015) based on the idea of RC control (Ambike, Paquet, Latash, & Zatsiorsky, 2013; Ambike et al., 2015; Zhou, Solnik, Wu, & Latash, 2014b). According to this idea, RC for a performance variable drifts slowly towards the actual value of this variable (RC-back-coupling) reflecting the natural tendency of physical systems to move towards a minimum of potential energy. Note that M_{TOT} was computed with respect to an axis passing through the mid-point between the middle and ring fingers. This was an arbitrarily selected point, which was likely shifted with respect to the point of application of the resultant finger force during natural pressing tasks (closer to the middle finger, Scholz et al., 2002). So, it was possible that in the absence of visual feedback the computed M_{TOT} drifted towards a value corresponding to the preferred point of application of the resultant.

Concluding comments

The main message of this study is that ME is a robust phenomenon that is observed following a sequence of quick actions leading to the same values of task-specific performance variables. Hence, voluntary actions may be viewed as descending perturbations into abundant systems. This finding supports the scheme of

motor control based on the idea that a family of solutions is facilitated to stabilize values of important performance variables.

Chapter 6

CONCLUSIONS

The main goal of this dissertation has been to quantify the extent to which perturbations introduced into redundant motor systems lead to motor equivalence with respect to task-specific performance variables and, alternatively, to changes in the performance. We explored the changes in the amount of ME and nME components at different phases of a variety of purposeful actions, and at several instants immediately following the perturbation onset, as well as the effects of visual feedback to provide insights about the neurophysiological sources for the motor equivalence phenomenon.

In the following sections, the specific aims and hypothesis will be reviewed and the respective findings will be summarized.

6.1 Aim 1 Findings

In experiments within Aim 1, individuals were instructed to reach to cylindrical and spherical targets, while an elastic band was placed across the elbow joint that limited elbow extension during the perturbed reaches. The motor equivalence indices were quantified and averaged within each 10% (~80 ms) of the reach trajectory. Aim 1 of this dissertation was **to determine how perturbations applied to the elbow joint lead to the use of motor equivalent joint configurations when individuals reach to targets with different constraints.**

Hypothesis 1.1: *Motor equivalence effects ($ME > nME$) with respect to the pointer tip position and the hand orientation will be present early in the reach and persist until movement termination. Such effects will increase after the perturbation onset, and a further increase is expected when the perturbation is stronger.*

As predicted, most of the differences in joint configuration between perturbed and non-perturbed trajectories led to preservation of the pointer-tip position and the hand orientation throughout the reach, i.e. $ME > nME$ with respect to both performance variables. Additionally, the ME values increased with the magnitude of the perturbation, but these effects were only present after ~30-40% of the reach trajectory, at approximately the time that the elbow joint motion was affected by the perturbation. The ME component was larger for the stronger perturbation (High-K condition) compared to the weaker perturbation (Low-K), while the effects of the magnitude of the perturbation were weaker on the nME component.

Hypothesis 1.2: *When the pointer is inserted into the cylindrical target, the motor equivalence effects will be larger with respect to hand orientation than position. In contrast, larger motor equivalence effects with respect to hand position than orientation are expected when individuals touch with the pointer the spherical target.*

The contrast between the stabilization of hand position *versus* orientation when movements were performed to spherical and cylindrical targets tested whether motor equivalence was modulated with respect to task constraints. Contrary to one of our hypotheses, the target type had no influence on the ME values with respect to either the pointer-tip position or the hand orientation. The task performance had an effect on the ME values after ~40% of the reach trajectory. The ME component was similar for the pointer-tip position and hand orientation. However, the nME component was

larger for the pointer-tip path than for the hand orientation regardless of whether the subjects had to only touch the spherical target with the pointer or to appropriately orient the pointer into the cylindrical target.

***Hypothesis 1.3:** The inter-trial variance in the joint configuration space will be structured in a specific way such that most of joint-configuration variance will lead to stable pointer tip position and hand orientation ($V_{UCM} > V_{ORT}$).*

The comparison between the motor equivalence analysis and the traditional UCM-based inter-trial variance approach tested for similarities between these approaches. Unlike the motor equivalence results, the UCM variance analysis, performed across repetitions of perturbed and non-perturbed trajectories, led to no effects or interactions among any of the factors manipulated during the experiment, i.e. magnitude of the perturbation, target type, and task performance. For all conditions, we found significantly larger V_{UCM} as compared to V_{ORT} , the component of joint configuration variance that reflects changes of the pointer-tip position or hand orientation.

6.2 Aim 2 Findings

The motor equivalence measured at the level of movement kinematics (Mattos et al., 2011; Scholz et al., 2007) reflects not only changes in neural commands but also mechanical coupling among the joint rotations (Hollerbach & Flash, 1982). The electrical activity of muscles is a closer estimate of the modulation of the neural drive to the motoneuronal pools that innervate the muscles. It has been suggested that muscles are united into groups as opposed to being controlled individually (d'Avella &

Bizzi, 2005; d'Avella et al., 2006; Tresch et al., 2006). Some authors (Krishnamoorthy, Goodman, et al., 2003) view these muscle groupings (M-modes) as an intermediate step in stabilization of task-specific performance variables. Within this aim, the motor equivalence analysis was applied at the level of muscle activations, treating the M-modes as the elemental variables stabilizing hand position and orientation during reaching. **The Aim 2 of this dissertation was to determine whether muscle modes (M-modes) would be reorganized in a task-specific way when the elbow joint was partially blocked (perturbed) while subjects inserted a pointer into a cylindrical target.**

***Hypothesis 2.1:** Motor equivalence effects ($ME > nME$) will be present in the M-mode space with respect to the pointer tip position and hand orientation. These effects will increase across successive time windows of 50 ms immediately after the perturbation onset corresponding to the action of local reflexes, pre-programmed reactions and voluntary responses. The motor equivalence effects will be stronger for hand orientation than pointer-tip position.*

The deviation in M-mode values in the perturbed reaches was observed starting 50-ms after the first visible changes in the EMG activity induced by the perturbation. The deviations in M-modes were larger in the ME component as compared with the nME component, computed for the pointer-tip position and hand orientation. The comparison of the ME and nME components between the phases before the perturbation and at 50 ms post-perturbation was close to significance, with a tendency for the ME component being larger than the nME component. When comparing the pre-perturbation with the Post-Pert100 phases (100 ms after perturbation onset), ME increase was significantly higher than the nME component. Both ME and nME

components increased equally between the pre-perturbation and “Post-Pert > 100” phases. Qualitatively similar results were observed in the motor equivalence analysis performed in the joint configuration space. The motor equivalence analysis had similar values with respect to the pointer-tip and the hand orientation.

Therefore, the observed changes in the magnitude of the M-modes suggest contributions from local reflexes (40–60 ms postperturbation), preprogrammed reactions (~70–100 ms), and voluntary corrections (>100 ms). Contrary to our expectation, no differences in the motor equivalence analysis with respect the hand pointer-tip position or hand orientation could be observed in the space of M-modes. However, the hypothesis that the motor equivalence effects would be stronger for hand orientation than pointer-tip position was confirmed at the level of joint rotations.

***Hypothesis 2.2:** The motor equivalence effects after the perturbation are not primarily due to an increase in the index of co-contraction between elbow flexors and elbow extensors at the post-perturbation phases as compared to unperturbed reaches.*

The index of co-contraction between the muscles acting at the elbow joint increased during the reaching movement, without major differences between the perturbed and unperturbed conditions. Therefore, it is unlikely that the increase in motor equivalence post-perturbation was due to changes in muscle co-contraction.

6.3 Aim 3 Findings

The previous experiments involving analysis of motor equivalence within the spaces of joint rotations and M-modes have suggested that a continuous perturbation leads to an increase in the deviation of the components of the synergy starting

immediately after the perturbation. Most of the changes in the motor components led to the task-specific stability with contributions from reflexes, pre-programmed and voluntary responses. The perturbation, however, was continuously applied to the effectors, which induced kinematic changes due to mechanical factors. **The Aim 3 of this dissertation was to determine whether a signature of motor equivalence (ME > nME) would be present after a transient positional perturbation applied to an element (the middle finger) during a multi-element task (accurate four-finger cyclic force production).** The perturbations consisted of a well-controlled lift of the finger, and after a few seconds the finger was lowered back to the initial position. A secondary goal was to investigate stabilization of multiple task performance variables simultaneously (Hsu & Scholz, 2012; Zhang et al., 2008). This was done by comparisons of motor equivalence and across-trials variance in finger forces with respect to total moment of force (M_{TOT}) and total force (F_{TOT}), while only the latter was used as feedback for the subjects. Similar analysis was performed in the finger mode space (hypothetical neural commands that can be modified independently, Danion et al., 2003).

***Hypothesis 3.1:** Motor equivalence effect (ME > nME) with respect to F_{TOT} and M_{TOT} values will be present in-between the lifting and lowering phases of the transient perturbation of the middle finger in the spaces of both finger forces and modes. The motor equivalence effect will persist after the transient perturbation is over.*

Motor equivalence analysis with respect to F_{TOT} (macro-analysis): Our analysis showed that elemental variables changed with the perturbation in the spaces of both finger forces and modes. However, there was a dramatic increase in the ME

component during and after the perturbation. In fact, the ME component was larger than the nME component even in the cycles before the perturbation, reflecting the fact that changes in the finger forces were primarily along the space leading to no changes in F_{TOT} . The ME component was larger than the nME during all steady-state phases of the task.

Motor equivalence analysis with respect to M_{TOT} (macro-analysis): In contrast to F_{TOT} that was consistently preserved across phases, motor equivalence in the M_{TOT} was found only during the perturbation, when the middle finger was kept in a lifted position. Before the perturbation, the nME component was larger than the ME component. When the perturbation was over, there was no difference between ME and nME components in the mode space; while in the force space the nME was larger than the ME component, both results suggesting that there was no motor equivalence with respect to M_{TOT} .

***Hypothesis 3.2:** Motor equivalence in F_{TOT} ($ME > nME$) will increase across successive time windows of 50-ms immediately after the perturbation onset in the spaces of finger forces and modes corresponding to local reflexes, pre-programmed reactions and voluntary responses.*

Motor equivalence analysis with respect to F_{TOT} (micro-analysis): We confirmed this hypothesis: The ME component increased gradually over the 50-ms time windows accompanied by a smaller and less consistent increase in the nME component. The ME component was larger in the period between 1 and 50 ms post-perturbation, before any effect mediated by reflex loops could be expected. The substantial increase of the ME component in the subsequent phases post-perturbation

suggest contributions of local reflexes, pre-programmed and voluntary actions to the motor equivalence.

Hypothesis 3.3: *Most of the inter-trial variance in the spaces of finger forces and modes will be compatible with stable values of F_{TOT} and M_{TOT} ($V_{UCM} > V_{ORT}$) at steady-states pre-, during-, and after- the middle finger perturbation.*

UCM-Variance analysis with respect to F_{TOT} (macro-analysis): Analysis of across-cycle variance performed for each phase of the cycle confirmed our predictions that most variance in both finger force and mode spaces would stabilize F_{TOT} ($V_{UCM} > V_{ORT}$). Moreover, there was increase in the across-trials variance During- and Post-Pert lying primarily in the space compatible with no changes in F_{TOT} .

UCM-Variance analysis with respect to M_{TOT} (macro-analysis). The analysis of variance was also performed with respect to M_{TOT} in both force and mode spaces. Overall, contrary to our prediction, the across-trials variance in the force and mode space did not stabilize M_{TOT} . In the mode space, there was a progressive increase in V_{ORT} during and post-perturbation. In the force space, V_{ORT} magnitude was not affected during the perturbation, but it increased after the perturbation was over. In contrast, V_{UCM} in both subspaces was larger during the perturbation, but didn't change after the perturbation.

Note that for the non-explicitly instructed performance variable (M_{TOT}) the results of the motor equivalence and UCM-based variance analyses were in opposite directions. During the period of middle finger lift, the changes in finger modes/force were motor equivalent with respect to M_{TOT} , but the values of M_{TOT} were not stabilized by the across-trials co-variation of finger modes and forces.

6.4 Aim 4 Findings

The goal of Aim 4 was **to determine whether changes in the action performed by an abundant system would lead to a motor equivalence signature ($ME > nME$).** A secondary goal was **to investigate the effects of removal of visual feedback on the components of motor equivalence.** The tasks in this experiment involved accurate production of total finger force and moment (F_{TOT} ; M_{TOT}) while pressing with four-fingers. Visual feedback was provided on both variables in the initial state, and then feedback was provided on one of the variables (either F_{TOT} or M_{TOT}) only, while the analysis was performed with respect to both variables. The last goal was to explore the structure of the inter-trial variance in the finger mode space to link the current experiment to previous studies.

***Hypothesis 4.1:** An action that a priori lies primarily within the nME space, will induce a change in the ME component.*

We confirmed the first hypothesis. When the performance changed, there were changes not only in the nME component, but also in the ME with respect to both performance variables (F_{TOT} and M_{TOT}).

***Hypothesis 4.2:** When the target values of the performance variables are changed back to their original values, the nME components will return to the original values, while the ME components will not.*

The second hypothesis was also confirmed. After a sequence of target jumps that led to transient changes in the performance variables, there was a large increase in the ME component, while the differences between the nME component prior to and after the target jumps were smaller. Similar motor equivalent effects were observed

after the step perturbation of the *I*-finger. This experiment extended the motor equivalence findings to transient changes in the action in absence of mechanical perturbations.

Hypothesis 4.3: *The amount of ME change will be insensitive to presence of visual feedback, while nME change will increase without visual feedback.*

We partially confirmed the third hypothesis. When no visual feedback was provided, the nME component increased, accompanied by inconsistent changes in the ME component. The increase in the ME component was smaller for the variable that received no visual feedback (frozen-feedback variable) in the F_{TOT} analysis. However, no difference in the amount of ME component at the post-perturbation phase was observed in the M_{TOT} analysis. These results show that visual feedback influences mostly components orthogonal to the UCM (nME).

Hypothesis 4.4: *The synergic structure of variance ($V_{UCM} > V_{ORT}$) will be observed for the variable receiving visual feedback but not for the “frozen-feedback” variable.*

This hypothesis was confirmed. The performance variable that had visual feedback (continuous-feedback variable) was stabilized by the inter-trial co-variation in the finger mode space. Similarly, there was a strong motor equivalence effect (ME > nME) after the sequence of target jumps. Overall, these results were consistent across the two parts of the experiment, namely, the parts involving jumping targets and perturbations of the index finger.

6.5 Concluding Comments and Future Directions

The findings from this dissertation revealed that response to external perturbation as well as transient change in actions in redundant (or abundant) systems are largely motor equivalent at the level of the task performance. This reorganization of motor elements is mediated by slow (i.e. voluntary) and fast motor responses (<~ 100 ms post-perturbation). This is the first set of studies that explored the potential feedback loops acting to reestablish synergies during purposeful tasks.

A typical observation in the experiments that was evident from the first study was a pronounced increase of the ME component immediately after the perturbation onset. This finding was consistent in the reaching and finger-pressing experiments and across the different levels of description (joint rotations, M-modes, finger modes, and finger forces). We acknowledge that motor equivalence effects could also be a consequence of the perturbation in the UCM space. The perturbation has components parallel and orthogonal to the UCM. Thus, one limitation of this study is the inability to distinguish how much of the motor equivalence effect is caused by the perturbation and how much comes from neural reorganization in response to the perturbation. We designed follow-up studies to estimate the extent to which motor equivalence effects are neurally organized. In Aim 2 we investigated motor equivalence at the level of M-modes, and we observed effects of motor equivalence within the first 50 ms after the beginning of perturbation. In Aim 3, we showed that motor equivalence increases across time windows of 50 ms post-perturbation, and remains large after a transient external perturbation, when the system comes to a new steady-state. Also, the results from Aim 4 show that motor equivalence increases as a result of transient changes in the action, which is expected to lie primarily orthogonal to the UCM. This robust observation indicates that the motor equivalence is of a neural origin, although effects

of muscle mechanics could also have contributions. The increase in the motor equivalence at short time delays followed by a progressive increase in motor equivalence with time suggests that the motor equivalence phenomenon involves a superposition of mechanics, reflex circuits at the spinal cord, pre-programmed reactions, as well as voluntary commands. In addition, findings from the fourth study suggest that vision is critical for the task-specific stability after perturbation in the pressing-task, with (if any) small effects on the ME component. In the previous studies, the effects of visual and proprioceptive/cutaneous feedbacks were not systematically controlled. Future experiments could involve experimental manipulations of these two feedback loops. This would be important to determine how the amount of ME is affected by the diminished ability of the fingers to detect quick errors in performance. Moreover, one could estimate at which instant in time after the perturbation the presence of visual feedback would have an effect on the task-specific stability.

In all of the studies, motor equivalence was evident not only after the perturbation, but also before changes in external conditions were induced to the multi-DOFs system. The early motor equivalence effect does not reflect the compensation of motor elements, but it is more likely to be a consequence of the natural variability during sequential actions due to spontaneous changes in internal states of biological systems and the interactions with the environment.

The essence of the UCM-based variance analysis and the motor equivalence analysis are similar because they reflect the synergic organization of motor elements. The method applied in this dissertation analyzes task-specific stability within a trial by comparing directions of actions, reactions, and motions induced by perturbations in

the multi-DOF space of elemental variables. Using perturbations is a more direct method to test task-specific stability when compared to the across-trials variance measure. However, unlike the across-trials variance analysis, the motor equivalence approach is sensitive to changes in the mean values of the performance variables and its results are not always expected to be similar to those of the UCM-based variance analysis. For example, in Aim 1 the inter-trial variance analysis did not capture effects of magnitude of perturbation, while a stronger perturbation led to stronger motor equivalence effects. Additional experiments exploring the inter-relations between the UCM-based analysis of variance and motor equivalence are encouraged.

Motor equivalence reflects the flexibility/adaptability feature of abundant systems and it is likely to involve numerous neurophysiological mechanisms, from feedback loops in the spinal cord to those involving higher CNS levels. An increase in motor equivalence to compensate for errors in the task-related performance variables is incompatible with most of the optimization approaches, since motor equivalence quantifies the changes in motor elements that do not affect performance variable. The results of this dissertation speak in favor of an alternative scheme of motor control that makes use of the abundant DOFs. This strategy resists changes in motor elements that lead to changes in important task-specific performance variables, while combinations of motor elements that do not affect those variables have more freedom to vary.

The UCM-framework provides a quantitative measure of how different motor elements are coordinated to produce natural behaviors. This approach is relatively new, and its applications to different populations have been limited. Links to neurophysiological mechanisms are still largely unknown, in part due to the difficulty in addressing these issues with behavioral measures in humans. Given the multiple

routes that remain to be explored using the UCM-framework, one of the natural paths is to study the findings of the current dissertation in populations with movement disorders to better understand features of synergic control and to ultimately improve treatment.

REFERENCES

- Abend, W., Bizzi, E., & Morasso, P. (1982). Human arm trajectory formation. *Brain*, 105(Pt 2), 331-348.
- Alessandro, C., Carbajal, J. P., & d'Avella, A. (2013). A computational analysis of motor synergies by dynamic response decomposition. *Front Comput Neurosci*, 7(191), 1-20.
- Ambike, S., Paquet, F., Latash, M. L., & Zatsiorsky, V. M. (2013). Grip-force modulation in multi-finger prehension during wrist flexion and extension. *Exp Brain Res*, 227(4), 509-522.
- Ambike, S., Zatsiorsky, V. M., & Latash, M. L. (2015). Processes underlying unintentional finger-force changes in the absence of visual feedback. *Exp Brain Res*, 233(3), 711-721.
- Arbib, M. A., Iberall, T., & Lyons, D. (1985). *Coordinated control programs for movements on the hand*. Berlin: Springer-Verlag.
- Arimoto, S., Nguyen, P., Han, H., & Doulgeri, Z. (2000). Dynamics and control of a set of dual fingers with soft tips. *Robotica*, 18(1), 71-80.
- Arimoto, S., Tahara, K., Yamaguchi, M., Nguyen, P., & Han, H. (2001). Principle of superposition for controlling pinch motions by means of robot fingers with soft tips. *Robotica*, 19(1), 21-28.
- Asaka, T., Wang, Y., Fukushima, J., & Latash, M. L. (2008). Learning effects on muscle modes and multi-mode postural synergies. *Exp Brain Res*, 184(3), 323-338.
- Atkeson, C. G., & Hollerbach, J. M. (1985). Kinematic features of unrestrained vertical arm movements. *J Neurosci*, 5(9), 2318-2330.
- Berkinblit, M. B., Gel'fand, I. M., & Fel'dman, A. G. (1986). A model of control of the movement of the multiarticular extremity. *Biofizika*, 31(1), 128-138.
- Berniker, M., Jarc, A., Bizzi, E., & Tresch, M. C. (2009). Simplified and effective motor control based on muscle synergies to exploit musculoskeletal dynamics. *Proc Natl Acad Sci U S A*, 106(18), 7601-7606.

- Bernstein, N. A. (1967). *The coordination and regulation of movements*. Oxford: Pergamon Press.
- Borzelli, D., Berger, D. J., Pai, D. K., & d'Avella, A. (2013). Effort minimization and synergistic muscle recruitment for three-dimensional force generation. *Front Comput Neurosci*, 7, 186.
- Brown, I. E., & Loeb, G. E. (2000). A reductionist approach to creating and using neuromusculoskeletal models. In J. M. Winters & P. E. Crago (Eds.), *Biomechanics and neural control of posture and movement* (pp. 148-163). New York: Springer.
- Chan, C. W., Jones, G. M., Kearney, R. E., & Watt, D. G. (1979). The 'late' electromyographic response to limb displacement in man. I. Evidence for supraspinal contribution. *Electroencephalogr Clin Neurophysiol*, 46(2), 173-181.
- Cheung, V. C., d'Avella, A., & Bizzi, E. (2009). Adjustments of motor pattern for load compensation via modulated activations of muscle synergies during natural behaviors. *J Neurophysiol*, 101(3), 1235-1257.
- Cole, K. J., & Abbs, J. H. (1987). Kinematic and electromyographic responses to perturbation of a rapid grasp. *J Neurophysiol*, 57(5), 1498-1510.
- Cruse, H., & Bruwer, M. (1987). The human arm as a redundant manipulator: the control of path and joint angles. *Biol Cybern*, 57(1-2), 137-144.
- Cruse, H., Bruwer, M., & Dean, J. (1993). Control of Three- and Four-Joint Arm Movement: Strategies for a Manipulator With Redundant Degrees of Freedom. *J Mot Behav*, 25(3), 131-139.
- d'Avella, A., & Bizzi, E. (2005). Shared and specific muscle synergies in natural motor behaviors. *Proc Natl Acad Sci U S A*, 102(8), 3076-3081.
- d'Avella, A., Fernandez, L., Portone, A., & Lacquaniti, F. (2008). Modulation of phasic and tonic muscle synergies with reaching direction and speed. *J Neurophysiol*, 100(3), 1433-1454.
- d'Avella, A., & Lacquaniti, F. (2013). Control of reaching movements by muscle synergy combinations. *Front Comput Neurosci*, 7, 42.
- d'Avella, A., Portone, A., Fernandez, L., & Lacquaniti, F. (2006). Control of fast-reaching movements by muscle synergy combinations. *J Neurosci*, 26(30), 7791-7810.

- Danion, F., Schoner, G., Latash, M. L., Li, S., Scholz, J. P., & Zatsiorsky, V. M. (2003). A mode hypothesis for finger interaction during multi-finger force-production tasks. *Biol Cybern*, *88*(2), 91-98.
- Danna-Dos-Santos, A., Degani, A. M., & Latash, M. L. (2008). Flexible muscle modes and synergies in challenging whole-body tasks. *Exp Brain Res*, *189*(2), 171-187.
- Danna-Dos-Santos, A., Shapkova, E. Y., Shapkova, A. L., Degani, A. M., & Latash, M. L. (2009). Postural control during upper body locomotor-like movements: similar synergies based on dissimilar muscle modes. *Exp Brain Res*, *193*(4), 565-579.
- Danna-Dos-Santos, A., Slomka, K., Zatsiorsky, V. M., & Latash, M. L. (2007). Muscle modes and synergies during voluntary body sway. *Exp Brain Res*, *179*(4), 533-550.
- de Freitas, S. M., Scholz, J. P., & Stehman, A. J. (2007). Effect of motor planning on use of motor abundance. *Neurosci Lett*, *417*(1), 66-71.
- de Rugy, A., & Sternad, D. (2003). Interaction between discrete and rhythmic movements: reaction time and phase of discrete movement initiation during oscillatory movements. *Brain Res*, *994*(2), 160-174.
- Desmurget, M., Grea, H., & Prablanc, C. (1998). Final posture of the upper limb depends on the initial position of the hand during prehension movements. *Exp Brain Res*, *119*(4), 511-516.
- Desmurget, M., Prablanc, C., Rossetti, Y., Arzi, M., Paulignan, Y., Urquizar, C., & Mignot, J. C. (1995). Postural and synergic control for three-dimensional movements of reaching and grasping. *J Neurophysiol*, *74*(2), 905-910.
- Dickinson, M. H., Farley, C. T., Full, R. J., Koehl, M. A., Kram, R., & Lehman, S. (2000). How animals move: an integrative view. *Science*, *288*(5463), 100-106.
- Diedrichsen, J., Shadmehr, R., & Ivry, R. B. (2010). The coordination of movement: optimal feedback control and beyond. *Trends Cogn Sci*, *14*(1), 31-39.
- Domkin, D., Laczko, J., Djupsjobacka, M., Jaric, S., & Latash, M. L. (2005). Joint angle variability in 3D bimanual pointing: uncontrolled manifold analysis. *Exp Brain Res*, *163*(1), 44-57.
- Domkin, D., Laczko, J., Jaric, S., Johansson, H., & Latash, M. L. (2002). Structure of joint variability in bimanual pointing tasks. *Exp Brain Res*, *143*(1), 11-23.

- Enderle, J. D., & Wolfe, J. W. (1987). Time-optimal control of saccadic eye movements. *IEEE Trans Biomed Eng*, 34(1), 43-55.
- Feldman, A. G. (1966). On the functional tuning of the nervous system in movement control or preservation of stationary pose. II. Adjustable parameters in muscles. *Biofizika*, 11(3), 498-508.
- Feldman, A. G. (1986). Once more on the equilibrium-point hypothesis (lambda model) for motor control. *J Mot Behav*, 18(1), 17-54.
- Feldman, A. G. (2009). Origin and advances of the equilibrium-point hypothesis. *Adv Exp Med Biol*, 629, 637-643.
- Feldman, A. G., Goussev, V., Sangole, A., & Levin, M. F. (2007). Threshold position control and the principle of minimal interaction in motor actions. *Prog Brain Res*, 165, 267-281.
- Feldman, A. G., & Levin, M. F. (1995). The origin and use of positional frames of reference in motor control. *Behavioral and brain sciences*, 18, 83.
- Feldman, A. G., & Orlovsky, G. N. (1972). The influence of different descending systems on the tonic stretch reflex in the cat. *Exp Neurol*, 37(3), 481-494.
- Feldman, S., Rachmilewitz, E. A., & Izak, G. (1966). The effect of central nervous system stimulation on erythropoiesis in rats with chronically implanted electrodes. *J Lab Clin Med*, 67(5), 713-725.
- Flash, T., & Hogan, N. (1985). The coordination of arm movements: an experimentally confirmed mathematical model. *J Neurosci*, 5(7), 1688-1703.
- Franklin, D. W., Osu, R., Burdet, E., Kawato, M., & Milner, T. E. (2003). Adaptation to stable and unstable dynamics achieved by combined impedance control and inverse dynamics model. *J Neurophysiol*, 90(5), 3270-3282.
- Freitas, S. M., & Scholz, J. P. (2009). Does hand dominance affect the use of motor abundance when reaching to uncertain targets? *Hum Mov Sci*, 28(2), 169-190.
- Freitas, S. M., Scholz, J. P., & Latash, M. L. (2010). Analyses of joint variance related to voluntary whole-body movements performed in standing. *J Neurosci Methods*, 188(1), 89-96.
- Friedman, J., Latash, M. L., & Zatsiorsky, V. M. (2011). Directional variability of the isometric force vector produced by the human hand in multijoint planar tasks. *J Mot Behav*, 43(6), 451-463.

- Friedman, J., Skm, V., Zatsiorsky, V. M., & Latash, M. L. (2009). The sources of two components of variance: an example of multifinger cyclic force production tasks at different frequencies. *Exp Brain Res*, *196*(2), 263-277.
- Fukson, O. I., Berkinblit, M. B., & Feldman, A. G. (1980). The spinal frog takes into account the scheme of its body during the wiping reflex. *Science*, *209*(4462), 1261-1263.
- Gelfand, I. M., & Latash, M. L. (1998). On the problem of adequate language in motor control. *Motor Control*, *2*(4), 306-313.
- Gera, G., Freitas, S., Latash, M., Monahan, K., Schoner, G., & Scholz, J. (2010). Motor abundance contributes to resolving multiple kinematic task constraints. *Motor Control*, *14*(1), 83-115.
- Gielen, C. C., Ramaekers, L., & van Zuylen, E. J. (1988). Long-latency stretch reflexes as co-ordinated functional responses in man. *J Physiol*, *407*, 275-292.
- Goodman, S. R., & Latash, M. L. (2006). Feed-forward control of a redundant motor system. *Biol Cybern*, *95*(3), 271-280.
- Goodman, S. R., Shim, J. K., Zatsiorsky, V. M., & Latash, M. L. (2005). Motor variability within a multi-effector system: experimental and analytical studies of multi-finger production of quick force pulses. *Exp Brain Res*, *163*(1), 75-85.
- Gorniak, S. L., Feldman, A. G., & Latash, M. L. (2009). Joint coordination during bimanual transport of real and imaginary objects. *Neurosci Lett*, *456*(2), 80-84.
- Gorniak, S. L., Zatsiorsky, V. M., & Latash, M. L. (2007). Hierarchies of synergies: an example of two-hand, multi-finger tasks. *Exp Brain Res*, *179*(2), 167-180.
- Gorniak, S. L., Zatsiorsky, V. M., & Latash, M. L. (2009). Hierarchical control of static prehension: II. Multi-digit synergies. *Exp Brain Res*, *194*(1), 1-15.
- Graziano, M. S., Taylor, C. S., & Moore, T. (2002). Complex movements evoked by microstimulation of precentral cortex. *Neuron*, *34*(5), 841-851.
- Graziano, M. S., Taylor, C. S., Moore, T., & Cooke, D. F. (2002). The cortical control of movement revisited. *Neuron*, *36*(3), 349-362.
- Grea, H., Desmurget, M., & Prablanc, C. (2000). Postural invariance in three-dimensional reaching and grasping movements. *Exp Brain Res*, *134*(2), 155-162.

- Gribble, P. L., Ostry, D. J., Sanguineti, V., & Laboissiere, R. (1998). Are complex control signals required for human arm movement? *J Neurophysiol*, *79*(3), 1409-1424.
- Guigon, E., Baraduc, P., & Desmurget, M. (2007). Computational motor control: redundancy and invariance. *J Neurophysiol*, *97*(1), 331-347.
- Gutman, S. R., & Gottlieb, G. L. (1992). Basic functions of variability of simple pre-planned movements. *Biol Cybern*, *68*(1), 63-73.
- Gutman, S. R., Latash, M. L., Almeida, G. L., & Gottlieb, G. L. (1993). Kinematic description of variability of fast movements: analytical and experimental approaches. *Biol Cybern*, *69*(5-6), 485-492.
- Hansen, E., Grimme, B., Reimann, H., & Schoner, G. (in press). Carry-over coarticulation in joint angles. 1-28.
- Hasan, Z. (1986). Optimized movement trajectories and joint stiffness in unperturbed, inertially loaded movements. *Biol Cybern*, *53*(6), 373-382.
- Hogan, N., & Sternad, D. (2007). On rhythmic and discrete movements: reflections, definitions and implications for motor control. *Exp Brain Res*, *181*(1), 13-30.
- Holdefer, R. N., & Miller, L. E. (2002). Primary motor cortical neurons encode functional muscle synergies. *Exp Brain Res*, *146*(2), 233-243.
- Hollerbach, J. M., & Flash, T. (1982). Dynamic interactions between limb segments during planar arm movement. *Biol Cybern*, *44*, 67-77.
- Hsu, W. L., & Scholz, J. P. (2012). Motor abundance supports multitasking while standing. *Hum Mov Sci*, *31*(4), 844-862.
- Hsu, W. L., Scholz, J. P., Schoner, G., Jeka, J. J., & Kiemel, T. (2007). Control and estimation of posture during quiet stance depends on multijoint coordination. *J Neurophysiol*, *97*(4), 3024-3035.
- Hughes, O. M., & Abbs, J. H. (1976). Labial-mandibular coordination in the production of speech: implications for the operation of motor equivalence. *Phonetica*, *33*(3), 199-221.
- Ivanenko, Y. P., Cappellini, G., Dominici, N., Poppele, R. E., & Lacquaniti, F. (2007). Modular control of limb movements during human locomotion. *J Neurosci*, *27*(41), 11149-11161.

- Jackson, J. (1889). On the comparative study of diseases of the nervous system. *Br Med J*, 355-362.
- Kang, N., Shinohara, M., Zatsiorsky, V. M., & Latash, M. L. (2004). Learning multi-finger synergies: an uncontrolled manifold analysis. *Exp Brain Res*, 157(3), 336-350.
- Kawato, M. (1999). Internal models for motor control and trajectory planning. *Curr Opin Neurobiol*, 9(6), 718-727.
- Kawato, M., & Wolpert, D. (1998). Internal models for motor control. *Novartis Found Symp*, 218, 291-304; discussion 304-297.
- Kelso, J. A., Tuller, B., Vatikiotis-Bateson, E., & Fowler, C. A. (1984). Functionally specific articulatory cooperation following jaw perturbations during speech: evidence for coordinative structures. *J Exp Psychol Hum Percept Perform*, 10(6), 812-832.
- Kilbreath, S. L., & Gandevia, S. C. (1994). Limited independent flexion of the thumb and fingers in human subjects. *J Physiol*, 479, 487-497.
- Kinoshita, H., Kawai, S., & Ikuta, K. (1995). Contributions and co-ordination of individual fingers in multiple finger prehension. *Ergonomics*, 38(6), 1212-1230.
- Klous, M., Mikulic, P., & Latash, M. L. (2011). Two aspects of feedforward postural control: anticipatory postural adjustments and anticipatory synergy adjustments. *J Neurophysiol*, 105(5), 2275-2288.
- Klous, M., Mikulic, P., & Latash, M. L. (2012). Early postural adjustments in preparation to whole-body voluntary sway. *J Electromyogr Kinesiol*, 22(1), 110-116.
- Krishnamoorthy, V., Goodman, S., Zatsiorsky, V., & Latash, M. L. (2003). Muscle synergies during shifts of the center of pressure by standing persons: identification of muscle modes. *Biol Cybern*, 89(2), 152-161.
- Krishnamoorthy, V., Latash, M. L., Scholz, J. P., & Zatsiorsky, V. M. (2003). Muscle synergies during shifts of the center of pressure by standing persons. *Exp Brain Res*, 152(3), 281-292.
- Krishnamoorthy, V., Latash, M. L., Scholz, J. P., & Zatsiorsky, V. M. (2004). Muscle modes during shifts of the center of pressure by standing persons: effect of instability and additional support. *Exp Brain Res*, 157(1), 18-31.

- Krishnamoorthy, V., Scholz, J. P., & Latash, M. L. (2007). The use of flexible arm muscle synergies to perform an isometric stabilization task. *Clin Neurophysiol*, *118*(3), 525-537.
- Latash, M. L. (1994). Reconstruction of equilibrium trajectories and joint stiffness patterns during single-joint voluntary movements under different instructions. *Biol Cybern*, *71*(5), 441-450.
- Latash, M. L. (2000). There is no motor redundancy in human movements. There is motor abundance. *Motor Control*, *4*, 259-261.
- Latash, M. L. (2008). Evolution of Motor Control: From Reflexes and Motor Programs to the Equilibrium-Point Hypothesis. *J Hum Kinet*, *19*(19), 3-24.
- Latash, M. L. (2010a). Motor synergies and the equilibrium-point hypothesis. *Motor Control*, *14*(3), 294-322.
- Latash, M. L. (2010b). Stages in learning motor synergies: a view based on the equilibrium-point hypothesis. *Hum Mov Sci*, *29*(5), 642-654.
- Latash, M. L. (2010c). Two Archetypes of Motor Control Research. *Motor Control*, *14*(3), e41-e53.
- Latash, M. L. (2012a). The bliss (not the problem) of motor abundance (not redundancy). *Exp Brain Res*, *217*(1), 1-5.
- Latash, M. L. (2012b). *Fundamentals of motor control*: Elsevier.
- Latash, M. L., Danion, F., Scholz, J. F., Zatsiorsky, V. M., & Schoner, G. (2003). Approaches to analysis of handwriting as a task of coordinating a redundant motor system. *Hum Mov Sci*, *22*(2), 153-171.
- Latash, M. L., Gorniak, S., & Zatsiorsky, V. M. (2008). Hierarchies of Synergies in Human Movements. *Kinesiology (Zagreb)*, *40*(1), 29-38.
- Latash, M. L., & Gottlieb, G. L. (1990). Compliant characteristics of single joints: preservation of equifinality with phasic reactions. *Biol Cybern*, *62*(4), 331-336.
- Latash, M. L., Levin, M. F., Scholz, J. P., & Schoner, G. (2010). Motor control theories and their applications. *Medicina (Kaunas)*, *46*(6), 382-392.
- Latash, M. L., Li, Z. M., & Zatsiorsky, V. M. (1998). A principle of error compensation studied within a task of force production by a redundant set of fingers. *Exp Brain Res*, *122*(2), 131-138.

- Latash, M. L., Scholz, J. F., Danion, F., & Schoner, G. (2001). Structure of motor variability in marginally redundant multifinger force production tasks. *Exp Brain Res*, *141*(2), 153-165.
- Latash, M. L., Scholz, J. F., Danion, F., & Schoner, G. (2002). Finger coordination during discrete and oscillatory force production tasks. *Exp Brain Res*, *146*(4), 419-432.
- Latash, M. L., Scholz, J. P., & Schoner, G. (2002). Motor control strategies revealed in the structure of motor variability. *Exerc Sport Sci Rev*, *30*(1), 26-31.
- Latash, M. L., Scholz, J. P., & Schoner, G. (2007). Toward a new theory of motor synergies. *Motor Control*, *11*(3), 276-308.
- Latash, M. L., Shim, J. K., Smilga, A. V., & Zatsiorsky, V. M. (2005). A central back-coupling hypothesis on the organization of motor synergies: a physical metaphor and a neural model. *Biol Cybern*, *92*(3), 186-191.
- Leijnse, J. N., Snijders, C. J., Bonte, J. E., Landsmeer, J. M., Kalker, J. J., Van der Meulen, J. C., . . . Hovius, S. E. (1993). The hand of the musician: the kinematics of the bidigital finger system with anatomical restrictions. *J Biomech*, *26*(10), 1169-1179.
- Lemay, M. A., & Grill, W. M. (2004). Modularity of motor output evoked by intraspinal microstimulation in cats. *J Neurophysiol*, *91*(1), 502-514.
- Levin, O., Wenderoth, N., Steyvers, M., & Swinnen, S. P. (2003). Directional invariance during loading-related modulations of muscle activity: evidence for motor equivalence. *Exp Brain Res*, *148*(1), 62-76.
- Lewis, G. N., MacKinnon, C. D., Trumbower, R., & Perreault, E. J. (2010). Co-contraction modifies the stretch reflex elicited in muscles shortened by a joint perturbation. *Exp Brain Res*, *207*(1-2), 39-48.
- Li, S. (2013). Analysis of increasing and decreasing isometric finger force generation and the possible role of the corticospinal system in this process. *Motor Control*, *17*(3), 221-237.
- Li, Z. M., Latash, M. L., Newell, K. M., & Zatsiorsky, V. M. (1998). Motor redundancy during maximal voluntary contraction in four-finger tasks. *Exp Brain Res*, *122*(1), 71-78.
- Li, Z. M., Latash, M. L., & Zatsiorsky, V. M. (1998). Force sharing among fingers as a model of the redundancy problem. *Exp Brain Res*, *119*(3), 276-286.

- Martin, J. R., Budgeon, M. K., Zatsiorsky, V. M., & Latash, M. L. (2011). Stabilization of the total force in multi-finger pressing tasks studied with the 'inverse piano' technique. *Hum Mov Sci*, 30(3), 446-458.
- Martin, V. (2007). *A dynamical systems account of the uncontrolled manifold and motor equivalence in human pointing movements*. (Doctoral), Ruhr Universitat Bochum.
- Martin, V., Scholz, J. P., & Schoner, G. (2009). Redundancy, self-motion, and motor control. *Neural Comput*, 21(5), 1371-1414.
- Matthews, P. B. (1959). A study of certain factors influencing the stretch reflex of the decerebrate cat. *J Physiol*, 147(3), 547-564.
- Mattos, D., Kuhl, J., Scholz, J. P., & Latash, M. L. (2013). Motor equivalence (ME) during reaching: is ME observable at the muscle level? *Motor Control*, 17(2), 145-175.
- Mattos, D., Schoner, G., Zatsiorsky, V. M., & Latash, M. L. (2015). Motor equivalence during multi-finger accurate force production. *Exp Brain Res*, 233(2), 487-502.
- Mattos, D. J., Latash, M. L., Park, E., Kuhl, J., & Scholz, J. P. (2011). Unpredictable elbow joint perturbation during reaching results in multijoint motor equivalence. *J Neurophysiol*, 106(3), 1424-1436.
- Morasso, P. (1981). Spatial control of arm movements. *Exp Brain Res*, 42(2), 223-227.
- Murray, R. M., Li, Z., & Sastry, S. S. (1994). *A Mathematical Introduction to Robotic Manipulation*. Boca Raton: CRC.
- Newell, K. M., Carton, L. G., & Hancock, P. A. (1984). Kinetic analysis of response variability. *Psychol Bull*, 96(1), 133-151.
- Nishikawa, K. C., Murray, S. T., & Flanders, M. (1999). Do arm postures vary with the speed of reaching? *J Neurophysiol*, 81(5), 2582-2586.
- Ohtsuki, T. (1981). Inhibition of individual fingers during grip strength exertion. *Ergonomics*, 24(1), 21-36.
- Oldfield, R. C. (1971). The assessment and analysis of handedness: the Edinburgh inventory. *Neuropsychologia*, 9(1), 97-113.

- Osu, R., Burdet, E., Franklin, D. W., Milner, T. E., & Kawato, M. (2003). Different mechanisms involved in adaptation to stable and unstable dynamics. *J Neurophysiol*, *90*(5), 3255-3269.
- Overduin, S. A., d'Avella, A., Carmena, J. M., & Bizzi, E. (2012). Microstimulation activates a handful of muscle synergies. *Neuron*, *76*(6), 1071-1077.
- Park, J., Sun, Y., Zatsiorsky, V. M., & Latash, M. L. (2011). Age-related changes in optimality and motor variability: an example of multifinger redundant tasks. *Exp Brain Res*, *212*(1), 1-18.
- Penrose, R. (1955). *A generalized inverse for matrices*. Paper presented at the Cambridge Philosophical Society.
- Prilutsky, B. I., & Zatsiorsky, V. M. (2002). Optimization-based models of muscle coordination. *Exerc Sport Sci Rev*, *30*(1), 32-38.
- Prochazka, A., Clarac, F., Loeb, G. E., Rothwell, J. C., & Wolpaw, J. R. (2000). What do reflex and voluntary mean? Modern views on an ancient debate. *Exp Brain Res*, *130*(4), 417-432.
- Raibert, M. H. (1977). Motor control and learning by the state space model . *Technical Report AI-M-351*. Cambridge, MA: Massachusetts Institute of Technology.
- Raptis, H., Burtet, L., Forget, R., & Feldman, A. G. (2010). Control of wrist position and muscle relaxation by shifting spatial frames of reference for motoneuronal recruitment: possible involvement of corticospinal pathways. *J Physiol*, *588*(Pt 9), 1551-1570.
- Reisman, D. S., & Scholz, J. P. (2003). Aspects of joint coordination are preserved during pointing in persons with post-stroke hemiparesis. *Brain*, *126*(Pt 11), 2510-2527.
- Reisman, D. S., & Scholz, J. P. (2006). Workspace location influences joint coordination during reaching in post-stroke hemiparesis. *Exp Brain Res*, *170*(2), 265-276.
- Reisman, D. S., Scholz, J. P., & Schoner, G. (2002a). Coordination underlying the control of whole body momentum during sit-to-stand. *Gait Posture*, *15*(1), 45-55.
- Reisman, D. S., Scholz, J. P., & Schoner, G. (2002b). Differential joint coordination in the tasks of standing up and sitting down. *J Electromyogr Kinesiol*, *12*(6), 493-505.

- Robert, T., & Latash, M. L. (2008). Time evolution of the organization of multi-muscle postural responses to sudden changes in the external force applied at the trunk level. *Neurosci Lett*, *438*(2), 238-241.
- Roh, J., Rymer, W. Z., & Beer, R. F. (2012). Robustness of muscle synergies underlying three-dimensional force generation at the hand in healthy humans. *J Neurophysiol*, *107*(8), 2123-2142.
- Rosenbaum, D. A., Meulenbroek, R. G., Vaughan, J., & Jansen, C. (1999). Coordination of reaching and grasping by capitalizing on obstacle avoidance and other constraints. *Exp Brain Res*, *128*(1-2), 92-100.
- Rosenbaum, D. A., Meulenbroek, R. J., Vaughan, J., & Jansen, C. (2001). Posture-based motion planning: applications to grasping. *Psychol Rev*, *108*(4), 709-734.
- Ross, K. T., & Nichols, T. R. (2009). Heterogenic feedback between hindlimb extensors in the spontaneously locomoting preammillary cat. *J Neurophysiol*, *101*(1), 184-197.
- Rothwell, J. (1994). *Control of human voluntary movement* (2 ed.): Chapman & Hall.
- Rouiller, E. M., Moret, V., Tanne, J., & Boussaoud, D. (1996). Evidence for direct connections between the hand region of the supplementary motor area and cervical motoneurons in the macaque monkey. *Eur J Neurosci*, *8*(5), 1055-1059.
- Saltiel, P., Wyler-Duda, K., D'Avella, A., Tresch, M. C., & Bizzi, E. (2001). Muscle synergies encoded within the spinal cord: evidence from focal intraspinal NMDA iontophoresis in the frog. *J Neurophysiol*, *85*(2), 605-619.
- Santello, M., & Soechting, J. F. (2000). Force synergies for multifingered grasping. *Exp Brain Res*, *133*(4), 457-467.
- Schieber, M. H. (1991). Individuated finger movements of rhesus monkeys: a means of quantifying the independence of the digits. *J Neurophysiol*, *65*(6), 1381-1391.
- Schmidt, R. A., & Lee, T. D. (2005). *Motor Control and Learning: A Behavioral Emphasis*. Champaign, IL: Human Kinetics.
- Scholz, J. P., Danion, F., Latash, M. L., & Schoner, G. (2002). Understanding finger coordination through analysis of the structure of force variability. *Biol Cybern*, *86*(1), 29-39.

- Scholz, J. P., Dwight-Higgin, T., Lynch, J. E., Tseng, Y. W., Martin, V., & Schoner, G. (2011). Motor equivalence and self-motion induced by different movement speeds. *Exp Brain Res*, 209(3), 319-332.
- Scholz, J. P., & Schoner, G. (1999). The uncontrolled manifold concept: identifying control variables for a functional task. *Exp Brain Res*, 126(3), 289-306.
- Scholz, J. P., & Schoner, G. (2014). Use of the uncontrolled manifold (UCM) approach to understand motor variability, motor equivalence, and self-motion. *Adv Exp Med Biol*, 826, 91-100.
- Scholz, J. P., Schoner, G., Hsu, W. L., Jeka, J. J., Horak, F., & Martin, V. (2007). Motor equivalent control of the center of mass in response to support surface perturbations. *Exp Brain Res*, 180(1), 163-179.
- Scholz, J. P., Schoner, G., & Latash, M. L. (2000). Identifying the control structure of multijoint coordination during pistol shooting. *Exp Brain Res*, 135(3), 382-404.
- Schoner, G. (1990). A dynamic theory of coordination of discrete movement. *Biol Cybern*, 63(4), 257-270.
- Schoner, G. (1995). Recent developments and problem in human movement science and their conceptual implications. *Ecol Psychol*, 7(4), 291-314.
- Schoner, G., & Kelso, J. A. (1988). Dynamic pattern generation in behavioral and neural systems. *Science*, 239(4847), 1513-1520.
- Schoner, G., Martin, V., Reimann, H., & Scholz, J. (2008). *Motor Equivalence and the uncontrolled manifold*. Paper presented at the 8th International Seminar on Speech Production, Strasbourg, France.
- Scott, S. H. (2004). Optimal feedback control and the neural basis of volitional motor control. *Nat Rev Neurosci*, 5(7), 532-546.
- Shadmehr, R., & Moussavi, Z. M. (2000). Spatial generalization from learning dynamics of reaching movements. *J Neurosci*, 20(20), 7807-7815.
- Shadmehr, R., & Mussa-Ivaldi, F. A. (1994). Adaptive representation of dynamics during learning of a motor task. *J Neurosci*, 14(5 Pt 2), 3208-3224.
- Shim, J. K., Latash, M. L., & Zatsiorsky, V. M. (2003). Prehension synergies: trial-to-trial variability and hierarchical organization of stable performance. *Exp Brain Res*, 152(2), 173-184.

- Shim, J. K., Olafsdottir, H., Zatsiorsky, V. M., & Latash, M. L. (2005). The emergence and disappearance of multi-digit synergies during force-production tasks. *Exp Brain Res*, *164*(2), 260-270.
- Slifkin, A. B., Vaillancourt, D. E., & Newell, K. M. (2000). Intermittency in the control of continuous force production. *J Neurophysiol*, *84*(4), 1708-1718.
- Soderkvist, I., & Wedin, P. A. (1993). Determining the movements of the skeleton using well-configured markers. *J Biomech*, *26*, 1473-1477.
- Soechting, J. F., Buneo, C. A., Herrmann, U., & Flanders, M. (1995). Moving effortlessly in three dimensions: does Donders' law apply to arm movement? *J Neurosci*, *15*(9), 6271-6280.
- Soechting, J. F., & Lacquaniti, F. (1989). An assessment of the existence of muscle synergies during load perturbations and intentional movements of the human arm. *Exp Brain Res*, *74*(3), 535-548.
- Sternad, D., de Rugy, A., Pataky, T., & Dean, W. J. (2002). Interaction of discrete and rhythmic movements over a wide range of periods. *Exp Brain Res*, *147*(2), 162-174.
- Sun, Y., Zatsiorsky, V. M., & Latash, M. L. (2011). Prehension of half-full and half-empty glasses: time and history effects on multi-digit coordination. *Exp Brain Res*, *209*(4), 571-585.
- Thomas, J. S., Corcos, D. M., & Hasan, Z. (2003). Effect of movement speed on limb segment motions for reaching from a standing position. *Experimental Brain Research*, *148*(3), 377-387.
- Tillery, S. I., Ebner, T. J., & Soechting, J. F. (1995). Task dependence of primate arm postures. *Exp Brain Res*, *104*(1), 1-11.
- Ting, L. H. (2007). Dimensional reduction in sensorimotor systems: a framework for understanding muscle coordination of posture. *Prog Brain Res*, *165*, 299-321.
- Todorov, E. (2004). Optimality principles in sensorimotor control. *Nat Neurosci*, *7*(9), 907-915.
- Todorov, E., & Jordan, M. I. (2002). Optimal feedback control as a theory of motor coordination. *Nat Neurosci*, *5*(11), 1226-1235.
- Torres, E., & Andersen, R. (2006a). Space-time separation during obstacle-avoidance learning in monkeys. *J Neurophysiol*, *96*(5), 2613-2632.

- Torres, E., & Andersen, R. (2006b). Space-time separation during obstacle-avoidance learning in monkeys. *Journal of Neurophysiology*, *96*(5), 2613-2632.
- Torres, E. B., & Zipser, D. (2002). Reaching to grasp with a multi-jointed arm. I. A computational model. *Journal of Neurophysiology*, *88*, 1-13.
- Tresch, M. C., Cheung, V. C., & d'Avella, A. (2006). Matrix factorization algorithms for the identification of muscle synergies: evaluation on simulated and experimental data sets. *J Neurophysiol*, *95*(4), 2199-2212.
- Trumbower, R. D., Ravichandran, V. J., Krutky, M. A., & Perreault, E. J. (2010). Contributions of altered stretch reflex coordination to arm impairments following stroke. *J Neurophysiol*, *104*(6), 3612-3624.
- Tseng, Y., Scholz, J. P., & Schoner, G. (2002). Goal-equivalent joint coordination in pointing: affect of vision and arm dominance. *Motor Control*, *6*(2), 183-207.
- Tseng, Y. W., & Scholz, J. P. (2005a). The effect of workspace on the use of motor abundance. *Motor Control*, *9*(1), 75-100.
- Tseng, Y. W., & Scholz, J. P. (2005b). Unilateral vs. bilateral coordination of circle-drawing tasks. *Acta Psychol (Amst)*, *120*(2), 172-198.
- Tseng, Y. W., Scholz, J. P., Schoner, G., & Hotchkiss, L. (2003). Effect of accuracy constraint on joint coordination during pointing movements. *Exp Brain Res*, *149*(3), 276-288.
- Tseng, Y. W., Scholz, J. P., & Valere, M. (2006). Effects of movement frequency and joint kinetics on the joint coordination underlying bimanual circle drawing. *J Mot Behav*, *38*(5), 383-404.
- Turvey, M. T. (1990). Coordination. *Am Psychol*, *45*(8), 938-953.
- Turvey, M. T. (2007). Action and perception at the level of synergies. *Hum Mov Sci*, *26*(4), 657-697.
- Uno, Y., Kawato, M., & Suzuki, R. (1989). Formation and control of optimal trajectory in human multijoint arm movement. Minimum torque-change model. *Biol Cybern*, *61*(2), 89-101.
- Vaillancourt, D. E., & Russell, D. M. (2002). Temporal capacity of short-term visuomotor memory in continuous force production. *Exp Brain Res*, *145*(3), 275-285.

- Vaillancourt, D. E., Slifkin, A. B., & Newell, K. M. (2001). Intermittency in the visual control of force in Parkinson's disease. *Exp Brain Res*, *138*(1), 118-127.
- Valero-Cuevas, F. J., Smaby, N., Venkadesan, M., Peterson, M., & Wright, T. (2003). The strength-dexterity test as a measure of dynamic pinch performance. *J Biomech*, *36*(2), 265-270.
- Valero-Cuevas, F. J., Venkadesan, M., & Todorov, E. (2009). Structured variability of muscle activations supports the minimal intervention principle of motor control. *J Neurophysiol*, *102*(1), 59-68.
- Varadhan, S. K., Zatsiorsky, V. M., & Latash, M. L. (2010). Variance components in discrete force production tasks. *Exp Brain Res*, *205*(3), 335-349.
- Vereijken, B., Vanemmerik, R. E. A., Whiting, H. T. A., & Newell, K. M. (1992). Free(Z)ing Degrees of Freedom in Skill Acquisition. *Journal of motor behavior*, *24*(1), 133-142.
- Wang, Y., Asaka, T., Zatsiorsky, V. M., & Latash, M. L. (2006). Muscle synergies during voluntary body sway: combining across-trials and within-a-trial analyses. *Exp Brain Res*, *174*(4), 679-693.
- Wang, Y., Zatsiorsky, V. M., & Latash, M. L. (2005). Muscle synergies involved in shifting the center of pressure while making a first step. *Exp Brain Res*, *167*(2), 196-210.
- Wang, Y., Zatsiorsky, V. M., & Latash, M. L. (2006). Muscle synergies involved in preparation to a step made under the self-paced and reaction time instructions. *Clin Neurophysiol*, *117*(1), 41-56.
- Whitney, D. E. (1969). *Resolved motion rate control of manipulators and human prostheses*. Paper presented at the IEEE Transactions on Man-Machine Systems.
- Wilhelm, L., Zatsiorsky, V. M., & Latash, M. L. (2013). Equifinality and its violations in a redundant system: multifinger accurate force production. *J Neurophysiol*, *110*(8), 1965-1973.
- Wing, A. M. (2000). Motor control: Mechanisms of motor equivalence in handwriting. *Curr Biol*, *10*(6), R245-248.
- Wu, Y. H., Zatsiorsky, V. M., & Latash, M. L. (2012). Multi-digit coordination during lifting a horizontally oriented object: synergies control with referent configurations. *Exp Brain Res*, *222*(3), 277-290.

- Yang, J. F., & Scholz, J. P. (2005). Learning a throwing task is associated with differential changes in the use of motor abundance. *Exp Brain Res*, 163(2), 137-158.
- Yang, J. F., Scholz, J. P., & Latash, M. L. (2007). The role of kinematic redundancy in adaptation of reaching. *Exp Brain Res*, 176(1), 54-69.
- Zatsiorsky, V. M. (2002). *Kinetics of Human Motion*. Champaign, IL: Human Kinetics.
- Zatsiorsky, V. M., Li, Z. M., & Latash, M. L. (1998). Coordinated force production in multi-finger tasks: finger interaction and neural network modeling. *Biol Cybern*, 79(2), 139-150.
- Zatsiorsky, V. M., Li, Z. M., & Latash, M. L. (2000). Enslaving effects in multi-finger force production. *Exp Brain Res*, 131(2), 187-195.
- Zhang, W., Scholz, J. P., Zatsiorsky, V. M., & Latash, M. L. (2008). What do synergies do? Effects of secondary constraints on multidigit synergies in accurate force-production tasks. *J Neurophysiol*, 99(2), 500-513.
- Zhang, W., Zatsiorsky, V. M., & Latash, M. L. (2007). Finger synergies during multi-finger cyclic production of moment of force. *Exp Brain Res*, 177(2), 243-254.
- Zhou, T., Solnik, S., Wu, Y. H., & Latash, M. L. (2014a). Equifinality and its violations in a redundant system: control with referent configurations in a multi-joint positional task. *Motor Control*, 18(4), 405-424.
- Zhou, T., Solnik, S., Wu, Y. H., & Latash, M. L. (2014b). Unintentional movements produced by back-coupling between the actual and referent body configurations: violations of equifinality in multi-joint positional tasks. *Exp Brain Res*.

Appendix

COMPUTATION OF VARIANCE AND MOTOR EQUIVALENCE ANALYSES REFERENT TO AIM 3

The force data \mathbf{f} were converted into a mode vector \mathbf{m} by using the enslaving matrix \mathbf{E} , where $\mathbf{f} = [f_i, f_M, f_R, f_L]^T$ (T represents matrix transpose).

$$\mathbf{m} = [\mathbf{E}]^{-1} \cdot \mathbf{f} \quad (\text{A1})$$

The Jacobian matrix \mathbf{J} defining the linear map between changes in finger forces (df) modes (dm) and changes in *total force* dF_{TOT} was defined:

$$dF_{TOT} = [1 \ 1 \ 1 \ 1] \cdot df = [1 \ 1 \ 1 \ 1] \cdot \mathbf{E} \cdot dm \quad (\text{A2})$$

$$\therefore \mathbf{J}_F = [1 \ 1 \ 1 \ 1] \text{ and } \mathbf{J}_M = [1 \ 1 \ 1 \ 1] \cdot \mathbf{E} \quad (\text{A3})$$

The \mathbf{J} matrix defining the changes between the finger force and modes (\mathbf{f}/\mathbf{m}) and changes in *total moment* about the longitudinal axis of the forearm/hand with respect to the mid-point of the hand is:

$$\mathbf{J}_F = [d_i, d_M, d_R, d_L] \text{ and } \mathbf{J}_M = [d_i, d_M, d_R, d_L] \cdot \mathbf{E} \quad (\text{A4})$$

where the d_i entries representing the lever arm of fingers, $d_i = 4.5$ cm, $d_M = 1.5$ cm, $d_R = 1.5$ cm and $d_L = -4.5$ cm. The UCM is the null-space of the Jacobian matrix \mathbf{J} , spanned by the basis vectors $\boldsymbol{\varepsilon}_i$, solving:

$$\mathbf{J} \cdot \boldsymbol{\varepsilon}_i = 0 \quad (\text{A5})$$

For the variance analysis, the mean-free \mathbf{f}/\mathbf{m} (Δx_{jk}) for a given \mathbf{j} trial and \mathbf{k} phase (pre-, during- and post-perturbation) was computed:

$$\Delta x_j = x_j - \bar{x}_0 \quad (\text{A6})$$

where x was either force or mode. The Δx was projected into the null and orthogonal spaces of \mathbf{J} as follows:

$$f_{\parallel} = \sum_{i=1}^{n-p} (\boldsymbol{\varepsilon}_i^T \cdot \Delta x) \cdot \boldsymbol{\varepsilon}_i \quad (\text{A7})$$

$$f_{\perp} = \Delta x - f_{\parallel} \quad (\text{A8})$$

where f_{\parallel} is the f parallel component and f_{\perp} is the orthogonal component, n is the number of elemental variables (\mathbf{f}/\mathbf{m}), and p is the number of constraints defined by the performance variable. There are $n-p$ basis vectors, so that the null space has $n-p$ dimensions.

The variance across trials per degree of freedom along V_{ucm} and orthogonal V_{ort} to the UCM was computed.

$$V_{ucm} = \frac{\sum |f_{\parallel}|^2}{(n-p) N_{trials}} \quad (\text{A9})$$

$$V_{ort} = \frac{\sum |f_{\perp}|^2}{p N_{trials}} \quad (\text{A10})$$

For the motor equivalence analysis, the force/mode deviation vectors Δx_j were computed for each j trial by subtracting the mean pre-perturbed force/mode $x_{0,AV}$.

$$\Delta x_j = x_j - x_{0,AV} \quad (\text{A11})$$

The alignment between $x_{0,AV}$ and the x_j , involved temporal normalization of $x_{0,AV}$ for each cycle of j trial. The Δx_j was projected along and orthogonal to the UCM according to equations A7 and A8. The motor equivalence (ME) and non-motor equivalence components (nME) were computed as the length of the projection vector in each subspace, respectively, and normalized by the square root of the degrees of freedom of each space:

$$ME_j = \frac{|f_{\parallel}|}{\sqrt{n-p}} \quad (\text{A12})$$

$$nME_j = \frac{|f_{\perp}|}{\sqrt{p}} \quad (\text{A13})$$